DYNAMIC RESPONSE OF TIMBER RAILROAD BRIDGES

by

A. Shakoor Uppal

A Thesis
presented to the University of Manitoba
in partial fulfillment of
the requirements of the degree of
Doctor of Philosophy
in the Department of Civil Engineering

Winnipeg, Manitoba
Fall, 1990

National Library of Canada
Bibliothèque nationale du Canada

Canadian Theses Service
Service des thèses canadiennes

Ottawa, Canada
K1A 0N4

The author has granted an irrevocable non-exclusive licence allowing the National Library of Canada to reproduce, loan, distribute or sell copies of his/her thesis by any means and in any form or format, making this thesis available to interested persons.

L'auteur a accordé une licence irrévocable et non exclusive permettant à la Bibliothèque nationale du Canada de reproduire, prêter, distribuer ou vendre des copies de sa thèse de quelque manière et sous quelque forme que ce soit pour mettre des exemplaires de cette thèse à la disposition des personnes intéressées.

The author retains ownership of the copyright in his/her thesis. Neither the thesis nor substantial extracts from it may be printed or otherwise reproduced without his/her permission.

L'auteur conserve la propriété du droit d'auteur qui protège sa thèse. Ni la thèse ni des extraits substantiels de celle-ci ne doivent être imprimés ou autrement reproduits sans son autorisation.

ISBN 0-315-71803-X

Canada

DYNAMIC RESPONSE OF TIMBER RAILROAD BRIDGES

BY

A. SHAKOOR UPPAL

A thesis submitted to the Faculty of Graduate Studies of the University of Manitoba in partial fulfillment of the requirements of the degree of

DOCTOR OF PHILOSOPHY

© 1990

Permission has been granted to the LIBRARY OF THE UNIVERSITY OF MANITOBA to lend or sell copies of this thesis. to the NATIONAL LIBRARY OF CANADA to microfilm this thesis and to lend or sell copies of the film, and UNIVERSITY MICROFILMS to publish an abstract of this thesis.

The author reserves other publication rights, and neither the thesis nor extensive extracts from it may be printed or otherwise reproduced without the author's written permission.

I hereby declare that I am the sole author of this thesis.

I authorize the University of Manitoba to lend this thesis to other institutions or individuals for the purpose of scholarly research.

I further authorize the University of Manitoba to reproduce this thesis by photocopying or by other means, in total or in part, at the request of other institutions or individuals for the purpose of scholarly research.

A. Shakoor Uppal

The University of Manitoba requires that all persons using or photocopying this thesis give their signatures, their addresses, and the date of use:

ABSTRACT

In the 1970's, it was reported that there were approximately 2300 track miles of timber railroad bridges in the United States and Canada. For short spans, they offer an attractive alternative to other types of bridges, as they are economical, faster to construct, and easy to maintain. Current design practices do not allow an independent consideration of the effects of the dynamic loads in sizing the bridge components, because very little information is available on the subject.

Dynamic tests were carried out at two timber railroad bridge sites under the passage of trains at speeds varying from 1 mph (i.e., crawl) to 50 mph. The loads at wheel-rail interfaces, the vertical displacements and the accelerations were measured at several locations on the bridge spans, the bridge approaches and the normal track sections. The maximum values of the dynamic load factors and the dynamic displacements factors obtained were as follows:

	Dynamic Load Factor	Dynamic Displacement Factor
Bridge span	1.50	1.32
Bridge approach	1.65	1.00
Normal track	1.85	1.15

Further, an analytical model was employed to simulate the test results. The model consisted of a multi-degree-of-freedom system with each vehicle having bounce, pitch, and roll movements. Two parallel chords, each having its distributed mass lumped at discrete points, were used to idealize the bridge spans. A computer program written on this basis was used to predict the loads at wheel-rail interfaces, the vertical displacements and the

accelerations at the discrete points on the spans.

The maximum predicted and measured loads at the wheel-rail interfaces were found to be within 22% of each other, while the value of the maximum predicted displacements were within 16% of the measured net values. This discrepancy was attributed in part to the partial continuity of the bridge spans over their supports.

Both the test results and the computer programs were used to study the effect of the speed and other factors on the dynamic response of open-deck and ballast-deck bridges.

ACKNOWLEDGEMENTS

The writer wishes to express his sincere gratitude and appreciation to his advisor, Dr. Sami H. Rizkalla, Professor, Civil Engineering Department, University of Manitoba, for his invaluable guidance and encouragement during the course of this study. The writer is also thankful to the members of his thesis examining committee, Dr. R. Bruce Pinkney, Dr. Al Lansdown, Dr. Neil Popplewell, and Dr. M. Saeed Mirza, for their valuable comments.

The writer is thankful to the Transportation Institute of the University of Manitoba for providing the financial support for this work and the Canadian National Railway - Prairie Region for permission to use the test facilities.

The writer wishes to thank Mr. Ron D. Miles, retired Regional Chief Engineer, CN Rail for his constant support, Mr. Russ B. Ferrier, retired General Superintendent - Transportation for his help, and Messrs. Ed Lemke, Moray McVey and Dave Fedorowich of the Structural Laboratory of the University of Manitoba for their assistance. The writer also wishes to thank the members of the Bridges and Structures Staff and many others in Engineering - CN Rail Prairie Region for their encouragement and help during the course of this work.

Special thanks are due to Mr. Rob Graham for his assistance with the computers, Messrs. Keith Loucks and Jingshu Wu for their assistance during the tests, and Ms. Wendy Seversen for typing this thesis expertly.

Lastly, the writer expresses his most sincere gratitude to his wife, Firdouse and to his daughters, Fatima, Hatima, Nazima, Saima, and Asima for their love, understanding, encouragement and patience, which have been the key factors in the completion of this work.

TABLE OF CONTENTS

Page

ABSTRACT i

ACKNOWLEDGEMENTS iii

TABLE OF CONTENTS v

LIST OF TABLES ix

LIST OF FIGURES xii

LIST OF SYMBOLS xx

CHAPTER 1 Introduction

1.1 General 1-1
1.2 Objectives 1-1
1.3 Scope 1-3

CHAPTER 2 Literature Review

2.1 General 2-1
2.2 Experimental Work 2-1
2.3 Theoretical Work 2-8
2.4 Necessity of the Research Program 2-18

CHAPTER 3 Experimental Program

3.1 General 3-1
3.2 Selection of Test Sites 3-2
3.2.1 Bridges
3.2.1.1 The Ballast-Deck Bridge
3.2.1.2 The Open-Deck Bridge
3.2.2 Bridge Approaches
3.2.3 Track Sections
3.3 Test Trains 3-4
3.4 Instrumentation 3-5
3.4.1 Loads at Wheel-Rail Interfaces
3.4.2 Vertical Displacements
3.4.2.1 Support Systems for Displacement Gauges (LVDT)
3.4.3 Accelerations
3.4.4 Data Acquisition System

3.5 Tests 3-10
3.5.1 Calibration Tests
3.5.2 Dynamic Tests
3.6 Test Results 3-14
3.6.1 Calibration Tests
3.6.2 Loads at Wheel-Rail Interfaces
3.6.3 Vertical Displacements
3.6.4 Accelerations
3.7 Analysis of Test Results 3-19
3.7.1 Calibration Tests
3.7.1.1 Modulus of Elasticity
3.7.1.2 Track Moduli for Bridge Approach and Normal Track Section
3.7.2 Loads at Wheel-Rail Interfaces
3.7.2.1 Dynamic Load Factor; DLF = L_d/L_s
3.7.3 Vertical Displacements
3.7.3.1 Dynamic Displacement Factor, DDF = D_d/D_s
3.7.4 Accelerations
3.7.4.1 Damping in Bridge Spans

CHAPTER 4 Analytical Model

4.1 General 4-1
4.2 Vehicle Model 4-2
4.2.1 Assumptions
4.2.2 Equations of Motion
4.3 Bridge Span Model 4-6
4.3.1 Assumptions
4.3.2 Equations of Motion
4.3.2.1 Mass Matrix
4.3.2.2 Stiffness Matrix
4.3.2.3 Damping Matrix
4.3.3 Fundamental Frequencies of Chords
4.4 Vehicle-Bridge Span Interaction 4-11
4.4.1 Assumptions
4.4.2 Loads at Wheel-Rail Interfaces
4.4.3 Relationship between Displacements under the i^{th} Wheel and at its Neighbouring Nodal Points
4.4.4 Effect of Wheel Positions
4.4.4.1 Generalized Masses
4.4.4.2 Generalized Stiffnesses
4.4.4.3 Generalized Forces

4.5 Overall Dynamic System 4-25
- 4.5.1 Overall Equations of Motion
- 4.5.2 Location of Wheels in Chord Segments
- 4.5.3 Solution of Equations of the Motion of the System
- 4.5.4 Computer Program

4.6 Numerical Example 4-31
- 4.6.1 Effect of Train Speed
- 4.6.2 Effect of Train Consists
- 4.6.3 Effect of Bridge Deck Type
- 4.6.4 Effect of Low Spot at Bridge Approach
- 4.6.5 Effect of Damping Coefficient
- 4.6.6 Method of Integration

CHAPTER 5 Discussion

5.1 Experimental Work 5-1
- 5.1.1 Calibration Tests
- 5.1.2 Loads at Wheel-Rail Interfaces
  - 5.1.2.1 Dynamic Load Factor
  - 5.1.2.2 Impact
- 5.1.3 Vertical Displacements
  - 5.1.3.1 Dynamic Displacement Factor
  - 5.1.3.2 Cycles of Vibration
- 5.1.4 Accelerations

5.2 Theoretical Work 5-12
- 5.2.1 Dynamic Model
  - 5.2.1.1 Influence of Assumptions
  - 5.2.1.2 Input Data
  - 5.2.1.3 Tests versus Analysis

5.3 Comparison Between Experimental and Analytical Results 5-15
- 5.3.1 Loads at Wheel-Rail Interfaces
- 5.3.2 Vertical Displacements
- 5.3.3 Accelerations

CHAPTER 6 Summary and Conclusions 6-1

CHAPTER 7 Suggestions for Future Research 7-1

LIST OF REFERENCES R-1

TABLES T-1

FIGURES F-1

LISTING OF COMPUTER PROGRAM A5-1

LIST OF TABLES

Table 3.1	Scale weights of locomotives and cars
Table 3.2	Static displacements and stiffnesses
Table 3.3	Maximum recorded loads, at wheel-rail interfaces, L_d (kips). BDB Site - Test Train No. 2 - September 16, 1986
Table 3.4	Maximum recorded loads, at wheel-rail interfaces, L_d (kips). ODB Site - Test Train No. 2 - September 16, 1986
Table 3.5	Maximum recorded vertical displacements, D_d (mm) BDB Site - Test Train No. 2 - September 16, 1986
Table 3.6	Maximum recorded vertical displacements, D_d (mm). ODB Site - Test Train No. 2 - September 16, 1986
Table 3.7	Maximum and minimum recorded accelerations (g) BDB Site - Test Train 2 - Bridge span S3
Table 3.8	Maximum and minimum recorded accelerations (g) ODB Site - Test Train No. 2 - Bridge Span S2
Table 3.9	Track modulus K (kips/in/in) - Linear approach
Table 3.10	Track modulus K (kips/in/in) - Bi-linear approach
Table 3.11	Upper limits of dynamic load factors, DLF - BDB and ODB Sites - Test Train No. 2
Table 3.11A	Upper limits of dynamic load factors, DLF versus static wheel loads for BDB and ODB sites.
Table 3.12	Values of maximum shear, moment and deflections at mid-point of a span per chord
Table 3.13	Computed damping coefficients. BDB Site - Ballast-Deck Span S3

Table 3.14	Computed damping coefficients. ODB Site - Open-Deck Span S2
Table 4.1	Bridge spans data
Table 4.2	Vehicle trains data
Table 4.3	Effect of train speed. Test Train No. 2 - Mid-point of open-deck bridge, Span S2
Table 4.3A	Effect of train speed. Test Train No. 2 - Mid-point of ballast-deck bridge, Span S3
Table 4.4	Effect of train consist. Test Train No. 2 - Mid-point of open-deck bridge, Span S2, Speed 50 mph
Table 4.5	Effect of bridge deck type. Test Train No. 2 - Mid-point of spans
Table 4.6	Effect of low spots at bridge approach. Test Train No. 2 - Mid-point of open-deck bridge, Span S2, Speed 50 mph
Table 4.7	Effect of damping coefficient, Test Train No. 2 - Bridge spans - Speed 50 mph
Table 4.8	Effect of method of numerical integration. Test Train No. 2 - Open-deck Bridge, Span S2, Speed 50 mph
Table 5.1	Measured versus computed static displacements
Table 5.2	Percentage of the DLF values below 30% impact. Loads at Wheel-rail interfaces - BDB and ODB Sites - Test Train No. 2
Table 5.3	Comparison between computed and measured dynamic load factors, DLF
Table 5.4	Measured rigid body movements (mm) at mid-points of bridge spans - Test Train No. 2
Table 5.5	Ratio of displacements - open versus ballast deck
Table 5.6	Average dynamic bending stresses (psi)

Table 5.7	Maximum loads at wheel-rail interfaces (kips) - Test Train No. 2 - Midpoint of bridge spans
Table 5.7A	Ratios of maximum loads at wheel-rail interfaces (kips) - Test Train No. 2 - Midpoint of bridge spans
Table 5.8	Maximum vertical displacements (mm) - Test Train No. 2 - Midpoint of bridge spans
Table 5.8A	Ratios of maximum vertical displacements (mm) - Test Train No. 2 - Midpoint of bridge spans
Table 5.9	Maximum and minimum accelerations (g) Test Train No. 2 - Midpoint of bridge spans
Table 5.10	Maximum values of predicted and measured dynamic load factors, DLF - Test Train No. 2 - Speed range 1-50 mph
Table 5.11	Maximum values of predicted and measured dynamic displacement factors, DDF - Test train No. 2 - Speed range 1-50 mph

LIST OF FIGURES

Figure 3.1 Elevation and typical cross-section of the ballast-deck bridge

Figure 3.2 Elevation and typical cross section of the open-deck bridge

Figure 3.3 Arrangement of locomotives and cars in test trains No. 1 and 2

Figure 3.4 Photograph showing a typical test train

Figure 3.5 Location of shear circuits, LVDT's and accelerometers - ballast deck bridge site

Figure 3.6 Location of shear circuits, LVDT's and accelerometers - open deck bridge site

Figure 3.7 Detail of strain gauges in shear-load circuit

Figure 3.8 Typical support system for LVDT's

Figure 3.9 Photograph showing typical support system for LVDT's

Figure 3.10 Typical outline of circuitry for dynamic tests

Figure 3.11 Test equipment in truck trailer

Figure 3.12 Photograph showing test equipment in truck trailer

Figure 3.13 Set-up for calibration tests

Figure 3.14 Photograph showing calibration test in progress

Figure 3.15 Load-displacement characteristics
BDB Site - Locations S3, A and T (given in Fig. 3.5)
- Test Train No. 1

Figure 3.16 Load-displacement characteristics
ODB Site - Locations S2, A and T (given in Fig. 3.6)
- Test Train No. 2

Figure 3.17 Loads at wheel-rail interfaces versus time
BDB Site - Midpoint of Span S3 - Test Train No. 2
Speed 1 mph

Figure 3.18	Loads at wheel-rail interfaces versus time BDB Site - Midpoint of Span S3 - Test Train No. 2 Speed 30 mph
Figure 3.19	Loads at wheel-rail interfaces versus time BDB Site - Midpoint of Span S3 - Test Train No. 2 Speed 50 mph
Figure 3.20	Loads at wheel-rail interfaces versus time BDB Site - Bridge approach - Test Train No. 2 Speed 1 mph
Figure 3.21	Loads at wheel-rail interfaces versus time BDB Site - Bridge approach - Test Train No. 2 Speed 30 mph
Figure 3.22	Loads at wheel-rail interfaces versus time BDB Site - Bridge approach - Test Train No. 2 Speed 50 mph
Figure 3.23	Loads at wheel-rail interfaces versus time BDB Site - Normal track section - Test Train No. 2 Speed 1 mph
Figure 3.24	Loads at wheel-rail interfaces versus time BDB Site - Normal track section - Test Train No. 2 Speed 30 mph
Figure 3.25	Loads at wheel-rail interfaces versus time BDB Site - Normal track section - Test Train No. 2 Speed 50 mph
Figure 3.26	Loads at wheel-rail interfaces versus time ODB Site - Midpoint of span S2 - Test Train No. 2 Speed 1 mph
Figure 3.27	Loads at wheel-rail interfaces versus time ODB Site - Midpoint of Span S2 - Test Train No. 2 Speed 30 mph
Figure 3.28	Loads at wheel-rail interfaces versus time ODB Site - Midpoint of Span S2 - Test Train No. 2 Speed 50 mph
Figure 3.29	Loads at wheel-rail interfaces versus time ODB Site - Bridge approach - Test Train No. 2 Speed 1 mph

Figure 3.30 Loads at wheel-rail interfaces versus time
ODB Site - Bridge approach - Test Train No. 2
Speed 30 mph

Figure 3.31 Loads at wheel-rail interfaces versus time
BDB Site - Bridge approach - Test Train No. 2
Speed 50 mph

Figure 3.32 Loads at wheel-rail interfaces versus time
Test Site 3 - Normal track section - Test Train No. 2
Speed 1 mph

Figure 3.33 Loads at wheel-rail interfaces versus time
ODB Site - Normal track section - Test Train No. 2
Speed 30 mph

Figure 3.34 Loads at wheel-rail interfaces versus time
ODB Site - Normal track section - Test Train No. 2
Speed 50 mph

Figure 3.35 Vertical displacement versus time
BDB Site - Midpoint of Span S3 - Test Train No. 2
Speed 1 mph

Figure 3.36 Vertical displacement versus time
BDB Site - Midpoint of Span S3 - Test Train No. 2
Speed 30 mph

Figure 3.37 Vertical displacement versus time
BDB Site - Midpoint of Span S3 - Test Train No. 2
Speed 50 mph

Figure 3.38 Vertical displacement versus time
BDB Site - Midpoint of Span S2 - Test Train No. 2
Speed 1 mph

Figure 3.39 Vertical displacement versus time
BDB Site - Midpoint of Span S2 - Test Train No. 2
Speed 30 mph

Figure 3.40 Vertical displacement versus time
BDB Site - Midpoint of Span S2 - Test Train No. 2
Speed 50 mph

Figure 3.41	Vertical displacement versus time BDB Site - Normal track section - Test Train No. 2 Speed 1 mph
Figure 3.42	Vertical displacement versus time BDB Site - Normal track section - Test Train No. 2 Speed 30 mph
Figure 3.43	Vertical displacement versus time BDB Site - Normal track section - Test Train No. 2 Speed 50 mph
Figure 3.44	Vertical displacement versus time ODB Site - Midpoint of span S2 - Test Train No. 2 Speed 1 mph
Figure 3.45	Vertical displacement versus time ODB Site - Midpoint of Span S2 - Test Train No. 2 Speed 30 mph
Figure 3.46	Vertical displacement versus time ODB Site - Midpoint of Span S2 - Test Train No. 2 Speed 50 mph
Figure 3.47	Vertical displacement versus time ODB Site - Bridge approach - Test Train No. 2 Speed 1 mph
Figure 3.48	Vertical displacement versus time ODB Site - Bridge approach - Test Train No. 2 Speed 30 mph
Figure 3.49	Vertical displacement versus time ODB Site - Bridge approach - Test Train No. 2 Speed 50 mph
Figure 3.50	Vertical displacement versus time ODB Site - Normal track section - Test Train No. 2 Speed 1 mph
Figure 3.51	Vertical displacement versus time ODB Site - Normal track section - Test Train No. 2 Speed 30 mph

Figure 3.52	Vertical displacement versus time ODB Site - Normal track section - Test Train No. 2 Speed 50 mph
Figure 3.53	Acceleration versus time BDB Site - Midpoint of Span S3 - Test Train No. 2 Speed 1 mph
Figure 3.54	Acceleration versus time BDB Site - Midpoint of Span S3 - Test Train No. 2 Speed 30 mph (Channel #1 not working)
Figure 3.55	Acceleration versus time BDB Site - Midpoint of Span S3 - Test Train No. 2 Speed 50 mph
Figure 3.56	Acceleration versus time ODB Site - Midpoint of Span S2 - Test Train No. 2 Speed 1 mph
Figure 3.57	Acceleration versus time ODB Site - Midpoint of Span S2 - Test Train No. 2 Speed 30 mph
Figure 3.58	Acceleration versus time ODB Site - Midpoint of Span S2 - Test Train No. 2 Speed 50 mph
Figure 3.59	Dynamic load factors versus speed BDB Site - Midpoint of Span S3 - Test Train No. 2
Figure 3.60	Dynamic load factors versus speed BDB Site - Bridge Approach - Test Train No. 2
Figure 3.61	Dynamic load factors versus speed BDB Site - Normal track section - Test Train No. 2
Figure 3.62	Dynamic load factors versus speed ODB Site - Midpoint of Span S3 - Test Train No. 2
Figure 3.63	Dynamic load factors versus speed ODB Site - Bridge Approach - Test Train No. 2
Figure 3.64	Dynamic load factors versus speed ODB Site - Normal track section - Test Train No. 2

Figure 3.65	Dynamic load factors versus static wheel load BDB Site - Midpoint of span S3 - Test Train No. 2
Figure 3.66	Dynamic load factors versus static wheel load BDB Site - Bridge approach - Test Train No. 2
Figure 3.67	Dynamic load factors versus static wheel load BDB Site - Normal track section - Test Train No. 2
Figure 3.68	Dynamic load factors versus static wheel load ODB Site - Midpoint of span S3 - Test Train No. 2
Figure 3.69	Dynamic load factors versus static wheel load ODB Site - Bridge approach - Test Train No. 2
Figure 3.70	Dynamic load factors versus static wheel load ODB Site - Normal track section - Test Train No. 2
Figure 3.71	Maximum displacement at midpoint of span S3 and span S2 and track section - BDB Site - Test train no. 2
Figure 3.72	Maximum displacements at midpoint of span S2, bridge approach and track section - ODB Site - Test train no. 2
Figure 3.73	Dynamic displacement factors, DDF versus speed BDB Site - Mid-point of Spans S3, S2, and Track Section
Figure 3.74	Dynamic displacement factors, DDF versus speed ODB Site - Mid-point of span S2, Bridge approach and track section
Figure 3.75	Damping coefficient versus train speed - Test train No. 2 - Ballast deck bridge span S3
Figure 3.76	Damping coefficient versus train speed - Test train No. 2 - Open deck bridge span S2
Figure 4.1	Vehicle suspension system
Figure 4.2	Idealized vehicle model
Figure 4.3	Photograph showing wheel-rail contact point
Figure 4.4	Ballast and open deck bridge spans
Figure 4.5	Idealized bridge span model
Figure 4.6	Flexibility influence coefficient - simple span

Figure 4.7	Vehicle-Bridge interaction
Figure 4.8	Relationship between displacements under i^{th} wheel and its neighbouring nodal points j and j+1
Figure 4.9	Location of wheels on chord segments
Figure 4.10	Typical predicted vertical displacement versus time Midpoint of ballast-deck span S3 - Test Train No. 2 Speed 30 mph
Figure 4.11	Typical predicted vertical displacement versus time Midpoint of open-deck span S2 - Test Train No. 2 Speed 30 mph
Figure 4.12	Typical predicted acceleration versus time Midpoint of ballast-deck span S3 - Test Train No. 2 Speed 30 mph
Figure 4.13	Typical predicted acceleration versus time Midpoint of open-deck span S2 - Test Train No. 2 Speed 30 mph
Figure 4.14	Predicted vertical displacement versus time Midpoint of open-deck span S2 - Locomotive of Test Train No. 2 - Speed 30 mph
Figure 4.15	Predicted vertical displacement versus time Midpoint of open-deck span S2 - Locomotive and one car of test train no. 2 - Speed 30 mph
Figure 4.16	Predicted vertical displacement versus time Midpoint of open-deck span S2 - Locomotive and two cars of test train No. 2 - speed 30 mph
Figure 4.17	Predicted vertical displacement versus time Midpoint of open-deck span S2 - Test Train No. 2 - Speed 50 mph - no low spot approach
Figure 4.18	Predicted vertical displacement versus time Midpoint of open-deck span S2 - Test Train No. 2 - Speed 50 mph - Low spot at approach = 0.5 in

Figure 4.19	Predicted vertical displacement versus time Midpoint of open-deck span S2 - Test Train No. 2 - Speed 50 mph - Low spot at approach = 1.0 in
Figure 4.20	Predicted vertical displacement versus time Midpoint of open-deck span S2 - Test train No. 2 - speed 50 mph - Low spot at approach = 1.5 in
Figure 4.21	Predicted vertical displacement versus time Midpoint of open deck span S2 - Test Train No. 2 - speed 50 mph - Low spot at approach = 2.0 in
Figure 4.22	Effect of damping coefficient on predicted vertical displacement - Test Train No. 2 at 50 mph
Figure 5.1	Percentage of DLF values falling below given percent of impact - bridge span S3, bridge approach and track section, BDB Site
Figure 5.2	Percentage of DLF values falling below given percent of impact - bridge span S2, bridge approach and track section, ODB Site
Figure 5.3	Comparison of theoretical with measured dynamic load factors, DLF - 40" dia. wheels
Figure 5.4	Comparison of theoretical with measured dynamic load factors, DLF - 33" dia. wheels
Figure 5.5	Measured maximum impact versus speed Test train no. 2 - BDB Site
Figure 5.6	Measured maximum impact versus speed Test train no. 2 - ODB Site
Figure 5.7	Comparison between measured and predicted displacement versus time - BDB Span S3 - Test train No. 2 at 30 mph
Figure 5.8	Comparison between measured and predicted displacement versus time - ODB Span S2 - Test train No. 2 at 30 mph

LIST OF SYMBOLS

Chapter 2

E = modulus of elasticity of material of beam (lb/in^2)

I = moment of inertia of beam (in^4)

m = mass per unit length of beam ($lb\text{-}sec^2/in$)

$u(x,t)$ = beam displacement of a point at position x and time t (in)

x = distance from left hand support of beam (in)

t = time (sec)

$F(x,t)$ = forcing function (lb)

$\eta(t)$ = distance of mass M from left hand support of beam at time t(in)

g = acceleration due to gravity (386.4 in/sec^2)

$\delta(x)$ = Dirac Delta function

$[M]$ = mass matrix of beam having lumped masses

$[C]$ = damping matrix of beam having lumped masses

$[K]$ = stiffness matrix

$[A]$ = matrix defining influence coefficients for interacting forces P_i

$\{D\}$, $\{\dot{D}\}$ and $\{\ddot{D}\}$ = vectors of generalized coordinates (in), velocities (in/sec) and accelerations (in/sec^2), respectively

$\{P\}$ = vector of interacting forces (lb)

Chapter 3

E = modulus of elasticity of material (lb/in^2)

P = point load or wheel load at midspan of simple beam or wheel load (lb)

Δ = displacement under load P (in)

I = moment of inertia of one chord or a rail along horizontal axis (in^4)

L = span length centre to centre of bents (in)

δP = increment of load P (lb)

$\delta\Delta$ = increment in displacement Δ (in)

w_m = maximum displacement measured under load P (in)

K = track support stiffness, modulus of track elasticity or simply track modulus (lb/in^2) or (lb/in/in)

L_d = measured dynamic load at wheel-rail interface (kips)

L_s = measured static load at wheel-rail interface (kips)

DLF = dynamic load factor L_d/L_s

D_d = measured dynamic displacement under a chord of stringers or under the rail base (mm)

$D_{calib,compu,crawl}$ = measured static, computed static, or crawl speed displacement of a chord of stringers or a rail base (mm)

DDF = dynamic displacement factor $D_d/D_{calib,\ compu,\ crawl}$

n = 1,2,3,..., mode of vibration of span

f_n = frequency of vibration for mode n (Hz) for n=1 it is natural or fundamental frequency

w = weight of chord per unit length (lb/in)

g = acceleration due to gravity (386.4 in/sec^2)

T_n = time period of decay curve after n^{th} cycle (sec)

U_n = response amplitude of decay curve after n^{th} cycle (mm), U_1 = response amplitude of the first cycle

ω_d = damped frequency of the chord (Hz)

X_n = response amplitude of decay curve after time of n^{th} cycle t_n (mm)

ξ = modal damping coefficient

δ = logarithmic decrement

Chapter 4

General:

v = speed of train (in/sec)

g = acceleration due to gravity (386.4 in/sec^2)

t = time for the 1st axle of train taken to travel a distance of x (in) from the left hand end of the bridge span (in)

Vehicles:

Subscript r, where r=1,2,...,4 used to indicate the vehicle number.
Sub or superscript i where i=1,2,...,n_w is used to indicate the wheel number.

W_T = scale weight of vehicle, i.e., locomotive or car (lb)

M_{br} = body mass of vehicle r including truck frames (lb/sec^2/in)

M_s^i = sprung mass associated with wheel i of vehicle $M_{br}/8$ (lb-sec^2/in)

M_u^i = unsprung mass per wheel i of vehicle, i.e., half the mass of axle-set (lb-sec^2/in)

y_{br}, $\dot{y}_{br}$ and $\ddot{y}_{br}$ = vertical displacement (in), velocity (in/sec) and acceleration (in/sec^2) of vehicle r, respectively.

I_{br} = pitch moment of inertia of vehicle r (lb/in/sec^2)

ϕ_{br}, $\dot{\phi}_{br}$, $\ddot{\phi}_{br}$ = pitch moment of inertia of vehicle r (lb-in-sec^2)

J_{br} = roll moment of inertia of vehicle r (lb-in-sec^2)

θ_{br}, $\dot{\theta}_{br}$ and $\ddot{\theta}_{br}$ = roll displacement (rad), (velocity (rad/sec) and acceleration (rad/sec^2) of vehicle r, respectively.

k_{ypr} = vertical spring stiffness of primary suspension per wheel of vehicle r (lb/in)

k_{ysr} = vertical spring stiffness of secondary suspension per wheel of vehicle r (lb/in)

k_{vr} = equivalent vertical spring stiffness per wheel of vehicle r (lb/in)

ℓ_{tr} = one-half distance between the truck centres of vehicle r (in)

ℓ_{wr} = one-half distance between the wheel base, i.e., between two wheel-axle sets of a truck, of vehicle r (in)

d_{cr} = one-half distance between the wheel-rail contact points of a wheel-axle set (in) = 1/2 (d_f-d_n)

ℓ_r^i = distance of the centre of gravity of vehicle r to the i^{th} wheel (in)

ℓ_{vr} = distance between the last axle of a vehicle r and the first axle of the rear vehicle, i.e., r+1 (in)

u_j^i, $\dot{u}_j^i$, and $\ddot{u}_j^i$ = vertical displacement (in), velocity (in/sec) and acceleration (in/sec^2) of node j due to wheel i on segment between nodes j and j+1

u_{br}^i, $\dot{u}_{br}^i$, and $\ddot{u}_{br}^i$ = vertical displacement (in), velocity (in/sec) and acceleration (in/sec^2) of the wheel-rail contact point for the i^{th} wheel of the r^{th} vehicle at any time t

F_r^i = load at wheel-rail interface for i^{th} wheel of vehicle r (lb)

Bridge Span:

ρ = mass density of the material of chord (lb/sec^2/in)

w = dead weight of track and deck material per unit length (lb/in)

A_g = gross cross-sectional area of chord (in^2)

I = moment of inertia of chord material (in^4)

E = modulus of elasticity of chord material (lb/in^2)

ξ = damping coefficient of chord as a fraction of the critical damping

ℓ = length of span centre to centre of bents (in)

ℓ_s = length of chord segment (in)

d = distance centre to centre of chords (in)

d_n = distance between right hand chord and right hand rail (in)

d_f = distance between right hand chord and left hand rail (in)

x^i = distance if i^{th} wheel from node j on segment defined by nodes j and j+1 (in)

n = number of active nodes

n_s = number of equal segments in a chord = n+1

$\alpha^i = x^i/\ell_s$, $\beta^i = 1 - x^i/\ell_s = 1 - \alpha^i$

$\gamma = d_n/d$, $\bar{\gamma} = 1 - d_n/d = 1 - \gamma$

$\delta = d_f/d$, $\bar{\delta} = 1 - d_f/d = 1 - \delta$

L_{dc} = computed dynamic load at wheel-rail interface at midpoint of bridge span (lb)

L_{sc} = computed static load at wheel-rail interface at midpoint of bridge span (lb)

DLF_c = computed dynamic load factor of bridge span

D_{dc} = computed dynamic displacement at midpoint of bridge span (in)

D_{sc} = computed static displacement at midpoint of bridge span (in)

DDF_c = dynamic displacement factor of bridge span

Chapter 5

P, P_s = static wheel load (lb)

P_v = dynamic wheel load at speed V (lb)

V = speed of vehicle (mph)

A_w = contact area of wheel with diameter w (in^2)
for w = 33" $A_{33} = 0.190\ in^2$
w = 40" $A_{40} = 0.240\ in^2$

D_w = diameter of wheel (in)

DLF_{AREA}, DLF_{Talbot} = dynamic load factors computed by methods suggested by AREA and Talbot, respectively.

CONVERSION FROM ENGLISH TO SI UNITS

Length, displacement, translation, bounce

1 ft = 0.3048 m	= 304.8 mm	
1 in = 25.40 mm	= 2.54 cm	

Area

1 ft^2 = 0.092903 m^2	= 92903 mm^2
1 in^2 = 645.16 mm^2	= 6.45 cm^2

Volume, Section Modulus

1 ft^3 = 0.028316 m^3	= 28316000 mm^3
1 in^3 = 16387 mm^3	= 16.387 cm^3

Moment of Inertia

1 ft^4 = 0.008631 m^4	= 8631000000 mm^4
1 in^4 = 416231 mm^4	= 41.623 cm^4

Mass

1 lb-sec^2/in	= 0.45359 kg

Weight, Force

1 kip	= 4.44822 kN
1 lb	= 4.44822 N

Force per Unit Length, Spring Stiffness

1 kip/ft	= 14.594 kN/m
1 lb/in	= 0.1751 N/mm

Force per Unit Area, Stress, Modulus of Elasticity, Pressure

1 psf	= 47.880 Pa
1 psi	= 6.89476 kPa = 0.006894 MPa

Moment

1 kip-ft	= 1.35582 kN.m
1 kip-in	= 112.985 N.m

Angular Measure, Roll, Pitch, Yaw

1°(degree)	= 0.0174 rad

Velocity

1 ft/sec	= 0.3048 m/s
1 in/sec	= 25.40 mm/s
1°(degree)/sec	= 0.0174 rad/s

Acceleration

1 ft/sec^2	= 0.3048 m/s^2
1 in/sec^2	= 25.4 mm/s^2
1°(degree)/sec^2	= 0.0174 rad/s^2
1 g	= 9.80664 m/s^2

Frequency

1 cycle/sec	= Hz

Damping Coefficient

1 lb-sec/in	= 0.1751 N.s/mm

Mass Moment of Inertia (in roll, pitch, yaw)

1 lb-in-sec^2	= 0.1129 N.m/s^2 = 0.113 kg.m^2
	= 112.985 N.mm/s^2 = 112985 kg/mm^2

USEFUL DATA

Newton: force that will give 1-kg mass an acceleration of 1 m/s^2 = N

One newton per sq. m (N/m^2) = 1 pascal

Joule: work done by a force of 1 N over a displacement of 1 m = J

One foot-pound (ft-lb) = 1.356 J

Chapter 1

INTRODUCTION

1.1 GENERAL

In the seventies, it was reported [121] that there were approximately 2300 track miles of timber railroad bridges in service in the United States and Canada. Although their number has been dropping since then due to replacements in other materials and branchline abandonments, they still represent a significant portion of the railroad bridge inventory. For short spans, they offer an attractive alternative to other types of bridges as they are economical, faster to construct, and easy to maintain [29, 31, 35, 84]. Current design practices do not allow an independent consideration of the effects of the dynamic loads in sizing of the bridge components, because very little information is available on the subject.

To study the dynamic response, tests were carried out in 1986 on timber bridge spans at two test sites using test trains consisting of a locomotive unit, two loaded hopper cars, and a caboose.

An analytical approach was also introduced to simulate the dynamic response of the bridge spans.

1.2 OBJECTIVES

The main objectives of this work are as follows:

(a) To carry out dynamic field tests on railroad timber bridges including the adjacent bridge approaches and the track sections, under the passage of the test trains at varying speeds. The main objectives of the experimental program are:

(i) to determine the magnitude of the dynamic loads at the wheel-rail interfaces and vertical displacements at different locations and their comparison with those obtained under static conditions.

(ii) to evaluate the dynamic load factors and the dynamic displacement factors based on the measured loads at wheel-rail contact points and the measured vertical displacements. This also includes examination of the influence of speed, static wheel loads and other parameters on these factors.

(iii) to measure accelerations at the mid-points of the bridge spans to determine the damping coefficients of the two deck systems using the logarithmic decrement technique.

(iv) to compare the behaviour of the ballast-deck timber bridge span to the open-deck bridge span and the comparison between the bridge approaches and the track sections at the two test sites.

(b) To develop an analytical model to simulate the dynamic response of the timber bridge spans. Based on the correlation between the measured and the predicted quantities such as loads, displacements and accelerations, the model will be used to define the behaviour of the spans under the railway loading.

(c) To use the analytical model to study the influence of different parameters such as train speed, train consist, static wheel loads and initial conditions of motion on the dynamic factors.

(d) To introduce recommendations for design considerations regarding appropriate dynamic factors for use in the sizing of the timber bridge components, if warranted by the extent of the findings of the study.

1.3 SCOPE

The program of this study consisted of two parts, namely, experimental and theoretical. The experimental work involved field tests at two timber railroad bridge sites using test trains running at speeds varying from 1 mph (i.e., crawl) to 50 mph.

At each site, the bridge spans, the bridge approaches, and the normal track sections were instrumented to measure the loads at wheel-rail interfaces, the vertical displacements and the accelerations. Each test train consisted of a locomotive unit, two open-top hopper cars loaded with ballast, and a caboose.

The theoretical work involved the development of a mathematical model for determining the dynamic response of timber railroad bridge spans. The data on geometrical and material characteristics of test trains and test bridge spans were used in a computer program based on the model to determine the values measured in the field.

The computer program was employed to examine the influence of several parameters such as speed, train consist, deck type, and low bridge approach, on the dynamic response of timber railroad bridge spans.

Chapter 2

LITERATURE REVIEW

2.1 GENERAL

Vibrations of railroad bridges under the effects of trains depend on the characteristics of locomotives and cars in the trains, the characteristics of the bridge components, and the characteristics of the wheel-rail interfaces. The study of the dynamic response of bridges can be traced back to the beginning of the nineteenth century, the time of erection of early railway bridges. Since that time, numerous researchers have worked on and are working on this problem. This chapter summarizes the literature review that pertains primarily to the behaviour and research related to railway bridges. Bibliographies of other published literature related to bridge dynamics may also be found in papers by Huang [51], Fryba [36], Genin, Ginsberg and Ting [42, 106], Ting and Yener [103], Ganga Rao [37, 38], Rao [87], and Gupta [45].

2.2 EXPERIMENTAL WORK

Experimental work in the laboratory as well as in the field also commenced in the middle of the nineteenth century, when a large number of railroad bridges were built. The first known discussion on the dynamic effects of the moving loads over structures was in the 1849 "Report of the Commissioners appointed to inquire into the Application of Iron to Railway Structures" [122].

In 1885, the first dynamic tests were reported by Robinson [90]. His tests involved thirteen railway bridges belonging to four different railroads. He found the blow resulting from the first drop of the heaviest part of a locomotive, followed by repeated impulses, to be the main cause of vibration. He suggested ways to avoid the cumulative effect of vibration and proposed equations for computing the natural and loaded time periods of the railroad bridge.

In Great Britain, the first comprehensive scientific attempt to investigate the problem of impact in railway bridges was conducted by the Bridge Stress Committee [5] under the chairmanship of Sir Alfred Ewing in March of 1923. Their report was published in October of 1928, and contained details of experiments on several steel bridges as well as dealing with analytical work on the subject. Amongst many findings of this investigation, the most important were as follows:

(1) The most important dynamic effects in railway bridges are caused by eccentric forces of the balancing weights of the driving wheels of the locomotive. These forces vary harmonically and are not increased by the train.

(2) The maximum impact occurred when the revolutions per second of the driving wheels coincided closely with the natural rate of vibration of the loaded structure. There is, therefore, a critical speed for every bridge which depends on its flexibility, the dead and live loads, and the diameter of the driving wheels of the locomotive.

(3) In short spans, i.e., less than 40 feet, the frequency of the pulsating force (i.e., hammer blow of driving wheels) is too low for synchronism to occur. The effect of the hammer blow is of the nature of a push, and it can almost be regarded as

a static load. At each blow, the girder deflects an amount proportional to the loads and recovers. There is, practically speaking, no oscillation.

In long spans, 250 ft and greater, at the highest speeds, the frequency of the pulsating load is too high for synchronism to occur. There may be resonance at lower speeds, but the hammer blow is then smaller, for its intensity varies as the square of the speed. At spans between 100 and 200 feet, synchronism will occur at high speeds. Further, in bridges with spans from 130 to 150 feet, not only were large oscillations set up at speeds corresponding with the natural frequency of the loaded bridge, but oscillations of even greater amplitudes occurred at speeds well above the critical speed.

In the United States, the first complete series of tests were reported in 1911 by the Committee on Impact of the American Railway Engineering and Maintenance of Way Association under the direction of Turneaure [110]. The tests were conducted on 21 plate girder spans up to 100 ft in length and on 24 truss spans from 100 to 250 ft in length, employing speeds from 10 mph to 60 mph. These tests provided ample evidence of the effect of synchronous speed and the effect of locomotive counterbalancing. For speeds of less than 15 mph, impact was found to be practically zero. The main causes of impact were unbalanced locomotive drivers, rough and uneven track, flat or irregular wheels, eccentric wheels, rapidity of application of loads, and deflection of beams and stringers.

In addition to the test data, the report contained an interesting discussion on the theory of oscillations and span frequencies. Impact values based on the data presented were used in the design of steel railroad bridges until 1935.

To obtain data on the damping coefficients in bridges, Hunley [52] secured static and dynamic readings on 39 different railroad spans under about 300 different locomotives. The detailed results of tests and the dynamic magnifiers and the damping coefficients obtained under different classes of locomotives are given in his report published by A.R.E.A. in 1935. His work did form the basis for the code used between 1936 and 1948. Thereafter, diesel locomotives were introduced eliminating the hammer blow effect of the steam locomotives and hence a need for two impact factors -- one for diesel locomotives and the other for steam locomotives.

Earlier measurements were done by means of mechanical or optical instruments which were cumbersome, and simultaneous readings at different points were difficult to obtain. This problem was eliminated with the introduction of electronic equipment and electrical resistance gauges in the nineteen-thirties. Until that time, most of the tests were on steel railway bridges. Later, with the development of the highway networks, interest in experiments on highway bridges grew rapidly. Since then, many other papers [9, 15, 32, 46, 50, 68, 80, 109, 123] have appeared which discuss dynamic tests on railway and highway bridges. These tests were carried out in the laboratory or in the field, and were mainly on steel or concrete structures.

In the late nineteen-forties, the Association of American Railroads [99, 100], at the request of the A.R.E.A. Committee, conducted exploratory tests on timber railway bridge approaches for the first time as a part of their extensive tests on steel bridges. The objective of the tests was to determine the relationship between the railway loads and stresses in timber trestles. The tests at each site comprised measurements of strain gauges installed at the top and bottom of stringers at the centre, and the top of stringers at one end of a span, as well as on the individual piles of a bent under a test train operating at speeds of 5 to 50 mph.

For the tests on two open deck spans, the results were as follows:

(a) The recorded static stresses in stringers at the centre of the span were lower than those calculated for a simple span, but greater than those calculated on the assumption that stringers were fully continuous.

(b) In one case, there was a fair agreement between the compressive and tensile stresses, whereas in the others, the compressive stresses were higher than the tensile stresses.

(c) There was a considerable variation in stresses in several stringers and timber under the rail carrying most of the load, and

(d) There was considerable variation in the magnitude of the total impact. Percentages of impact for the stringer chord determined by the increase in the stress over the static stress occurring at slow speed were between 57% to 35%.

Tests by the A.A.R. on a ballast deck consisting of longitudinal members only (without transverse floor planks) also indicated the same results mentioned in (a) and (c) above. However, the maximum average value of stresses due to total impact recorded was as high as 70.6% greater than the static stress.

Later, Leggett [65] reported the American Association of Railroads tests carried out under the sponsorship of the A.R.E.A. Committee 7--Wood Bridges and Trestles. These tests comprised the following:

(a) Fatigue bending tests on full-size stringers and standard block shear tests on small clear specimens, at Purdue University Engineering Experiment Station, and

(b) Standard bending tests on small clear specimens at the U.S. Forest Products Laboratory, Madison, Wisconsin.

The program involved two species of wood, namely, Douglas Fir and Southern Pine. In total, twelve timber stringers 8" x 16" x 14'-6" (6 of each species) in unseasoned condition were subjected to fatigue bending tests using the Krouse-Purdue fatigue machine, which was hydraulically activated and electronically controlled. Constant repeated loads were transmitted at one-third points of a 13' simple span, and the observations obtained from data procured on such timber under repeated loading were as follows:

(a) When the span-depth ratio is ten or less, failure can be expected in longitudinal shear rather than in bending.

(b) Tests were too few to permit the establishment of S-N curves.

(c) Failure in horizontal shear was sudden, and occurred at locations near the centroidal axis where the checks were usually the deepest.

(d) The number of checks increased from drying during the tests.

(e) After an initial sudden failure in horizontal shear, the deflection was approximately doubled while the original load on the specimen was maintained.

(f) Shear failure generally originated at the end of the span.

The above tests were the first, a survey was conducted which indicated no previous record of any repeated stress experiments on timber of the size commonly used in railway trestles and similar structures. Further tests were carried out on the railroad timber trestles during the fifties by the A.A.R. at the request of the A.R.E.A. These have been reported by Ruble [91] and Drew [27]. The main objectives of the tests were to study the effect of the duration of stress on impact, and the cumulative effect of the repetitive train loading on the fatigue strength of the trestles. Ruble stated that the present design of timber railroad structures is based on static loads only and that the dynamic or impact effects should be considered if the design of timber trestles is to be based on science. He also commented that timber has twice the strength under suddenly applied loads as it has under the same load applied statically. Further, the stress under a suddenly applied load goes from zero to a maximum in about $^1/_{100}$ of a second, while under a high speed locomotive it takes about $^3/_{100}$ of a second for a stress to reach a maximum, or about 30 times longer.

Drew's [27] conclusions were as follows:

(a) The maximum live load stresses in trestle stringers can reasonably be expected to accumulate to less than one year during their service lives rather than ten years, as currently assumed in design.

(b) The railroad loading need not be considered "long-time loading". At least a 10 percent increase in design stresses should be permitted, but such an increase should apply only to fiber stresses unless seasoning checks can be controlled.

(c) Fatigue tests indicate that failure in horizontal shear can be expected during the service life of a stringer with longitudinal checks.

A summary of additional tests on timber trestles have been reported by Magee [72]. Some of his conclusions were, "(1) Static and dynamic stresses and fatigue strength of timber trestles are known from extensive research; (2) Better inspection devices for detecting internal defects in timber are needed; and (3) Research has not yet developed a satisfactory fire-retardant treatment for timber trestles." Byer [13, 14] used the data obtained from a number of different test programs on steel spans which varied in design characteristics and distributions of span lengths and test speeds, and found that the test results do indicate that under a given set of conditions, the distribution of impact magnitudes can be approximated by a normal distribution and that when the conditions are changed, impact tends to increase with increase in speed and decrease with increase in span length.

2.3 THEORETICAL WORK

One of the first persons to work on an analytical approach to the problem of bridge vibrations was Willis [122] who, in 1849 derived the differential equation for the deflection under a moving mass load for a beam of negligible mass, and gave an approximate solution. An exact solution of the equation which he formulated was obtained by Stokes [97] in 1883 by means of power series. The equation as derived is of some use in the case of railway loads because of the high ratio of the loads to the weight of the bridge. The other significant contribution to the problem was made by Krylov [63] in 1905, when he obtained a solution for the case of the mass of the load being negligible compared to the mass of the bridge. This is equivalent to a constant force moving across the span. Timoshenko [102, 105] in 1922 pointed out three major causes of vibrations in railroad bridges: The live load effect of a smoothly rolling load, the impact effect of the balance weights of the locomotive driving wheels, and the impact effect due to irregularities of the track and the flat spots in the wheels. He examined two possible extreme cases of the live load effect: the mass of the moving load is either large or small in comparison to the mass of the beam. Timoshenko is also credited with the solution to the problem of the effects of a harmonic force moving over a beam at a constant speed, an idealization of the effect of counterweights on the locomotive driving wheels. From his analyses, which were based on energy methods, he concluded that the live load effect of a smoothly running load was always small, not exceeding 10% and therefore could be neglected. The impact of the balance weights of locomotive driving wheels became of practical importance, especially under conditions involving resonance. The most unfavorable condition was where resonance could occur. For a short span bridge, this was not likely, because of so high a natural frequency. The additional dynamic effect due to irregularities in the track and flats on the wheels was of importance only for bridge parts directly subjected to the action of moving loads and high speed in short spans.

Krylov and Timoshenko included the effect of beam mass in the Willis equation, and solved by using series expansion techniques. In their work, they neglected the transverse inertia of the moving mass particle. Based on the work of Krylov and Timoshenko, an enormous number of approximate solutions to boundary value problems with different types of loading conditions and boundary conditions were reported in the literature. Lowan [69, 71] in 1935 and Bondar [12] solved the case of moving variable loads with the aid of Green's function. Lowan's general equation for displacement of a simple beam is equally applicable to the case of stationary loads of constant or fluctuating magnitude, and any system of concentrated or continuously distributed loads which traverse the beam with velocities which are prescribed functions of time.

The problem involving both the load mass and the beam mass, being somewhat more complicated, was first examined by Saller [92] in 1921 and then Jeffcott [55] in 1929, who considered cases involving massless, light to massive uniform beam simply supported and an unsprung or a sprung mass under the action of constant or fluctuating force moving uniformly along the span, and also including damping. The particular integral of the basic equation of motion he used was evaluated by a method of successive approximation. The iterative approach used for solution became divergent in some cases. Different techniques for solution of the equations were employed by Fryba [36], Wen [118], and Bolotin [11]. Fryba solved many cases of loadings using the method of integral transformation. Wen analyzed the response of beams traversed by two-axle loads on the assumption that the dynamic deflection was proportional to the static deflection due to the weight of the beam and the loads and using the numerical solution by Newmark. Bolotin used the approximate method asymptotic solutions in quadrature.

Inglis [53] in 1934 used harmonic analysis to solve several practically important cases of dynamics of railway bridges traversed by steam locomotives, i.e., motion of a concentrated force, sprung and unsprung masses, and harmonic forces acting on a beam, etc., including the influence of damping. The process of harmonic analysis which he used is based on the assumption that any distribution of live load, concentrated or distributed, can, for the purposes of calculating deflections, be replaced by a harmonic series of sinusoidal distributions of load which, for a simply supported beam, gives rise to a similar sinusoidal distribution of deflection. His results were in excellent agreement with the experimental findings of the Bridge Stress Committee [5], and were later compared by Chilver [17] with those arrived at by Mise and Kunii [77]. The difference of analysis between Inglis and Mise and Kunii is in the solution of the differential equation which in the latter case also gives approximate solution with the aid of elliptical functions, which is a mathematically more precise treatment of the problems studied by Inglis. Inglis stated that, in short span bridges, the damping was large and the maximum dynamic effects due to hammer blows could be estimated by treating the hammer blows as static forces superimposed upon the corresponding axle loads, the hammer blow being computed for the highest speed permissible.

Inglis established that the oscillations of a railway bridge are dominated almost entirely by the "hammer-blow" effect of a steam locomotive; he found that for loads of constant magnitude, moving at typical speeds, the dynamic deflections of a railway bridge due to oscillation are not large; for uniformly distributed advancing load, the deflection is almost free of oscillation and may be taken as the "static crawl deflection." These conclusions indicate that a more critical condition may arise when a single concentrated mass traverses a bridge; a theoretical analysis to be of practical value should take account of the "hammer-blow" effects of the locomotive and damping effects in the bridge.

Schallenkamp [93] in 1937 presented a rigorous solution for the case of a smoothly rolling load which considered both the mass of the load and the mass of the bridge. He introduced a method of using Fourier series with unknown coefficients. Although his solution does include most of the important variables involved, it is not in a form convenient for computation.

Up to that time, the vehicle had been idealized by a single mass point. However, in the early 1950's, idealization of the vehicle as a sprung and unsprung mass was attempted. Hillerborg [50] was first to obtain the solution of the motion of sprung masses on a beam by means of Fourier's method, and the method of numerical differences. Further advances were made possible by the arrival of digital computers. The formulation involving both the sprung and unsprung masses was solved by Looney [67] and Biggs et al. [10] using the Inglis method. The basic assumptions made in the numerical procedures presented by both are that the bridge is a simple beam, of which only the first or fundamental mode of vibration is considered, and that the deflected shape of the bridge can be approximated by a half sine wave. The methods used are essentially the same, i.e., the differential equations are written for the fundamental mode of the bridge and solved numerically, except that Looney assumes a smoothly rolling load, whereas Biggs et al. include the effect of the vehicle springing. Tung et al. [109] used Hillerborg's method.

Ting et al. [106] illustrated the kinematical relationship involved, considering the interaction of a moving vehicle and bridge where the system was modelled as a Bernoulli-Euler beam carrying a single mass particle. The differential equation governing the transverse displacement of the beam took the form

$$EI\frac{\partial^4 u}{\partial x^4} + m\frac{\partial^2 u}{\partial t^2} = F\ (x,t) \tag{2.1}$$

where EI is the bending rigidity of the beam, m the mass per unit length of the beam, and u(x,t) is the transverse displacement of a point on the beam at position x and time t. F(x,t) is the reaction force exerted by the mass particle on the beam. When the mass is at position $\eta(t)$, the forcing function F(x,t) can be related to the transverse acceleration of the particle by Newton's second law, yielding

$$F = -M\ [g + \frac{d^2u}{dt^2}\ (\eta,t) \bullet \delta(x-\eta)] \tag{2.2}$$

where Mg represents the weight of the particle and $\delta(x)$ is the Dirac Delta function. Since the particle position η is a time-dependent function, the explicit form of the transverse acceleration can be shown to be

$$\frac{d^2u}{dt^2} = \frac{\partial^2 u}{\partial t^2} + 2\left(\frac{d\eta}{dt}\right)\frac{\partial^2 u}{\partial x \partial t} + \left(\frac{d\eta}{dt}\right)^2\frac{\partial^2 u}{\partial x^2} + \left(\frac{d^2\eta}{dt^2}\right)\frac{\partial u}{\partial u} \quad (2.3)$$

The mathematical difficulty of the solution lies in handling the delta function and the mixed derivative on the right-hand-side of the last equation. Therefore, the methods of solution found in the earlier works were based on the use of simplifying assumptions which did not fully treat the kinematically coupled terms and thus were restricted to simple boundary conditions for which a closed form solution could be obtained.

To fully treat the basic kinematical characteristics, the analysis becomes considerably involved. Its mathematical complexity has been demonstrated by Stanisic et al. [95], as they concluded that the exact analytical solution is beyond hope. Most of the existing analytical solutions which include the beam-mass interaction were obtained by series expansion methods or modal expansion techniques where the numerical data are computed using series truncation procedures and usually an iterative process is necessary for including the coupling terms. Ting et al. [106] have discussed the modal expansion technique and the integral formulation. They stated that the equations of motion obtained by the modal expansion technique could be solved by the method of the moving force approximation, the successive iteration or the direct finite differences depending on the magnitude of a certain quantity. Similarly, the equations of motion obtained by the integral formulation which is based on Green's function are discretized and could be solved by various numerical schemes.

The use of high speed computers has allowed significant progress in research into dynamic response of both railway and highway bridges. The vehicles as well as the bridge components have been idealized as multi-degree-of-freedom systems. The vehicle has been idealized as a single axle or multiple axle system with linear or non-linear springs and viscous or Coulomb friction dash pots. Differing degrees of sophistication in idealizations are discussed by Huang [51] and Genin et al. [42]. Similarly, the single-span bridge has been idealized as a "one-dimensional bridge", where the effect of width-wise flexibility is insignificant, or as a "two-dimensional bridge", where the effect of width-wise flexibility is significant. In the case of sprung vehicles crossing a bridge, discrete beam systems have been used. The discretizations have included lumped masses [8, 18-22], rigid bar replacements [32] and eigen-function expansions [109, 118]. For two-dimensional bridges, the discretizations have been achieved by the finite element method, by eigen-function expansion [77A], and by finite differences. The two-dimensional model is used for simple-span and continuous bridges.

The equations of motion have been derived using d'Alemberts' principle or Lagrangean energy equations.

The equations of motion of the system, regardless of the degrees of freedom, can be written as

$$[M]\{\ddot{D}\} + [C]\{\dot{D}\} + [K]\{D\} = [A]\{P\} \tag{2.4}$$

in which $\{\ddot{D}\}$, $\{\dot{D}\}$ and $\{D\}$ are, respectively, the generalized accelerations, velocities, and displacements, [M] is the mass matrix, [K] is the stiffness matrix; [C] represents the viscous damping matrix; and [A] defines the influence coefficients for interacting forces P_i. The matrix [A] is determined by the location of the vehicle on bridge, and thus depends on time and the velocity of the vehicle. The forces P_i depend on the generalized coordinates of the vehicle-bridge system and their time derivatives:

$$P_i = P_i(\dot{u}, \dot{z}, u, z, t) \tag{2.5}$$

where u and z are the generalized displacements of bridge and of vehicle, respectively, and $\dot{u}$ and $\dot{z}$ are their first derivatives.

It is usually assumed that a vehicle maintains a constant speed, or some assigned variations, as it crosses a bridge. This assumption about the vehicle-bridge system implies that some non-conservative energy from the vehicle engine must be supplied. Initial conditions of motion of both vehicle and bridge are usually specified when a vehicle enters a bridge.

Chu et al. [18, 19, 20, 21] in 1978 presented a more exact analysis of the dynamic response of a steel girder and a steel truss span under the passage of one or a series of railway vehicles. He found that the impact factor with two vehicles was lower than that for a single vehicle due to axle spacing. The 2% bridge structural damping assumed reduced the impact factor only slightly. For the girder span, the maximum computed impact factor was lower than that given in the A.R.E.A. design specifications. The measured values were also lower than the maximum moment and shears in girders and axial forces in most of the members in trusses.

Wiriyachai et al. [124] used the deterministic approach to calculate the maximum impact effects of flat wheels, bridge pier settlement, camber errors, and various track irregularities on a steel truss span bridge investigated by Chu et al. They used simulation to general rail profiles associated with various track irregularities.

He found the two most important sources of impact to be: (1) initial vehicle deflection and roll; and (2) track roughness. For selected members subjected to 70 ton cars travelling at 50 mph, the 0.25 in initial deflection and 0.02 radian initial roll of cars developed more than 40% of total impact, and specified track roughness caused 40% or less impact. A smooth running train developed 3.3-11.4% of the impact, and the remaining impact was caused by flat wheels, pier settlement, and camber errors. The fast Fourier transform was applied to these profiles resulting in spectra that were the same as those given in other findings by Garivaltis and Garg [41]. Chu, Garg and Bhatti [18] developed a multi-degree-of-freedom model for a freight car to account for all the significant geometric and suspension non-linearities and studied the behaviour over the truss span bridge used in their earlier studies.

The findings of this study were that (1) greater approach irregularities produce higher impact factors and dynamic forces in bridge members; (2) impact factors in members with low static stress are high, but dynamic stress produced are low; (3) impact factors reduce slightly due to bridge damping; and (4) the dynamic forces in the lower lateral bracing members are low as compared to their allowable values.

Gesund and Young [39], Florance [34], Knowles [61], Kessel and Schlack [60] investigated the dynamic response of beams under different loading conditions. Steele [96] worked out the analytical dynamic response of a simply supported Euler-Bernoulli beam with or without elastic foundation by method of images. His solution converged rapidly for a simply supported, long beam with a high velocity, moving concentrated load. The Fourier integrals were evaluated in closed form for the beam with elastic foundation. In particular, the asymptotic results a solution for the "critical" load velocity, for which a "steady state" solution does not exist and for the limiting case of infinite load velocity, for which the beam is given an initial uniform velocity. Tung [108] studied response of highway bridges on a probabilistic basis. His solution gave response quantities such as the probability distribution foundation and the expected rate of threshold crossings of the response. His results showed that for all practical purposes, the first few terms gave reasonably good results. Higher accuracy could be achieved by simply taking more terms in the expansion. Meacham and Ahlbeck [74] examined the dynamic loads caused by wheel-rail interaction, rail joints, car rocking and corrugated rails. They concluded that from the computer analyses of the dynamic loads and the manner in which various parameters of vehicle and track structure affected these loads, it was possible to decide more intelligently how to alleviate the high wheel-rail stresses caused by today's unique traffic and track conditions through better track maintenance and changes in stiffness and damping trucks and track structure itself. Dhar [40] proposed a method of analysis of the dynamic response of a girder and a truss span under railroad vehicles. He found that in order to get the maximum impact, the train should occupy almost the whole span. Matsuura [73] investigated the dynamic behaviour of bridge girders in high speed railway. He concluded that the effect of periodic axle arrangement of a long train was a predominant factor for producing a resonant condition in a railway bridge girder at high speeds. This condition depended on the input amplitude of the train and the damping factor of the girder. He also suggested a lower limit of the bending rigidity of the girder in terms of the natural frequency. Bhatti [8] used the analysis approach similar to Dhar , but included the vehicle-track-bridge interaction in both vertical and horizontal directions. Palamas [81] et al. used a simple degree-of-freedom oscillator as the vehicle dynamics model and analyzed the system using a Rayleigh-Ritz method. He found that the effect of the local surface irregularities on the dynamic amplification factor (DAF) in terms of deflections was two to three times greater than those given in the international design codes. He commented that his model was an extreme idealization of a real vehicle and so the best values of DAF should be between his results and those given in the design codes.

Other studies mainly on the steel and concrete highway bridges involve cantilever bridges by Veletsos and Huang [112], plate simply supported by Yoshida and Weaver [111], or continuous over flexible beams by Ng and Kulkarni [77A], or multispan bridges as by Fleming and Romualdi [32] and Louw [68]. Other researchers who carried out work on highway bridges are Garg [40], Cantiani [15], Gupta [45], Osogoly and Agarwal [80], Wilson [123] and more recently, Hathout [46].

Considerable analytical work has been carried out on the study of vehicle-guideway dynamics by investigators such as Chiu et al. [17A], Wormley et al. [125], Richardson and Wormley [89], Kaplan et al. [57] and Minnetyn et al. [76].

The studies carried out on wheel-rail interaction are covered by Radford [86], Hedrick [48], and Hedrick et al. [49], and on the performance of the railway track and road surface are covered by El-Aini [28], Raymond et al. [88], Corbin and Kangman [24], Fazio and Corbin [30], Koof and Tyworth [62], Grassie and Cox [44] and Al-Rashid [3]. The discussion of the above studies is beyond the scope of this review.

To the author's knowledge, predictions of the dynamic response of a timber railroad bridge span has never been attempted before. The algorithm used in the analytical model for this dissertation will follow the one employed by Chu et al.

2.4 NECESSITY OF THE RESEARCH PROGRAM

The A.R.E.A. Manual [4] states, "the dynamic increment of load due to the effect of speed, roll, and track irregularities is not well established for timber structures. The total effect of the aforementioned factors is estimated to be less than the increase in strength which timber exhibits for short cumulative duration of loading to which railroad bridges are subjected in service, and is taken into consideration in the derivation of allowable working stresses for design ... The live load per track consists of Cooper loading, which produces a loading effect equivalent to that caused by the heaviest engine or train load expected to be moved over the completed structure during its expected life."

The current design is based on static loads only, and in comparison to the design of steel and concrete bridges, it does not consider any impact of the loads. Therefore, in order to bring the design of timber bridges up to the same scientific base as the other materials and in order to make the design more meaningful in terms of the distribution of stresses due to different types of loads, it is necessary that appropriate dynamic increments (i.e., dynamic load factors and dynamic displacement factors, etc.) be considered in sizing their components as well.

From the foregoing literature review, it is quite apparent that there is not sufficient experimental information available, nor is there any theoretical work undertaken so far on the subject of the dynamic response of timber railroad bridges.

The work presented in this dissertation is an attempt to determine both experimentally and theoretically the dynamic response including the load factors and the displacement factors for timber railroad bridge spans and to study the influence of various parameters on such behaviour.

Chapter 3

EXPERIMENTAL PROGRAM

3.1 GENERAL

Railroad timber bridges [4] consist of relatively short spans, i.e., usually ranging from 10 to 15 feet in length, which are supported on timber bents. The bents may either be made up of caps and piles braced together as in "pile-bents" or be made up of caps, posts and sills braced together as in "frame-bents" and supported on wood blockings, concrete footings or on round timber piles. The longitudinal members that span between the bents are "stringers" and a bunch of stringers under each rail of track is a "chord".

In a ballast-deck span, the stringers are floored with wooden planks. The rails are fastened to track ties which are partially embedded in a layer of ballast placed between the ties and the planks.

In an open-deck span, the rails are fastened to bridge ties which rest directly on and alternately fastened to the stringers by means of lining spikes.

Both types of spans constitute a system of interconnected components such that the stresses induced by loads applied at the wheel-rail interfaces redistribute with a time lag from the rails to the stringers.

The locomotives and the cars of the trains consist of two dual-axle trucks each. The spacing between the axles of the trucks is such that at instances only a single axle occupies the short spans of the bridge.

The test program in this investigation was designed to measure the loads at the wheel-rail interfaces and the vertical displacements under each rail at the bridge approaches, at the normal track sections, and at the mid-span of the stringers of the bridges. The accelerations were measured only at the mid-points of the spans.

The measurements taken at different locations on the rails in the field revealed the presence of small track surface and gauge irregularities. Though no measurements were taken on any of the wheels itself, some irregularities could be expected in the wheel running surfaces as well. Since these irregularities were considered to be small, it is assumed that these would not influence the results significantly.

3.2 SELECTION OF TEST SITES

One of the early efforts in this experimental program was to select two adequate test sites, one with a ballast-deck bridge and another with an open-deck bridge which were close to each other, accessible by road, and a single-storey height for ease of instrumentation. The sites chosen were approximately 25 miles northwest of Winnipeg near Grosse Isle, Manitoba, at Miles 16.50 and 19.50, respectively of the Canadian National Railway's branchline, named the Oak Point Subdivision.

3.2.1 Bridges

3.2.1.1 The Ballast-Deck Bridge. The ballast-deck bridge, Figure 3.1, was a slough crossing located at Mile 16.50 Oak Point Subdivision, consisting of a four-span ballast-deck pile trestle with an overall length of 45'10" and a height of 9'-4". It was built in 1943 using treated Douglas Fir material. Its deck was made up of 10" x 4" x 13'-6" transverse planks nailed onto ten 8" x 16" spaced stringers (including two jack stringers) possessing an average span length of 11'-2½". The majority of the stringers were two spans long and alternately continuous over intermediate bents. The bents consisted of a 12" x 14" by 14'-0" long cap resting over five piles each, driven with a penetration varying from 16' to 24'.

3.2.1.2 **<u>The Open-Deck Bridge</u>**. The open-deck bridge, Figure 3.2, was a slough crossing at Mile 19.50 Oak Point Subdivision, consisting of a three span, open-deck pile trestle with an overall length of 36'-5½" and a height of 5'-4". It was built in 1945/46 using treated Douglas Fir material. Its deck was made up of thirty-six, 8" x 8" by 12'-0" long bridge ties spaced at 12" centres which were renewed in 1975. The ties rested on eight 8" x 16" chorded stringers possessing an average span length of 11'-6¼". The majority of the stringers were two spans long, and alternately continuous over intermediate bents. The bents consisted of a 12" x 14" by 14'-0" long caps supported over five piles each, driven with a penetration of approximately 23'.

The elevation and typical cross-sections of the ballast-deck and the open-deck bridges are shown in Figures 3.1 and 3.2, respectively.

Despite their ages, the bridges did not show any signs of deterioration, which could have affected their original capacity. However, prior to the tests loose members were shimmed and all fasteners were tightened to ensure adequate performance of all components.

3.2.2 Bridge Approaches

The section of the track situated immediately behind (within 15 ft. length) the dumpwalls which provided a transition between the track and the bridge is referred to here as a "bridge approach", or simply an "approach". The approach sections at both sites were in good condition, and possessed a full section of gravel and pit-run material. The approach to the open-deck bridge possessed the transition track ties.

3.2.3 Track Sections

A section of the track beyond a bridge approach (approximately 50 ft. from the dumpwall and beyond) is referred to here as a "track section".

The alignment of the track sections at both test sites was tangent. The grade at the ballast-deck bridge was level, whereas at the open-deck bridge it was 0.02% rising north.

The track consisted of 85-lb. (sec. 137 Algoma Canada MRC 85 lb HF-1944) jointed rails in lengths of 36' to 39' and 7½" x 11" double-shouldered tie plates spiked to 8" x 6" by 8'-0" long no. 2 ties spaced at approximately 22" centres and embedded in a ballast section of gravel and pit run material. On the ballast-deck bridge, the ballast section consisted of about 12" deep crushed limestone material.

The zone speed over the stretch of track covered by these tests was 30 mph with a maximum weight limit of 220,000 lbs. for a 4-axle car. Therefore, to accommodate speeds of up to 50 mph for the tests, the track was upgraded. Upgrading included spot surfacing and track lining.

3.3 TEST TRAINS

The trains used for the tests were similar to the trains normally operated on this line for hauling limestone from Steep Rock, Manitoba. Since the trains were required at two different times, they differed in cars and their weights. However, both trains were made up of a GR-20 Series 4-axle type diesel locomotive, two ballast-loaded open top hopper cars and a caboose. The open-top hopper cars possessed transverse beams at their mid-length just below their bodies which facilitated jacking of the cars for static (i.e., cars in stationery position) tests.

The test trains were scale weighed by their trucks (2 axle assembly) at the local tower scale in CN's Symington Yard before leaving for the test sites.

Figure 3.3 show the typical arrangement, dimensions, and weights of the locomotives and cars of the two test trains. Table 3.1 gives the scale weights of locomotives and cars for the test trains nos. 1 and 2. The photograph of the typical test train used in this investigation is shown in Figure 3.4.

3.4 INSTRUMENTATION

The bridges, their approaches, and the normal track sections were instrumented to measure the loads at wheel-rail interfaces, the vertical displacements under the rail points, and the accelerations at mid-points of bridge spans, under the test trains moving at different speeds.

Figures 3.5 and 3.6 show the locations of the shear-load circuits used to measure the loads at the wheel-rail interfaces, accelerometers, and the LVDT's for the vertical displacements at the two bridges.

3.4.1 Loads at Wheel-Rail Interfaces

There are several methods available for measuring the loads at wheel-rail interfaces. However, the method used here is based on instrumented rails which employ the vertical load measurement circuit adapted from strain gauge pattern reported by ORE [1, 2, 75].

As shown in Figure 3.7, eight gauges were installed at each measurement point, i.e., four on either side of the rail neutral axis. This pattern, often called a shear-load circuit, measured the net shear differential between the two gauged regions, a-b and c-d, with the gauge pattern placed between the rail support points (i.e., the spaces between the bridge ties or the track ties, as the case may be), and the circuit output is directly proportional to the vertical load P as it passes between the gauges.

The influence zone of the pattern is very short, i.e., a few inches either side of the mid-point between a-b and c-d, so that only a sample of short duration is provided from each passing wheel. The pattern has been found to exhibit excellent linearity and minimal sensitivity to lateral load (cross talk) or to the lateral position of the vertical load [2]. This arrangement of the strain gauges (pattern) was tested in the Structural Laboratory of the University of Manitoba, prior to its installation in the field.

The shear circuits were temperature compensated using dummy gauges which were located near the active gauges. Initial readings were also taken for each loading case prior to using the same set-up for recording the measurements, which were recorded within a maximum duration of time of seventy-five seconds for the test train at crawl speed.

The electrical gauges used for the tests were Constantan Strain gauges of type #CEA-06-250UW-350 with fully encapsulated grid and exposed copper-coated integral solder tabs.

The web areas of the rails were ground and polished and the strain gauges were installed in accordance with M-M Instruction Bulletin #B-127-9 "Strain Gage Installations with M-Bond 200 Adhesive" dated 1979.

There were six shear circuits installed for each bridge, as shown in Figure 3.5 for the ballast deck, and Figure 3.6 for the open-deck bridge.

3.4.2 Vertical Displacements

The vertical displacements were measured at the same points as where the wheel-rail contact loads were measured. The linear variable differential transducers (LVDT) were installed either under the chord of stringers or under the rail bases, i.e., locations span S3, approach A and track T for the ballast deck bridge site as given in Figure 3.5 and span S2, approach A and track T for the open deck bridge span as given in Figure 3.6. For the BDB site, an additional set of displacement gauges was provided under the chords of span S2.

The LVDT's used were Hewlett Packard 7 DCDT Series displacement transducers. The ranges of the LVDT's varied between 1/4"± and 1"± with accuracies varying between ±.001" and ±.005".

The core of the LVDT's was connected to the moving member, and the coil was mounted to a mechanical reference point in a HP 14072A Mounting Block. This mounting set-up had provision for adjusting both the radial and axial alignment between the coil and the core. The mounting blocks were non-magnetic, using aluminum or 303 stainless steel materials.

3.4.2.1 Support System for Displacement Gauges (LVDT).

Four-inch diameter PVC pipes were pushed into the augered holes located about 8'-6" from the centreline of the track below the measurement points. A two-inch diameter steel pipe was inserted into each of the PVC pipes and driven into the ground. The annular spaces between the pipes were kept hollow except at the top, where they were filled with poly-foam rings and then covered with plastic wrappings. This type of support system was used to prevent vibrations produced by train dynamics in the ground from affecting the LVDT readings.

Details of a typical example of the support systems is given in Figures 3.8 and 3.9.

There were four such supports installed for the ballast-deck bridge at T, A, S2 and S3 as shown in Figure 3.5 and three for the open-deck bridge at T, A, and S2 as shown in Figure 3.6. Readings were taken with a laser instrument of the elevations at the top of the supports with respect to previously established bench marks on shore, under no traffic, as well as under traffic conditions on the bridges. No measurable vibrations were found to have developed in the support systems at both bridges. It was therefore assumed that the support systems were firm and stable for the intended test purposes.

3.4.3 Accelerations

Vibrations due to accelerations were measured using two Bruel and Kjaer 4366 type accelerometers which were mounted to the underside of stringer chords with Thermogrip hot melt glue using a Bostik 260 Type Electric gun. These locations are shown in Figure 3.5 as locations #S3, positions #7 and 8 for the ballast-deck bridge and as locations #S2, positions #7 and 8 in Figure 3.6 for the open-deck bridge.

The accelerometers were connected to a pair of Bruel and Kjaer 2626 Conditioning Amplifiers which in turn were also connected to the Data Acquisition System. A tee electronic connector was used to allow the incoming data to be monitored also by a Hewlett Packard HP 3582A Spectrum Analyzer during the test.

3.4.4 Data Acquisition System

A 16-Channel Techmar Lab Master data acquisition system (D.A.S.) was employed for recording loads, displacements and accelerations as measured from moving test trains. This unit possessed a conversion rate of 40 kHz, resolution of 12 bits and user selectable 16 single-ended or 8 true differential analog inputs (ranges +5 mv, +10v) and a programmable gain capability.

A Lab Master card hooked to an IBM-PC was used to convert the analog data into digital data and store it on floppy diskettes.

The rate of acquisition available was 1600 readings per second, or 100 readings per second for each of the sixteen channels. The above D.A.S. was supplemented by:

(a) Nicolet Explorer Digital Oscilloscope: Model 204 Digitizing Rate 20 MHZ. This unit had 2 channels and was used for selective viewing plots and storing information on wheel-rail interface loads and vertical displacements during the tests.

(b) Hewlett Packard Spectrum Analyzer: Model #HP 3582A, Rate 25 KHZ equipped with an X-Y Plotter. This unit had two channels and was tee-connected to the main circuitry for viewing the accelerations during the tests.

An outline of the circuitry of the above set-up is shown in a block diagram in Figure 3.10. The sensitivities of the measuring devices are given on pages A2-1 to 3 as well as in Uppal [111a]. This arrangement allowed simultaneous measurement on 16 channels, plus instant viewing of data on another 4 channels. In addition to the above, an IBM-PC complete with printer and plotter was also available at the sites to obtain hard copies of the data and various plots immediately after each test run.

The D.A.S. and other pieces of equipment were housed in a 40' long air-conditioned truck-trailer unit which had its own 5 kWH regulated power supply. The layout of the equipment inside the trailer and the trailer is shown in Figures 3.11 and 3.12.

During the tests, the truck-trailer unit was parked on the shoulder of Highway #6, some 50-60 feet from the test sites. The shielded cables and their connections were kept dry. Also to prevent problems with long cables, after the calibration tests, the cables were left undisturbed until all tests were completed.

3.5 TESTS

Tests were carried out in the field on two different days. Test series 1, comprising static and dynamic tests of the ballast-deck bridge, was conducted on July 11, 1986. The dynamic tests included runs of a full test train followed by runs of the locomotive alone at different speeds. Test series 2 were conducted on September 16, 1986, and consisted of similar tests of the open-deck bridge, and a repeat of the dynamic tests of the ballast-deck bridge. A detailed schedule of each test series is given in Uppal [111a].

3.5.1 Calibration Tests

The purpose of these tests was two-fold: firstly, to calibrate the system for dynamic tests, and secondly, to determine the stiffnesses of the bridge spans, the bridge approaches, and the normal track sections.

For the ballast-deck bridge, the middle of one of the hopper cars (i.e., #CN 090151) was centered over the load measurement locations one at a time, i.e., span S3, approach A and track T in Figure 3.5. A load cell, a jack and a segmental railway car wheel were installed between the transverse beam of the car body and the rail at each of the two rail points, as shown in Figure 3.13. The segmental wheels were used over the rails to simulate the actual wheel-rail contact conditions for the static situations.

The description of the load cells, jacks and jacking pumps used were as follows:

(a) Load Cells: (two types were used)

(i) Baldwin HBM Load Cell, 200 kips capacity, 4" deep, and

(ii) STRAINSET Compression Flat Load Cell Model F1, 100 kips capacity, 3½" deep. Both load cells were calibrated in the Structural Lab of the University of Manitoba on July 9, 1986.

(b) Jacks: Two 100 kips Enerpac Jacks Model #RLC 100 with 2 1/4" stroke, collapsed height of 5 9/16", and extended height of 7 13/16".

(c) Pump: Enerpac Type hand pump Model #P-85, pressure rating 0 to 10,000 psi and piston stroke of 1".

The pressure gauges were also calibrated (i.e., gauge reading in psi vs. machine load in kips) in the Structural Laboratory of the University of Manitoba on July 9, 1986. The test setup for the jacking operation are shown in Figure 3.14.

Once the car was centered over each shear circuit location, the jack was located between the transverse beam of the hopper car and the rails, the load was applied by means of the Enerpac hand pump. The deflection of the rails induced voltages in shear-load circuits, which were used to calibrate the system. The applied load per rail was raised to a maximum of 20 kips and then lowered to zero. The load per rail was also applied gradually at each LVDT location to determine the load-deflection relationship of the system. After carrying out the test at each bridge span, the procedure was repeated at the approach and track locations.

At the open-deck bridge location, the arrangement of the calibration tests was identical to the ballast-deck, except for the following:

(i) the car used for the calibration tests was CN #090159; and

(ii) the maximum jacking load applied per rail was raised to 30 kips. This was done to correspond to the magnitude of the maximum wheel load of the test train, so no extrapolation for the load-displacement curve would be necessary for finding the deflections at static wheel load levels.

Figure 3.14 shows the calibration test in progress.

3.5.2 Dynamic Tests

In spite of all the preparations made for the testing date, including the test train, the weather on July 11, 1986 was less than ideal, in that it rained heavily and continuously the day and night before the tests, as well as during the day of the tests. Consequently, the tests of the ballast-deck bridge were conducted while the deck, bridge timber, and the road bed were very wet. There was an unexpected amount of water under the bridges which delayed the installation of the LVDT's and the accelerometers. The wet conditions also resulted in malfunction of a few gauges.

The dynamic tests were carried out for the ballast-deck bridge, with test train no. 1 runs at crawl speed (i.e., 1 mph), 5, 10, 15, 20, 30, 40, and 50 mph. The measurements of loads, displacements and accelerations were recorded and stored on floppy diskettes. The locomotive (i.e., #CN 5516) was uncoupled from the rest of the test train and tests were carried out with locomotive runs at crawl speed (i.e., 1 mph), 5, 10, 20, 30, 40, and 50 mph, and the measurements were recorded and stored on floppy diskettes.

Due to the bad weather conditions, it was decided to postpone the remaining tests to another day.

The second series of tests took place on September 16, 1986. The weather conditions were quite favorable at the outset. The tests commenced at the open-deck bridge after the gauges were checked and verified the day before. Following the static tests, the dynamic tests were carried out using test train no. 2 running at crawl speed (i.e., 1 mph), 5, 10, 15, 20, 30, 40, and 50 mph. Runs at crawl speed, 30, and 50 mph were repeated several times to duplicate some of the data from different channels on the Nicolet Explorer Digital Oscilloscope.

No uncoupling of the locomotive was conducted for the open-deck bridge. The same test train and truck-trailer unit were moved to the test site of the ballast-deck bridge. The circuits of strain gauges already in place were verified. The LVDT's and accelerometers were installed again. The calibration tests from series 1 were used.

The dynamic tests were repeated for the ballast-deck bridge using test train no. 2 with runs at crawl speed (1 mph), 10, 30, and 50 mph. Similarly, a couple of additional runs were made at 30 and 50 mph to record data from different channels on the Nicolet Explorer Digital Oscilloscope. The light drizzle which started falling in the course of the tests at site 1 and affected only the function of the gauges at positions #1 and 4, shown in Figure 3.5.

For all dynamic tests, the speed of the test trains was maintained by the enginemen in the cabin. A Decatur Ray Gun Speed Measuring Device (Model No. T1, Range 8 to 99 mph) was used to verify the actual test speeds. The readings from both sources corresponded very well, except at speeds of 5 mph and less, for which the radar device was not considered to be reliable.

3.6 TEST RESULTS

The experimental work at both sites involved twelve calibration tests (6 at each site) and forty dynamic tests (24 for the ballast-deck site, BDB and 16 for the open-deck site, ODB). Data on each static test was recorded on 4 channels and data on each dynamic test on 16 channels. In addition, some of the data were also recorded on the Nicolet Explorer Digital Oscilloscope and the HP Spectrum Analyzer. Massive data were collected for the dynamic and static tests for both bridges. Only selected data has been presented in the following sections.

3.6.1 Calibration Tests

The calibration tests of the shear-load circuits at the mid-span of the bridges, the approaches and the track for both sites (i.e., BDB and ODB) are given in Figures 3.15 and 3.16, respectively. Figure 3.15 shows the load-displacement characteristics at locations S3, A and T (only left rail, i.e., channels 2, 4, and 6) of the BDB under test train no. 1. Figure 3.16 shows the load-displacement characteristics at locations S2, A and T (average of the left and right rails, i.e., channels 1 to 6) of the ODB under test train no. 2.

The following are some of the observations based on the results of the calibration tests:

(a) The load-displacement curves for the bridge spans were fairly linear, whereas those for the approaches and the track sections were non-linear within the range of the measurements.

(b) The bridge spans were stiffer than the approaches and in turn, the approaches were stiffer than the track sections.

Since the maximum load limits used for the two test sites differed, some plots were linearly extrapolated to obtain the displacements at a load of 31.73 kips (which represented the weight of the heaviest wheel of the test trains). Using the values of rail displacements for this load level, the values of the stiffnesses were computed, and are given in Table 3.2.

In comparing the values, it may be noted that the ballast deck bridge span was stiffer than the open-deck bridge span despite the fact that this span is 6" longer. This could be attributed to the fact that (a) the deck planks act compositely with the stringers in carrying some of the load, and (b) the load had a better dispersion through ballast and the deck plank floor system.

The bridge approach of the open deck bridge was stiffer by approximately 13% than that of the ballast-deck bridge. This could be attributed to the fact that the former possessed transition ties.

The track sections for both sites had about the same stiffness.

3.6.2 Loads at Wheel-Rail Interfaces

The loads at the rail-wheel interfaces are transmitted across a small contact area on the running surface, except when the wheel flange is also in contact with the rail, in which case, a two-point load path does exist [2, 86].

The loads at the wheel-rail interfaces for a railway vehicle in motion may be influenced by the following factors:

(a) the static weight of the vehicle;

(b) the dynamic forces due to wheel-rail irregularities on the running surface, such as wheel out-of-roundness, wheel flats and rail joints, the presence of these adds to the impact between wheel and rail;

(c) the dynamic forces such as bounce, roll, pitch and yaw generated due to suspension system of the vehicle in motion;

(d) the track geometry irregularities such as gauge, surface and line;

(e) the external disturbances such as wind, self-excited hunting motions (a wheel set rolling along a tangent track wherein the wheels banging from rail to rail, describe a sinusoidal path called "hunting". The oscillations set up by such motion increase depending on the conicity of wheels and the speed and decrease with an increase in the axle loads), wheel and rail creep and flange forces; and

(f) the speed of the vehicle.

When the vehicle passes over a bridge span, the characteristics of the span and its supports also affect the loads at wheel-rail interfaces, which continuously fluctuate about their static values. Figures 3.17 through 3.25 show typical plots of loads versus time for the BDB for the left and right rail under the passage of test train no. 2 for speeds of 1, 30 and 50 mph. Figures 3.17 to 3.19 are for the mid-point of the bridge span S3. The sudden shift of the datum in Figure 3.19 is mainly due to the instrumentation malfunction. The results from the locomotive and car no. 1 were the only data used from this figure. Figures 3.20 to 3.22 are load versus time plots for the bridge approach, and Figures 3.23 to 3.25 are for the track section for the DBD site. Some instrumentation problem experienced in Figure 3.19 for the 50 mph speed is repeated in Figures 3.22 and 3.25.

Similarly, Figures 3.26 through 3.34 show typical plots of the loads versus time of the ODB site under the passage of test train no. 2. Figures 3.26 to 3.28 are for the mid-point of the bridge span S2 for speeds of 1, 30 and 50 mph. Figures 3.29 to 3.31 are for the bridge approach and Figures 3.32 to 3.34 are for the track section.

The above plots give the dynamic wheel loads for both rails which exhibit significant variations from their static values. Tables 3.3 and 3.4 provide the maximum recorded loads at wheel-rail interfaces for the two test sites. Additional information on the loads at wheel-rail interfaces can be found in Uppal [111a].

3.6.3 Vertical Displacements

The vertical displacements are influenced by the magnitude of the loads at the wheel-rail interfaces, the stiffnesses and the damping characteristics of the systems that are provided by the components of the bridge spans, and the nature of both the track and the approach sections.

Since a fair amount of variation in the data measured for the loads at the wheel-rail interfaces was observed, the reasons of which were described in section 3.6.2, the same was to be expected for the vertical displacements.

Figures 3.35 through 3.43 show typical plots of the vertical displacements of the left and right rails versus time at the BDB site for mid-point of the bridge span S3, and span S2, and the normal track section, respectively, under the passage of test train no. 2 at speeds of 1, 30 and 50 mph. The maximum values of the displacements are given in Table 3.5.

In the case of the span S3, Figures 3.35 to 3.37, the values of maximum displacement under the left-hand chord were consistently higher than those under the right-hand chord. This could be attributed to the fact that the track was accentric with respect to the bridge span by an amount of 0.33 inch. These displacements showed little increase with increase in the speed. For span S2, Figures 3.38 to 3.40, the values of maximum displacement were recorded only for the right-hand chord. These displacements also showed little increase with increase in the train speed.

For normal track section, Figures 3,41 to 4.43, the values of maximum displacements under the left-hand rail were higher than those under the right-hand rail, probably due to a soft spot under the right rail. These displacements increased with increase in train speed.

Similarly, Figures 3.44 through 3.52 show typical plots of the vertical displacements versus time for the ODB site for mid-point of bridge span S2, the bridge approach and the normal track section, respectively under the passage of test train no. 2 at speeds of 1, 30 and 50 mph. The maximum values of the displacements ar given in Table 3.6.

In the case of the span S2, Figures 3.44 to 3.47, the values of maximum displacements for both chords were found to be fairly consistent and their average values exhibited an increasing trend with increase in the train speed.

For the bridge approach, Figures 3.47 to 3.49, the maximum displacements under the right-hand rail were slightly higher than those under the left-hand rail. The displacements reduced with increase in the train speed.

For the normal track section, Figures 3.50 to 3.52, the maximum displacements under the left-hand rail were slightly higher than those under the right-hand rail. These displacements first decreased with increase in the train speed, and then increased with increase in the train speed.

Additional information on the maximum values of vertical displacements and the wheels under which they occurred is given in Uppal [111a].

3.6.4 Accelerations

The typical output of the recorded acceleration versus time for the mid-point of the span S3 of the ballast-deck bridge and for the mid-point of span S2 of the open-deck bridge under test train no. 2, at speeds of 1, 3, and 50 mph are shown in Figures 3.53 to 3.55, and 3.56 to 3.58, respectively. The maximum and minimum values are given in Tables 3.7 and 3.8.

The tabulated values indicated that the acceleration increased and their range widened as the speed increased. For the ballast deck bridge, the maximum acceleration ranged from +10.08 g to -7.00 g at 50 mph as shown in Figure 3.55, but unfortunately for the open deck bridge at a speed of 20 mph and beyond, the range exceeded the measurement limits of the instrumentation which was set from +10.8 g to -10.8 g as shown in Figures 3.57 and 3.58.

3.7 ANALYSIS OF TEST RESULTS

3.7.1 Calibration Tests

3.7.1.1 Modulus of Elasticity. As stated in Section 3.6.1, the load-displacement relationship for the bridge spans at both test sites shown in Figures 3.1 and 3.2 was found to be fairly linear. Assuming the stringers of the spans to be simply supported at one end and continuous at the other end of a two span beam, the following expression was used to compute the modulus of elasticity of the bridge span material.

$$E = (P/\Delta) \bullet L^3/(69 \times I) \tag{3.1}$$

where:

P = Load applied at mid-point of span (lbs.)

Δ = Deflection under load P (inches)

L = Span length (inches)

I = Moment of inertia (inches^4) of one chord

The values of E were found to be as follows:

BD Bridge, Span S3: $E = 1.48 \times 10^6$ psi

OD Bridge, Span S2: $E = 1.17 \times 10^6$ psi

The actual values of E are expected to be higher than the above values, mainly because of the following reasons:

(i) the measured deflections were the average of the two middle out of four stringers of each chord, meaning that average deflection of the chord would be smaller;

(ii) the timber being wet by rain, possibly exhibited lower value of E than for relatively dry conditions;

(iii) the measured deflection values may include some play in the components of the spans; and

(iv) the actual sizes of stringers may be smaller than those used for the computations.

The A.R.E.A. manual [4] gives values for the Modulus of Elasticity, E, for different grades of Douglas Fir which range from 1.20×10^6 to 1.76×10^6 psi.

Although the calculated values of E based on the measured load-deflection relationship are for the bridge span and not for the timber material alone, they do fall within the above range. The value of E used for subsequent computations in this study is taken as 1.65×10^6 psi, which is close to the middle of the range and is commonly accepted.

3.7.1.2 **<u>Track Moduli for Bridge Approach and Normal Track Section</u>**. Within the range of the measurements, the load-displacement curves for the bridge approaches and normal track sections were non-linear, as given in Figures 3.15 and 3.16. However, the rate of change of load versus displacement $\delta P/\delta\Delta$ was fairly constant with the increasing magnitude of the load. According to Talbot [98], beyond certain load levels this relationship could be assumed linear for all tracks, despite the fact that for the weaker tracks, it could initially behave non-linearly. This behaviour could be due to the effect of slackness in the components of track which will become insignificant to the overall load-displacement behaviour with increasing levels of load.

Since the values of $\delta P/\delta\Delta$ were constant near the maximum wheel load of 31.73 kips, the track moduli K for the bridge approach and normal track sections could be calculated using the following Talbot formula [58, 98]:

$$K = \frac{1}{4}\sqrt[3]{\frac{1}{(EI)}\left(\frac{P}{\omega_m}\right)^4} \tag{3.2}$$

where; P = Wheel load (lbs)

ω_m = Deflection of rail measured under wheel load P (inches)

E = Modulus of elasticity of rail steel (psi)

I = Moment of inertia of rail section along horizontal section (inch^4). For 85 lb rail = 29.49

K = Modulus of track elasticity or track support stiffness or simply termed as track modulus (lb/in/in.)

The calculated values based on the measured loads and deflections are given in Table 3.9. It should be noted that the modulus of track at both the BDB and the ODB sites is similar, whereas the modulus of bridge approach for the ODB site is higher than that for the BDB site. This may be attributed to the presence of transition ties, which assisted in better dispersion of axle load, thereby reducing the deflection of rails.

The term "modulus of track elasticity", "track support stiffness", or simply "track modulus", is defined [47] as the load per unit length of rail required to depress one tie by one unit divided by the tie spacing.

Rail, fastening, tie, ballast, and subgrade are components that enter into the stiffness of the track and determine the value of the track modulus. The track modulus is not only important in several track analysis equations, but it is also highly important as a measure of track strength, quality, and life.

The track modulus depends on rail weight, tie spacing, quality of ballast, and subgrade, which exhibit a certain amount of play or looseness. The modulus, being a measure of support stiffness, should be free of any play in the components and hence by displacement, which is not elastic.

Railway engineering [47], Second Edition, p. 261, Table 15.1 for #85 rail, 8" x 6" x 8'-0" ties at 22" spacings on 6" limestone on a loam and clay road bed gives a track modulus value of 970 before tamping and 1080 after tamping. Although the bridge approach and the normal track sections tested here had gravel and pitrun on a silty clay roadbed, the values obtained experimentally are somewhat lower than those quoted above. This could be due to play in the wet track and the subgrade components.

Since the load-displacement behaviour was found to be non-linear for the track within the range of the train loads, a bi-linear analysis of the track modulus was also attempted as suggested by Kerr and Shenton [59], and the results are given in Table 3.10.

In Table 3.10, w_o may be considered as the play or the compliance factor associated with K_o and K_1 to be the value of the track moduli. The values of K_1 are significantly higher than the values of K obtained by the linear approach.

The linear analysis is quite valid here because of the compressible nature of the roadbed material which is clay in this instance, as opposed to the bi-linear approach which would be more suitable for the frictional type of roadbed materials such as sand or gravel etc., and ω_o will represent the actual value of play.

3.7.2 Loads at Wheel-Rail Interfaces

3.7.2.1 Dynamic Load Factor: DLF=L_d/L_s. For the purpose of this report, the dynamic load factor or DLF is defined as the ratio of the measured load at wheel-rail interface, L_d, at a given location (i.e., the bridge span, the bridge approach, or the normal track section) for a given speed, to the scale wheel in question.

Like the loads at wheel-rail interface L_d, the dynamic load factors DLF are influenced by several factors mentioned in section 3.6.2.

The wheel-rail running surface irregularities (i.e., wheel-out-of-roundness, wheel flats and rail joints, etc.) and the track geometry irregularities (i.e., wide or tight gauge, rail being out of surface and/or out of line, etc.) can produce severe impact between wheel and rail which can occur at any position along the track and may not increase linearly with speed [56].

In addition to the above, the other factors that influence in a significant way are the axle loads, the make-up and position of the axles (i.e., the spacing and eccentricity) and the stiffness of the bridge/track structure. Hunting is usually pronounced in empty cars [47].

Only the effect of the speed and the static axle loads is considered here.

Figures 3.59 to 3.61 show the plots of the dynamic load factors for the bridge span S3, the bridge approach and the normal track section, respectively, at the BDB site (for left and right rails) versus speeds ranging from 1 to 50 mph.

Similarly, Figures 3.62 to 3.64 show the plots of the dynamic load factors for the bridge span S2, the bridge approach and the normal track section, respectively at the ODB site (for left and right rails), versus speed ranging from 1 to 50 mph. As indicated in the above figures, a few values of DLFs belonging mainly to the cabooses in the test trains were found to be inconsistent with the rest of the experimental data. These values were left out of the upper and lower limit lines trends, so the envelopes in fact represent approximately 95% of the actually measured values. The upper values of the DLF's for each site are given in Table 3.11. It should be noted that in general, these factors are found to increase with increase in the train speed.

The dynamic load factors are also related to their respective static wheel loads in Figures 3.65 to 3.70 for the bridge spans, the bridge approach, and the normal track sections (both rails) for both the BDB and ODB sites. The maximum values of the DLF's by maximum static wheel loads of cars for both sites are given in Table 3.11A.

In general, these factors were found to decrease with increase of the static wheel loads. This demonstrates that the heavier axles such as of locomotives and cars are more stable with respect to rolling action than the lighter axles such as of the cabooses. Moreover, the weights of their wheels are more evenly distributed while in motion, a condition which helps to reduce the vibrations due to the rolling action of the vehicles.

3.7.3 Vertical Displacements

Figure 3.71 shows the maximum dynamic displacements versus speed of test train No. 2 (average of L & R rails) at the mid-points of the bridge spans S3 and S2 and the normal track section T, for the BDB site.

The measured values of displacements for the spans did exhibit little effect of the increase in speed. However, the displacements in the track section increased as the speed increased.

Similarly, Figure 3.72 shows plots of the maximum dynamic displacements (average of L & R rails) at mid-point of the bridge span S2, the bridge approach and the normal track section, respectively for test site 2 versus speed of test train no. 2. The values of displacements of the span S2 and the normal track increased with increase in speed, whereas the approach fluctuated somewhat without showing the real effect of speed.

3.7.3.1 Dynamic Displacement Factors: $DDF = D_d/D_s$. The dynamic displacement factor is defined as the ratio of the measured displacement at a given speed, D_d, to the static displacement, D_s, for a particular location on the bridge span, bridge approach, or track section.

The different types of DDF's used in this report are:

(a) $$DDF_{calibration} = D_d/D_{calib}$$

This is the ratio of the measured value of the maximum displacement at a given speed of the test train, D_d, and the value of the static displacement under a load equivalent to the heaviest wheel based on the static calibration test, D_{calib}.

(b) $$DDF_{computed} = D_d/D_{compu}$$

This is the ratio of the measured value of the maximum displacement at a given speed of the test train, D_d, and the value of the static displacement, computed assuming the train to be a series of moving loads, D_{compu}.

(c) $$DDF_{crawl} = D_d/D_{crawl}$$

This is the ratio of the measured value of the maximum displacement at a given speed of the test train, D_d, and the value of the displacement at crawl speed at the same point, D_{crawl}.

For computing the above ratios, the values of D_{calib} for the bridge spans, the bridge approaches and the track sections were determined from the relationships shown in Figures 3.15 and 3.16. The computed displacement, D_{compu} were calculated using the method of influence lines considering the test train a series of moving loads, and assuming the bridge span to be partially continuous as shown in Table 3.12, and assuming the approaches and track sections as infinite beams on elastic foundation [58, 59]. The maximum values of shear, bending and displacements per chord of timber span are given in Table 3.12.

The various values of the dynamic displacement factors, DDF for mid-point of span S3 of the BDB site under the passage of test train no. 2 were computed for different speeds, and the ranges over which these values (i.e., average of both rails) varied were as follows:

$$D_d/D_{calib} = 1.64 \text{ to } 1.80$$
$$D_d/D_{compu} = 1.71 \text{ to } 1.89, \text{ and}$$
$$D_d/D_{crawl} = 0.95 \text{ to } 1.01$$

The behaviour indicates that the dynamic displacement factors were not sensitive to speed.

The dynamic displacement factors, DDF, for the mid-point of span S2 and track section of the BDB site under the passage of test train no. 2 were computed for different speeds. The variations in their values within the range of measurements were as follows:

DDF	Span S2	Track Section
D_d/D_{calib}	-	0.93 to 1.02
D_d/D_{crawl}	0.99 to 1.12*	1.00 to 1.10
D_d/d_{compu}	-	0.94 to 1.04

* Based on reading at one rail.

It was found that for span S2, the dynamic displacement factors initially (i.e., at low speeds) decreased and then increased with an increase in the speed, whereas for the track section, the factors initially stayed almost constant, however, increased with increase in the speed. Figure 3.73 shows the maximum values of DDF_{crawl} for the mid-point of span S3, the Span S2 and the track section T at the BDB site. Similarly, the various dynamic displacement factors, DDF for mid-point of span S2 of the ODB site, for test train no. 2 were also computed for different speeds. The range by which their magnitudes varied over a speed of 50 mph is given below:

$$D_d/D_{calib} = 2.13 \text{ to } 2.80$$
$$D_d/D_{compu} = 2.80 \text{ to } 3.68$$
$$D_d/D_{crawl} = 1.00 \text{ to } 1.32$$

It was found that the dynamic displacement factors increased with an increase in the speed. The dynamic displacement factor, DDF, for the approach and the track section of the ODB site for different speeds were plotted. The ranges over which these values varied were as follows:

DDF	Bridge Approach	Normal Track Section
D_d/D_{calib}	1.11 to 1.15	1.04 to 1.21
D_d/D_{compu}	1.19 to 1.24	1.05 to 1.22
D_d/D_{crawl}	0.97 to 1.00	0.98 to 1.13

It was found that they indicated some fluctuation at low speeds, but after that the readings remained unaffected by an increase in speed. However, these factors for the track section showed an initial decrease after which their values tended to increase with increase in speed. Figure 3.73 shows the maximum values of DDF_{crawl} for the mid-points of spans S3 and S2, and the track section T at the BDB site. Figure 3.74 shows the maximum values of DDF_{crawl} for the mid-point of span S2, the bridge approach A and the track section T at the ODB site.

3.7.4 Accelerations

Figures 3.53 and 3.58 show the plots of accelerations versus speeds of 1, 30, and 50 mph for mid-points of spans S3 and S2 for the first and second test bridges, respectively. The behaviour indicated that the accelerations and the range of acceleration widened as the speed increased. For the ballast-deck bridge, the maximum acceleration ranged from +10.08 g to -6.78 g, but unfortunately for the open-deck bridge at 20 mph and beyond, the range exceeded the measurement limits of instrumentation which was set from +10.08 to -10.08.

3.7.4.1 Damping in Bridge Spans. The fundamental frequency of each bridge span chord was computed using the following mathematical expression [7, 54]:

$$f_n = \left(\frac{n^2\pi}{2L^2}\right)\sqrt{\frac{EIg}{w}} \tag{3.3}$$

where n = 1,2,3,..., mode of vibration

L = Span length (inches)

E = Modulus of elasticity of the span material (lb/inch^2)

I = Moment of inertia of a chord (inch^4)

g = Acceleration due to gravity = 386.4 (in/sec^2)

w = Weight of chord per unit length (lb/inch)

f_n = Frequency of vibration for n^{th} mode (Hz)

The values of "f_1" for the ballast and open-deck bridge spans were as follows:

Ballast deck bridge span S3:

	Natural Frequency (Hz/chord)	
1. Simply supported chord	22.37	(20.01)*
2. Chord-continuous over two or more spans	22.55	(22.85)

Open deck bridge span S2:

	Natural Frequency (Hz/chord)
1. Simply supported chord	34.24
2. Chord-continuous over two spans	34.16

* Values in parentheses include jack stringers

In section 3.6.1, the behaviour of the bridge spans was observed to be linearly elastic and the fact that in free vibration, the fundamental mode dominates the other modes, the logarithmic decrement technique [6, 22, 85] was employed to the free vibration portions of the accelerations versus time plots of both types of bridge spans for calculating the damping coefficients, using the following relationships:

(a) $\xi \approx \delta/2\pi$

(b) $f_1 = 1/T = \omega_d/2n$

(c) $\delta = 1/n \; \ell n \; (U_1/U_n)$, and

(d) $\xi = (\ell n \; x_1/x_n)/(2\pi f_1 \Delta T)$ (3.4)

where f_1 = Natural frequency for mode 1 (Hertz)

T = Period time (sec.)

ω_d = Damped frequency of span (Hertz)

δ = Logarithmic decrement

n = 1,2,3,...., mode of vibration

U_1 = Response amplitude of decay curve at first cycle (mm)

U_n = Response amplitude of decay curve after nth cycles (mm)

x_1 = Response amplitude at time t_1 (sec)

x_n = Response amplitude at time t_n (sec)

$\Delta T = (t_n - t_1)$

ξ = Modal damping coefficient

The values of damping coefficients using equation (3.3) for spans S3 and S2 are given in Tables 3.13 and 3.14, respectively.

Based on the relationships of the damping coefficients as shown in Figures 3.75 and 3.76, the following observations could be made:

(a) The ballast-deck span had about 50% higher average damping coefficient than the open-deck span.

(b) More consistent values of damping coefficients were obtained from the acceleration versus time plots for the open-deck span as opposed to the ballast-deck span which were found to be erratic. This may be due to the wet condition of span components, particularly the ballast.

(c) The damping coefficient did not exhibit any relationship with the speed of the train.

Chapter 4

ANALYTICAL MODEL

4.1 GENERAL

A multi-degree-of-freedom vehicle-span system was considered for the analytical model. It consisted of a maximum of four railway vehicles coupled one to another with universal joints to simulate the test trains of Chapter 3 (made up of a locomotive, two open-top hopper cars loaded with ballast, and a caboose) used for the experimental work. Each vehicle in the train was assumed to possess three degrees of freedom, namely, bounce, roll, and pitch. The bridge span consisted of two parallel chords. Each chord was divided into a number of equal segments and it was assumed that the distributed masses of the track system, the deck and the chords were concentrated at discrete segment connection points or nodes according to tributary area.

The approach used involves the following steps:

1. Formulating the equations of motion of the vehicle bodies and the equations of motion of the bridge span chords.
2. Determining expressions for the forces at the wheel-rail interfaces.
3. Establishing the relationship between displacement under a wheel and at its neighbouring nodal points.
4. Constructing the mass, damping and stiffness matrices for the overall dynamic system from the above.
5. Positioning of the wheels with respect to a given segment of the chord and, using generalized coordinates, determining and adding contribution of the wheels to their

appropriate places in the matrices of 4, above.

6. Re-arranging terms associated with the unknown variables in the equations of motion of the system.

7. Solving the equations of motion of the overall dynamic system by means of numerical integration.

A computer program was developed, based on the proposed analytical model, and was used to predict the loads at wheel-rail interfaces, and the vertical displacements and accelerations at the discrete points on the spans (i.e., nodes), while traversed by a train travelling at a constant speed.

The program was utilized to study the effect of speed and other parameters on the dynamic response of open-deck and ballast-deck bridges.

4.2 VEHICLE MODEL

Each vehicle of the system comprises a car body supported by dual axle trucks at each end. The body rests on the bolster centre plate with or without stops mounted on the side frames. The analysis considers the car body as a rigid body.

The major truck components [56, 64, 89, 20] are the two side frames, the bolster and the two wheel sets as shown in Figure 4.1. The wheel set has two wheels rigidly connected by an axle which is assumed to be isolated from the truck frame by a primary suspension system, consisting of the bearing box and the side frame, and by the flexibility of the side frame itself. The only flexibility in this connection is due to the bending of the side frame, while damping is provided through friction of the bearing boxes sliding vertically in their guides.

The secondary suspension consists of the coil springs between bolsters and sideframes, friction snubbers that also act between side frames and bolsters, and friction at the centre plate that resists rotation of the truck relative to the car body. The side frames also prevent the car body from rolling excessively.

4.2.1 Assumptions

Each vehicle has been idealized as a rigid body and four axle-sets having three degrees of freedom corresponding to bounce, y_b, pitch, ϕ_b, and roll, θ_b, as shown in Figure 4.2(a). The two dual-axle trucks are assumed to be part of the vehicle body. The axes of reference of the vehicle body are assumed to pass through its centre of mass. The vertical springs in the primary suspension (i.e., between the wheel-axle set and the truck frame, with a spring constant, k_{yp}) and the secondary suspension system (i.e., between the vehicle body and the truck frame, with spring constant, k_{ys}) are treated as linear springs acting in series with an equivalent spring constant k_y as shown by the following relationship:

$$k_y = \frac{1}{\left(\frac{1}{k_{yp}} + \frac{1}{k_{ys}}\right)} \qquad (4.1)$$

The damping in the suspension systems of the vehicles is small (21), and is not liable to change significantly while the vehicle traverses a short bridge span and therefore is neglected. The effects of lateral or longitudinal movements in the vehicle components resulting from hunting, sway or braking actions are neglected. The couplings between the vehicles are assumed to be provided by universal joints so that the effects of the degrees-of-freedom of one vehicle are not transferred to another vehicle. All vehicles in a train cross the bridge at a constant speed.

4.2.2 Equations of Motion

Assuming no damping in the suspension systems and using Newton's second law of motion, the equations of motion for a vehicle with three degrees of freedom may be expressed as follows:

$$M_{b_r}\, \ddot{y}_{b_r} + \sum_{i=1}^{8} k_{y_r}\, y_r^i = 0 \qquad \text{Vertical Displacement}$$

$$I_{b_r}\, \ddot{\phi}_{b_r} + \sum_{i=1}^{8} k_{y_r}\, y_r^i(\pm \ell_r^i) = 0 \qquad \text{Pitch Displacement} \tag{4.2}$$

and $$J_{b_r}\, \ddot{\theta}_{b_r} + \sum_{i=1}^{8} k_{y_r}\, y_r^i(\pm d_{c_r}) = 0 \qquad \text{Roll Displacement}$$

where for vehicle r, see Figure 4.2(b)

M_{b_r}, I_{b_r} and J_{b_r} = the body mass, the body pitch moment of inertia and the body roll moment of inertia, respectively.

ℓ_r^i = distance from the centre of gravity of vehicle to the i[th] wheel

d_{c_r} = one-half the distance between the wheel-rail contact points of a wheel-axle set

k_{y_r} = equivalent vertical spring stiffness per wheel of the vehicle

$\ddot{y}_{b_r}$, $\ddot{\phi}_{b_r}$, and $\ddot{\theta}_{b_r}$ = the accelerations due to the bounce, the pitch, and the roll of the centre of mass of the vehicle body.

where y_r^i = $(y_{b_r} \pm \ell_r^i\phi_{b_r} \pm d_{c_r}\theta_{b_r} - u_{b_r}^i)$ and

$u_{b_r}^i$ = the vertical displacement of the wheel-rail contact point for the i[th] wheel of r[th] vehicle at any time t.

The sign notation of the following quantities for different wheels of the r^{th} vehicle is taken as follows:

Quantity	Wheels	Sign
$\ell_r^i \phi_{b_r}$	1 to 4	+
$\ell_r^i \phi_{b_r}$	5 to 8	-
$d_{c_r} \theta_{b_r}$	Odd number	+
$d_{c_r} \theta_{b_r}$	Even number	-

Also,

$\ell_r^i = \ell_{t_r} - \ell_{w_r}$ for wheels 3 to 6, and

$\ell_r^i = \ell_{t_r} + \ell_{w_r}$ for other wheels.

By substituting for the above quantities and letting

ϕ_{b_r} and $\theta_{b_r} = 0$ for bounce

y_{b_r} and $\theta_{b_r} = 0$ for pitch, and

y_{b_r} and $\phi_{b_r} = 0$ for roll,

for a vehicle whose displacements at and about its centre of mass are chosen as the generalized coordinates, and by rearranging the terms, Eq. (4.2) can be represented in the following decoupled matrix form:

$$\begin{bmatrix} M_{b_r} & 0 & 0 \\ 0 & I_{b_r} & 0 \\ 0 & 0 & J_{b_r} \end{bmatrix} \begin{Bmatrix} \ddot{y} \\ \ddot{\phi}_{b_r} \\ \ddot{\theta}_{b_r} \end{Bmatrix} + k_{y_r} \begin{bmatrix} 8 & 0 & 0 \\ 0 & 8(\ell_{t_r}^2 + \ell_{w_r}^2) & 0 \\ 8 & 0 & 8d_{c_r} \end{bmatrix} \begin{Bmatrix} y_{b_r} \\ \phi_{b_r} \\ \theta_{b_r} \end{Bmatrix}$$

$$= \sum_{i=1}^{8} k_{y_r} u_{b_r}^i \begin{Bmatrix} 0 \\ \pm \ell_r^i \\ \pm d_{c_r} \end{Bmatrix}$$

or simply

$$[M_r]\{\ddot{y}_r\} + [K_{v_r}]\{y_r\} = \{F_{v_r}\} \tag{4.3}$$

where both $[M_r]$ and $[K_{v_r}]$ are diagonal matrices, $\{F_{v_r}\}$ is a force vector, and damping is neglected. Similar expressions can be derived for other vehicles in the train, and the entire train can be represented in matrix form.

4.3 BRIDGE SPAN MODEL

A timber railroad bridge [4] consists of relatively short spans supported by bents. The spans are made up of structural members called stringers which run parallel to the track. The stringers may be simply supported, or may be alternately continuous over the bents and may be spaced apart or closely packed together in a chord under each rail. The spans are often classified according to the type of deck they carry, i.e., a ballast-deck or an open-deck as shown in Figure 4.4. In a ballast-deck, the track ties are partially embedded in ballast which is laid between the rails and wooden flooring planks secured to the stringers, whereas in an open-deck the ties are laid transversely between the rails and stringers.

4.3.1 Assumptions

A bridge span can be modelled as two parallel chords (i.e., beams) which are simply supported over bents as shown in Figure 4.5. Each chord is divided into a number of equal segments approximating the tie spacing of an open-deck. The distributed mass of the track, the deck, and the chord is considered to be lumped (or concentrated) at the segment connections or nodes. Only a vertical degree of freedom is assigned to each node and only the fundamental mode of vibration is considered. All displacements are assumed to be small. The effect of rotary inertia is neglected. The span material is assumed to possess linear behaviour. The experimental work confirmed this to be valid within the limits of operating loads. The span is considered to have viscous damping, which is proportional to the velocity of vibration.

The bridge span is assumed to be at rest before the train of vehicles enters the span.

4.3.2 Equations of Motion

For a dynamic system possessing stiffness and viscous damping, such as a stringer chord with lumped masses, the following equations of motion are obtained by means of d'Alembert's principle [19, 23, 107].

$$[M_c]\{\ddot{u}(t)\} + [D_c]\{\dot{u}(t)\} + [K_c]\{u(t)\} = \{F_c(x,t)\} \tag{4.4}$$

in which

$[M_c]$ = mass matrix of the chord with "m" masses lumped at "n" nodal points. This is a diagonal matrix

$[K_c]$ = stiffness matrix of the chord. This is a symmetric matrix

$[D_c]$ = equivalent viscous damping matrix of the chord

$\{F_c(x,t)\}$ = vector of applied nodal loads due to interaction between the moving vehicle and the bridge span chord, and

$\{\ddot{u}(t)\}$, $\{\dot{u}(t)\}$, and $\{u(t)\}$ are, respectively, the accelerations, the velocities and the vertical displacements with respect to time at the nodal points. Similarly, the equations of motion for the second chord were derived and the two were combined to form the equations of motion for the bridge span.

4.3.2.1 __Mass Matrix__. Assuming that a bridge span chord is divided into n_s equal segments of ℓ_s length each and that the chord is of uniform cross-section, the mass of each segment is given by

$$m = (w/g + A_g\,\rho)\ell_s$$

where w = dead weight per unit length of track and deck material

A_g = gross cross-sectional area of chord

ρ = mass density of the material of chord

ℓ_s = length of a chord segment, and

g = acceleration due to gravity

The lumped masses of chords 1 and 2 can be expressed as $\sum_{j=1}^{n} m_{j,j}$ and $\sum_{j'=n+1}^{2n} m_{j',j'}$, respectively, where "n" is the number of nodal points, equal to n_s-1. The mass matrix for a bridge span is a diagonal matrix of order 2n.

4.3.2.2 __Stiffness Matrix__. The stiffness matrix of a chord is obtained by inversion of the flexibility matrix, the elements of which are obtained by summation of the flexibility influence coefficients, $f_{i,j}$ [23]. For the simple span ℓ shown in Figure 4.6, the flexibility coefficient, $f_{i,j}$, represents deflection at point i (=x from L.H.S.) caused by a unit load applied at node j (=a from L.H.S.), and is given by the following expressions [101].

$$f_{i,j} = A\ell_s^4(n_s-j)i\{2n_sj - (i^2+j^2)\}, \qquad \text{for } i \leq j$$

$$f_{i,j}' = A\ell_s^4(n_s-i)j\{2n_si - (i^2+j^2)\}, \qquad \text{for } i \geq j \tag{4.5}$$

where $A = \dfrac{1}{6EIn_s\ell_s}$

The flexibility coefficients of chords 1 and 2 are expressed as $\sum_{\substack{j=1\\k=1}}^{n} f_{j,k}$ and $\sum_{\substack{j'=n+1\\k'=n+1}}^{2n} f_{j',k'}$ respectively, the individual inversions of which give the elements of the stiffness matrices which for chord 1 are $\sum_{\substack{j=1\\k=1}}^{n} S_{j,k}$ and, for chord 2, are $\sum_{\substack{j'=n+1\\k'=n+1}}^{2n} S_{j',k'}$. The stiffness matrix for a bridge span is a symmetric matrix of order 2n.

4.3.2.3 <u>Damping Matrix</u>. The damping for each chord was considered to be viscous and is taken as a linear combination of $[M_c]$ and $[K_c]$, i.e.

$[D_c] = \alpha\,[M_c] + \beta\,[K_c]$, in which α and β are arbitrary proportionality factors and the expression satisfies the orthogonality condition. Thus, for normal modes for which each mass undergoes harmonic motion of the same frequency, passing simultaneously through the equilibrium position, the above expression can be put into the following uncoupled form [23],

$$[D_c] = 2\xi\omega_m\,[M_c]$$

where ξ = damping coefficient of chords as a fraction of critical damping

ω_m = circular frequency for m^{th} mode. For m=1, it is the fundamental circular frequency.

The damping matrix of the bridge span is a diagonal matrix similar to the mass matrix.

4.3.3 <u>Fundamental Frequencies of Chords</u>

When the damping is small, it has little influence on the natural frequencies of the system and therefore the calculation of natural frequency assumed no damping. For a freely vibrating undamped chord with lumped masses [66, 107], the equations of motion may be expressed in the following form:

$$[M_c]\{\ddot{U}\} + [K_c]\{U\} = 0, \quad \text{or simply}$$

$$M_c\ddot{U} + K_cU = 0 \tag{4.6}$$

where M_c are lumped masses, and K_c are stiffnesses.

Assuming the response of the chord to be harmonic, the displacement U(t) can be given as

$$U(t) = U_o \sin(\omega t + \theta) \tag{4.7}$$

where U_o = the shape of the chord which does not change with time

θ = the phase angle, and

ω = the undamped natural frequency.

Differentiating Eq. 4.6 twice with respect to t to obtain accelerations and substituting U and $\ddot{U}$ into Eq. 4.6, we obtain

$$[K_c - \omega^2 M_c]U_o \sin(\omega t + \theta) = 0 \quad \text{or, since } \sin(\omega t + \theta) \neq 0$$

$$[K_c - \omega^2 M_c]U_o = 0 \tag{4.8}$$

Now if, instead of K_c, the flexibility matrix for the chord f_c (i.e., $f_{i,j}$) is known, then multiplying Eq. 4.8 by $(1/\omega^2 f_c)$ and rearranging the terms, we get

$$[1/\omega^2 I - f_c M_c]U_o = 0 \tag{4.9}$$

where I is an identity matrix of order n.

Eq. 4.9 is a set of homogeneous equations which can have non-zero solutions provided the determinant of the coefficient matrix vanishes. Thus, the frequency equation in this case is

$$\left| \frac{1}{\omega^2} I - f_c M_c \right| = 0 \tag{4.10}$$

Eq. 4.10 represents a characteristic-value problem, so the roots of the equation are characteristic numbers or eigenvalues which are equal to reciprocals of the squares of the natural circular frequencies of the modes. Since we are interested in the fundamental mode, we need the largest eigenvalue, which corresponds to the smallest frequency.

4.4 VEHICLE-BRIDGE SPAN INTERACTION

The vehicle-bridge span interaction [103, 106] takes place at the wheel-rail contact surfaces (or interfaces) as shown in Figure 4.3. The load that a wheel exerts on a rail is a function of the masses and the suspension systems of the vehicle and the elastic and other characteristics of the span. These loads at the wheel-rail interfaces fluctuate continuously about their static values as the vehicle moves over the bridge span.

4.4.1 Assumptions

The wheels of the vehicle are assumed to remain in contact with the rails at all times. The surfaces of the wheel treads are assumed to be smooth and round, and the track surface irregularities are assumed to be negligible. The rails and bridge ties for the open-deck and flooring planks for the ballast-deck are assumed to be pin-connected to the stringers at the nodal points. There is no play in the components of the span.

Consider the i^{th} wheel of the r^{th} vehicle, as shown in Figure 4.7. There are two masses--a sprung mass (i.e., part of the vehicle body) $M^i_{s_r}$, supported by a spring system of stiffness k_{y_r}, and the unsprung mass (i.e., the wheel and half of the axle) $M^i_{u_r}$, which is always in contact with the rail. Damping in the vehicle is assumed to be zero.

4.4.2 Load at the Wheel-Rail Interface

The loads at the wheel-rail interfaces (or the interacting forces) F^i_r, for the i^{th} wheel are given by the following expression [9].

$$F^i_r = (M^i_{u_r} + M^i_{s_r})g + k_{y_r}\, y^i_r\, M^i_{u_r} - \ddot{u}^i_{b_r} \tag{4.11}$$

Rearranging the terms,

$$F^i_r = M^i_{u_r}(g - \ddot{u}^i_{b_r}) + k_{y_r}\, y^i_r + M^i_{s_r}\, g \tag{4.12}$$

where y^i_r, as before, is

$$y^i_r = (y_{b_r} \pm \ell^i_r\, \phi_{b_r} \pm y_{c_r}\, \theta_{b_r} - \ddot{u}^i_{b_r}) \tag{4.13}$$

4.4.3 Relationship Between Displacements Under the i^{th} wheel and at its Neighbouring Nodal Points

It is assumed that, in the deflected state, the segments of the chords between the nodal points remain straight. Therefore, the displacement under the i^{th} wheel, $u^i_{b_r}$, shown in Figure 4.8 can be expressed in terms of the nodal displacements u^i_j, u^i_{j+1} for chord 1 (or $u^i_{j'}$, $u^i_{j'+1}$ for chord 2) using linear interpolation by the following relationship.

$$u^i_{b_r} = \bar{\gamma}(\alpha^i u^i_{j+1} + \beta^i u^i_j) + \gamma(\alpha^i u^i_{j'+1} + \beta^i u^i_{j'}) \tag{4.14}$$

where $\alpha^i = \frac{x_i}{\ell_s}$, $\beta^i = 1 - \frac{x_i}{\ell_s} = 1 - \alpha^i$

$$\gamma = \frac{d_n}{d} \text{ and } \bar{\gamma} = 1 - \frac{d_n}{d} = 1 - \gamma$$

$$\delta = \frac{d_f}{d} \text{ and } \bar{\delta} = 1 - \frac{d_f}{d} = 1 - \delta$$

Differentiating Eq. 4.14 twice, the following expression for acceleration is obtained.

$$\ddot{u}^i_{b_r} = \bar{\gamma}\ (\alpha^i \ddot{u}^i_{j+1} + \beta^i \ddot{u}^i_j) + \gamma\ (\alpha^i \ddot{u}^i_{j'+1} + \beta^i \ddot{u}^i_{j'}) \tag{4.15}$$

The substitution of Equations 4.13 and 4.15 into 4.12 yields the values of F^i_r.

The combined effects of all the wheels on the displacement and acceleration at a given node j are u_j and $\ddot{u}_j$, respectively.

4.4.4 Effect of Wheel Positions

The contributions of the effect of the i^{th} and $(i+1)^{th}$ wheels on the chord segments defined by nodes j and j+1, and j' and j'+1, are obtained assuming linear interpolation and the generalized coordinates [23, 114] for the rigid body masses, stiffnesses, dampings and interaction forces.

Using Figure 4.8, the following wheel contributions are obtained.

4.4.4.1 **Generalized Masses**. The expression for the generalized masses m* is given by

$$m^* = \sum m_i \psi_i^2 \tag{4.16}$$

where m_i = the mass of the i^{th} wheel = M_u^i, and

ψ_i = the value of the shape form at i of the deflected segment, and is here assumed to be equal to $(1 - \frac{x_i}{\ell_s})$ or $(\frac{x_i}{\ell_s})$, depending upon the reference point of x^i

Also, as before let

$$\delta = \frac{d_f}{d}$$

$$\bar{\delta} = (1 - \frac{d_f}{d}) = 1 - \delta$$

At point k due to i^{th} wheel,

$$m_k^* = M_u^i (1 - \frac{x_i}{\ell_s})^2 \quad \text{, and}$$

At node j, due to i^{th} wheel,

$$m_j^* = M_u^i (1 - \frac{x_i}{\ell_s})^2 (1 - \frac{d_n}{d})^2$$

Similarly, at node j', due to $(i+1)^{th}$ wheel,

$$m_j^* = M_u^i(1 - \frac{x_i}{\ell_s})^2 (1 - \frac{d_f}{d})^2$$

Now, the effect of the i^{th} and the $(i+1)^{th}$ wheel on different nodal points of the panel is shown:.

<u>Direct Effect on Nodes</u>

(a) Node "j" due to i^{th} and $(i+1)^{th}$ wheel

$$m_{jj} = \underbrace{M_u^i (1 - \frac{x^i}{\ell_s})^2(1 - \frac{d_n}{d})^2}_{i^{th}} + \underbrace{M_u^i (1 - \frac{x_i}{\ell_s})^2 (1 - \frac{d_f}{d})^2}_{(i+1)^{th}}$$

$$= M_u^i \beta^{i2}\bar{\gamma}^2 + M_u^i \beta^{i2}\bar{\delta}^2$$

$$= M_u^i(\bar{\gamma}^2 + \bar{\delta}^2)\beta^{i2}$$

$$\equiv A \qquad (4.17)$$

Similarly,

(b) Node "j+1" due to i^{th} and $(i+1)^{th}$ wheel

$$m_{j+1,j+1} = M_u^i(\bar{\gamma}^2 + \bar{\delta}^2)\alpha^{i2}$$

$$\equiv C \qquad (4.18)$$

(c) Node "j'" due to i^{th} and $(i+1)^{th}$ wheel

$$m_{j'j'} = M_u^i(\gamma^2 + \gamma^2)\beta^{i2}$$

$$\equiv A' \qquad (4.19)$$

(d) Node "j' +1" due to i^{th} and $(i+1)^{th}$ wheel

$$m_{j'+1,j'+1} = M_u^i(\gamma^2 + \delta^2)\alpha^{i2}$$

$$\equiv C' \qquad (4.20)$$

Effect of one node on other nodes:

1. Adjacent Nodes:

(a) On node "j" due to node "j+1"

$$m_{j,j+1} = \underbrace{M_u^i\left(\frac{x^i}{\ell_s}\right)\left(1 - \frac{x^i}{\ell_s}\right)\left(1 - \frac{d_n}{d}\right)}_{i^{th}} + \underbrace{M_u^i\left(\frac{x_i}{\ell_s}\right)\left(1 - \frac{x^i}{\ell_s}\right)\left(1 - \frac{d_f}{d}\right)}_{(i+1)^{th}}$$

$$= M_u^i\alpha^i\beta^{i2}\bar{\gamma}^2 + M_u^i a^i\beta^{i2}\bar{\delta}^2$$

$$= M_u^i(\bar{\gamma}^2 + \bar{\delta}^2)\alpha^i\beta^i$$

$$\equiv B$$

$$= m_{j+1,j} \qquad (4.21)$$

(b) On node "j'" due to node "j' +1" and vice versa

$$m_{j',j'+1} = M_u^i(\gamma^2 + \delta^2)\alpha^i\beta^i$$

$$\equiv B'$$

$$= m_{j'+1,j'} \qquad (4.22)$$

2. Opposite Nodes:

(a) On node "j" due to node "j'" and vice versa (near nodes)

$$m_{j,j'} = \underbrace{M_u^i\,(1 - \frac{x^i}{\ell_s})^2(\frac{d_n}{d})(1 - \frac{d_n}{d})}_{i^{th}} + \underbrace{M_u^i\,(1 - \frac{x_i}{\ell_s})(\frac{d_f}{d})(1 - \frac{d_f}{d})^2}_{(i+1)^{th}}$$

$$= M_u^i \beta^{i2}\gamma\bar{\gamma} + M^i\beta^{i2}\delta\bar{\delta}$$

$$= M_u^i(\gamma\bar{\gamma} + \delta\bar{\delta})\beta^{i2}$$

$$\equiv D$$

$$= m_{j',j} \tag{4.23}$$

(b) On node "j+1" due to node "j'+1" and vice versa (for nodes)

$$m_{j+1,j'+1} = M_u^i(\gamma\bar{\gamma} + \delta\bar{\delta})\alpha^{i2}$$

$$\equiv F$$

$$= m_{j'+1,j+1} \tag{4.24}$$

3. Diagonal Nodes:

(a) On node "j" due to node "j'+1" and vice versa

$$m_{j,j'+1} = \underbrace{M_u^i(\frac{x_i}{\ell_s})(1 - \frac{x_i}{\ell_s})(\frac{d_n}{d})(1 - \frac{d_n}{d})}_{i^{th}} + \underbrace{M_u^i(\frac{x_i}{\ell_s})(1 - \frac{x^i}{\ell_s})(\frac{d_f}{d})(1 - \frac{d_f}{d})}_{(i+1)^{th}}$$

$$= M_u^i\alpha^i\beta^i\gamma\bar{\gamma} + M^i\alpha^i\beta^i\delta\bar{\delta}$$

$$= M_u^i(\gamma\bar{\gamma} + \delta\bar{\delta})\,\alpha^i\beta^i$$

$$\equiv E$$

$$= m_{j',j+1} \tag{4.25}$$

4.4.4.2 Generalized Stiffnesses. The expression for the generalized stiffness k^* is given by

$$k^* = \sum k_i(\psi_i'')^2 \tag{4.26}$$

where $k_i =$ the equivalent spring stiffness per wheel of vehicle $r = k_{y_r}$, and

$\psi_i'' =$ the slope of the deflected segment, and here it is assumed to be

$= (1 - \frac{x^i}{\ell_s})$ or $(\frac{x^i}{\ell_s})$ depending upon the reference point of x^i

The derivation of the wheel contributions is exactly the same as for the generalized masses, and their values are as follows:

$$k_{j,j} = k_{y_r}(\bar{\gamma}^2 + \bar{\delta}^2)\beta^{i2} \qquad \equiv A1$$

$$k_{j+1,j+1} = k_{y_r}(\bar{\gamma}^2 + \bar{\delta}^2)\alpha^{i2} \qquad \equiv C1$$

$$k_{j',j'} = k_{y_r}(\gamma^2 + \delta^2)\beta^{i2} \qquad \equiv A'1$$

$$k_{j'+1,j'+1} = k_{y_r}(\gamma^2 + \delta^2)\alpha^{i2} \qquad \equiv C'1$$

$$k_{j,j+1} = k_{y_r}(\bar{\gamma}^2 + \bar{\delta}^2)\alpha^i\beta^i \qquad \equiv B1 = k_{j+1,j}$$

$$k_{j',j'+1} = k_{y_r}(\gamma^2 + \delta^2)\beta^{i2} \qquad \equiv B'1 = k_{j'+1,j}$$

$$k_{j,j'} = k_{y_r}(\gamma\bar{\gamma} + \delta\bar{\delta})\beta^{i2} \qquad \equiv D1 = k_{j',j}$$

$$k_{j+1,j'+1} = k_{y_r}(\gamma\bar{\gamma} + \delta\bar{\delta})\alpha^{i2} \qquad \equiv F1 = k_{j'+1,j+1}$$

and

$$k_{j,j'+1} = k_{y_r}(\gamma\bar{\gamma} + \delta\bar{\delta})\alpha^i\beta^i \qquad \equiv E1 = k_{j',j+1}$$

4.4.4.3 Generalized Forces. The expression for the rigid bodies generalized forces p^* is given by

$$p^* = \sum p_i\,\psi_i \tag{4.27}$$

where p_i = the force due to i^{th} wheel = $(M^i_{s_r} + M^i_{u_r})g$ or k_{y_r}, as the case may be, and

ψ_i = shape of the deflected segment as before.

1. <u>Effect of Wheel Weights</u>

(a) Node "j" due to i^{th} and $(i+1)^{th}$ wheel

$$= (M^i_{s_r} + M^i_{u_r})\, g\, (1 - \frac{x^i}{\ell})\, \{(1 - \frac{d_n}{d}) + (1 - \frac{d_f}{d})\}$$

$$= (\bar{\gamma} + \bar{\delta})\beta^i(M^i_{s_r} + M^i_{u_r})\, g$$

$$\equiv A2$$

Similarly,

(b) Node "j+1" due to i^{th} and $(i+1)^{th}$ wheel

$$= (\bar{\gamma} + \bar{\delta})\alpha^i(M^i_{s_r} + M^i_{u_r})\, g$$

$$\equiv B2$$

(c) Node "j'"

$$= (\gamma + \delta)\beta^i(M^i_{s_r} + M^i_{u_r})\, g$$

$$\equiv A'2 \qquad \text{and}$$

(d) Node "j'+1"

$$= (\gamma + \delta)\alpha^i(M^i_{s_r} + M^i_{u_r})\, g$$

$$\equiv B'2 \qquad \text{and}$$

2. <u>Effect of Wheel Bounce</u>

(a) On node "j" of bounce of i^{th} and $(i+1)^{th}$ wheel,

$$= \underbrace{-k_{y_r}(1 - \frac{d_n}{d})(1 - \frac{x^i}{\ell_s})}_{i^{th}} + \underbrace{k_{y_r}(1 - \frac{d_f}{d})(1 - \frac{x^i}{\ell_s})}_{(i+1)^{th}}$$

$$= -k_{y_r}\{(1 - \frac{d_n}{d}) + (1 - \frac{d_f}{d})\}(1 - \frac{x^i}{\ell_s})$$

$$= -k_{y_r}(\bar{\gamma} + \bar{\delta})\beta^i$$

$$\equiv G$$

Similarly,

(b) Node "j'+1" due to i^{th} and $(i+1)^{th}$ wheel

$$= -k_{y_r}(\bar{\gamma} + \bar{\delta})\alpha^i \equiv H$$

(c) Node "j'"

$$= -k_{y_r}(\gamma + \delta)\beta^i \equiv G', \qquad \text{and}$$

(d) Node "j'+1"

$$= -k_{y_r}(\gamma + \delta)\alpha^i$$

$$\equiv H'$$

3. **Effect of Wheel Pitch**

(a) On node "j" of pitch of i^{th} and $(i+1)^{th}$ wheel

$$\pm \mid k_{y_r}(\bar{\gamma} + \bar{\delta})\beta^i \mid \ell_r^i = \pm \mid G \mid \ell_r^i \equiv N$$

(b) Node "j+1"

$$\pm \mid k_{y_r}(\bar{\gamma} + \bar{\delta})\alpha^i \mid \ell_r^i = \pm \mid H \mid \ell_r^i \equiv Q$$

(c) Node "j'"

$$\pm \mid k_{y_r}(\gamma + \delta)\beta^i \mid \ell_r^i = \pm \mid G' \mid \ell_r^i \equiv N'$$

(d) Node "j'+1"

$$\pm \mid k_{y_r}(\gamma + \delta)\alpha^i \mid \ell_r^i = \pm \mid H' \mid \ell_r^i \equiv Q'$$

4. **Effect of Wheel Roll**

(a) On node "j" of roll of i^{th} and $(i+1)^{th}$ wheel,

$$\pm \mid G \mid d_{c_r} \equiv R$$

Similarly,

(b) Node "j+1"

$$\pm|H|d_{c_r} \equiv S$$

(c) Node "j"

$$\pm|G'|d_{c_r} \equiv R', \qquad \text{and}$$

(d) Node "j'+1"

$$\pm|H'|d_{c_r} \equiv S'$$

5. **Wheel Stiffness Effect**

(a) In bounce

$$= 8k_{y_r} \qquad \equiv T$$

(b) In pitch

$$= 8k_{y_r}\,(\ell_{t_r}^2 + \ell_{w_r}^2) \qquad \equiv U$$

(c) In roll

$$= 8k_{y_r}\,d_{c_r} \qquad \equiv W$$

where all wheels in a vehicle are the same, then

$$M_{u_r}^{i} = M_{u_r}^{i+1} = M_{u_r}$$

and where all axles are parallel to each other, then

$$\alpha^{i} = \alpha^{i+1} = \alpha, \text{ and}$$

$$\beta^{i} = \beta^{i+1} = \beta$$

The above contributions are added to their appropriate places in the mass, damping and stiffness matrices of the overall dynamic system. The contribution of the generalized masses of one axle (i.e., i^{th} and $(i+1)^{th}$ wheels) on one segment of the span (described by nodes j and j+1 and j' and j'+1) to the overall mass matrix is as follows:

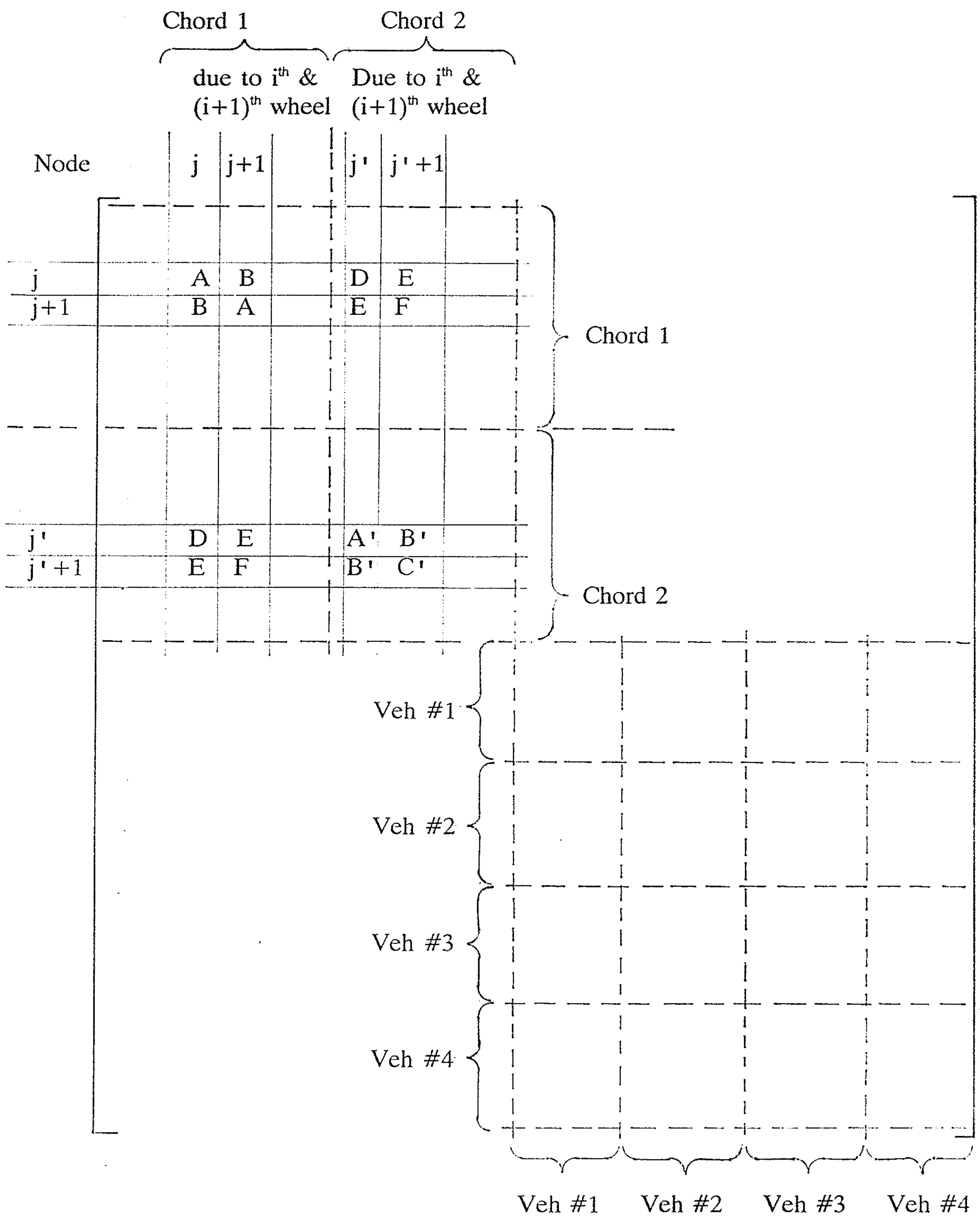

Order = $(2n + 3\ \ell_{car}) \times (2n + 3\ \ell_{car})$

Overall Mass Matrix

where other axles and segments are involved, their contributions would be added to their appropriate locations in the matrix. Where the other axles and segments are involved, their contributions would be added to their appropriate locations in the matrix.

The contributions of the generalized forces of one axle (i.e., i^{th} and $(i+1)^{th}$ wheels) on segment (described by j and j+1 and j' and j'+1) on the overall force vector is as follows:

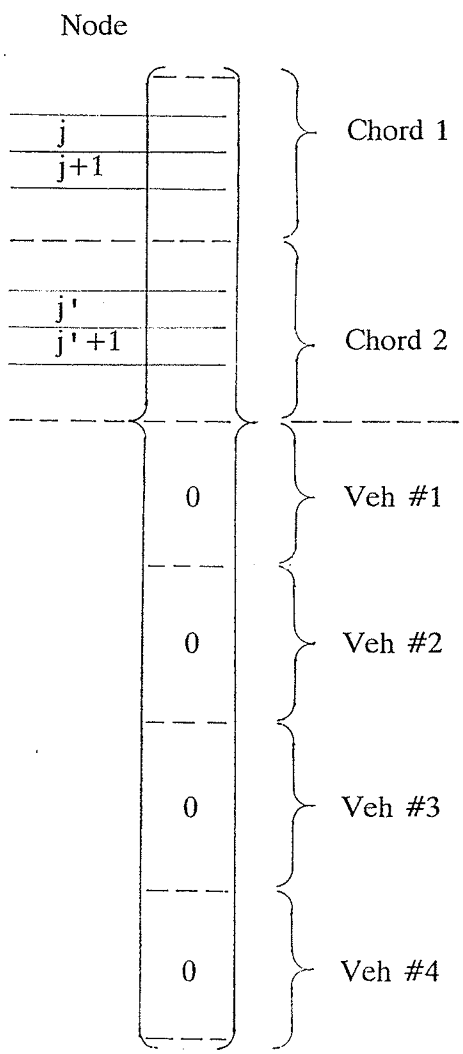

Order = $(2n + 3\ \ell_{car})$

Overall Force Vector

The contribution of the generalized stiffnesses of one axle (i.e., i^{th} and $(i+1)^{th}$ wheels of vehicle #1) on one segment of the span (described by nodes j and j+1 and j' and j'+1) to the overall stiffness matrix is as follows:

		Chord 1		Chord 2													
		Due to i^{th} and $(i+1)^{th}$ wheel		Due to i^{th} and $(i+1)^{th}$ wheel		Veh #1			Veh #2			Veh #3			Veh #4		
	Node	j	j+1	j'	j'+1	y_{b_1}	ϕ_{b_1}	θ_{b_1}	y_{b_2}	ϕ_{b_2}	θ_{b_2}	y_{b_3}	ϕ_{b_3}	θ_{b_3}	y_{b_4}	ϕ_{b_4}	θ_{b_4}
Chord 1	j	A1	B1	D1	E1	G	N	R									
	j+1	B1	C1	E1	F1	H	Q	S									
Chord 2	j'	D1	E1	A'1	B'1	G'	N'	R'									
	j+1	E1	F1	B'1	C'1	H'	Q'	S'									
Veh #1	y_{b_1}	G	H	G'	H'	T											
	ϕ_{b_1}	N	Q	N'	Q'		U										
	θ_{b_1}	R	S	R'	S'			W									
Veh #2	y_{b_2}																
	ϕ_{b_2}																
	θ_{b_2}																
Veh #3	y_{b_3}																
	ϕ_{b_3}																
	θ_{b_3}																
Veh #4	y_{b_4}																
	ϕ_{b_4}																
	θ_{b_4}																

Order = $(2n + 3\,\ell_{car}) \times (2n + 3\,\ell_{car})$

Overall Stiffness Matrix

Where the other axles and segments are involved, their contributions would be added to their appropriate locations in the vector.

4.5 OVERALL DYNAMIC SYSTEM

Each chord is divided into $n_s = n+1$ equal segments or n effective nodal points. Every node is assigned one degree of freedom, namely, the vertical displacement. Therefore, a bridge span possesses 2n degrees of freedom. Further, there are three degrees of freedom assigned to each vehicle, so a train consisting of N_c number of cars has $3N_c$ degrees of freedom. The overall dynamic system therefore comprises $(2n + 3N_c)$ degrees of freedom.

4.5.1 Overall Equations of Motion

From Equations 4.3, 4.4, 4.12, and section 4.4.4, the equations of motion for the overall train-bridge span system may be expressed as

$$\left[\begin{array}{c|c} M_{bt} & \\ \hline & M_t \end{array}\right] \left\{\begin{array}{c} \ddot{U} \\ \hline \ddot{Y} \end{array}\right\} + \left[\begin{array}{c|c} C & \\ \hline & C_v \end{array}\right] \left\{\begin{array}{c} \dot{U} \\ \hline \dot{Y} \end{array}\right\} + \left[\begin{array}{c|c} K_b & K_{bt} \\ \hline K_{tb} & K_t \end{array}\right] \left\{\begin{array}{c} U \\ \hline Y \end{array}\right\} = \left\{\begin{array}{c} F_b \\ \hline F_t \end{array}\right\}.$$

where

M_{b_t} = the mass matrix comprising the lumped masses of chords 1 and 2 (i.e., $[M_c]$) plus the effects of wheel masses

M_t = the mass matrix comprising the car bodies (i.e., $[M_r]$) in the train

K_b = the stiffness matrix comprising wheel contributions on chord segments

K_{bt} = the stiffness matrix comprising wheel contributions on chord segments = K^T_{tb}

K_t = the stiffness matrix comprising vehicle bodies

C_b = the damping matrix comprising chords 1 and 2 (i.e., $[D_c]$ plus) the effects of wheels

C_v = the damping matrix comprising vehicle suspension system assumed zero

F_b and F_t = the vectors of force due to interaction at wheel-rail interfaces

$\ddot{U}$, $\dot{U}$, and U and $\ddot{Y}$, $\dot{Y}$ and Y = the accelerations, velocities, and

displacement associated with chords $\ddot{u}$, $\dot{u}$, and u and with vehicle body $\ddot{y}_r$, $\dot{y}_r$, and y_r, respectively

The above equations may also be represented as

$$[M_o]\{\ddot{D}\} + [C_o]\{\dot{D}\} + [K_o]\{D\} = \{F_o\} \tag{4.28}$$

in which $[M_o]$, $[C_o]$, and $[K_o]$ are, respectively, the overall matrices of mass, damping and stiffness, and $\{F_o\}$ is the vector of force including the effect of vehicle-bridge span interactions. and $\{\ddot{D}\}$, $\{\dot{D}\}$, and $\{D\}$ are the vectors of acceleration, velocity, and displacement, respectively, at the nodal points of the span, as well as the successive derivatives with respect to time t for the vehicle motions. The sizes of the matrices and the vectors for the overall system depend on the number of segments which a bridge span is divided into, and the number of vehicles considered in a train. The equations of motion of the overall system possess purely stiffness coupling terms which are composed of contributions from individual wheel motions (i.e., bounce, pitch and roll). This is because the damping in the suspension system is neglected. The orthogonality characteristics were used to uncouple the stiffness matrix.

The equations 4.28 represent an uncoupled linear multi-degree-of-freedom system, the responses of which were obtained separately in normal modes and then superimposed to provide the overall response.

4.5.2 Location of Wheels on Chord Segments

As a train or vehicle moves over a bridge span, the position of a certain wheel on a given chord segment is identified from the first axle of the train by $y_1 = Vt$ as shown in Figure 4.9. The time t is measured from the instant that the first wheel enters the span at a constant velocity V. Other distance relationships, y_r^i (i for wheel and r for vehicle) are as follows:

Vehicle No. 1

$$\left.\begin{aligned}
y_1^1 &= Vt = y_1^2 \\
y_1^3 &= y_1^1 - 2\ell_{w1} = y_1^4 \\
y_1^5 &= y_1^1 - 2\ell_{t1} = y_1^6, \text{ and} \\
y_1^7 &= y_1^1 - 2\ell_{w1} - 2\ell_{t1} = y_1^8
\end{aligned}\right\} \tag{4.29}$$

and for the subsequent vehicles, i.e., r = 2, 3, ...

$$\left.\begin{aligned}
y_4^1 &= y_{r-1}^8 - \ell_{v(r-1,r)} = y_r^2 \\
y_4^3 &= y_{r-1}^8 - 2\ell_{wr} = y_r^4 \\
y_r^5 &= y_{r-1}^8 - 2\ell_{tr} = y_r^6, \text{ and} \\
y_r^7 &= y_{r-1}^8 - 2\ell_{tr} - 2\ell_{wr} = y_r^8
\end{aligned}\right\} \tag{4.30}$$

The location of a wheel is obtained by comparison of y_r^i with $j\ell_s$ and $(j+1)\ell_s$.

It can be seen that if all vehicles are identical, then

$$\left.\begin{aligned}
&\ell_{t_1} = \ell_{t_2} = \ldots = \ell_t \\
&\ell_{w_1} = \ell_{w_2} = \ldots = \ell_w, \text{ and} \\
&\ell_{v_{12}} = \ell_{v_3} = \ldots = \ell_v \\
&\text{Also eventually,} \\
&\ell_{c_1} = \ell_{c_2} = \ldots = \ell_c
\end{aligned}\right\} \tag{4.31}$$

4.5.3 Solution of the Equations of Motion of the System

A computer program [115, 116, 117] was developed to solve the equations of motion for the overall dynamic system using different methods of numerical integration. The outline of the procedure of analysis employed in the program is given in the following steps:

(a) Compute the constant parameters of the system and construct the mass and stiffness matrices for each vehicle and each chord individually [43, 79, 83] as shown in Equations 4.3 and 4.4, respectively.

(b) Obtain the fundamental circular frequency ω_1 of the chords by eigenvalue analysis [66, 107], assuming undamped harmonic motion with the aid of Equation 4.10. The analysis was carried out by the power method of Mises. Choose the damping coefficient ξ of the chord and construct the damping matrix of the span using Equation 4.6.

(c) Establish the distance vectors from the configuration of wheels in each vehicle and the distances between the vehicles as in Equations 4.29 and 4.30.

(d) Choose a time step, t and calculate the position of the wheels by algebraically adding $y_1^1 = Vt$ to all the terms of the distance vector and determine the number of wheels on a chord in question.

(e) For every wheel, determine the position with respect to the chord segment it occupies, i.e., the distance y^i, from node j and j+1 (or j' and j'+1 for the other chord), as shown in Figure 4.8, and, using the general coordinates for mass, stiffness and interacting force as in Equations 4.16, 4.26 and 4.27, determine the contributions of wheel position to be included to the overall mass, damping, and stiffness matrices and force vector.

(f) Formulate the equations of motion of the overall dynamic system (i.e., Equations 4.28) by constructing the overall mass, $[M_o]$, damping, $[C_o]$, and stiffness, $[K_o]$ matrices and the force vectors $\{F_o\}$.

(g) Solve the equations of motion for the overall system by using one of the following numerical integration techniques:

(i) Newmark's ß-method, or

(ii) Houbolt's method

to find the dynamic displacements, velocities and accelerations, etc., at the nodal points.

A brief description of the above techniques is given by Rao [87] and Levy and Wilkinson [66].

(h) Choose the next time step $t + \Delta t$ and repeat the above procedure until the last axle of the train has gone past the span.

(i) With the aid of Equation 4.12, compute the wheel-rail interface loads at the nodal points.

(j) Denote the maximum wheel-rail interface load and the maximum vertical dynamic displacement at the mid-point of the bridge span by L_{d_c} and D_{d_c}, respectively. Assuming the maximum static wheel load L_s is known, determine the maximum static vertical displacement D_s at mid-point of the span by influence lines for rolling loads.

Compute the following factors for different train speeds:

(a) Dynamic load factor, $DLF_c = \dfrac{L_{d_c}}{L_s}$ and

(b) Dynamic displacement factor, $DDF_c = \frac{D_{d_c}}{D_s}$

4.5.4 Computer Program

The computer program, written in FORTRAN IV, is quite flexible in that it can be used for any length of span and for components having different material properties. Though at present, no provision exists for the track irregularities, the program could be adapted to incorporate the track line and surface irregularities by introducing initial displacements at the nodal points.

Up to four vehicles are currently in a train, but the program can be expanded to include more than four vehicles. Similarly, each chord is currently divided into ten equal segments, but this number can be increased or decreased as necessary.

Initial values of displacements for different degrees of freedom can be specified both for vehicles and for spans for predicting their influence on the dynamic response of the system.

To illustrate the capabilities of the program, the effect of the following parameters was studied:

(a) train speed

(b) train consist

(c) bridge deck type

(d) low spot at bridge approach, and

(e) damping coefficients

The listing of the computer program is appended to this thesis.

4.6 NUMERICAL EXAMPLE

The numerical examples are based on span no. 3 of the ballast-deck and span no. 2 of the open-deck test bridges, as shown in Figures 3.1 and 3.2, respectively, and for which measured data is available in Chapter 3 under test train no. 2 as shown in Figure 3.4.

The data on the spans and on the test train used as input for the computer program are given in Tables 4.1 and 4.2.

Figures 4.10 and 4.11 show typical computed vertical displacement versus time plots for the mid-point of span S3 of the ballast-deck and span S2 of the open-deck bridges, respectively, for train no. 2 at a speed of 30 mph. The maximum values of displacements of 4.12 mm occur under axle no. 9 and of 4.57 mm under axle no. 4, respectively.

Figures 4.12 and 4.13 show typical computed accelerations versus time plots for the above cases. The maximum ranges of acceleration values for the ballast-deck and open-deck spans were +0.86, -0.82 g and +1.71, -1.60 g, respectively,.

4.6.1 Effect of Train Speed

The predicted maximum loads at wheel-rail interfaces, the predicted maximum vertical displacements, and the predicted maximum and minimum accelerations for the mid-point of the open-deck bridge span S2 and ballast-deck bridge span S3 under different speeds of the test train no. 2 are given in Table 4.3 and 4.3A, respectively. It can be noted that the predicted values increase with increase in speed. The loads at wheel-rail interfaces increased by an average of 27.6% and 16.1% and the vertical displacements by an average of 18.1% and 19.9% for open-deck and ballast-deck spans, respectively over a speed range of 1 to 50 mph.

A comparison of the above predicted values with those obtained from the field tests is given in Tables 5.7, 5.8, and 5.9.

4.6.2 Effect of Train Consist

Table 4.4 shows the predicted maximum loads of wheel-rail interfaces, the predicted maximum vertical displacements, and the predicted maximum and minimum accelerations at mid-point of the open-deck bridge span S2 under the locomotive, the locomotive and a open-top hopper car, the locomotive and two open-top hopper cars, and the full test train no. 2 at 50 mph. It can be seen that as the train consist (i.e., the train make-up) increases in length, the loads at the wheel-rail interface increase, the vertical displacements also increase, but the accelerations do not seem to indicate any definite relationship with the train consists.

The displacement versus time plots for the above cases are given in Figures 4.14, 4.15, 4.16, and 4.17.

4.6.3 Effect of Bridge Deck Type

Table 4.5 shows a comparison of the response of the ballast-deck and the open-deck bridge spans. The loads at wheel-rail interfaces and the vertical displacements both increase with increase in speed. The rates of increase of loads as well as displacements are higher in case of the open deck as opposed to the ballast deck. Similarly, the vertical displacements of the open deck are consistently higher than those of the ballast-deck.

4.6.4 Effect of Low Spot at Bridge Approach

Various initial values of bounce were used to study the effect of the low spot at the bridge approaches. Table 4.6 shows the effect of 0.5" to 2.0" low spot on the maximum values of loads, vertical displacements and accelerations in the open-deck span S2 under the test train no. 2 at a speed of 50 mph. It may be noted that a 2 inch low spot increased the load at the wheel-rail interface by 19%, whereas the same increased the vertical displacement by 61.6%.

The displacement versus time plots for the above cases are given in Figures 4.18, 4.19, 4.20 and 4.21.

4.6.5 Effect of Damping Coefficient

Table 4.7 shows the effect of the choice of the damping coefficient values on the maximum vertical displacements at mid-points of bridge spans. The increase in the percentage of damping coefficient results in a decrease in the value of the predicted displacements except for the ballast-deck span, where the initial increases in the damping coefficients (i.e., up to ξ=2.5%) cause some increase in the displacements. Figure 4.22 shows a plot of the above values.

4.6.6 Method of Integration

Table 4.8 shows the values of the maximum loads at wheel-rail interfaces, the maximum vertical displacements, and the values of the maximum and the minimum accelerations of the open deck bridge span S2 under test train no. 2 at 50 mph obtained by the Newmark's ß-method and the Houbolt method. It may be noted that the values of the loads and the displacements computed by both techniques of integration are within a good agreement of each other.

Chapter 5

DISCUSSION

This chapter compares the results of the static and dynamic tests for the two test sites and how these results can be utilized for design purposes.

The assumptions made in the analytical model and their influence on the predicted values are discussed, as well as the sources and the quality of the input data for the computer program.

Finally, it compares the predicted and the measured values of the loads at wheel-rail interfaces, vertical displacements, and accelerations, as well as the dynamic load and dynamic displacement factors.

5.1 EXPERIMENTAL WORK

5.1.1 Calibration Tests

On the first day of the tests, the bridge components and track sections were wet due to heavy rain. This had softened the ballast in the bridge deck and track sections, and thus affected the results such as the values of E and K calculated from the measured values.

The static deflections were measured using maximum loads of 20 kips per rail at the BDB Site and 30 kips per rail at the ODB Site. These measurements were mainly intended for calibration purposes. However, the load-deflection relationships were used and extrapolated to examine the stiffnesses, the moduli of elasticity of the bridge and the track moduli.

The measured static displacements were compared to those computed assuming single concentrated loads at mid-points of partially continuous bridge spans as given in Table 5.1. Although the measured static displacements were slightly higher than the computed due to possible play in the components, they were within reasonable agreement.

The measured load-deflection curves were extrapolated to obtain the moduli of the bridge approach and normal track sections assuming linear and bi-linear relationships, as shown in Figures 3.15 and 3.16.

As the track modulus for a soft track varies with the axle load, the results of the linear analysis seem to be more appropriate for the nature of the roadbed of the test sites and for the limits of the load measurements in this investigation. However, if the measurements beyond the above mentioned limits were available indicative of a linear relationship, a bi-linear analysis would have been more meaningful [59].

Despite the fact that the stiffness of the bridge approach at each test site fell between that of the bridge span and the track section, the approach section was far from being ideal as a transition, in that its behaviour was much closer to that of the track section, as shown in Table 3.2. This is because the stiffness of the relatively short span was about three to four times the stiffness of the bridge approach, whereas the stiffness of the bridge approach was less than one and one-half times that of the track section.

Further, the approach for the open-deck bridge was found to be about thirteen percent stiffer than that for the ballast-deck. Possible reasons for this are: one, that the approach for the open-deck possessed transition ties, which allowed better dispersion of the axle load through the ballast, and two, that the value of the ballast may have been reduced on account of the wet conditions.

As a bridge approach is required to provide a smooth transition of stiffness from a track section to a bridge span to reduce the impact and the associated maintenance problems, there is a need to examine its current design with a view to further enhance its stiffness.

5.1.2 <u>Loads at Wheel-Rail Interfaces</u>

The measured values of loads at wheel-rail interfaces show a fair amount of variation even for tests at the same speed. The reasons for this kind of behaviour were discussed in section 3.6.2. However, the tendency of the dynamic load factors is to increase with increase in speed and decrease with increase in static wheel loads, as shown in Figures 3.59 to 3.64 and 3.65 to 3.70, respectively. This behaviour could be attributed amongst other factors discussed in Sections 3.6.2 and 3.7.2 to the fact that the lighter axles, i.e., of the caboose, being less stable yields larger values of dynamic load factors (DLF), compared to the heavier axles, i.e., of the locomotive and loaded cars, the masses of which lower their frequencies thereby moving away from the forcing frequencies. The forcing frequencies have resulted from a combination of track irregularities, the train speed and other factors.

Figures 5.1 and 5.2 show the percentage of the number of the dynamic load factor values which fell below a given percent of the impact for the bridge span, the bridge approach, and the track section at the BDB site and the ODB site, respectively.

The percentage of values of the dynamic load factor falling below 30% impact are given in Table 5.2. This indicates that over 90% of the recorded values possess an impact of 30% or less. Further, it indicates that those above 30% impact values generally belonged to lighter wheel loads, which appeared to be less stable than the heavier wheel loads.

5.1.2.1 Dynamic Load Factor. A comparison of two test sites, shown in Table 3.11, indicated that although the dynamic load factors for the bridge approaches and track sections were comparable, the DLF for the ballast deck span were higher than those obtained for the open deck span. This indicated that wheel impact was higher on rails with a stiffer span. However, as mentioned in Sections 3.6.2 and 3.7.2, this is attributable to several factors.

The DLF from the measurements at a speed of 50 mph has been found to be as high as 1.86 for rail over track ties, 1.65 for rail over approach ties, and 1.49 for rail over ties on the bridge span, as shown in Table 3.11. It may be noted that the maximum values of DLF occur under the axles of cabooses which are considerably lighter than the axles of locomotives or loaded cars, as shown in Table 3.11A.

Moving trains produce dynamic impacts from roll, slip, nosing etc., and vibration caused by unequal distribution of lading.

For bridge ties, A.R.E.A. Manual, Chapter, 7, Part 2, Paragraph 4 [4] states "Cross ties shall be of adequate size to distribute the track load to all stress carrying stringers...". The reference does, however, suggest an approximate method of analysis for determining the division of rail load to several stringers with different sizes and spacing of ties.

It further states, "Each tie shall be designed to carry not less than one-third of the maximum axle load, as well as to provide sufficient stiffness to properly distribute loads to the stringers. Ties shall be secured against bunching, and the maximum clear space between them, on open bridges, shall be 8 in." This investigation found that DLF for bridge ties was as high as 1.59, meaning the axle load may be carried by two consecutive ties.

For track ties, currently no real method of design has been suggested. The A.R.E.A. Manual, Chapter 3, Clause 1.4.2 states "Owing to the many variables involved, including strength of timber in its average condition in track, condition of roadbed, etc., it is not possible to calculate a design for a tie in the sense that a bridge member is designed."

No adequate way has in the past been devised to account for these effects. However, the inclusion of speed as a factor in the impact has existed for a long time.

Talbot [47, 98] has suggested that the static load be increased by 1% per mph over a speed of 5 mph, i.e.,

$$P_v/P_s = 1 + 0.01\ (V\text{-}5),\ \text{or}$$

$$DLF_{Talbot} = 1 + 0.01\ (V\text{-}5) \tag{5.1}$$

The above expression is based on 33 in. dia. wheels. Larger diameter wheels with greater contact area impose less impact on the track and give rise to an impact factor of f_1 equal to the ratio between the contact area of a 33 in. diameter wheel and that of a wheel of different diameter, i.e.,

$$f_1 = A_{33}/A_w \tag{5.2}$$

where A_{33} = contact area of a 33 in. diameter wheel = 0.19 sq. in.

A_w = contact area of a wheel of different diameter. For 40 in. diameter = 0.24 sq. in.

P_s and P_v are static and dynamic wheel loads, respectively, and

V = speed in mph

Therefore, the modified Talbot equation is

$$DLF_{Talbot} = 1 + 0.01\,(V\text{-}5)f_1 \tag{5.3}$$

The A.R.E.A. Manual, page 22-3-15 [4] applies the same procedure, but omits the 5 mph static effect. The ratio is also between the diameter D_{33} and D_w rather than between the contact areas.

$$P_v = P + \theta P \tag{5.4}$$

where

P = static wheel load

$$\theta = (D_{33} \times V)/(D_w \times 100) \tag{5.5}$$

Therefore,

$$DLF_{AREA} = 1 + \theta \tag{5.6}$$

Since the locomotives and the cars used in the test trains had wheels of 40 in. and 33 in. diameters, respectively, the above expressions for the 40 in. wheels used in this investigation would be as follows:

$$DLF_{Talbot} = 1 + 7.917 \times 10^{-3}(V\text{-}5) \tag{5.7}$$

$$DLF_{AREA} = 1 + 8.250 \times 10^{-3}(V) \tag{5.8}$$

The computed values, as well as the measured values of the DLF's are given in Table 5.3.

The above values have also been shown graphically for 33" diameter and 40" diameter wheels in Figures 5.3 and 5.4, respectively. It may be noted that at low speeds the measured values of the dynamic load factors, DLF, are higher than the computed values, except in case of cabooses for which they are generally higher than those computed from Talbot and AREA. This difference is significant in that the Talbot and AREA formulae underestimate the values at low speeds and overestimate the values at high speeds.

From the findings of this investigation, the expression of Eq. 5.8 has been modified as follows:

$$DLF_{Uppal} = 1.13 + 5.80 \times 10^{-3}V \tag{5.9}$$

These DLF's could be considered in the design of track and bridge ties as an allowance to account for the dynamic affects. However, more experimental work would be necessary to establish such factors over a wide range of speeds.

5.1.2.2 <u>Impact</u>.

The equation for impact is:

$$I = (\frac{L_d}{L_s} - 1) \times 100 \tag{5.10}$$

The values of impact, as a percentage of static loads, L_s, for the maximum values of DLF at different speeds, are given in Figures 5.5 and 5.6 for BDB and ODB sites, respectively. A majority of the plotted values correspond to lighter axles in case of these tests. As mentioned earlier in Section 3.6.2, these values are influenced by several parameters.

5.1.3 Vertical Displacements

On the ballast-deck span S3 the vertical displacements were found to be independent of speed, whereas on the ballast deck span S2, the values of vertical displacements increased slightly with increase in speed, as shown in Figures 3.71 and 3.72, respectively.

On the open-deck span S2, the vertical displacements showed a definite increase with increase in speed, but no effect was observed in the bridge approach due to increase in speed. At both test sites in the normal track sections, the vertical displacement also increased with increase in speed.

From the examination of the magnitude of the measured displacements in the bridge spans, the bridge approaches, and the normal track sections, it became evident that they were made up of three parts, namely,

(a) the rigid body movement comprising play in the components and settlement of the support points under load,

(b) the static displacement caused by rolling loads, and

(c) the displacement attributed to dynamics of the load.

Therefore, in order to ascertain the real increase in the displacement due to increase in the speed of the train, it is important to consider the amount of the rigid body movement in the bridge span.

Although the experimental set-up was not designed to isolate the amount of the rigid body movement, it was possible to obtain its value as the minimum value of displacement from the vertical displacement versus time plots, as shown in Figure 5.7 and 5.8. These values are summarized in Table 5.4. It is obvious that there is more rigid body movement in the components of the open deck bridge as opposed to the ballast-deck bridge. It may also be noted that the rigid body movement depends on the train speed, i.e., it is higher for low speeds and lower at high speeds.

The measured displacements in the open-deck span were greater than in the ballast-deck span, and the ratio of open to ballast deck displacements increased with increase in speed as shown in Table 5.5.

This could be attributed to the fact that ballast in the ballast-deck provides a cushion, thereby damping the effect of dynamic loads, in this case displaying virtually no effect of speed on the displacements.

The measured values of displacements possess the elements of rigid body movement. Consequently, the real displacements are smaller than those measured, and accordingly the actual bending stresses computed from them would also be lower than the values given above.

Similarly, in the track section, the ballast and the roadbed provided a good cushion and heavy damping occurred with the consequence that the dynamic response varied between 10 and 13 percent over that of the crawl speed.

On earlier tests [99, 100] on a bridge span of a similar configuration, it was found that the neutral axes were located at approximately one-half the depth of the stringers. This, together with the fact that the vertical displacements are proportional to the moments generated in a simple span under moving loads, the bending (including the dynamic effect) stresses were computed from the measured average net displacements for different train speeds in both the ballast deck and the open deck spans. The values obtained are given in Table 5.6.

According to the AREA Manual, for commercial grade Douglas Fir, subject to 10 years of cumulative load duration, the allowable bending stresses and moduli of elasticity are as follows:

Service Condition	Allowable Bending Stress	Modulus of Elasticity
Continuously dry	1500 - 2100 psi	1.76×10^6 psi
Wet	1500 - 2100 psi	1.60×10^6 psi

The values of the computed stresses based on the measured net displacements given in Table 5.6 are generally below the above range, indicating that the actual spans still possess significant reserve moment capacity.

It may also be observed that measured displacements under the rails of the normal track section at the ODB Site were greater than those of the same section at the BDB Site. The explanation for this is that the track at the BDB Site was of slightly better quality, i.e., was stiffer than that at the ODB Site, as this was also evident from the calibration tests.

5.1.3.1 <u>Dynamic Displacement Factor</u>. Since the measured net loads at crawl speed were fairly close to those obtained statically, they were used to calculate the dynamic load factors, DLF. For the ballast-deck, these DLF were found to be very close to unity, indicating that the span did not undergo measurable dynamic displacement under the test train within the range of the measurements, as shown in Figure 3.73.

The damping of wood and the construction of the bridge appears to have a significant influence on the displacements which, in the case of the ballast deck, exhibited virtually no response whereas in case of the open-deck span, the maximum value of DDF was 1.32, i.e., a 32% increase over the crawl speed due to dynamic effects, as shown in

Figure 3.74.

5.1.3.2 **Cycles of Vibration**. For bridge spans, approaches, and normal track sections, the displacement versus time relationships shown in Figures 3.35 to 3.52, exhibited one full cycle of vibration per truck (a truck consists of a pair of axles, see Figure 3.3) for the first and the last trucks, and one full cycle each for a pair of trucks for each of the intermediate trucks of the test train, i.e., the test train produced a total of five distinct cycles of displacement as it passed over a measurement point.

The theoretical plots of the vertical displacements for the bridge spans in Figures 4.10, 4.11, and 4.17 to 4.21 exhibited one full cycle of vibration per truck, except when the spacing of these trucks were closer where there was one full cycle of vibration for a pair of trucks, i.e., the test train produced a total of seven distinct cycles of displacement as it passed over a measurement point.

The difference between the experimental and the theoretical plots could be attributed besides factors discussed in Sections 3.6.2 and 3.7.2, to the greater stiffness of the actual spans due to partial continuity and due to the values of the damping coefficients chosen for the analytical model.

The peak values of displacement, given in Uppal [111a], seem to depend on the spacing of axles in a truck, spacing between consecutive trucks, the axle weights, and the train speed.

Further, it also appears that the bridge spans, the approaches, and the normal track sections act as mechanical systems comprising rails, ties, ballast, and stringers or roadbed where the redistribution of load from one component to another takes some time. In case of bridge spans, this time lag at higher speeds appears to be significant in comparison to the time needed for the test train to pass over a measurement point. Consequently, in such instances, the redistribution of load was not fully realized and the gauges were not able to pick up the full load.

This problem occurred during test series 1 for train speeds exceeding 30 mph. However, the problem was rectified for subsequent tests by increasing the rate of measurements (i.e., number of measurements per second). The results of the test series 1 are not included in this dissertation.

5.1.4 Accelerations

The acceleration measurements were obtained at the mid-points of the spans only. In the absence of a knowledge of the magnitudes of the accelerations for the railroad timber bridge span, the instrumentation range was set at +-10.08 g. However, apparently, the actual values at certain speeds exceeded the limit. Therefore, the measured accelerations were not used in this investigation as intended as another means of verification for the measured displacements.

5.2 THEORETICAL WORK

5.2.1 Dynamic Model

5.2.1.1 Influence of Assumptions. In this investigation, several assumptions were made to simplify the development of the theoretical model. The effect of some of the assumptions was quite evident on the predicted results, while for the others, it was nullified by their counterbalancing nature. Only the main assumptions are discussed here.

(a) The dynamic behaviour of a railway vehicle is very complex due to the number of components involved, each of which is non-linear in nature and contribute to its multiple degrees of freedom and its overall springing and damping characteristics. For the sake of simplicity, the vehicle model assumed in the analysis was only a three DOF linear system with no damping. The degrees of freedom considered were the bounce, the pitch and the roll movements because of their effect on the vertical loads and displacements. The initial values of motion as the vehicle entered the span were either assigned or assumed as zero.

The effect of the low spot at the bridge approach, which was taken as initial vertical displacement, is shown in Figure 4.17 to 4.21 and Table 4.6.

(b) The dispersion of wheel load in a ballast-deck span was superior to that in an open deck span. This was because of the composite action of the deck planks and the cushioning effect of the layer of ballast between the rails and the deck, whereas in an open-deck span, the transfer of load takes place through the bridge ties and is more concentrated. Therefore, for an open-deck, the distribution of the wheel load over a stringer chord was assumed to be parabolic with approximately three-quarters of the stringers effective in carrying the load and for the ballast-deck, all stringers were considered to be effective, except the jack stringers which were too far from the rails to take any live loads of trains.

Good agreement between the measured and computed values of loads at wheel-rail interfaces and vertical displacements justifies this assumption.

(c) The mass of timber bridge spans is neither uniformly distributed nor concentrated at any particular points. However, the model assumed the mass to be lumped at discrete points. Since the spans are short, the discrete points were fairly close to each other.

(d) The spans were assumed to be linearly elastic. This was confirmed by the calibration tests to be valid within the working range of loads.

(e) The model assumed that the wheels of the vehicle were always in contact with rails and the track surface level, and gauge was perfect and wheel surfaces were smooth and truly round. At higher speeds, aerodynamic conditions could develop, resulting in momentary loss of wheel-rail contact. Further, the drop of wheels would generate additional impact. No matter how ideal the conditions, there would always be some rail or wheel surface irregularities, however small, which would influence the dynamic response. The effect of these is that the increase in the values of the loads at wheel-rail interfaces and the vertical displacements with increase in the train speed is more consistent in the case of the predicted values in comparison to the measured values, as evident in Tables 5.7 and 5.8.

(f) A train comprising a number of cars while in motion is subject to numerous internal and external forces, some of which may be transferred from one car to another and affect the overall dynamic behaviour of the train. This may further be magnified by the geometric irregularities of the running surfaces. The model did not consider the transfer of any of such forces from one car to another. This is evident from the smoothness of the computed curves.

5.2.1.2 Input Data. The choice of input data affected the predicted values.

(a) The sprung and unsprung masses used in the numerical example were obtained by scale weighing the cars by their trucks. The spring constants and moments of inertia for different motions were assessed from a comparison of the published information on similar locomotives and cars. Therefore, the above values are, at best, estimates of the real values.

(b) Similarly, the distributed masses, and the geometric and elastic properties of the chords were computed from the available information and no attempt was made to verify them by means of tests.

5.2.1.3 Tests versus Analysis

(a) There is some degree of structural continuity inherent in the way the railroad bridge spans are constructed. Since the analytical model assumed the spans to be simply supported, the predicted values of vertical displacements are greater than those that would have been obtained with partial continuity at the end of the span as in the case of the actual bridges tested.

(b) Experimental work indicated that the values of the vertical displacements were composed of three parts: (i) the rigid body movement due to settlement of supports, and play in components, (ii) the static displacement, and (iii) the displacement due to dynamic effect of the load. The predicted values were free from any rigid body movement resulting from play in the components and settlement of the support points under load. The measured net displacements were compared with the predicted displacements in Table 5.8.

(c) In the analysis, no compression of the caps and piles was taken into account for the analytical model, though such elastic deformations could be present as a part of the rigid body movement in the bents of the test bridges under the train loads.

(d) The values of damping coefficients computed from the test data on both spans were found to have a fair amount of variation. The values used for analysis were therefore the average values.

5.3 COMPARISON BETWEEN EXPERIMENTAL AND ANALYTICAL RESULTS

5.3.1 Loads at Wheel-Rail Interfaces

The maximum value of the loads at the wheel-rail interface, as predicted by the analytical model and as measured from the tests in the field under test train no. 2 at mid-point of the spans are given in Tables 5.7 and 5.7A.

The predicted values of the maximum loads at the wheel-rail interfaces were based on absolutely smooth wheel and rail surfaces which in the case of the test bridges did have small irregularities. These irregularities affected the loads. However, in most instances, the difference between the two was about 22%.

5.3.2 Vertical Displacements

The measured net displacement is equal to the actual measured displacement less the displacement due to the rigid body movement due to the settlement of the support points of span and play in bridge components.

The maximum values of the predicted and the measured net displacements at the mid-points of the spans for the above cases are given in Tables 5.8 and 5.8A.

By comparison of the values, it may be noted that the maximum predicted displacement values increase with the increase in speed. The average values are within 16% of the measured displacements. This was expected because of the assumption used in the analytical model which assumed the spans to be simply supported, whereas, in actual fact, they were partially continuous over their supports.

Figures 5.7 and 5.8 show the comparison between the measured and predicted displacements versus time plots for the BDB Span S3 and the ODB Span S2, respectively, for test train No. 2 at 30 mph. The figures also show the rigid body movements for both spans. The effect of the semi-continuous span in the experimental plot is quite evident from the simply supported span of the analytical model. It could be noted that there is a good agreement between the measured and predicted graphs.

Table 5.10 shows the maximum values of the predicted and the measured dynamic load factors over a speed range of 1-50 mph of test train no. 2 for the ballast deck span S3 and the open deck span S2. Table 5.11 shows the maximum values of the predicted and the measured dynamic displacement factors for the same. It is evident that for the open-deck span the predicted and the measured dynamic displacement factor are 1.20 and 1.12 respectively, and in the case of the ballast deck span, these are 1.18 and 1.57, respectively. The predicted value in case of the open deck being lower may be attributed, among other factors, to the value of the damping coefficient used for the theoretical analysis.

Chapter 6

SUMMARY AND CONCLUSIONS

The investigation of the dynamic response of timber railway bridges was divided into an experimental and theoretical phase. The experimental phase involved static and dynamic tests on two types of timber bridge spans, a ballast-deck and an open-deck. Bridge approaches, and the adjacent sections of track under the passage of test trains at different speeds were also included in this investigation. The tests provided measurements of loads at wheel-rail interfaces, vertical displacements and accelerations at several locations. The theoretical phase involved the development of an analytical model to simulate the dynamic response of the bridge spans. The analytical approach was also applied to study the effects of other parameters on the dynamic behaviour of the spans, such as the effects of train speed, the low spots, and the train consist.

Based on the test results and the analytical model considered in this investigation, the following conclusions have been drawn:

1. Factors such as track irregularities, wheel running surface irregularities, rolling and hunting action of cars in trains have an effect on loads at wheel-rail interfaces, vertical displacements, and accelerations.
2. The load-deflection behaviour of the bridges is fairly linear, in contrast to the non-linear behaviour of the bridge approaches and the normal track sections.
3. The ballast-deck bridge span is comparably stiffer than the similar open deck one. Both types of bridge span are substantially stiffer than the bridge approaches, which, in turn, are stiffer than the normal track sections.

4. Although the stiffness of the bridge approach fell between the stiffnesses of the bridge span and the normal track section, its value was in fact much closer to that of the track rather than to the bridge. In general, this means that the bridge approaches should be stiffened to be able to act more effectively as transitions.

5. It was also found that the practice of using the transition ties improves the stiffness of the bridge approach by approximately 13% due to dispersion of the axle loads through the ballast section.

6. The values of track moduli for the normal track sections at both test sites were fairly close to each other and comparable to the values given by the other sources for similar quality track.

7. For both types of bridge spans, the dynamic load factors, $DLF = L_d/L_s$, increase in value with the increase of train speed. The maximum values of the measured DLF for a speed of 50 mph were as follows:

BDB Site		ODB Site	
Span S3	= 1.49	Span S2	= 1.48
Approach	= 1.61	Approach	= 1.65
Track	= 1.86	Track	= 1.78

8. The dynamic load factors decrease with increase in the static wheel loads. For the BDB Span S3, the maximum value of DLF decreased from 1.49 for the wheel of the caboose to 1.15 for the locomotive. Similarly, for ODB Span S2, the maximum value of DLF decreased from 1.48 for the wheel of the caboose to 1.30 for the locomotive.

9. For normal track sections, the values of DLF_{crawl} computed from the field measurements taken at lower speeds are generally greater than those obtained from

the empirical relationships given by Talbot and AREA. Consequently, a modified form of the relationship has been suggested for DLF.

10. For the open deck span, the dynamic displacement factors, DDF_{crawl}, increased with increase in speed with a maximum value of 1.32 over the crawl speed. On the other hand, for the ballast-deck span, speeds of up to 50 mph, did not show any effect on the dynamic displacement factors.

11. Similarly, the dynamic displacement factors, DDF_{crawl}, for normal track sections also increased with increase in speed. Their maximum values were 1.10 for the BDB Site and 1.13 for ODB Site, respectively.

12. The bending stresses in the bridge spans based on the net dynamic displacements (i.e., the dynamic displacements less the rigid body movement) were found to be lower than the permissible values given by AREA for Douglas Fir.

13. Although both types of bridge spans appeared to be heavily damped, the damping in the ballast deck was found to be approximately 50% higher than that in the open deck span.

14. The analytical model was able to predict the dynamic response of timber railroad bridge spans. The developed computer program can be used for simply supported spans of steel or concrete bridges as well. The program could be expanded to include any number of vehicles in a train.

15. The analytical model, predicts that loads at wheel-rail interfaces, vertical displacements, and accelerations increase with increase in speed.

16. The predicted values of the maximum loads at the rail-wheel interfaces, and the maximum vertical displacements were compared to those measured in the field and

the results were as follows:

(a) The values of the predicted maximum loads at wheel-rail interfaces were in agreement within 22% of the measured values

(b) The values of the predicted maximum vertical displacements were in agreement within 16% of the measured values.

(c) The rigid body movement in the open-deck span was more than three times that in the ballast deck span.

(d) The predicted values of the accelerations were very low compared to the measured ones. This was because the measured values were taken for stringers located directly under the rails, whereas the predicted values are the average values for the chords under each rail.

(e) At a train speed of 50 mph, the predicted displacements decreased with an increase in the percentage of damping coefficients, except the BDB Span for which at $\xi = 2.5\%$, the displacement reached its peak value.

17. For a constant speed, the maximum displacement values in both types of spans increased with an increase in the train consist (i.e., make-up and length), as well as with increase in the depth of the low spot at their ends. The maximum values of the predicted and measured dynamic load factors for the spans over a speed range of 1 to 50 mph were found to be as follows:

<u>Ballast-deck Span S3</u>

$DLF_{pred.} = 1.17$ $\quad$ $DLF_{measured} = 1.05$

<u>Open-deck Span S2</u>

$DLF_{pred.} = 1.28$ $\quad$ $DLF_{measured} = 1.18$

The increase in speed resulted in increase in the values of DLF. On the other hand, the increase in the static wheel loads resulted in decrease in the values of DLF.

18. The maximum values of the predicted and the measured net dynamic displacement factors of the spans over a speed range of 1 to 50 mph were found to be as follows:

Ballast-deck Span S3

$DDF_{pred.} = 1.20 \qquad DDF_{measured} = 1.12$

Open-deck Span S2

$DDF_{pred.} = 1.18 \qquad DDF_{measured} = 1.57$

The increase in speed resulted in increase in the values of DDF. The increase in speed resulted in the decrease of the value of DDF. The differences between the predicted and measured values are attributed, amongst other factors, to the assumptions made in the analytical model, particularly with respect to the track line and surface irregularities of simply supported spans, whereas in actual fact they are partially continuous, the rigid body movements and the damping characteristics, etc.

Chapter 7

SUGGESTIONS FOR FUTURE RESEARCH

Based on the conclusions drawn from this study, the following suggestions are made for future research:

1. Many railroads are now using instrumented railway vehicles to determine the performance of their track or the track quality index. These vehicles travel over the lines and collect data on track geometry (i.e., line, cross-levels, curvature, superelevation and gauge, etc.) as well as data on the rail defects. This information is for dynamic conditions only, and as such is often quite different from the static conditions upon which most of the current maintenance criteria are based.

   Since the track modulus still remains a basic quantity which reflects the strength and stability of the track, research efforts should be directed towards determining the relationship between the track modulus and the track quality index.

2. The data obtained from these tests does establish the qualitative trends for the effects of speed as well as the effects of static wheel loads on the Dynamic Load Factors. However, these tests are not sufficient to establish definite Dynamic Load Factors that could be recommended for use in the design of track and bridge ties.

   Consequently, more tests are necessary for establishing the quantitative effects of speed and other parameters on the Dynamic Load Factors.

   Similar tests could also be carried out on track sections having concrete ties.

3. In the past, some research has been carried out on the influence of wheel out-of-roundness, wheel flats, track surface roughness and rail joints on normal track

sections. This research could be extended to bridge spans as well as to bridge approaches.

4. The measured dynamic displacements appeared to be composed of three parts:

   (a) the rigid body movement,

   (b) the static displacement, and

   (c) the dynamic effect of the moving vehicle.

   In order to obtain the true dynamic effects of a vehicle on a bridge span, the amount of rigid body movement must be determined. The method used for estimating the rigid body movement needs to be verified by instrumentation of bridge to measure the relative movements of the components under the train loads.

5. The bridge approach, although found to be stiffer than the normal track section, essentially is another piece of track and, as such, was not very effective as a transition between the bridges and the track. Since the bridge approaches are often the maintenance-prone areas, further research could be directed toward the design of a suitable bridge approach which would provide a smooth transition as well as involving minimal maintenance. This may require dynamic testing of approaches with varying factors that influence their performance, such as width and depth of ballast, size, length and spacing of approach ties, concrete versus wood ties, and other measures used to maintain full ballast section as well as the effect of tamping, etc.

6. The current study dealt primarily with the determination of the dynamic response of the mid-point of bridge spans. These spans are supported on timber pile or frame bents which by themselves may be subject to movement under traffic. Further, in the majority of cases the spans are partially-continuous over bent supports. Therefore,

for full appreciation of the dynamic response of the overall bridge structure, future work should include instrumentation of the stringer chord support points, piles at cut-off levels as well as at ground levels in order to assess the distribution of live loads on piles.

7. The damping coefficients used for the analytical model were computed from the "free vibration" portion of the acceleration versus time plots. The results obtain varied considerably and therefore the average values were used for the analytical model. The damping coefficients should be verified by obtaining them by other techniques, such as exciting bridge spans to resonant frequencies or subjecting the spans to free vibrations by suddenly applied impact loading.

8. There are several conclusions drawn from the tests carried out as a part of this study. However, the number of tests and the test results are not sufficient for making definite recommendations for the dynamic load factors and the dynamic displacement factors which should be considered for the design of timber bridge or track components. More tests are needed to develop quantitative values of such factors and to cover other cases.

9. The analytical model used for this study had many simplifying assumptions which could affect the results. It is suggested that the following items be considered in any future enhancement:

   (a) Vehicle models be modified to include more degrees of freedom, as well as the damping in the vehicle suspension system;

(b) The bridge span model should be modified to include some degree of continuity at the support points; and

(c) The program should be modified to account for the wheel and rail surface irregularities.

REFERENCES

LIST OF REFERENCES

1. Ahlbeck, D.R., Johnson, M.R., Harrison, H.C., and Tuten, J.M., "Measurement of Wheel/Rail Load on Class 5 Track", Report No. FRA/ORD - 80/19, February 1980.

2. Ahlbeck, D.R. and Harrison, H.D., "Techniques for Measurement of Wheel-Rail Forces", Bettelle, Columbus Laboratories, Columbus, Ohio, pp. 31-41.

3. Al-Rashid, N., "A Theoretical and Experimental Study of Dynamic Highway Loading", Ph.D. Thesis, The University of Texas at Austin, May 1970.

4. American Railway Engineering Association, "Specification for Steel Railway Bridges", Manual for Railway Engineering, Chapters 3, 7, 15, and 22, 1984.

5. Bridge Stress Committee, Report of the "Dept. of Scientific and Industrial Research, published under the authority of His Majesty's Stationery Office, London, 1928.

6. Beards, C.F., "Structural Vibration Analysis - Modelling, Analysis and Damping of Vibrating Structures", Ellis Harwood Ltd., 1983.

7. Bleich, H.H., "Frequency Analysis of Beam and Girder Floors", ASCE Transactions, Paper No. 2416, October 1949, pp. 1023-1064.

8. Bhatti, M.H., "Vertical and Lateral Dynamic Response of Railway Bridges due to Non-Linear Vehicles and Track Irregularities", Ph.D. Thesis, Illinois Institute of Technology, Chicago, Ill., December 1982.

9. Biggs, J.M., "Introduction to Structural Dynamics", Chapter 8, McGraw Hill Book Company, New York, 1964.

10. Biggs, J.M., Suer, H.S. and Louw, J.M., "Vibration of Simple-Span Highway Bridges", Journal of the Structural Division, Proc. of the ASCE, March 1957, pp. 291-318.

11. Bolotin, V.V., "On Dynamic Calculations of Railway Bridges with Consideration Given to the Mass of the Moving Load (Russian) Trudy Moskovskogo Instituta inzhenerore zheleznodorozhnogo transporta", Vol. 76, 1952, pp. 87-107.

12. Bondar, N.G., "Dynamic Calculations of Beams Subjected to Moving Load (in Russian)", Issledovaniya poteorii sooruzhen, Vol. 6, Strorizdat, Moscow, 1954, pp. 11-23.

13. Byers, W.G., "Impact from Railway Loading on Steel Girder Spans", Journal of Structural Division, ASCE, June 1970, pp. 1093-1103.

14. Byers, W.G., "Frequency of Railway Bridge Damage", Journal of Structural Engineering, Vol. III, No. 8, ASCE, August 1985, pp. 1635-1646.

15. Cantieni, R., "Dynamic Load Tests on Highway Bridges in Switzerland, 60 Years Experience of EMPA", Report No. 211, Swiss Federal Laboratories for Materials Testing and Research, 1983, pp. 1-79.

16. Causes of Deterioration and Protective Methods for Timber -- Progress of a Sub-Committee of the Committee on Timber Structures of the Structural Division, Proc. of the ASCE, Vol. 84, No. ST5, September 1958, pp. 1760-1-1760-10.

17. Chilver, A.H., "A Note on the Mise-Kunii Theory of Bridge Vibration", Quart. J. Mech. Appl. Math., 9 (1956), No. 2, pp. 433-436.

17A. Chiu, W., Smith, R., and Wormley, D.N., "Influence of Vehicle and Distributed Guideway Dynamic Interactions", J. Dynam. Syst. Meas. Control, Trans. ASME 93(1), p. 25, 1971.

18. Chu, K.H., Garg, V.K., and Bhatti, M.H., "Impact in Truss Bridge due to Freight Trains", Journal of Engineering Mechanics, ASCE, Vol. 111, No. 2, February 1985, Paper No. 19480, pp. 159-174.

19. Chu, K.H., Garg, V.K., and Dhar, C.L., "Railway-Bridge Impact: Simplified Train and Bridge Model", Journal of the Structural Division, Proceedings of the ASCE, Vol. 105, No. ST9, September 1979, pp. 1823-1844.

20. Chu, K.H., Garg, V.K., and Wang, T.L., "Impact in Railway Prestressed Concrete Bridges", Journ. of Struct. Eng. Vol. 112, No. 5, 1986, ASCE, Paper No. 20602, pp. 1036-1051.

21. Chu, K.H., Garg, V.K. and Wiriyachai, A., "Dynamic Interaction of Railway Trains and Bridges", Vehicle System Dynamics, Vol. 9, No. 4, July 1980, pp. 207-236.

22. Chu, F.H. and Wang, B.P., "Experimental Determination of Damping Materials and Structures", Damping Applications for Vibration Control, AMD-Vol. 38, ASME.

23. Clough, R.W. and Penzien, J., "Dynamics of Structures", Chapter 13, McGraw-Hill Book Company, 1975.

24. Corbin, J.C. and Kaufman, W.M., "Classifying Track by Power Spectral Density", Mechanics of Transportation Suspension Systems, AMD-Vol. 15, ASME, December 1975, pp. 1-20.

25. Craig, R.R, "Structural Dynamics -- An Introduction of Computer Methods" John Wiley & Sons, New York, 1981.

26. Dhar, C.L., "A Method of Computing Railway Bridge Impact", Ph.D. Thesis, Illinois Institute of Technology, Chicago, Ill., May 1978.

27. Drew, F.P., "Load Considerations for Beams", Journal of the Structural Division, Proceedings of the ASCE, Vol. 85, No. ST1, January 1959, pp. 113-122.

28. El-Aini, Y.M., "Effect of Foundation Stiffness on Track Buckling", Journal of Eng. Mech. Div. of the ASCE, Vol. 102, No. EM3, June 1976, pp. 531-545.

29. Eslyn, W.E. and Clark, J.W., "Wood Bridges -- Decay Inspection and Control", Agriculture Handbook No. 557, October 1979, U.S. Government Printing Office, Washington, D.C., 20402.

30. Fazio, A.E. and Corbin, J.L., "Track Quality Index for High Speed Track", Journal of Transportation Engineering, January 1986, pp. 46-61.

31. Fish, A., "Case Studies of Timber Bridges' Problems Caused by Unit Trains", Bulletin 678 - American Railway Engineering Association, pp. 532-535.

32. Fleming, J.F. and Romualdi, J.P., "Dynamic Response of Highway Bridges", Journal of the Structural Division, Proc. of the ASCE, Vol. 87, No. ST7, October 1961, pp. 31-61.

33. Fr'yba, L., "Vibration of a Beam under the Action of a Moving Mass System", Acta Technica Academiae Scientiarum Hangaricae, 55, 1966, No. 1-2, pp. 213-240.

34. Florence, A.L., "Travelling Force on a Timoshenko Beam", Transactions of the ASME, Journal of Applied Mechanics, June 1965, pp. 351-358.

35. Freas, A.D., "Forest Service Research on Structural Use of Wood", Journal of Structural Division, ASCE, Vol. 93, ST2, April 1967, pp. 91-126.

36. Fry'ba, L., "Vibration of Solids and Structures under Moving Loads", Academia Publishing House of the Czechoslovak Academy of Sciences, Prague, 1972.

37. Ganga Rao, H.V.S., "Research in Vibration Analysis of Highway Bridges", The Shock and Vibration Digest, Vol. 16, No. 9, Sept. 1984, pp. 17-22.

38. Ganga Rao, H.V.S., and Haslebacher,m C.A., "Vibration Analysis of Highway Bridges", The Shock and Vibration Digest, Vol. 13, No. 1, Jan. 1981, pp. 3-8.

39. Gesund, H. and Young, D., "Dynamic Response of Beams to Moving Loads", Mem. Assoc. Intern. Ponts et Charpentes, 21, 1961, pp. 95-110.

40. Garg, V.K., "Computer Models for Railway Vehicle Operation", Rail International, June 1978, pp. 381-395.

41. Garivaltis, D.S. and Barg, V.K., "The Response of a Six-Axle Locomotive to Random Track Input", Report No. R-312, Association of American Railroads, Chicago, Ill., June 1978.

42. Genin, J., Ginsberg, J.H., and Ting, E.G., "Longitudinal Track-Train Dynamics: A New Approach", Journal of Dynamic Systems, Measurement and Control, ASME, December 1974, pp. 466-469.

43. Gere, J.M., and Weaver, Jr. W., "Analysis of Framed Structures", Van Nostrand Reinhold Company, New York, 1965.

44. Grassie, S.L. and Cox, S.J., "The Dynamic Response of Railway Track with Unsupported Sleepers, "Proc. of the Inst. of Mech. Engineers, Vol. 199, No. D2, 1985, pp. 123-135.

45. Gupta, R.K. "Dynamic Loading of Highway Bridges", Journal of the Engineering Mechanics Division, Proceedings of ASCE, Vol. 106, No. EM2, April 1980, pp. 377-394.

46. Hathout, I.A., "Dynamic Response of Highway Bridges", Ph.D. Thesis, University of Waterloo, 1982.

47. Hay, W.W., "Railroad Engineering", Second Edition, John Wiley and Sons, New York, 1982.

48. Hedrick, J.K., "Simulation and Analysis of Rail-Vehicle Dynamics", Presented at the Mini-Conference on Transportation, University of Michigan, Ann Arbor, MI, April 20-22, 1977.

49. Hedrick, J.K., Billington, G.F. and Dreesbach, D.A., "Analysis, design and Optimization of High Speed Suspension Using State Variable Techniques", Journal of Dynamic Systems, Measurement and Control, ASMUE, June 1974, pp. 193-203.

50. Hillerborg, A., "Dynamic Influences of Smoothly Running Loads on Simply Supported Girders", Institute of Structural Engineering and Bridge Building, Royal Institute of Technology, Stockholm, Sweden, 1951.

51. Huang, T., "Vibration of Bridges", Shock and Vibration Digest, Vol. 8, No. 3, March 1976, pp. 61-76.

52. Hunley, J.B., "Impact in Steel Railway Bridges", A.R.E.A. Proceedings, Vol. 37, 1936, p. 747.

53. Inglis, C.E., "A Mathematical Treatise on Vibration in Railway Bridges", The University Press, Cambridge, 1934.

54. Jacobsen, L.S. and Ayres, R.S., "Engineering Vibrations with Applications to Structures and Machinery", McGraw-Hill Book Company, Inc., New York, 1958.

55. Jeffcott, H.H., "On the Vibration of Beams under the Action of Moving Loads", Philosophical Magazine, Vol. 8, Series 7, pp. 66-97, 1929.

56. Jenkins, H.H., Stephenson, J.E., Clayton, G.A., Moreland, G.W., and Lyon, D., "The Effect of Track and Vehicle Parameters on Wheel/Rail Vertical Dynamic Forces", REJ, January 1974, pp. 2-26.

57. Kaplan, A. et al., "Train Elevated Guideway Interactions", TRW Systems Group, Washington, D.C., 1970.

58. Kerr, A.C., "A Method for Determining the Track Modulus Using a Locomotive or Car on Multi-Axle Trucks", Proceedings, A.R.E.A., Vol. 84, 1983.

59. Kerr, A.D., and Shenton, H.H. III, "Railroad Track Analysis and Determination of Parameters", University of Delaware, Dept. of Civil Engineering Research Report CE-85-48, February 1985.

60. Kessel, P.G. and Schlack, A.L., Jr., "On the Response of a Beam Subjected to a Cyclic Moving Load", Journal of Engineering for Industry, Trans. of the ASME, November 1969, pp. 925-930.

61. Knowles, J.K. "On the Dynamic Response of a Beam to a Randomly Moving Load", Journal of Applied Mechanics, ASME, Paper No. 67-WA/APM-30,March, 1968, pp. 1-6.

62. Koot, R.S. and Tyworth, J.E., "Railroad Track Quality measurement by Multivariate Statistical Analysis", Transportation Journal, Fall 1985, pp. 51-65.

63. Krylov, A.N., "Mathematical Collection of Papers of Academy of Sciences", Vol. 61, Peterburg, 1905.

64. Law, E.H., and Cooperrider, N.K., "A Survey of Railway Vehicle Dynamic Research", Journal of Dynamic Systems, Measurements and Control, ASME, Vol. 26, No. 2, June 1974, pp. 132-146.

65. Leggett, J.L., "Investigations of Fatigue Strength of Railroad Timber Bridge Stringers", Advance Report of Committee 7 - Wood Bridges and Trestles, 1953, pp. 161-211.

66. Levy, S., and Wilkinson, J.P.D., "The Component Element Method in Dynamics -- with Application to Earthquake and Vehicle Engineering", McGraw-Hill Inc., 1976.

67. Looney, C.T.G., "High Speed Computer Applied to Bridge Impact", Journal of Struct. Div., Proc. of the ASCE, Vol. 84, No. ST5, September 1958, pp. 1759-1-1759-41.

68. Louw, J.M., "The Vibration of Two-Span and Simple Span Highway Bridges", The Civil Engineer in South Africa, December 1963, pp. 303-314.

69. Lowan, A.N., "Oscillations of Beams under the Action of Moving Variable Loads", Philosophical Magazine, Series 7, Vol. 19, 1935, pp. 708-715.

70. Licari, J.S. and Wilson, E.N., "Dynamic Response of a Beam Subjected to a Moving Force System", Proc. Fourth U.S. Mat'l Cong. Appl. Mech., 1962, p. 419.

71. Lowan, A.N., "On Transverse Oscillations of Beams under the Action of Moving Variable Loads", Philosophical Magazine, Series[7, Vol. 19, 1935, pp. 708-715.

72. Magee, G.M., "Wood Research in the Railroad Industry", Journal of the Structural Division, Proceedings of the ASCE, Vol. 93, No. ST2, April 1967, pp. 105-120.

73. Matsuura, A., "Dynamic Behaviour of Bridge Girder for High Speed Railway Bridge", Japanese Railway - Quarterly Report, Vol. 20, No. 2, 1979.

74. Meacham, H.C., and Ahlbeck, D.R., "A Computer Study of Dynamic Loads caused by Vehicle-track Interaction", J.Eng. for Industry, Trans. ASME, 91, Ser. 8, pp. 808-816, 1969.

75. "Measurements and Their Analysis in Railway Technology", Report No. 1, 5th Intl. Colloq. ORE/BVFA Railway Vehicle Tech., Vienna, Austria, Ore Colloquia, May 6-8, 1969, (Utrecht, October 1969 AZ40/RPI/E).

76. Minnetyan, L., Nelson, R.B., and Mingori, D.L., "Dynamics and Optimal Design of AGT System", Journal of the Structural Division, ASCE, Vol. 106, No. ST4, April, 1980, pp. 897-914.

77. Mise, K., and Kunii, S., "A Theory for the Forced Vibrations of a Railway Bridge under the Action of Moving Loads", Quart. Journ. Mech. and Applied Math., Vol. IX, Pt. 2, 1956, pp. 195-211.

77A. Ng, S.F., and Kulkarni, G.G., "On the Transverse Free Vibration of Beam-Slab Type Highway Bridges", J. Sound Vib. 21(3), April 1972, pp. 259-261.

78. Newmark, N.M., "A Method of Computation for Structural Dynamics", Journal of the Engineering Mechanics Division, Proceedings of the ASCE, Vol. 85, No. EM3, July, 1959, pp. 67-94.

79. Olsson, M., "Finite Element, Modal Coordinate Analysis of Structures Subjected to Moving Loads", Journal of Sound and Vibration, 1985, 99(1), 1-12.

80. Osagaly, P. and Agarwal, A., "Vibration Study of Continuous Bridges", Ontario Ministry of Transp. and Commun.

81. Palamas, J., Coussy, O. and Bamberger, Y., "Effects of Surface Irregularities Upon the Dynamic Response of Bridges under Suspended Moving Loads", Journal of Sound and Vibration, 1985, 99(2), pp. 235-245.

82. Paz, M., "Structural Dynamics -- Theory and Computation", Van Nostrand Reinhold Company, New York, 1985.

83. Pestel, E.C., and Leckie, F.A., "Matrix Methods in Elasto Mechanics", McGraw-Hill Book Company Inc., New York, 1963.

84. Purpee, C.M., "Pressure Preserved Wood for Permanent Structures", Jour. of Struct. Div., Proc. of the ASCE, Vol. 84, No. ST7, November 1958, pp. 1841-1-1841-10.

85. Plunkett, R., "Measurement of Damping", a paper presented at Colloquium on Structural Damping, held at the ASME Annual Meeting, Atlantic City, N.J., Dec. 1959, pp. 117-131.

86. Radford, R.W., "Wheel/Rail Vertical Forces in High Speed Railway Operation", Journal of Engineering for Industry, Vol. 99, No. 4, November 1977.

87. Rao, S.S., "Mechanical Vibrations", Addison-Wesley Publishing Company Inc., Don Mills, Ontario, 1986.

88. Raymond, G.P., Lamson, S.T., and Law, J.E., "A Review of Current Track Structure Design and Future Track Research Requirements", Canadian Institute of Guided Ground Transport, Kingston, Report No. 83-6, August 1983.

89. Richardson, H.H. and Wormley, D.N., "Transportation Vehicle/Beam Elevated Guideway Dynamic Interactions: A State-of-the-Art Review", Journal of Dynamic Systems, Measurement, and Control, ASME, June 1974, pp. 169-179.

90. Robinson, S.W., "Vibration of Bridges", Transactions, ASCE, Vol. 16, Paper No. 351, February 1887, pp. 42-65.

91. Ruble, E.J., "Impact in Railroad Bridges", Proceedings, ASCE, Vol. 81, Separate No. 736, July 1955, pp. 736-1-736-36.

92. Saller, H., "Einfluss bewegter Last auf Eisenbahnoberbau und Brucken", Kreidels Verlag, Berlin, 1921.

93. Schallenkamp, A., "Schwingungen von Tragern bei bewegten Lasten", Ingenieur - Archiv, 8, 1937, pp. 182-198.

94. Skeer, M.H. and Hribar, J.A., "Dynamic Response of Systems Subjected to Moving Mass Excitations", Journal of the Franklin Institute, Vol. 287, No. 4, April 1969, pp. 319-331.

95. Stanisic, M.M., Euler, J.A. and Montgomery, S.T., "On a Theory Concerning the Dynamic Behaviour of Structures Carrying Moving Masses", Ing.-Arch. 43(5), pp. 295, 1974.

96. Steele, C.R., "The Finite Beam with a Moving Load", Journal of Applied Mechanics, ASME, March 1967, pp. 111-118.

97. Stokes, G.G., "Discussion of a Differential Equation Related to the Breaking of Railway Bridges", Cambridge University Press, 1934.

98. "Stresses in Railroad Track - The Talbot Reports", compiled and produced by Susan K. Chambers, American Railway Engineering Association, 1980.

99. "Tests of a Ballasted Floor Wood Pile Trestle -- Southern Railway System", Advance Report of Committee 30 -- Impact and Bridge Stresses, ARR, pp. 121-133.

100. "Tests of an Open Flood Wood Pile Trestle -- Missouri-Kansas-Texas Railroad", Advance Report of Committee 30 -- Impact and Bridge Stresses, AAR, pp. 103-105.

101. Thompson, W.T., "Vibration Theory and Applications", Prentice-Hall Inc., Englewood Cliffs, N.J., 1965.

102. Timoshenko, S.P., "On the Forced Vibrations of Bridges", Phil. Mag., 43, London, 1922.

103. Ting, E.C., and Yener, M., "Vehicle-Structure Interaction in Bridge Dynamics", The Shock and Vibration Digest, Vol. 15, No. 12, Dec. 1983, pp. 3-9.

104. Timoshenko, S.P., and Young, D.H., "Vibration Problems in Engineering", 3rd Ed., D. Van Nostrand Co., New York, 1955.

105. Timoshenko, S.P., "Vibration of Bridges", Paper No. RR-50-9, ASME Transactions, Vol. 49-50, Part II, 1927-28, pp. 53-61.

106. Ting, E.C., Genin, J. and Ginsberg, J.H., "Dynamic Interaction of Bridge Structures and Vehicles", The Shock and Vibration Digest, Vol. 7, No. 11, Nov. 1975.

107. Tse, F.S., Morse, I.E., and Hinkle, R.T., "Mechanical Vibrations --Theory and Applications", Allyn and Bacon, Inc., 1978.

108. Tung, C.C., "Random Response of Highway Bridges to Vehicle Loads", Journ. of the Engineering Mech. Div., Proc. of the ASCE, Vol. 93, No. EM5, October 1967, pp. 79-94.

109. Tung, T.P., Goodman, L.E., Chen, T.Y., and Newmark, N.M., "Highway Bridge Impact Problems", Highway Research Board Bull. No. 124, pp. 111-134, 1955.

110. Turneaure, F.E. et al., "Report of Committee on Impact", A.R.E.A. Proceedings, Vol. 12, Part 3, 1911, p. 13.

111. Yoshida, D.M. and Weaver, W., "Finite Element Analysis of Beams and Plates with Moving Loads", Publication of Intern. Assoc. for Bridge and Structu. Engng. 31, 1971, pp. 179-195.

111a. Uppal, S., "Experimental Results of Testing Two Timber Railway Bridges", Technical Report, Civil Engineering Department, University of Manitoba, January, 1990.

112. Velestos, A.S. and Haung, T., "Analysis of Dynamic Response of Highway Bridges", Journal of the Engineering Mechanics Division, ASCE, Vol. 96, EM5, October 1970.

113. Verna, J.R., Graham, J.F., Jr., Shannon, J.M. and Sanders, P.H., "Timber Bridges: Benefits and Costs", Journal of Structural Engineering, ASCE, Vol. 110, No. 7, July 1984, pp. 1563-1571.

114. Vernon, J.B., "Linear Vibration Theory -- Generalized Properties and Numerical Methods;", John Wiley & Sons Inc., 1967.

115. Wang, C.K., "Computer Methods in Advanced Structural Analysis", Intext International Publishers, 1973, pp. 353-354.

116. Wang, P.C., "Numerical and Matrix Methods in Structural Mechanics with Applications to Computers", John Wiley & Sons, 1966, pp.l 290-294.

117. Weaver, W., Jr., "Computer Programs for Structural Analysis", D. Van Nostrand Co., Inc., Princeton, N.J., 1967.

118. Wen, R.K., "Dynamic Response of Beams Traversed by Two-Axle Loads", Journ. of the Engineering Mech. div., Proc. of the ASCE, October, 1960, EM5, 2624, pp. 91-111.

119. Wickens, A.H., "The Dynamic Stability of a Simplified Four-Wheeled Railway Vehicle Having Profiled Wheels", Int. J. Solid Structures, 1965, Vol. 1, pp. 385-406, Pergamon Press Ltd., Great Britain.

120. Wickens, A.H., "General Aspects of Dynamics of Railway Vehicles", J. Eng. for Industry, Trans. ASMUE, 91, Ser. B., pp. 869-878, 1969.

121. Williams, J.R., and Norton, K.J., "Decay in Timber Trestles: What is the Rate of Growth?", Railway Track and Structures Magazine, April 1976.

122. Willis, R., "The Effects Produced by Causing Weights to Travel Over Elastic Bars", Appendix to the Report of Commissioners, 1849, Published in Barlow, P.: A Treatise on the Strength of Timber, Cast and Malleable Iron, London, 1851.

123. Wilson, J.F., "Model Experiments for Span-Vehicle Dynamics", Journal of Eng. Mech. Div., Proc. of the ASCE, Vol. 103, No. EMA, August 1977, pp. 701-715.

124. Wiriyachai, A., Chu, K.H., and Garg, V.K., "Bridge Impact due to Wheel and Track Irregularities", Journal of the Engineering Mechanics Division, Proceedings of the ASCE, Vol. 108, No. EM4, August 1982, pp. 648-666.

125. Wormley, D.N., Garg, D.P. and Richardson, H.H., "A Comparative Study of the Non-linear and Linear Performance of Vehicle Air Cushion Suspensions Using Bond Graph Models", J. Dyn. Syst. Meas. and Control, Trans. ASME, 94(3), 1972, p. 189.

TABLES

Table 3.1 Scale weights of locomotives and cars

Description	Truck Weights (lbs) Leading	Truck Weights (lbs) Trailing	Total Weights (lbs)
(a) Test Train No. 1 -- 11 July 1986			
1. Locomotive CN #5516	124,220	123,560	247,780
2. Hopper Car CN #090151	101,740	104,700	206,440
3. Hopper Car CN #302360	96,090	101,700	197,760
4. Caboose CN #79384	31,300	31,520	62,820
(b) Test Train No. 2 - 16 September 1986			
1. Locomotive CN #5608	126,900	125,800	252,760
2. Hopper Car CN #090159	88,480	98,700	187,180
3. Hopper Car CN #090151	100,840	103,760	204,600
4. Caboose CN #79715	30,580	30,240	60,820

Table 3.2 Static displacements and stiffnesses

Location	Static Deflection mm @ load = 31.7 kips	Stiffness kips/inch
(a) BDB Site - Test Train No. 1		
Ballast Deck Bridge Span S3	2.40	335.76
Bridge Approach	9.78	82.90
Track Section (only LR)	11.64	69.23
(b) ODB Site - Test Train No. 2		
Open Deck Bridge Span S2	2.68	300.67
Bridge Approach	8.58	93.92
Track Section	12.06	66.82

Table 3.3 Maximum recorded loads at wheel-rail interfaces, L_d (kips)
BDB Site - Test Train No. 2 - September 16, 1986

Speed (mph)	Span S3		Approach		Track		Remarks
	Stat	Dyna	Stat	Dyna	Stat	Dyna	
1	31.45	34.57	31.45	34.13	31.73	35.64	
30	31.45	36.04	31.73	40.63	31.73	38.43	
50	31.73	36.00	31.73	50.93	31.73	43.60	

Table 3.4 Maximum recorded loads, at wheel-rail interfaces, L_d (kips)
ODB Site - Test Train No. 2- September 16, 1986

Speed (mph)	Span S2		Approach		Track		Remarks
	Stat	Dyna	Stat	Dyna	Stat	Dyna	
1	31.73	34.62	31.73	36.43	31.73	35.30	
30	31.45	40.77	31.73	41.26	31.45	38.43	
50	31.73	34.57	31.45	40.00	31.73	39.21	

Table 3.5 Maximum recorded vertical displacements, D_d (mm)
BDB Site - Test Train No. 2 - September 16, 1986

Speed (mph)	Span S3		Approach		Track		Remarks
	Stat	Dyna	Stat	Dyna	Stat	Dyna	
1	5.22	4.03	-	4.10	11.92	10.14	Test #8
30	5.46	4.00	-	4.14	12.43	9.89	Test #10A, 10A, 10
50	5.39	4.17	-	4.71	13.31	11.12	Test #11, 11A, 11

Note: * LVDT at L.R. Span S2 did not function.

Table 3.6 Maximum recorded vertical displacements, D_d (mm)
ODB Site - Test Train No. 2 - September 16, 1986

Speed (mph)	Span S2		Approach		Track		Remarks
	Stat	Dyna	Stat	Dyna	Stat	Dyna	
1	6.29	6.36	9.77	10.02	13.73	12.13	Test #22AA
30	7.54	6.43	9.45	10.16	13.87	13.12	Test #24AA, #24C
50	8.11	8.32	9.80	9.71	15.66	13.58	Test #25B, #25C

Table 3.7 Maximum and minimum recorded accelerations (g)
BDB Site - Test Train No. 2 - Bridge Span S3

Speed (mph)	Left Rail		Right Rail		Remarks
	Maximum	Minimum	Maximum	Minimum	
1	+0.75	-1.06	+0.08	-0.13	Test #8
30	+4.10	-4.86	+5.86	-2.09	Test #10A
50	*	-7.00	+3.16	-4.65	Test #11B

Table 3.8 Maximum and minimum recorded accelerations (g)
ODB Site - Test Train No. 2 - Bridge Span S2

Speed (mph)	Left Rail		Right Rail		Remarks
	Maximum	Minimum	Maximum	Minimum	
1	+0.23	-0.21	+0.33	-0.38	Test #22AA
30	*	*	*	*	Test #24
50	*	*	*	*	Test 25A

Table 3.9 Track modulus K (lbs/in^2) - Linear approach

Location	Bridge Approach	Normal Track
BDB Site	944.30	748.67
ODB Site	1124.38	714.11

Table 3.10 Track modulus K (lbs/in^2) - Bi-linear approach

Location	Bridge Approach	Normal Track
BDB Site		
K_o	290.11	196.82
w_o	0.08	0.21
K_1	1,129.26	1,306.88
ODB Site		
K_o	269.27	223.77
w_o	0.18	0.28
K_1	2425.22	1623.10

Table 3.11 Upper limits of dynamic load factors, DLF = L_d/L_s

Speed (mph)	Bridge Span S3, S2	Approach	Track
(a) BDB Site - Test Train No. 2			
1	1.25	1.23	1.13
10	1.28*	1.17*	1.23*
30	1.28*	1.47	1.40
50	1.49*	1.61*	1.86*
(b) ODB - Test Train No. 2			
1	1.16*	1.17*	1.11*
5	1.19*	1.16*	1.16*
10	1.26	1.43	1.19
15	1.25	1.23*	1.17*
20	1.36	1.23	1.28
30	1.43	1.40	1.59
40	1.39	1.43	1.45
50	1.48*	1.65	1.78

Note: * indicates incomplete information on a test train run.

Table 3.11A Maximum values of DLF by maximum static wheel loads of cars

(a) BDB Site - Test Train No. 2

Particulars	Heaviest Static Wheel (kips)	Maximum DLF		
		Span S3	Approach	Track
1. Locomotive	31.73	1.15	1.61*	1.37*
2. OTH Car #1	24.68	1.27	1.56	1.19
3. OTH Car #2	25.94	1.26	1.59	1.24
4. Caboose	7.65	1.49	1.60	1.86

(b) ODB Site - Test Train No. 2

Particulars	Heaviest Static Wheel (kips)	Maximum DLF		
		Span S3	Approach	Track
1. Locomotive	31.73	1.30	1.27	1.25
2. OTH Car #1	24.68	1.23	1.34	1.34
3. OTH Car #2	25.94	1.29	1.25	1.45
4. Caboose	7.65	1.48	1.65	1.78

* Not compatible with other values

Table 3.12 Values of maximum shear, moment and deflection for mid-point of a span per chord

Length (ft-in)	Shear (kips)	Moment (ft-kips)	Deflection (insx1000/EI)	Deflection[1] (mm)
		TEST TRAIN NO. 1		
Simple Span				
11'-3"	-14.51	+81.63	-1860.71	-2.68(-2.14)[2]
11'-6"	-14.87	+85.53	-2012.78	-2.89(-2.32)
12'-0"	-15.55	+93.30	-2340.65	-3.37(-2.71)
Continuous Three Span Bridge (11'-6½", 11'-6", 11'-6")*				
	-16.42	-24.18	-908.87	-1.31
	+14.07	+52.92	+690.81	+0.99
Continuous Four Span Bridge (10'-0", 12'-0", 11'-3", 11'-8")**				
	-16.83	-19.38	-899.39	-1.29(-1.04)
	+14.11	+51.96	+529.87	+0.08(+0.06)
Continuous Four Span Bridge (10'-0", 12'-0", 11'-3", 11'-8")***				
	-18.00	-13.76	-1140.28	-1.64(-1.31)
	+11.54	+58.88	+428.25	+0.62(+0.49)
		TEST TRAIN NO. 2		
Simple Span				
11'-3"	-14.79	83.20	-1897.34	-2.73(-1.31)
11'-6"	-15.16	87.18	-2052.40	-2.95(-2.36)
12'-0"	-15.85	95.10	-2386.73	-3.43(-2.75)
Continuous Three Span Bridge (11'-6 ½", 11'-6", 11'-6")*				
	-16.74	-24.62	-993.03	-1.43
	+14.34	+53.79	+703.08	+1.01
Continuous Four Span Bridge (10'-0", 12'-0", 11'-3", 11'-8")**				
	-17.15	-19.62	-928.36	-1.34(-1.07)
	+14.38	+52.58	+536.68	+0.77(+0.62)
Continuous Four Span Bridge (10'-0", 12'-0", 11'-3", 11'-8")***				
	-18.35	-14.02	-1126.86	-1.62(-1.30)
	+11.76	+58.61	+436.07	+0.63(+0.50)

Notes: 1. Deflections are based on:
(a) Modulus of elasticity, $E = 1.65 \times 10^6$ psi
(b) Moment of inertia, I per chord = 10,095.04 in^4 without jack stringers and = 12,616.30 in^4 with jack stringers
2. Values of deflections within parentheses are with I, including jack stringers
3. One inch = 25.4 millimeters
4. * Values for midspan ** Values for 11'-3" span
*** Values for 12'-0" span

Table 3.13 Computed damping coefficient - BDB Site - Span S3

Speed (mph)	Damping Coefficients (% age) Left Rail	Damping Coefficients (% age) Right Rail	Test #
10	5.92	5.28	9
30	3.62	6.57	10B
30	10.03	9.65	10B
30	4.83	-	10B
50	10.15	13.95	11B
50	18.60	19.19	11B
Mean $\bar{\xi}$ =	8.86	10.9	
Std. Deviation σ =	5.50	5.7	

Combined average $\bar{\xi}$ = 9.8% Std. Dev. σ = 5.4

Table 3.14 Computed Damping Coefficient - ODB Site - Span S2

Speed (mph)	Damping Coefficients (% age) Left Rail	Damping Coefficients (% age) Right Rail	Test #
10	6.37	9.09	23
10	6.14	6.85	23
30	4.99	3.91	24B
30	8.06	5.83	24B
30	4.74	3.20	24C
30	5.61	7.56	24C
30	8.63	-	24C
30	5.11	-	24C
50	5.09	5.82	25A
50	5.21	6.61	25A
50	6.68	-	25A
50	7.84	6.45	25C
Mean $\bar{\xi}$ =	6.21	6.15	
Std. Deviation σ =	1.34	1.78	

Combined average $\bar{\xi}$ = 6.2% Std. Dev. σ = 1.5

Table 4.1 Bridge span data

	Particulars	Ballast-deck Bridge, Span 3	Open-deck Bridge, Span 2
1.	Span length, 1 (in)	144.00	138.00
2.	No. of stringers per chord	5	4
3.	Effective no. of stringers per chord	4	3
4.	Nominal size of stringers (in x in)	8 x 16	8 x 16
5.	Density of Douglas Fir, ρ (lb/in^3)	0.34722×10^{-1}	0.34722×10^{-1}
6.	Weight of track and deck per chord, w (lb/in)	96.00	96.00
7.	Damping coefficient as percentage of critical damping, ξ	9.8	6.2
8.	No. of segments/chord, n_s	10	10
9.	Centre to centre spacing of chords, d (in)	60.28	60.97
10.	Dist. of 1st rail to near side chord d_n (in)	0.97	1.03
11.	Dist. of 2nd rail to near side chord, d_f (in)	59.97	60.03
12.	Modulus of elasticity of Douglas Fir, E (lb/in^2)	1.65×10^6	1.65×10^6

Notes: (i) Acceleration due to gravity, $g = 386.4$ in/sec^2

(ii) One inch = 25.4 mm

Table 4.2 Vehicle trains data

	Particulars	Locomotive	OTH Car	OTH Car	Caboose
Test Train No. 1		CN #5516	CN #090151	CN #302360	CN #79384
1.	Body mass, M_b (lb-sec^2/in)	641.25	534.27	511.80	162.58
2.	Sprung mass, M_c associated with each wheel (lb-sec^2/in)	69.11	62.25	59.44	15.66
3.	Unsprung mass, M_u associated with each wheel (lb-sec^2/in)	11.05	4.53	4.53	4.53
4.	Body pitch moment of inertia, I_b (lb-in-sec^2)	1.98x10^7	1.66x10^7	1.66x10^7	0.27x10^7
5.	Body roll moment of inertia, J_b (lb-in-sec^2)	1.17x10^6	1.28x10^6	1.28x10^6	0.24x10^6
6.	Vertical spring stiffness/wheel, K_v (lb/in)	3324.00	11020.00	11020.00	1600.00
7.	Half dist. between truck centers, l_t (in)	204.00	190.25	187.75	164.88
8.	Half dist. between two wheel-axle sets of a truck, l_w (in)	54.00	34.00	34.00	34.00
9.	Half dist. between two wheel-rail points of a wheel-axle set, d_c (in)	29.50	29.50	29.50	29.50
10.	Dist. between last axle of one vehicle and first axle of following vehicle, l_v (in)	0.00	138.25	82.50	118.50
Test Train No. 2		CN #5608	CN #090159	CN #090151	CN #79715
1.	Body mass, M_b (lb-sec^2/in)	654.14	484.42	529.50	157.40
2.	Sprung mass, M_c associated with each wheel (lb-sec^2/in)	70.62	56.02	61.66	15.10
3.	Unsprung mass, M_u associated with each wheel (lb-sec^2/in)	11.05	4.53	4.53	4.53
4.	Body pitch moment of inertia, I_b (lb-in-sec^2)	1.98x10^7	1.66x10^7	1.66x10^7	0.27x10^7
5.	Body roll moment of inertia, J_b (lb-in-sec^2)	1.17x10^6	1.28x10^6	1.28x10^6	0.24x10^6
6.	Vertical spring stiffness/wheel, K_v (lb/in)	3324.00	11020.00	11020.00	1600.00
7.	Half dist. between truck centers, l_t (in)	204.00	190.25	109.25	164.88
8.	Half dist. between two wheel-axle sets of a truck, l_w (in)	54.00	34.00	34.00	34.00
9.	Half dist. between two wheel-rail points of a wheel-axle set, d_c (in)	29.50	29.50	29.50	29.50
10.	Dist. between last axle of one vehicle and first axle of following vehicle, l_v (in)	0.00	138.25	82.50	118.50

Notes: (i) The vertical damping constant of vehicle(s), C_v taken as "0" lb-sec/in

(ii) Time step, Δt, used was = 0.001 seconds

(iii) Source of the vehicle trains data is CN Rail Equipment Department

Table 4.3 Effect of train speed - Test Train No. 2 - Mid-point of open-deck bridge, Span S2

(a) Predicted maximum loads at wheel-rail interfaces (kips)

Speed (mph)	Left Rail	Right Rail	Average
1	31.74	31.45	31.59
10	32.24	32.21	32.22
30	33.68	34.31	34.00
50	40.30	40.33	40.32

(b) Predicted maximum vertical displacements (mm)

Speed (mph)	Left Rail	Right Rail	Average
1	4.40	4.42	4.41
10	4.49	4.46	4.48
30	4.56	4.57	4.53
50	5.20	5.22	5.21

(c) Predicted maximum and minimum accelerations (g)

Speed (mph)	Left Rail		Right Rail	
	Maximum	Minimum	Maximum	Minimum
1	+0.19	-0.19	+0.06	-0.05
10	+0.45	-0.43	+0.46	-0.42
30	+1.71	-1.60	+1.49	-1.44
50	+3.70	-3.03	+3.69	-2.89

Table 4.3A Effect of train speed - Test Train No. 2 - Mid-point of ballast-deck bridge, Span S3

(a) Predicted maximum loads at wheel-rail interfaces (kips)

Speed (mph)	Left Rail	Right Rail	Average
1	31.78	31.25	31.52
10	32.15	32.76	31.96
30	33.77	34.94	34.36
50	36.47	36.68	36.58

(b) Predicted maximum vertical displacements (mm)

Speed (mph)	Left Rail	Right Rail	Average
1	3.68	3.76	3.72
10	3.97	4.05	4.01
30	4.03	4.12	4.07
50	4.41	4.50	4.46

(c) Predicted maximum and minimum accelerations (g)

Speed (mph)	Left Rail		Right Rail	
	Maximum	Minimum	Maximum	Minimum
1	+0.05	-0.07	+0.02	-0.05
10	+0.23	-0.28	+0.18	-0.17
30	+0.77	-0.82	+0.74	-0.72
50	+1.52	-1.47	+1.68	-1.50

Table 4.4 Effect of train consist - Test Train No. 2 - Mid-point of open-deck bridge, Span S2, Speed 50 mph

(a) Predicted maximum loads at wheel-rail interfaces (kips)

Train Consist	Left Rail	Right Rail	Average
(i) Locomotive	46.56	43.31	44.94
(ii) Locomotive and 1st OTH Car	49.22	42.64	45.93
(iii) Locomotive and two OTH Cars	45.37	44.39	44.88
(iv) Locomotive, two OTH Cars and Caboose	40.30	40.33	40.32

(b) Predicted maximum vertical displacements (mm)

Train Consist	Left Rail	Right Rail	Average
(i) Locomotive	4.04	4.05	4.05
(ii) Locomotive and 1st OTH Car	4.94	4.91	4.93
(iii) Locomotive and two OTH Cars	5.23	5.21	5.22
(iv) Locomotive, two OTH Cars and Caboose	5.20	5.22	5.21

(c) Predicted maximum and minimum accelerations (g)

Train Consist	Left Rail		Right Rail	
	Max	Min	Max	Min
(i) Locomotive	+5.22	-4.89	+6.76	-6.57
(ii) Locomotive and 1st OTH Car	+6.34	-5.54	+8.04	-10.14
(iii) Locomotive and two OTH Cars	+7.43	-7.80	+7.32	-7.39
(iv) Locomotive, two OTH Cars and Caboose	+3.70	-3.03	+3.69	-2.89

Table 4.5 Effect of bridge deck type - test train No. 2
- Mid-point of Spans S3 and S2

(a) Average max. predicted loads at wheel-rail interfaces (kips)

Speed (mph)	Ballast-deck Bridge Span S3	Open-deck Bridge Span S2
1	31.51	31.59
10	31.96	32.22
30	34.36	34.00
50	36.58	40.32

(b) Average max. predicted vertical displacements (mm)

Speed (mph)	Ballast-deck Bridge Span S3	Open-deck Bridge Span S2
1	3.72	4.41
10	4.01	4.48
30	4.07	4.53
50	4.46	5.21

Table 4.6 Effect of low spot at bridge approach
Test train No. 2 - Mid-point of open-deck bridge, span S2
- Speed 50 mph

(a) Predicted max. loads at wheel-rail interfaces (kips)

Low Spot (inch)	Left Rail	Right Rail	Average
0.0	40.30	40.33	40.32
0.5	40.16	41.76	40.96
1.0	41.70	42.97	42.34
1.5	44.43	44.19	44.32
2.0	50.59	45.41	48.00

(b) Predicted max. vertical displacements (mm)

Low Spot (inch)	Left Rail	Right Rail	Average
0.0	5.20	5.22	5.21
0.5	5.43	5.45	5.44
1.0	6.39	6.41	6.40
1.5	7.41	7.49	7.45
2.0	8.25	8.58	8.42

(c) Predicted max. and minimum accelerations (g)

Low Spot (inch)	Left Rail		Right Rail	
	Max.	Min.	Max.	Min.
0.0	+3.03	-3.70	+3.69	-2.89
0.5	+3.34	-4.64	+3.34	-3.78
1.0	+4.58	-5.47	+4.64	-5.18
1.5	+6.47	-7.15	+6.78	-7.19
2.0	+8.54	-8.82	+8.93	-9.36

Table 4.7 Effect of damping coefficient
Test Train No. 2 - Bridge spans - Speed 50 mph

Damping Coefficient $\xi\%$	Predicted maximum vertical displacements (mm)					
	Ballast-deck span S3			Open-deck span S2		
	Left Rail	Right Rail	Average	Left Rail	Right Rail	Average
0.0	4.52	4.55	4.54	5.35	5.37	5.36
2.5	4.71	4.79	4.75	5.24	5.26	5.25
5.0	4.62	4.72	4.67	5.21	5.23	5.22
6.2	-	-	-	5.20	5.22	5.21
7.5	4.50	4.60	4.55	5.18	5.20	5.19
9.8	4.41	4.50	4.45	-	-	-
10.0	4.40	4.49	4.45	5.14	5.15	5.15
12.5	4.32	4.41	4.37	-	-	-
15.0	4.25	4.35	4.30	5.05	5.06	5.05
20.0	4.16	4.24	4.20	4.96	4.98	4.97

Table 4.8 Effect of method of numerical integration
Open-deck bridge span S2 - Test train No. 2
- Speed 50 mph

(a) Maximum loads at wheel-rail interface (kips)

Method	Left Rail	Right Rail	Average
Newmark's-ß	40.30	40.33	40.32
Houbolt	41.10	40.53	40.81

(b) Maximum vertical displacements (mm)

Method	Left Rail	Right Rail	Average
Newmark's-ß	5.20	5.22	5.21
Houbolt	5.19	5.21	5.20

(c) Maximum and minimum accelerations (g)

Method	Left Rail		Right Rail		Average	
	Max.	Min.	Max.	Min.	Max.	Min.
Newmark's-ß	+3.70	-3.03	+3.69	-2.89	+3.70	-2.96
Houbolt	+1.68	-1.41	+1.68	-1.41	+1.68	-1.41

Table 5.1 Measured versus computed static displacements

	Measured Static Displacement (mm)	Computed Static Displacement (mm)
Ballast Deck Bridge		
Span S3	2.40	2.41
Open Deck Bridge		
Span S2	2.68	2.65

Note: The above is based on:
(1) Calibration tests
(2) Static displacements assuming partially continuously supported spans
(3) For the BDB bridge, the jack stringers assumed to be participating in carrying the train load

Table 5.2 Percent of the DLF values below 30% impact--Loads at wheel-rail interfaces. BDB and ODB Sites, Test Train No. 2

Particulars	Percentage < 30%
BDB Site	
Bridge Span S3	97.8
Approach	80.6
Track	92.1
ODB Site	
Bridge Span S2	94.8
Approach	96.9
Track	92.1

Table 5.3 Comparison between the computed and measured dynamic load factors, DLF

Speed (mph)	DLF_{Talbot} 40 in.	DLF_{Talbot} 33 in.	DLF_{AREA} 40 in.	DLF_{AREA} 33 in.	$DLF_{Measured}$ BDB Site 40 in.	BDB Site 33 in. Car	BDB Site 33 in. Caboose	ODB Site 40 in.	ODB Site 33 in. Car	ODB Site 33 in. Caboose
Stat	1.00	1.00	1.00	1.00	1.00	1.00	-	1.00	1.00	-
1	1.00	1.00	1.01	1.01	1.13	1.11	-	1.11	1.12	-
5	1.00	1.00	1.04	1.05	-	-	-	1.12	1.16	-
10	1.04	1.05	1.08	1.10	1.15	1.19	1.23	1.14	1.19	1.17
15	1.08	1.10	1.12	1.15	-	-	-	1.12	1.17	-
20	1.12	1.13	1.17	1.20	-	-	-	1.13	1.28	-
30	1.20	1.25	1.25	1.30	1.21	1.24	1.46	1.22	1.38	1.59
40	1.28	1.35	1.33	1.40	-	-	-	1.25	1.45	1.42
50	1.36	1.45	1.41	1.50	1.37	1.24	1.86	1.25	1.35	1.78

Table 5.4 Measured rigid body movements (mm) at mid-points of bridge spans - Test Train No. 2.

Speed (mph)	Ballast-deck Span S3 Left Rail	Ballast-deck Span S3 Right Rail	Ballast-deck Span S3 Average	Open-deck Span S2 Left Rail	Open-deck Span S2 Right Rail	Open-deck Span S2 Average
1	0.71	0.73	0.72	1.85	2.50	2.18
10	0.68	0.70	0.69	1.74	2.46	2.10
20	0.55	0.55	0.55	1.67	2.45	2.06
30	0.50	0.51	0.50	1.65	2.27	1.96
50	0.50	0.45	0.47	1.50	2.25	1.88

Table 5.5 Ratio of Measured Displacements, Open versus Ballast Deck

Speed (mph)	Ratio
1	1.05
10	1.09
30	1.20
50	1.44

Table 5.6 Average dynamic bending stresses (psi)

(a) Ballast Deck Span S3

Speed (mph)	Average Net Displacement (mm)	Average Bending Stress Including the Dynamic Effect (psi)
1	4.63 - 0.72 = 3.91	926.04
10	4.68 - 0.69 = 3.99	944.99
30	4.68 - 0.50 = 4.18	989.99
50	4.78 - 0.47 = 4.31	1020.78

Note: Measured static displacement by calibration test = 2.40 (mm) and the static bending stress = 568.4 (psi)

(b) Open Deck Span S2

Speed (mph)	Average Net Displacement (mm)	Average Bending Stress Including the Dynamic Effect (psi)
1	6.33 - 2.18 = 4.15	1070.19
10	6.45 - 2.10 = 4.35	1121.77
30	6.93 - 1.96 = 4.97	1281.65
50	8.08 - 1.88 = 6.22	1604.00

Note: Measured static displacement by calibration test = 2.68 (mm) and the static bending stress = 691.11 (psi)

Table 5.7 Maximum loads at wheel-rail interfaces (kips)
Test Train No. 2 - Midpoint of bridge spans

Speed (mph)	Predicted			Measured		
	Left Rail	Right Rail	Average	Left Rail	Right Rail	Average
(A) Ballast-deck bridge, span S3						
1	31.25	31.78	31.52	34.54	34.24	34.39
10	31.76	32.15	31.96	35.55	-	-
30	33.77	34.94	34.36	36.04	35.00	35.52
50	36.47	36.68	36.58	35.70	36.00	35.85
(B) Open-deck bridge, span S2						
1	31.74	31.45	31.59	34.62	33.06	33.84
10	32.24	32.21	32.23	35.60	34.18	34.89
30	33.68	34.31	34.00	40.77	36.04	38.41
50	40.30	40.33	40.32	31.20	34.57	32.89

Table 5.7A Ratios of maximum loads at wheel-rail interfaces (kips), DLF
- Test Train No. 2 - Midpoint of bridge spans

Speed (mph)	Predicted L_d/L_{crawl}			Measured L_d/L_{crawl}		
	Left Rail	Right Rail	Average	Left Rail	Right Rail	Average
(a) Ballast-deck bridge, Span S3						
1	1.00	1.00	1.00	1.00	1.00	1.00
10	1.02	1.01	1.01	1.03	-	1.03
30	1.08	1.10	1.09	1.04	1.02	1.03
50	1.17	1.15	1.16	1.03	1.05	1.04
(b) Open-deck bridge, Span S2						
1	1.00	1.00	1.00	1.00	1.00	1.00
10	1.02	1.02	1.02	1.03	1.04	1.03
30	1.06	1.09	1.08	1.18	1.09	1.14
50	1.27	1.28	1.28	0.90	1.05	0.98

Table 5.8 Maximum vertical displacements (mm)
Test Train No. 2 - Midpoint of bridge span

Speed (mph)	Predicted			Measured Net		
	Left Rail	Right Rail	Average	Left Rail	Right Rail	Average
(a) Ballast-deck bridge, span S3						
1	3.68	3.76	3.72	4.52	3.32	3.92
10	3.97	4.05	4.01	4.55	3.41	3.98
30	4.03	4.12	4.07	4.80	3.45	4.13
50	4.41	4.50	4.45	4.89	3.72	4.31
(b) Open-deck bridge, span S2						
1	4.40	4.42	4.41	4.44	3.86	4.15
10	4.49	4.46	4.48	4.75	3.94	4.35
30	4.56	4.57	4.53	5.78	4.16	4.97
50	5.20	5.22	5.21	6.33	6.07	6.20

Note: Measured net displacement is equal to the actual measured displacement less displacement due to the rigid body movement, i.e., tightening of the components of a span and the settlement of support points, etc. The values of the rigid body movements are given in Table 5.4.

Table 5.8A Ratios of maximum vertical displacements (mm), DDF
Test Train No. 2 - Midpoint of bridge spans

Speed (mph)	Predicted D_d/D_{crawl}			Measured D_d/D_{crawl}		
	Left Rail	Right Rail	Average	Left Rail	Right Rail	Average
(a) Ballast-deck Bridge, Span S3						
1	1.00	1.00	1.00	1.00	1.00	1.00
10	1.08	1.08	1.08	1.01	1.03	1.02
30	1.09	1.10	1.09	1.06	1.04	1.05
50	1.20	1.20	1.20	1.08	1.12	1.10
(b) Open-Deck Bridge, Span S2						
1	1.00	1.00	1.00	1.00	1.00	1.00
10	1.02	0.99	1.01	1.07	1.02	1.05
30	1.04	1.03	1.03	1.30	1.08	1.20
50	1.18	1.18	1.18	1.43	1.57	1.49

Table 5.9 Maximum and minimum accelerations (g)
Test Train No. 2 - Midpoint of bridge spans

Speed (mph)		Predicted Left Rail	Predicted Right Rail	Measured Left Rail	Measured Right Rail
(a) Ballast deck-bridge, span S3					
1	Max	-0.08	+0.02	+0.75	+0.08
	Min	+0.07	-0.02	-1.06	-0.13
10	Max	+0.21	+0.21	+4.52	+1.11
	Min	-0.24	-0.25	-5.18	-0.81
30	Max	+0.86	+0.72	+4.10	+5.86
	Min	-0.82	-0.73	-4.86	-2.09
50	Max	+1.37	+1.49	*	+3.16
	Min	-1.38	-1.43	-7.00	-4.65
(b) Open-deck Bridge, span S2					
1	Max	+0.19	+0.06	+0.23	+0.33
	Min	-0.19	-0.05	-0.21	-0.38
10	Max	+0.45	+0.46	+5.78	+3.07
	Min	-0.43	-0.42	-3.63	-2.51
30	Max	+1.71	+1.41	*	*
	Min	-1.60	-1.44	*	*
50	Max	+3.70	+3.69	*	*
	Min	-3.03	-2.87	*	*

Note: * $\pm$ 10.08 g was the limit set for measurement; these values exceeded the limit

Table 5.10 Maximum values of predicted and measured dynamic load factors, DLF - Test train No. 2 - Speed range 1 to 50 mph

Location	Predicted DLF $= L_d/L_{crawl}$	Measured DLF $= L_d/L_{crawl}$
BDB Site 1 Span S3	1.16	1.02
ODB Site 2 Span S2	1.28	1.14

Table 5.11 Maximum values of predicted and measured dynamic displacement factors, DDF - Test Train No. 2 - Speed range 1 to 50 mph

Location	Predicted DLF $= D_d/D_{crawl}$	Measured DLF $= D_d/D_{crawl}$
BDB Site Span S3	1.20	1.12
ODB Site Span S2	1.18	1.57

SENSITIVITIES OF MEASURING DEVICES

a) Test Series #1 - BDB Site - test train no. 1

Channel	Location	Measurement	Unit	Sensitivity mVolt/unit
1	S3-R	Load	kips	0.10E+00
2	S3-L	Load	kips	0.10E+00
3	A-R	Load	kips	0.10E+00
4	A-L	Load	kips	0.10E+00
5	T-R	Load	kips	0.10E+00
6	T-L	Load	kips	0.10E+00
7	S3-R	Accel.	g	0.13E+00
8	S3-L	Accel.	g	0.11E+00
9	S3-R	Displ.	mm	0.15E+00
10	S3-L	Displ.	mm	0.17E+00
11	S2-L	Displ.	mm	0.14E+00
12	S2-R	Displ.	mm	0.18E+00
13	A-R	Displ.	mm	0.17E+00
14	A-L	Displ.	mm	0.24E+00
15	T-R	Displ.	mm	0.18E+00
16	T-L	Displ.	mm	0.17E+00

Notes: 1. For locations of gauges, refer to Figure 3.5.
2. Channel #17 was control channel measuring time in seconds.

SENSITIVITIES OF MEASURING DEVICES

b) Test Series #2 - ODB Site - test train no. 2

Channel	Location	Measurement	Unit	Sensitivity mVolt/unit
1	S2-R	Load	kips	0.10E+00
2	S2-L	Load	kips	0.10E+00
3	A-R	Load	kips	0.10E+00
4	A-L	Load	kips	0.10E+00
5	T-R	Load	kips	0.10E+00
6	T-L	Load	kips	0.10E+00
7	S2-R	Accel.	g	0.99E+00
8	S2-L	Accel.	g	0.99E+00
9	S2-R	Displ.	mm	0.17E+00
10	S2-L	Displ.	mm	0.14E+00
11	-	-	-	-
12	-	-	-	-
13	A-R	Displ.	mm	0.15E+00
14	A-L	Displ.	mm	0.17E+00
15	T-R	Displ.	mm	0.23E+00
16	T-L	Displ.	mm	0.18E+00

Notes: 1. For locations of gauges, refer to Figure 3.6.
2. The channel numbers and gauge locations for the tests done with locomotive runs were the same as for the test train no. 1 runs.
3. Channel #17 was control channel measuring time in seconds.

SENSITIVITIES OF MEASURING DEVICES

c) Test Series #2 - BDB Site - test train no. 2

Channel	Location	Measurement	Unit	Sensitivity mVolt/unit
1	S3-R	Load	kips	0.10E+00
2	S3-L	Load	kips	0.10E+00
3	S2-R	Load	kips	0.10E+00
4	S2-L	Load	kips	0.10E+00
5	T-R	Load	kips	0.10E+00
6	T-L	Load	kips	0.10E+00
7	-R	Accel.	g	0.99E+00
8	-L	Accel.	g	0.99E+00
9	S3-R	Displ.	mm	0.14E+00
10	S3-L	Displ.	mm	0.14E+00
11	-	-	-	-
12	-	-	-	-
13	S2-R	Displ.	mm	0.15E+00
14	S2-L	Displ.	mm	0.17E+00
15	T-R	Displ.	mm	0.23E+00
16	T-L	Displ.	mm	0.18E+00

Notes: 1. For locations of gauges, refer to Figure 3.5.
2. Channel #17 was control channel measuring time in seconds.

LISTING OF COMPUTER PROGRAM

```
//DYTMOPN  JOB ',,,T=25M','UPPAL'
//STEP1  EXEC  WATFIV,SIZE=2000K
//GO.SYSIN  DD  *
$JOB  WATFIV   UPPAL
C
C  ----------------------------------------------------------------
C   PROGRAM NAME "DYTMOPN"
C  ----------------------------------------------------------------
C
C   THIS PROGRAM DETERMINES THE DYNAMIC RESPONSE OF A TIMBER RAILROAD
C   BRIDGE SPAN SUBJECTED TO ONE OR UPTO FOUR 4-AXLE RAILWAY VEHICLES
C   (I.E. LOCOMOTIVES OR CARS) MOVING AT A CONSTANT SPEED.
C
C  ----------------------------------------------------------------
C  VEHICLE MODEL
C  ----------------------------------------------------------------
C
C     A FOUR AXLE VEHICLE IS IDEALIZED AS A RIGID BODY WITH THREE
C     DEGREES OF FREEDOM I.E. BOUNCE, PITCH, AND ROLL MOTION.
C     THE VERTICAL SPRINGS ARE TAKEN AS LINEAR. VEHICLE DAMPERS
C     ARE TAKEN AS ZERO. UP TO FOUR VEHICLES HAVE BEEN CONSIDERED
C     IN THE MATHEMATICAL MODEL.
C     COUPLING BETWEEN THE VEHICLES ARE ASSUMED TO BE PROVIDED BY
C     UNIVERSAL JOINTS. VEHICLES MAY OR MAY NOT BE IDENTICAL.
C     THE WHEELS OF THE VEHICLES ARE ASSUMED TO ALWAYS REMAIN IN CONTACT
C     WITH THE RAILS OF THE TRACK AT ALL TIMES.
C
C  ----------------------------------------------------------------
C  BRIDGE SPAN MODEL
C  ----------------------------------------------------------------
C
C     A LUMPED MASS IS ASSUMED FOR THE RAILROAD BRIDGE SPAN.HTHE
C     SPAN IS ASSUMED TO BE SIMPLY SUPPORTED AT ITS ENDS.
C     EACH CHORD OF THE SPAN IS DIVIDED INTO TEN EQUAL SEGMENTS
C     AND DISTRIBUTED MASS OF THE TRACK SYSTEM AND CHORD IS
C     CONSIDERED AS CONCENTRATED AT THE SEGMENT CONNECTION POINTS
C     (OR NODES).
C     ONLY VERTICAL DEGREE OF FREEDOM IS ASSIGNED TO EACH NODE.
C     ALL DISPLACEMENTS ARE ASSUMED TO BE SMALL AND THE EFFECT OF
C     ROTARY INERTIA AND NON-LINEARITY OF MATERIAL ARE NEGLECTED
C     IN THE ANALYSIS.
C
C  ----------------------------------------------------------------
C  BASIS OF ANALYSIS
C  ----------------------------------------------------------------
C
C     1. FORMULATE EQUATIONS OF MOTION OF VEHICLES AND CHORDS OF SPAN
C        AS WELL AS EXPRESSIONS FOR THE INTERACTION FORCES BETWEEN
C        WHEELS AND RAILS.
C     2. CONSTRUCT MASS,DAMPING,AND STIFFNESS MATRICES FOR VEHICLE
C        BODIES AND CHORDS OF THE SPAN.
C          - STIFFNESS MATRIX OBTAINED BY INVERSION OF FLEXIBILITY MATRIX
C            OF CHORD.
C          - FUNDAMENTAL FREQUENCIES OF CHORDS OBTAINED BY EIGENVALUE
C            SOLUTION ASSUMING FREE HARMONIC VIBERATIONS.
C          - DAMPING MATRIX FOR CHORDS TAKEN AS PRODUCT OF DAMPING COEFF.
C            ,FUNDAMENTAL FREQUENCIES AND MASS MATRIX.
C     3. USING GENERAL COORDINATES FOR MASS,STIFFNESS AND LOAD, CONTRI-
C        BUTION OF WHEEL POSITION AT A GIVEN SPAN SEGMENT WAS ADDED TO
C        THE OVERALL MASS,DAMPING AND STIFFNESS MATRICES AND TO THE
```

```
C             FORCE VECTORS.
C          4. THE RESULTING EQUATIONS OF MOTION OF THE SYSTEM WERE INTEGRATED
C             USING NEWMARK BETA METHOD TO OBTAIN DYNAMIC DISPLACEMENTS,
C             VELOCITIES AND ACCELERATIONS.
C          5. FROM NO.4 AND THE STATIC DISPLACEMENTS, THE DYNAMIC DISPLACEMNT
C             FACTORS WERE COMPUTED.
C
C   -----------------------------------------------------------------
C
C   SYMBOLS USED IN PROGRAM
C   -----------------------------------------------------------------
C
C   CONTROL SYMBOLS:
C   ----------------
C
C       KK1 = 5; FOR READER
C       KK2 = 6; FOR PRINTER
C       VALUES OF KK1 AND KK2 MAY BE RE-ASSIGNED FOR READ/WRITE ON TAPE.
C
C       IPRNTM = 1; MASS,STIFFNESS,AND INVERT MATRICES ARE PRINTED
C       IPTM = 0;PRINT NODAL VALUES,=1;PRINT TIME VALUES,=2;ALSO PRINT
C                MATRICES IN DYNA SUBROUTINE AND OTHER NODAL VALUES.
C       LCAR = 1; FOR ONE VEHICLE; 2, FOR TWO ETC. UP TO FOUR  VEHICLES
C       EPS = SMALL NO. TO TEST WHETHER ANY DIAGONAL ELEMENT IS ZERO OR
C             NOT
C
C   BRIDGE SPAN SYMBOLS:
C   --------------------
C
C       N = ACTIVE NO. OF NODAL POINTS IN A CHORD
C       M = NO. OF NODAL POINTS IN BOTH CHORDS = 2.*N
C       NP = NO. OF CHORD SEGMENTS AFFECTED BY WHEEL LOADS
C       XPL = LENGTH OF A SEGMENT OF CHORD
C       AG = CROSS SECTIONAL AREA OF A CHORD
C       XI = MOMENT OF INERTIA OF A CHORD
C       RHO = MASS DENSITY OF MATERIAL OF CHORD
C       RO = WT. OF TRACK AND DECK OF BRIDGE PER CHORD PER INCH
C       E = MODULUS OF ELASTICITY OF MATERIAL OF CHORD
C       DC = DAMPING CONSTANT FOR BRIDGE CHORD
C       NDK = TYPE OF BRIDGE DECK; =0,FOR OPEN AND =1,FOR BALLAST
C       C = CENTER TO CENTER DISTANCE BET. TWO CHORDS
C       D1 = DISTANCE OF FIRST RAIL TO NEARSIDE CHORD
C       D2 = DISTANCE OF SECOND RAIL TO NEARSIDE CHORD
C
C   VEHICLES SYMBOLS:
C   -----------------
C
C       SM1,2,3,4 = SPRUNG MASSES ASSOCIATED WITH EACH WHEEL OF
C                   VEHICLE NO.1,2,3 AND 4 RESPECTIVELY
C       UM1,2,3,4 = UNSPRUNG MASSES OF WHEELS OF VEHICLES NO.1,2,3 & 4
C       XMB1,2,3,4 = BODY MASSES OF VEHICLES NO.1,2,3 & 4
C       XJJB1,2,3,4 = BODY PITCH MOMENT OF INERTIAS OF VEHICLES NO.1,2,3&4
C       XJB1,2,3,4 = BODY ROLL MOMENT OF INERTIAS OF VEHICLES NO. 1,2,3&4
C       NW = NO. OF ROLLING WHEELS ASSOCIATED WITH VEHICLE BODIES
C       XLB1,2,3,4 = HALF DISTANCES BET. TRUCK CENTERS OF VEHICLES 1,2,3&4
C       BB1,2,3,4 = HALF DISTANCES BET. TWO AXLE SETS OF VEHICLES 1,2,3&4
C       BA1,2,3,4 = HALF DISTANCES BET. RAIL-WHEEL CONTACT POINTS ON ONE
C                   WHEEL-AXLE SET FOR VEHICLE 1,2,3 AND 4 ETC.
C       XKY1,2,3,4 = VERTICAL SPRING STIFFNESSES PER WHEEL FOR VEH. 1,2,3,
C       CY1,2,3,4 = VERTICAL DAMPERS PER VEHICLE 1,2,3&4 ; TAKEN =0.
C       DIST1,2,3,4 = DISTANCES BET. LAST AXLE OF FRONT VEHICLE AND FIRST
C                     AXLE OF REAR VEHICLE ETC.
C
C   MISCELLANEOUS SYMBOLS:
```

```
C ---------------------
C
C     NN = 2*N+3*LCAR = M+3*LCAR OVERALL SIZE OF ROWS AND COLUMNS
C          IN RESULTING MATRICES AND VECTORS
C     DT = VALUE OF EACH TIME INCREMENT
C     NINC = NO. OF TIME INCREMENTS
C     G = ACCELERATION DUE TO GRAVITY
C     VEL = VELOCITY OF VEHICLE OR TRAIN OF VEHICLES
C
C ----------------------------------------------------------------

C DESCRIPTION OF THE INPUT DATA
C ----------------------------------------------------------------

C - CARD NO. 1 --------FORMAT:  6(D12.6)
C ----------------------------------------------------------------

C   COLUMNS:01 TO 12; MODULUS OF ELASTICITY =E ;LB/IN**2
C          :13 TO 24; ACCELERATION DUE TO GRAVITY =G ;386.4IN/SEC**2
C          :25 TO 36; MASS DENSITY OF MATERIAL =RO ;LB-SEC**2/IN
C ----------------------------------------------------------------

C --CARD NO.  2 -------FORMAT:  6(D12.6)  ---- SERIES OF 4 CARDS
C ----------------------------------------------------------------

C   COLUMNS:01 TO 12; CAR BODY MASS =XMB1 ;LB-SEC**2/IN
C          :13 TO 24; SPRING MASS ASSOCIATED WITH EACH WHEEL =SM1 ;LB
C                     -SEC**2/IN
C          :25 TO 36; UNSPRUNG MASS = MASS OF WHEEL =UM1 ;LB-SEC**2/IN
C          :37 TO 48; CAR BODY PITCH MOMENT OF INERTIA =XLLB1;B-IN-SEC2

C          :49 TO 60; CAR BODY ROLL MOMENT OF INERTIA =XJB1;LB-IN-SEC**

C ----------------------------------------------------------------

C --CARD NO.  3 -------FORMAT:  6(D12.6) ----- SERIES OF 4 CARDS
C ----------------------------------------------------------------

C   COLUMNS:01 TO 12; VERTICAL SPRING STIFFNESS PER WHEEL =XKY1,LB/IN
C          :13 TO 24; HALF DISTANCE BETWEEN TRUCK CENTERS =XLB1,IN
C          :25 TO 36; HALF DISTANCE BETWEEN TWO WHEEL AXLE SETS =BB1,IN

C          :37 TO 48; HALF DISTANCE BETWEEN TWO WHEELS ON ONE WHEEL
C                     AXLE SET =BA1,IN
C          :49 TO 60; CONSTANT FOR VERTICAL DAMPER OF VEHICLE =CY1
C          :61 TO 72; DIST. BET. LAST AXLE OF FIRST VEHICLE AND
C                      FIRST AXLE OF REAR VEHICLE =DIST1,IN
C ----------------------------------------------------------------

C --CARD NO.  4 -------FORMAT:  10I5
C ----------------------------------------------------------------

C   COLUMNS: 1 TO  5; NO. OF ACTIVE NODAL POINTS =N
C          : 6 TO 10; FOR IPRNTM=1, MASS MATRIX, STIFFNESS MATRIX AND
C                     INVERT MATRIX ARE PRINTED
C          :11 TO 15; FOR IPTM=1, MATRICES IN DYNAL SUBROUTINE PRINTED
C          :21 TO 25; FOR LCAR=1,ONE VEHICLE AND NOT=1, FOUR VEHICLES
C ----------------------------------------------------------------

C --CARD NO.  5 -------FORMAT:  (3(D12.6),1I4)
C ----------------------------------------------------------------

C   COLUMNS:01 TO 12; GROSS SECTIONAL AREA OF CHORD =AG ,IN**2
C          :13 TO 24; LENGTH OF CHORD SEGMENT =XPL ,IN
C          :25 TO 36; MOMENT OF INERTIA OF CHORD =XI ,IN**4
C          :37 TO 40; TYPE OF DECK =NDK ,=0 FOR OPEN,=1 FOR BALLAST
C ----------------------------------------------------------------

C --CARD NO.  6 -------FORMAT:  (3I4,3(D12.6))
C ----------------------------------------------------------------
```

```
C     COLUMNS:01 TO 04; NO. OF SEGMENTS AFFECTED BY WHEEL LOADS =NP
C            :05 TO 08; NO. OF ROLLING WHEELS ASSOCIATED WITH BODY =NW
C            :09 TO 12; NO. OF TIME INCREMENTS =NINC
C            :13 TO 24; VALUE OF EACH TIME INCREMENT =DT ,SEC
C            :25 TO 36; VELOCITY OF VEHICLE =VEL ,IN/SEC
C            :37 TO 48; DAMPING CONSTANT FOR TRESTLE SPAN(SCALAR QTY) =DC

C -------------------------------------------------------------------

C --CARD NO.  7 -------FORMAT:  (6(D12.6))
C -------------------------------------------------------------------

C     COLUMNS:01 TO 12; C/C DISTANCE BETWEEN TWO CHORDS =C ,IN
C            :13 TO 24; DISTANCE OF 1ST. RAIL TO NEARSIDE CHORD =D1 ,IN
C            :25 TO 36; DISTANCE OF 2ND. RAIL TO NEARSIDE CHORD =D2 ,IN
C -------------------------------------------------------------------

C --CARD NO.  8 -----FORMAT:  (32I2)
C -------------------------------------------------------------------

C     COLUMNS: 1 TO 48; FAC1(I)
C            :48 TO 96; FAC2(J)
C            :97 TO 144; FAC3(K)
C -------------------------------------------------------------------

C     ---------------------------------------------------------------

C
C     MAIN PROGRAM
C
C     ---------------------------------------------------------------

C
      IMPLICIT REAL*8(A-H,O-Z)
      COMMON/BLOCK 1/XLAMD1,XLAMD2,ZETA1,ZETA2
      DIMENSION SB(30,30),XMASS(30,30),FLEX(20,20),BS(20,20)
      DIMENSION XMSAT(10,10),FLEXI(10,10)
C
      CALL INDATA(E,G,RHO,N,IPRNTM,AG,XPL,XI,NP,NW,NINC,DT,VEL,DC,
     1NN,KK2,M,IPTM,LCAR,NDK,XMB1,UM1,SM1,XJJB1,XJB1,XMB2,UM2,SM2,
     2XJJB2,XJB2,XMB3,UM3,SM3,XJJB3,XJB3,XMB4,UM4,SM4,XJJB4,XJB4,XKY1,
     3XLB1,BB1,BA1,CY1,DIST1,XKY2,XLB2,BB2,BA2,CY2,DIST2,XKY3,XLB3,BB3,
     4BA3,CY3,DIST3,XKY4,XLB4,BB4,BA4,CY4,DIST4)
C
      CALL DYNAL(N,NN,E,SB,XL,XI,XPL,RHO,IPRNTM,XMASS,KK2,NW,VEL,NP,G,
     1DT,NINC,FLEX,AG,M,DC,IPTM,LCAR,BS,XMSAT,FLEXI,NDK,XMB1,UM1,SM1,
     2XJJB1,XJB1,XMB2,UM2,SM2,XJJB2,XJB2,XMB3,UM3,SM3,XJJB3,XJB3,
     3XMB4,UM4,SM4,XJJB4,XJB4,
     4XKY1,XLB1,BB1,BA1,CY1,DIST1,XKY2,XLB2,BB2,BA2,CY2,DIST2,
     5XKY3,XLB3,BB3,BA3,CY3,DIST3,XKY4,XLB4,BB4,BA4,CY4,DIST4)
C
      STOP
      END
C
C -------------------------------------------------------------------

C   THIS SUBROUTINE READS AND WRITES ALL INPUT DATA NECESSARY FOR
C   THE DYNAMIC ANALYSIS OF VEHICLE - SPAN SYSTEM
C -------------------------------------------------------------------

C
      SUBROUTINE INDATA(E,G,RHO,N,IPRNTM,AG,XPL,XI,NP,NW,NINC,DT,VEL,DC,

     1NN,KK2,M,IPTM,LCAR,NDK,XMB1,UM1,SM1,XJJB1,XJB1,XMB2,UM2,SM2,XJJB2,

     2XJB2,XMB3,UM3,SM3,XJJB3,XJB3,XMB4,UM4,SM4,XJJB4,XJB4,XKY1,XLB1,BB1

     3,BA1,CY1,DIST1,XKY2,XLB2,BB2,BA2,CY2,DIST2,XKY3,XLB3,BB3,BA3,CY3,
     4DIST3,XKY4,XLB4,BB4,BA4,CY4,DIST4)
C
      IMPLICIT REAL*8(A-H,O-Z)
```

```
      COMMON/BLOCK 1/XLAMD1,XLAMD2,ZETA1,ZETA2
C
      KK1=5
      KK2=6
C
C   INPUT OF GENERAL DATA .
C
C   **** READ CARD NO. 1 ****
C
      READ(KK1,10)E,G,RO
   10 FORMAT(6(D12.6))
      WRITE(KK2,20)
   20 FORMAT(1H1,//,20X,'*** PROGRAM INPUT DATA ***'///'*** UNITS ARE IN
     1 MILLIMETERS,POUNDS AND SECONDS UNLESS OTHERWISE STATED ***' /)
      WRITE(KK2,30)E,G,RO
   30 FORMAT(10X,'MODULUS OF ELASTICITY =',D14.6/10X,'GRAVITY =',D14.6/1
     10X,'DENSITY =',D14.6//)
      RHO=RO/G
C
C   DATA RELATED TO RAILWAY VEHICLE(S)
C
C   **** READ CARD SERIES NO. 2 ****
C
      READ(KK1,10)XMB1,UM1,SM1,XJJB1,XJB1
      READ(KK1,10)XMB2,UM2,SM2,XJJB2,XJB2
      READ(KK1,10)XMB3,UM3,SM3,XJJB3,XJB3
      READ(KK1,10)XMB4,UM4,SM4,XJJB4,XJB4
      WRITE(KK2,40)XMB1,UM1,SM1,XJJB1,XJB1
      WRITE(KK2,40)XMB2,UM2,SM2,XJJB2,XJB2
      WRITE(KK2,40)XMB3,UM3,SM3,XJJB3,XJB3
      WRITE(KK2,40)XMB4,UM4,SM4,XJJB4,XJB4
   40 FORMAT(10X,'CAR BODY MASS =',D14.6/10X,'UNSPRUNG MASS =',D14.6/10X
     1,'SPRUNG MASS =',D14.6/10X,'PITCH MOI =',D14.6/10X,'ROLL MOI =',D1
     24.6/)
C
C   **** READ CARD SERIES NO. 3 ****
C
      READ(KK1,10)XKY1,XLB1,BB1,BA1,CY1,DIST1
      READ(KK1,10)XKY2,XLB2,BB2,BA2,CY2,DIST2
      READ(KK1,10)XKY3,XLB3,BB3,BA3,CY3,DIST3
      READ(KK1,10)XKY4,XLB4,BB4,BA4,CY4,DIST4
      WRITE(KK2,50)XKY1,XLB1,BB1,BA1,CY1,DIST1
      WRITE(KK2,50)XKY2,XLB2,BB2,BA2,CY2,DIST2
      WRITE(KK2,50)XKY3,XLB3,BB3,BA3,CY3,DIST3
      WRITE(KK2,50)XKY4,XLB4,BB4,BA4,CY4,DIST4
   50 FORMAT(10X,'SPRING STIFFNESS =',D14.6/10X,'HLF DIST TRK CRS =',D14
     1.6/10X,'HLF LENGTH OF WHEEL BASE =',D14.6/10X,'HLF DIST BET TWO WH
     2EELS =',D14.6/10X,'VEHICLE DAMPING CONST =',D14.6/10X,'DIST BET TW
     3O VEHICLES =',D14.6//)
C
C   CODES FOR VARIOUS OUTPUT CONTROL OPTIONS
C
C   **** READ CARD NO. 4 ****
C
      READ(KK1,70)N,IPRNTM,IPTM,LCAR
      WRITE(KK2,60)N,IPRNTM,IPTM,LCAR
   60 FORMAT(10X,'NO OF ACT NOD PTS =',1I5/10X,'IPRNTM=1;FOR PRINT =',1I
     15/10X,'IPTM=2,FOR PRINT MATRICES IN DYNAL =',1I5/10X,
     2'LCAR=1,FOR ONE CAR =',1I5//)
   70 FORMAT(10I5)
      M=2*N
      NN=M+3*LCAR
C
```

```
C     DATA RELATED TO TIMBER BRIDGE SPAN
C
C     **** READ CARD NO. 5 ****
C
         READ(KK1,80)AG,XPL,XI,NDK
      80 FORMAT(3(D12.6),1I4)
         WRITE(KK2,90)AG,XPL,XI,NDK
      90 FORMAT(10X,'X-SECTIONAL AREA OF CHORD =',D14.6/10X,'SEGMENT LENGTH
        1 =',D14.6/10X,'MOI OF CHORD =',D14.6/10X,'TYPE OF DECK =',1I4//)
C
C     DATA FOR DYNAL SUBROUTINE
C
C     **** READ CARD NO. 6 ****
C
         READ(KK1,100)NP,NW,NINC,DT,VEL,DC
         WRITE(KK2,110)NP,NW,NINC,DT,VEL,DC
     100 FORMAT(3I4,3(D12.6))
     110 FORMAT(10X,'NO. OF SEGMENTS =',I14/10X,'NO OF WHEELS =',I14/10X,
        1'NO OF TIME INC =',I14/10X,'VALUE OF TIME INC =',D14.6/10X,'VELOCI
        2TY OF VEHICLE =',D14.6/10X,'DAMPING CONST OF SPAN =',D14.6//)
         IF(LCAR.EQ.1) NW=8
         IF(LCAR.EQ.2) NW=16
         IF(LCAR.EQ.3) NW=24
         IF(LCAR.EQ.4) NW=32
C
C     **** READ CARD NO. 7 ****
C
         READ(KK1,10)C,D1,D2
         WRITE(KK2,120)C,D1,D2
     120 FORMAT(10X,'CC DIST BET TWO CHORDS =',D14.6/10X,'DIST BET 1ST RAIL
        1AND NS CHORD =',D14.6/10X,'DIST BET 2ND RAIL AND NS CHORD =',
        2D14.6//)
         XLAMD1=D1/C
         XLAMD2=1.-XLAMD1
         ZETA1=D2/C
         ZETA2=1.-ZETA1
         RETURN
         END
C
C     ----------------------------------------------------------------
C     THIS SUBROUTINE COMPUTES THE DYNAMIC RESPONSE OF RAILROAD TIMBER
C     BRIDGE SPAN DUE TO VEHICLE - SPAN INTERACTION
C     ----------------------------------------------------------------
C
C     XMASS(NN,NN) = OVERALL MASS MATRIX OF TWO CHORDS PLUS CONTRIBUTION
C                    OF VEHICLE BODIES
C     XMSAT(N,N) =
C     SB(NN,NN) = STIFFNESS MATRIX OF CHORD
C     FLEX(M,M) = FLEXIBILITY MATRIX
C     DAMP(M,M) = DAMPING MATRIX OF CHORD ONE AND TWO
C     BS(NN,NN) =
C     FLXI(N,N) =
C     EIGV(N) = EIGENVALUES FOR ONE CHORD
C     SV(M) = DEAD LOAD SHEAR FORCE VECTOR
C     BM(M) = DEAD LOAD BENDING MOMENT VECTOR
C     Y(NW) = DIST. OF A PARTICULAR WHEEL FROM THE ORIGIN
C     FR(NN) = EXTERNAL FORCE VECTOR
C     DELTA(N,N) = FLEXIBILITY MATRIX OF ONE CHORD
C
         SUBROUTINE DYNAL(N,NN,E,SB,XL,XI,XPL,RHO,IPRNTM,XMASS,KK2,NW,VEL,
        1NP,G,DT,NINC,FLEX,AG,M,DC,IPTM,LCAR,BS,XMSAT,FLEXI,NDK,XMB1,UM1,
        2SM1,XJJB1,XJB1,XMB2,UM2,SM2,XJJB2,XJB2,XMB3,UM3,SM3,XJJB3,XJB3,
        3XMB4,UM4,SM4,XJJB4,XJB4,
        4XKY1,XLB1,BB1,BA1,CY1,DIST1,XKY2,XLB2,BB2,BA2,CY2,DIST2,XKY3,
        5XLB3,BB3,BA3,CY3,DIST3,XKY4,XLB4,BB4,BA4,CY4,DIST4)
C
```

```
      IMPLICIT REAL*8(A-H,O-Z)
      COMMON/BLOCK 1/XLAMD1,XLAMD2,ZETA1,ZETA2
      INTEGER FAC1(32),FAC2(32),FAC3(32)
      DIMENSION SB(NN,NN),XMASS(NN,NN),Y(32)
      DIMENSION FLEX(M,M),BS(M,M),XMSAT(N,N),FLEXI(N,N)
      DIMENSION DAMP(30,30);FR(30),SBT(30,30),XMASST(30,30)
      DIMENSION UO(30),VO(30),AAO(30),UU(30),V(30),AC(30),US(18),DDF(18)
      DIMENSION SV(18),BM(18),EIGV(10),FREQ(20),FF(18)
      DATA EPS/0.1D-04/
C
C     **** READ CARD SERIES NO. 8 ****
C
  100 READ(5,120) (FAC1(I),I=1,32)
      READ(5,120) (FAC2(J),J=1,32)
      READ(5,120) (FAC3(K),K=1,32)
  120 FORMAT(32I2)
C
C     INITIAL DISPLACEMENT AND VELOCITY VECTORS
C
      DO 140 J=1,NN
      UO(J)=0.
  140 VO(J)=0.
      UO(20)=+0.0008110
      IF(LCAR.EQ.1) GO TO 160
      UO(23)=-0.0024373
      IF(LCAR.EQ.2) GO TO 160
      UO(26)=-0.0006963
      IF(LCAR.EQ.3) GO TO 160
      UO(29)=+0.0006444
  160 CONTINUE
C
C     MASS MATRIX
C
  180 CALL XMASB(N,NN,AG,XPL,RHO,KK2,IPRNTM,M,XMASS,LCAR,XMSAT,NDK,XMB1,
     1XJJB1,XJB1,XMB2,XJJB2,XJB2,XMB3,XJJB3,XJB3,XMB4,XJJB4,XJB4,G)
C
C     STIFFNESS MATRIX
C
      CALL STIFF(N,NN,XI,E,XPL,KK2,M,SB,FLEX,IPRNTM,DAMP,BS,LCAR,FLEXI,
     1XKY1,XLB1,BB1,BA1,CY1,XKY2,XLB2,BB2,BA2,CY2,XKY3,XLB3,BB3,BA3,CY3,
     2XKY4,XLB4,BB4,BA4,CY4)
C
      DO 240 J=1,NN
      FR(J)=0.
      IF(XMASS(J,J).EQ.0.0) GO TO 200
      AAO(J)=FR(J)/XMASS(J,J)
      GO TO 220
  200 AAO(J)=0.
  220 CONTINUE
      DO 240 K=1,NN
      SBT(J,K)=SB(J,K)
  240 XMASST(J,K)=XMASS(J,K)
C
C     EIGENVALUES SOLUTION FOR NATURAL FREQUENCIES
C
      CALL EIGEN(FLEXI,XMSAT,N,N,EPS,EIGV,KK2,IPRNTM)
C
      DO 280 K=1,N
  260 FREQ(K)=1.*DSQRT(EIGV(1))
  280 CONTINUE
      DO 300 J=1,N
      JJ=J+N
  300 FREQ(JJ)=FREQ(J)
C
C     DAMPING MATRIX
C
      DO 320 I=1,M
      DO 320 J=1,M
```

```
  320 DAMP(I,J)=XMASST(I,J)*FREQ(I)*DC*2.
  340 CONTINUE
C
      IF(NDK.EQ.0) GO TO 370
      IF(NDK.EQ.1) GO TO 360
      GO TO 430
  360 WRITE(KK2,420)
      GO TO 430
  370 WRITE(KK2,400)
  400 FORMAT(1H1,//,20X,' **** DYNAMIC RESPONSE OF TIMBER RAILROAD BRIDG
     1E ****'//30X,' *** OPEN     DECK *** '///28X,' ** OUTPUT AS FOLLOW
     2S ** '//)
  420 FORMAT(1H1,//,20X,' **** DYNAMIC RESPONSE OF TIMBER RAILROAD BRIDG
     1E ****'//30X,' *** BALLAST  DECK *** '///28X,' ** OUTPUT AS FOLLOW
     2S ** '//)
  430 CONTINUE
C
      T=0.
      XL=(N+1)*XPL
      VL1=2.*(XLB1+BB1)+DIST1
      VL2=2.*(XLB2+BB2)+DIST2+VL1
      VL3=2.*(XLB3+BB3)+DIST3+VL2
      VL4=2.*(XLB4+BB4)+DIST4+VL3
      IF(LCAR.EQ.1) XLT=VL1/XL+1.5
      IF(LCAR.EQ.2) XLT=VL2/XL+1.5
      IF(LCAR.EQ.3) XLT=VL3/XL+1.5
      IF(LCAR.EQ.4) XLT=VL4/XL+1.5
C
C     START OF TIME INTEGRATION
C
C     ICOUNT = DYNAMIC DISPLACEMENT FOR CHORD
C     JCOUNT = STATIC DISPLACEMENT FOR CHORD
C     MCOUNT = LOAD AT WHEEL - RAIL INTERFACE
C     NUMB TO SET THE WRITE INTERVAL AT EVERY "NKN" VALUE
      ICOUNT=0
      JCOUNT=0
      MCOUNT=0
      NUMB=0
C
C     CONTROL OF WRITE INTERVT WHEEL-RAIL INTERFACE
C
      DLTX=VEL*DT
      NKN=2
      DLXX=2.*DLTX
C
C     THE BIG TIME LOOP BEGINS   ******
C
      DO 5040 J=1,NINC
C
      ICOUNT=ICOUNT+1
      JCOUNT=JCOUNT+1
      MCOUNT=MCOUNT+1
      NUMB=NUMB+1
C
      IF(NINC.EQ.1) GO TO 620
C
      DO 520 L=1,NN
      FR(L)=0.
      DO 520 K=1,NN
      SB(L,K)=SBT(L,K)
  520 XMASS(L,K)=XMASST(L,K)
C
      IF(IPTM.NE.2) GO TO 600
      WRITE(KK2,2400)(FR(K),K=1,NN)
      DO 540 I=1,NN
  540 WRITE(KK2,2400)(SB(I,K),K=1,NN)
      DO 560 I=1,NN
```

```
      560 WRITE(KK2,2400)(XMASS(I,K),K=1,NN)
          DO 580 I=1,NN
      580 WRITE(KK2,2400)(DAMP(I,K),K=1,NN)
      600 CONTINUE
C
      620 T=J*DT
          XX=VEL*T
          XXL=XX/XL
          IF(XXL.GT.XLT) GO TO 6000
C
C     POSITIONING OF WHEELS ON CHORD SEGMENTS
C
C     VEHICLE NO. 1
C
          Y(1)=VEL*T
          Y(2)=Y(1)
          Y(3)=Y(1)-2.*BB1
          Y(4)=Y(3)
          Y(5)=Y(1)-2.*XLB1
          Y(6)=Y(5)
          Y(7)=Y(1)-2.*BB1-2.*XLB1
          Y(8)=Y(7)
          IF(LCAR.EQ.1) GO TO 640
C
C     VEHICLE NO. 2
C
          Y(9)=Y(8)-DIST2
          Y(10)=Y(9)
          Y(11)=Y(9)-2.*BB2
          Y(12)=Y(11)
          Y(13)=Y(9)-2.*XLB2
          Y(14)=Y(13)
          Y(15)=Y(9)-2.*BB2-2.*XLB2
          Y(16)=Y(15)
          IF(LCAR.EQ.2) GO TO 640
C
C     VEHICLE NO. 3
C
          Y(17)=Y(16)-DIST3
          Y(18)=Y(17)
          Y(19)=Y(17)-2.*BB3
          Y(20)=Y(19)
          Y(21)=Y(17)-2.*XLB3
          Y(22)=Y(21)
          Y(23)=Y(17)-2.*BB3-2.*XLB3
          Y(24)=Y(23)
          IF(LCAR.EQ.3) GO TO 640
C
C     VEHICLE NO. 4
C
          Y(25)=Y(24)-DIST4
          Y(26)=Y(25)
          Y(27)=Y(25)-2.*BB4
          Y(28)=Y(27)
          Y(29)=Y(25)-2.*XLB4
          Y(30)=Y(29)
          Y(31)=Y(25)-2.*BB4-2.*XLB4
          Y(32)=Y(31)
      640 CONTINUE
C
C     NODE SELECTION LOOP BEGINS ****
C
          DO 1900 JJ=1,NP
          J1=JJ-1
          J2=JJ
          X1=XPL*JJ
          X2=XPL*(JJ-1)
          K=1
C
C     WHEEL SELECTION LOOP BEGINS ****
C
```

```
      DO 1800 JJM=1,NW
      K=-K
      IF(K) 660,680,680
  660 FAT1=XLAMD1
      FAT2=XLAMD2
      GO TO 700
  680 FAT1=ZETA1
      FAT2=ZETA2
  700 CONTINUE
C
      IF(Y(JJM).GT.X1.OR.Y(JJM).LT.X2) GO TO 1800
      X=Y(JJM)-(JJ-1)*XPL
      ALPHA=X/XPL
      BETA=1.-ALPHA
      J3=J1+N
      J4=J2+N
C
C     COMPUTATION OF CONSTANTS FOR EACH MATRIX FOR EACH TIME STEP
C
       C1=FAT2*FAT2*BETA*BETA
       C2=FAT2*FAT2*BETA*ALPHA
       C3=FAT1*FAT2*BETA*BETA
       C4=FAT1*FAT2*BETA*ALPHA
       C5=FAT2*FAT2*ALPHA*ALPHA
       C6=FAT1*FAT2*ALPHA*ALPHA
       C7=FAT1*FAT1*BETA*BETA
       C8=FAT1*FAT1*BETA*ALPHA
       C9=FAT1*FAT1*ALPHA*ALPHA
       C10=FAT2*BETA
       C11=FAT2*ALPHA
       C12=FAT1*BETA
       C13=FAT1*ALPHA
C
C     COMPUTATION OF DISTRIBUTIONS TO MASS, STIFFNESS MATRICES AND TO
C     LOAD VECTORS
C
       IF(JJM.GE.1.AND.JJM.LE.8) XKY=XKY1
       IF(JJM.GE.9.AND.JJM.LE.16) XKY=XKY2
       IF(JJM.GE.17.AND.JJM.LE.24) XKY=XKY3
       IF(JJM.GE.25.AND.JJM.LE.32) XKY=XKY4
       IF(JJM.GE.1.AND.JJM.LE.8) UM=UM1
       IF(JJM.GE.9.AND.JJM.LE.16) UM=UM2
       IF(JJM.GE.17.AND.JJM.LE.24) UM=UM3
       IF(JJM.GE.25.AND.JJM.LE.32) UM=UM4
       IF(JJM.GE.1.AND.JJM.LE.8) SM=SM1
       IF(JJM.GE.9.AND.JJM.LE.16) SM=SM2
       IF(JJM.GE.17.AND.JJM.LE.24) SM=SM3
       IF(JJM.GE.25.AND.JJM.LE.32) SM=SM4
       IF(J1.EQ.0) GO TO 900
C
C     WHEELS ON CHORD NO. 1
C     ---------------------
C
C     VEHICLE NO. 1
C
       XMASS(J1,J1)=C1* UM+XMASS(J1,J1)
       SB(J1,J1)=C1*XKY+SB(J1,J1)
       IF(JJM.GT.8) GO TO 800
C
       SB(J1,M+1)=SB(J1,M+1)-C10*XKY1
       SB(J1,M+2)=SB(J1,M+2)+(FAC1(JJM)*XLB1+FAC2(JJM)*BB1)*XKY1*C10
       SB(J1,M+3)=SB(J1,M+3)+FAC3(JJM)*BA1*XKY1*C10
       SB(M+1,J1)=SB(M+1,J1)-C10*XKY1
       SB(M+2,J1)=SB(M+2,J1)+(FAC1(JJM)*XLB1+FAC2(JJM)*BB1)*XKY1*C10
       SB(M+3,J1)=SB(M+3,J1)+FAC3(JJM)*BA1*XKY1*C10
C
       IF(LCAR.EQ.1) GO TO 880
C
C     VEHICLE NO. 2
C
  800 IF(JJM.GT.16) GO TO 820
```

```
      SB(J1,M+4)=SB(J1,M+4)-C10*XKY2
      SB(J1,M+5)=SB(J1,M+5)+(FAC1(JJM)*XLB2+FAC2(JJM)*BB2)*XKY2*C10
      SB(J1,M+6)=SB(J1,M+6)+FAC3(JJM)*BA2*XKY2
      SB(M+4,J1)=SB(M+4,J1)-C10*XKY2
      SB(M+5,J1)=SB(M+5,J1)+(FAC1(JJM)*XLB2+FAC2(JJM)*BB2)*XKY2*C10
      SB(M+6,J1)=SB(M+6,J1)+FAC3(JJM)*BA2*XKY2*C10
      IF(LCAR.EQ.2) GO TO 880
C
C     VEHICLE NO. 3
C
  820 IF(JJM.GT.24) GO TO 840
      SB(J1,M+7)=SB(J1,M+7)-C10*XKY3
      SB(J1,M+8)=SB(J1,M+8)+(FAC1(JJM)*XLB3+FAC2(JJM)*BB3)*XKY3*C10
      SB(J1,M+9)=SB(J1,M+9)+FAC3(JJM)*BA3*XKY3*C10
      SB(M+7,J1)=SB(M+7,J1)-C10*XKY3
      SB(M+8,J1)=SB(M+8,J1)+(FAC1(JJM)*XLB3+FAC2(JJM)*BB3)*XKY3*C10
      SB(M+9,J1)=SB(M+9,J1)+FAC3(JJM)*BA3*XKY3*C10
      IF(LCAR.EQ.3) GO TO 880
C
C     VEHICLE NO. 4
C
  840 IF(JJM.GT.32) GO TO 880
      SB(J1,M+10)=SB(J1,M+10)-C10*XKY4
      SB(J1,M+11)=SB(J1,M+11)+(FAC1(JJM)*XLB4+FAC2(JJM)*BB4)*XKY4*C10
      SB(J1,M+12)= SB(J1,M+12)+FAC3(JJM)*BA4*XKY4*C10
      SB(M+10,J1)=SB(M+10,J1)-C10*XKY4
      SB(M+11,J1)=SB(M+11,J1)+(FAC1(JJM)*XLB4+FAC2(JJM)*BB4)*XKY4*C10
      SB(M+12,J1)=SB(M+12,J1)+FAC3(JJM)*BA4*XKY4*C10
C
  880 CONTINUE
C
      FR(J1)=FR(J1)+C10*(UM+SM)*G
C
  900 IF(J1.EQ.0.OR.J2.EQ.NP) GO TO 920
C
      XMASS(J1,J2)=C2*UM+XMASS(J1,J2)
      XMASS(J2,J1)=C2*UM+XMASS(J2,J1)
C
      SB(J1,J2)=C2*XKY+SB(J1,J2)
      SB(J2,J1)=C2*XKY+SB(J2,J1)
  920 IF(J2.EQ.NP) GO TO 1060
C
C     VEHICLE NO. 1
C
      XMASS(J2,J2)=C5*UM+XMASS(J2,J2)
      SB(J2,J2)=C5*XKY+SB(J2,J2)
C
      IF(JJM.GT.8) GO TO 940
      SB(J2,M+1)=SB(J2,M+1)-C11*XKY1
      SB(J2,M+2)=SB(J2,M+2)+(FAC1(JJM)*XLB1+FAC2(JJM)*BB1)*XKY1*C11
      SB(J2,M+3)=SB(J2,M+3)+FAC3(JJM)*BA1*XKY1*C11
      SB(M+1,J2)=SB(M+1,J2)-C11*XKY1
      SB(M+2,J2)=SB(M+2,J2)+(FAC1(JJM)*XLB1+FAC2(JJM)*BB1)*XKY1*C11
      SB(M+3,J2)=SB(M+3,J2)+FAC3(JJM)*BA1*XKY1*C11
C
      IF(LCAR.EQ.1) GO TO 1040
C
C     VEHICLE NO. 2
C
  940 IF(JJM.GT.16) GO TO 960
      SB(J2,M+4)=SB(J2,M+4)-C11*XKY2
      SB(J2,M+5)=SB(J2,M+5)+(FAC1(JJM)*XLB2+FAC2(JJM)*BB2)*XKY2*C11
      SB(J2,M+6)=SB(J2,M+6)+FAC3(JJM)*BA2*XKY2*C11
      SB(M+4,J2)=SB(M+4,J2)-C11*XKY2
      SB(M+5,J2)=SB(M+5,J2)+(FAC1(JJM)*XLB2+FAC2(JJM)*BB2)*XKY2*C11
      SB(M+6,J2)=SB(M+6,J2)+FAC3(JJM)*BA2*XKY2*C11
      IF(LCAR.EQ.2) GO TO 1040
C
C     VEHICLE NO. 3
C
  960 IF(JJM.GT.24) GO TO 980
```

```
      SB(J2,M+7)=SB(J2,M+7)-C11*XKY3
      SB(J2,M+8)=SB(J2,M+8)+(FAC1(JJM)*XLB3+FAC2(JJM)*BB3)*XKY3*C11
      SB(J2,M+9)=SB(J2,M+9)+FAC3(JJM)*BA3*XKY3*C11
      SB(M+7,J2)=SB(M+7,J2)-C11*XKY3
      SB(M+8,J2)=SB(M+8,J2)+(FAC1(JJM)*XLB3+FAC2(JJM)*BB3)*XKY3*C11
      SB(M+9,J2)=SB(M+9,J2)+FAC3(JJM)*BA3*XKY3*C11
      IF(LCAR.EQ.3) GO TO 1040
C
C     VEHICLE NO. 4
C
  980 IF(JJM.GT.32) GO TO 1040
      SB(J2,M+10)=SB(J2,M+10)-C11*XKY4
      SB(J2,M+11)=SB(J2,M+11)+(FAC1(JJM)*XLB4+FAC2(JJM)*BB4)*XKY4*C11
      SB(J2,M+12)=SB(J2,M+12)+FAC3(JJM)*BA4*XKY4*C11
      SB(M+10,J2)=SB(M+10,J2)-C11*XKY4
      SB(M+11,J2)=SB(M+11,J2)+(FAC1(JJM)*XLB4+FAC2(JJM)*BB4)*XKY4*C11
      SB(M+12,J2)=SB(M+12,J2)+FAC3(JJM)*BA4*XKY4*C11
C
 1040 CONTINUE
C
      FR(J2)=FR(J2)+C11*(UM+SM)*G
C
 1060 IF(J1.EQ.0.OR.J3.EQ.N) GO TO 1080
C
      XMASS(J1,J3)=C3*UM+XMASS(J1,J3)
      XMASS(J3,J1)=C3*UM+XMASS(J3,J1)
C
      SB(J1,J3)=C3*XKY+SB(J1,J3)
      SB(J3,J1)=C3*XKY+SB(J3,J1)
 1080 IF(J3.EQ.N) GO TO 1340
C
C     WHEELS ON CHORD NO. 2
C     ---------------------
C
C     VEHICLE NO. 1
C
      XMASS(J3,J3)=C7*UM+XMASS(J3,J3)
      SB(J3,J3)=C7*XKY+SB(J3,J3)
C
      IF(JJM.GT.8) GO TO 1200
      SB(J3,M+1)=SB(J3,M+1)-C12*XKY1
      SB(J3,M+2)=C1(JJM)*XLB1+FAC2(JJM)*BB1)*XKY1*C12
      SB(J3,M+3)=SB(J3,M+3)+FAC3(JJM)*BA1*XKY1*C12
      SB(M+1,J3)=SB(M+1,J3)-C12*XKY1
      SB(M+2,J3)=SB(M+2,J3)+(FAC1(JJM)*XLB1+FAC2(JJM)*BB1)*XKY1*C12
      SB(M+3,J3)=SB(M+3,J3)+FAC3(JJM)*BA1*XKY1*C12
C
      IF(LCAR.EQ.1) GO TO 1300
C
C     VEHICLE NO. 2
C
 1200 IF(JJM.GT.16) GO TO 1220
      SB(J3,M+4)=SB(J3,M+4)-C12*XKY2
      SB(J3,M+5)=SB(J3,M+5)+(FAC1(JJM)*XLB2+FAC2(JJM)*BB2)*XKY2*C12
      SB(J3,M+6)=SB(J3,M+6)+FAC3(JJM)*BA2*XKY2*C12
      SB(M+4,J3)=SB(M+4,J3)-C12*XKY2
      SB(M+5,J3)=SB(M+5,J3)+(FAC1(JJM)*XLB2+FAC2(JJM)*BB2)*XKY2*C12
      SB(M+6,J3)=SB(M+6,J3)+FAC3(JJM)*BA2*XKY2*C12
      IF(LCAR.EQ.2) GO TO 1300
C
C     VEHICLE NO. 3
C
 1220 IF(JJM.GT.24) GO TO 1260
      SB(J3,M+7)=SB(J3,M+7)-C12*XKY3
      SB(J3,M+8)=SB(J3,M+8)+(FAC1(JJM)*XLB3+FAC2(JJM)*BB3)*XKY3*C12
      SB(J3,M+9)=SB(J3,M+9)+FAC3(JJM)*BA3*XKY3*C12
      SB(M+7,J3)=SB(M+7,J3)-C12*XKY3
      SB(M+8,J3)=SB(M+8,J3)+(FAC1(JJM)*XLB3+FAC2(JJM)*BB3)*XKY3*C12
      SB(M+9,J3)=SB(M+9,J3)+FAC3(JJM)*BA3*XKY3*C12
      IF(LCAR.EQ.3) GO TO 1300
C
```

```
C     VEHICLE NO. 4
C
 1260 IF(JJM.GT.32) GO TO 1300
      SB(J3,M+10)=SB(J3,M+10)-C12*XKY4
      SB(J3,M+11)=SB(J3,M+11)+(FAC1(JJM)*XLB4+FAC2(JJM)*BB4)*XKY4*C12
      SB(J3,M+12)=SB(J3,M+12)+FAC3(JJM)*BA4*XKY4*C12
      SB(M+10,J3)=SB(M+10,J3)-C12*XKY4
      SB(M+11,J3)=SB(M+11,J3)+(FAC1(JJM)*XLB4+FAC2(JJM)*BB4)*XKY4*C12
      SB(M+12,J3)=SB(M+12,J3)+FAC3(JJM)*BA4*XKY4*C12
C
 1300 CONTINUE
C
      FR(J3)=FR(J3)+C12*(UM+SM)*G
C
 1340 IF(J2.EQ.NP.OR.J3.EQ.N) GO TO 1360
C
      XMASS(J2,J3)=C4*UM+XMASS(J2,J3)
      XMASS(J3,J2)=C4*UM+XMASS(J3,J2)
C
      SB(J2,J3)=C4*XKY+SB(J2,J3)
      SB(J3,J2)=C4*XKY+SB(J3,J2)
C
 1360 IF(J1.EQ.0.OR.J4.GT.M) GO TO 1380
C
      XMASS(J1,J4)=C4*UM+XMASS(J1,J4)
      XMASS(J4,J1)=C4*UM+XMASS(J4,J1)
C
      SB(J1,J4)=C4*XKY+SB(J1,J4)
      SB(J4,J1)=C4*XKY*SB(J4,J1)
C
 1380 IF(J4.GT.M) GO TO 1500
C
C     VEHICLE NO. 1
C
      XMASS(J4,J4)=C9*UM+XMASS(J4,J4)
      SB(J4,J4)=C9*XKY+SB(J4,J4)
C
      IF(JJM.GT.8) GO TO 1400
      SB(J4,M+1)=SB(J4,M+1)-C13*XKY1
      SB(J4,M+2)=SB(J4,M+2)+(FAC1(JJM)*XLB1+FAC2(JJM)*BB1)*XKY1*C13
      SB(J4,M+3)=SB(J4,M+3)+FAC3(JJM)*BA1*XKY1*C13
      SB(M+1,J4)=SB(M+1,J4)-C13*XKY1
      SB(M+2,J4)=SB(M+2,J4)+(FAC1(JJM)*XLB1+FAC2(JJM)*BB1)*XKY1*C13
      SB(M+3,J4)=SB(M+3,J4)+FAC3(JJM)*BA1*XKY1*C13
      GO TO 1480
C
C     VEHICLE NO. 2
C
 1400 IF(JJM.GT.16) GO TO 1440
      SB(J4,M+4)=SB(J4,M+4)-C13*XKY2
      SB(J4,M+5)=SB(J4,M+5)+(FAC1(JJM)*XLB2+FAC2(JJM)*BB2)*XKY2*C13
      SB(J4,M+6)=SB(J4,M+6)+FAC3(JJM)*BA2*XKY2*C13
      SB(M+4,J4)=SB(M+4,J4)-C13*XKY2
      SB(M+5,J4)=SB(M+5,J4)+(FAC1(JJM)*XLB2+FAC2(JJM)*BB2)*XKY2*C13
      SB(M+6,J4)=SB(M+6,J4)+FAC3(JJM)*BA2*XKY2*C13
      IF(LCAR.EQ.2) GO TO 1480
C
C     VEHICLE NO. 3
C
 1440 IF(JJM.GT.24) GO TO 1460
      SB(J4,M+7)=SB(J4,M+7)-C13*XKY3
      SB(J4,M+8)=SB(J4,M+8)+(FAC1(JJM)*XLB3+FAC2(JJM)*BB3)*XKY3*C13
      SB(J4,M+9)=SB(J4,M+9)+FAC3(JJM)*BA3*XKY3*C13
      SB(M+7,J4)=SB(M+7,J4)-C13*XKY3
      SB(M+8,J4)= SB(M+8,J4)+(FAC1(JJM)*XLB3+FAC2(JJM)*BB3)*XKY3*C13
      SB(M+9,J4)=SB(M+9,J4)+FAC3(JJM)*BA3*XKY3*C13
      IF(LCAR.EQ.3) GO TO 1480
C
C     VEHICLE NO. 4
C
 1460 IF(JJM.GT.32) GO TO 1480
```

```
      SB(J4,M+10)=SB(J4,M+10)-C13*XKY4
      SB(J4,M+11)=SB(J4,M+11)+(FAC1(JJM)*XLB4+FAC2(JJM)*BB4)*XKY4*C13
      SB(J4,M+12)=SB(J4,M+12)+FAC3(JJM)*BA4*XKY4*C13
      SB(M+10,J4)=SB(M+10,J4)-C13*XKY4
      SB(M+11,J4)= SB(M+11,J4)+(FAC1(JJM)*XLB4+FAC2(JJM)*BB4)*XKY4*C13
      SB(M+12,J4)=SB(M+12,J4)+FAC3(JJM)*BA4*XKY4*C13
C
 1480 CONTINUE
C
      FR(J4)=FR(J4)+C13*(UM+SM)*G
C
 1500 IF(J2.EQ.NP.OR.J4.GT.M) GO TO 1600
C
      XMASS(J2,J4)=C6*UM+XMASS(J2,J4)
      XMASS(J4,J2)=C6*UM+XMASS(J4,J2)
C
      SB(J2,J4)=C6*XKY+SB(J2,J4)
      SB(J4,J2)=C6*XKY+SB(J4,J2)
C
 1600 IF(J3.EQ.N.OR.J4.GT.M) GO TO 1700
C
      XMASS(J3,J4)=C8*UM+XMASS(J3,J4)
      XMASS(J4,J3)=C8*UM+XMASS(J4,J3)
C
      SB(J3,J4)=C8*XKY+SB(J3,J4)
      SB(J4,J3)=C8*XKY+SB(J4,J3)
C
 1700 CONTINUE
C
 1800 CONTINUE
C
C     WHEEL SELECTION LOOP ENDS ****
C
 1900 CONTINUE
C
C     NODE SELECTION LOOP ENDS ****
C
      IF(IPTM.NE.2) GO TO 2500
      WRITE(KK2,2000)
 2000 FORMAT(2X,'MATRICES AT THE END OF EACH TIME INCREMENT BEFORE INTE
     1GRATION. '/)
      DO 2100 I=1,NN
 2100 WRITE(KK2,2400)(XMASS(I,K),K=1,NN)
      DO 2200 I=1,NN
 2200 WRITE(KK2,2400)(SB(I,K),K=1,NN)
      DO 2300 I=1,NN
 2300 WRITE(KK2,2400)(DAMP(I,K),K=1,NN)
      WRITE(KK2,2400)(FR(K),K=1,NN)
 2400 FORMAT(2X,10(E11.4,1X)/10(E11.4,1X)/10(E11.4,1X))
 2500 CONTINUE
C
C     DIRECT STEP BY STEP INTEGRATION
C
C   -----------------------------------------------------------------

C     NOTE: REMOVE "C" FROM COL. 1 OF CALL STATEMENT FOR THE METHOD
C           OF INTEGRATION BEING USED.
C   -----------------------------------------------------------------

C
C     NEWMARK,S BETA METHOD
      CALL INTGR1(J,DT,XMASS,SB,FR,DAMP,NN,UO,VO,AAO,UU,V,AC,EPS)
C
C     HOUBOLT METHOD
C     CALL INTGR2(J,DT,XMASS,SB,FR,DAMP,NN,UO,VO,AAO,UU,V,AC,EPS)
C
C     WILSON THETA METHOD
C     CALL INTGR3(J,DT,XMASS,SB,FR,DAMP,NN,UO,VO,AAO,UU,V,AC,EPS)
C
C     DYNAMIC DISPLACEMENTS, VELOCITIES, AND ACCELERATIONS
C
```

```
       IF(IPTM.EQ.1.AND.ICOUNT.LT.NINC) GO TO 2520
       IF(ICOUNT-NINC) 2640,2520,2520
  2520 IF(J.NE.1) GO TO 2580
       WRITE(KK2,2540)
  2540 FORMAT( /,'*** DYNAMIC DISPLACEMENTS,VELOCITIES AND ACCELERATIONS
      1 ***'//)
       WRITE(KK2,2560)
  2560 FORMAT(5X,'TIME',10X,'DDISP(5)',8X,'DDISP(14)',8X,'ACCEL(5)',
      18X,'ACCEL(14)',8X,'DELTIME',8X,'DISTANCE',8X,'XXL RATIO'/)
  2580 IF(NUMB.LT.NKN) GO TO 2620
C     CONVERT DISPL. AND ACCEL. INTO MM AND G RESPECTIVELY
       UU5=UU(5)*25.4
       UU14=UU(14)*25.4
       AC5=AC(5)/386.4
       AC14=AC(14)/386.4
C
C   -----------------------------------------------------------------

C     NOTE: REMOVE "C" FROM THE NEXT AND THE CORRESP. STATEMENTS IF DISP.

C     , VEL., ACCEL. ARE NOT REQUIRED.
C   -----------------------------------------------------------------

C      GO TO 2601
C
       WRITE(KK2,2600)T,UU5,UU14,AC5,AC14,J
C      WRITE(KK2,2600)T,UU(5),UU(14),AC(5),AC(14),J,XX,XXL
  2600 FORMAT(2X,D14.6,2X,D14.6,2X,D14.6,2X,D14.6,2X,D14.6,2X,I5,2X,
      1D14.6,2X,D14.6 )
C
C2601 CONTI. C
       IF(NUMB.GE.NKN) NUMB=0
  2620 IF(IPTM.EQ.1.AND.ICOUNT.LT.NINC) GO TO 2640
       ICOUNT=0
  2640 CONTINUE
C
  2660 IF(IPTM.NE.2) GO TO 2780
C
C     STATIC DISPLACEMENTS
C
       CALL STATIC(FLEX,M,FR,NN,US,KK2)
C
       IF(IPTM.EQ.1.AND.JCOUNT.LT.NINC) GO TO 2680
       IF(JCOUNT-NINC) 2780,2680,2680
  2680 IF(J.NE.1) GO TO 2740
       WRITE(KK2,2700)
  2700 FORMAT( /,' *LACEMENTS ***'/)
       WRITE(KK2,2720)
  2720 FORMAT(5X,'TIME',10X,'SDISP(5)',8X,'SDISP(14)',8X,
      1'DELTIME',8X,'DISTANCE',8X,'XXL RATIO'/)
  2740 IF(NUMB.LT.NKN) GO TO 2760
       DDF(5)=UU(5)/US(5)
       DDF(14)=UU(14)/US(14)
C     CONVERT STAT. DISPL. INTO MM
       US5=US(5)*25.4
       US14=US(14)*25.4
       WRITE(KK2,2600)T,US5,US14,DDF(5),DDF(14),J
C      WRITE(KK2,2600)T,US(5),US(14),DDF(5),DDF(14),J,XX,XXL
       IF(NUMB.GE.NKN) NUMB=0
  2760 IF(IPTM.EQ.1.AND.JCOUNT.LT.NINC) GO TO 2780
       JCOUNT=0
  2780 CONTINUE
C   -----------------------------------------------------------------

C     NOTE: PLACE "C" IN COL.OF THE NEXT STATEMENT IF THE RAIL-WHEEL
C           INTERFACE FORCES ARE REQUIRED.
C   -----------------------------------------------------------------

  2800 IF(IPTM.NE.2) GO TO 5020
C
C     COMPUTATION OF WHEEL - RAIL INTERFACE FORCES
C
```

```
C
      CALL CONFOR(N,M,NN,G,UU,AC,XKY1,UM1,SM1,XLB1,BA1,XKY2,UM2,SM2,
     1XLB2,BA2,XKY3,UM3,SM3,XLB3,BA3,XKY4,UM4,SM4,XLB4,BA4,FAC1,FAC2,FAC
     23,LCAR,NW,Y,XPL,FF,DT,VEL,NP,J)
C
      IF(IPTM.EQ.1.AND.MCOUNT.LT.NINC) GO TO 3080
      IF(MCOUNT-NINC) 5020,3080,3080
 3080 IF(J.NE.1) GO TO 4040
      WRITE(KK2,4000)
 4000 FORMAT( /,' *** LOADS AT WHEEL - RAIL INTERFACES *** '/)
      WRITE(KK2,4020)
 4020 FORMAT(6X,'TIME',10X,'CON FOR(5)',8X,'CON FOR(14)',8X,'WHEEL NO',
     18X,'DELTIME',8X,'DISTANCE',8X,'XXL RATIO'/)
 4040 CONTINUE
      FF5=FF(5)
      FF14=FF(14)
      IF(FF5.LE.0.0.AND.FF14.LE.0) GO TO 4080
      WRITE(KK2,4060)T,FF5,FF14,J,XX,XXL
 4060 FORMAT(2X,D14.6,2X,D14.6,2X,D14.6,2X,I5,2X,D14.6,
     12X,D14.6)
 4080 CONTINUE
 5000 IF(IPTM.EQ.1.AND.MCOUNT.LT.NINC) GO TO 5020
      MCOUNT=0
 5020 CONTINUE
 5040 CONTINUE
C
C     THE BIG TIME LOOP ENDS ******
C
 6000 RETURN
      END
C
C  -----------------------------------------------------------------
C  THIS SUBROUTINE CALCULATES MASS MATRIX OF A TIMBER RAILROAD BRIDGE
C  SPAN INCLUDING THE EFFECTS OF MASSES OF VEHICLE.
C  -----------------------------------------------------------------
C
C     XMASS(NN,NN) = MASS MATRIX OF TWO CHORDS AND VEHICLE SPRUNG BODY
C     XMSAT(N,N)  = MASS MATRIX OF ONE CHORD
C
      SUBROUTINE XMASB(N,NN,AG,XPL,RHO,KK2,IPRNTM,M,XMASS,LCAR,XMSAT,
     1NDK,XMB1,XJJB1,XJB1,XMB2,XJJB2,XJB2,XMB3,XJJB3,XJB3,XMB4,XJJB4,
     2XJB4,G)
C
      IMPLICIT REAL *8(A-H,O-Z)
      DIMENSION XMASS(NN,NN),XMSAT(N,N)
C
C     INITIALIZATION OF MASS MATRIX
C
      DO 10 J=1,NN
      DO 10 K=1,NN
   10 XMASS(J,K) =0.
      DO 20 I=1,N
      DO 20 J=1,N
   20 XMSAT(I,J)=0.
C
C     DISTNCTION BETWEEN TWO TYPES OF BRIDGE DECKS
C
C     FAC = A FACTOR TO ACCOUNT FOR THE DEAD WEIGHT OF TRACK AND DECK
C           OF CHORD
C     FAC = 22.000 LBS/IN, FOR OPEN DECK PER CHORD
C     FAC = 96.000 LBS/IN, FOR BALLAST DECK PER CHORD
      IF(NDK.EQ.0) FAC=22.000
      IF(NDK.EQ.1) FAC=96.000
      IF(NDK.NE.0.AND.NDK.NE.1) FAC=22.000
C
C   FORMULATION OF MASS MATRIX OF A CHORD
C
      DO 40 J=1,N
```

```
      XMASS(J,J)=(FAC/G+AG*RHO)*XPL
   40 CONTINUE
      DO 50 J=1,N
   50 XMSAT(J,J)=XMASS(J,J)
      DO 60 J=1,N
      JJ=J+N
   60 XMASS(JJ,JJ)=XMASS(J,J)
C
C     INCLUSION OF EFFECTS OF VEHICLE BODIES
C
C    VEHICLE NO. 1
C
      XMASS(M+1,M+1)=XMB1
      XMASS(M+2,M+2)=XJJB1
      XMASS(M+3,M+3)=XJB1
      IF(LCAR.EQ.1) GO TO 80
C
C    VEHICLE NO. 2
C
      XMASS(M+4,M+4)=XMB2
      XMASS(M+5,M+5)=XJJB2
      XMASS(M+6,M+6)=XJB2
      IF(LCAR.EQ.2) GO TO 80
C
C    VEHICLE NO. 3
C
      XMASS(M+7,M+7)=XMB3
      XMASS(M+8,M+8)=XJJB3
      XMASS(M+9,M+9)=XJB3
      IF(LCAR.EQ.3) GO TO 80
C
C    VEHICLE NO. 4
C
      XMASS(M+10,M+10)=XMB4
      XMASS(M+11,M+11)=XJJB4
      XMASS(M+12,M+12)=XJB4
C
   80 CONTINUE
      IF(IPRNTM.NE.1) GO TO 150
      WRITE(KK2,90)
   90 FORMAT(1H1, /,30X,'*** MASS MATRIX OF TWO CHORDS AND VEHICLE BODY
     1 ***'/)
      DO 100 I=1,NN
  100 WRITE(KK2,120)I,(XMASS(I,J),J=1,NN)
  120 FORMAT(1X,I2,1X,10(E11.4,1X)/10(E11.4,1X))
  150 CONTINUE
      RETURN
      END
C
C   ----------------------------------------------------------------------

C   THIS SUBROUTINE COMPUTES THE STIFFNESS MATRIX OF A CHORD OF A TIMBER

C   RAILROAD SPAN INCLUDING THE EFFECT OF CONSTANT PART OF VEHICLE(S).
C   ----------------------------------------------------------------------

C
C    SB(NN,NN) = OVERALL STIFFNESS MATRIX OF CHORD ONE AND TWO
C    FLEX(M,M) = FLEXIBILITY MATRIX FOR CHORD ONE AND TWO
C    DB(NN,NN) = DAMPING MATRIX OF VEHICLE
C    BS(M,M) = INVERTED FLEXIBILITY MATRIX
C    FLEXI(N,N) = MATRIX FOR STORING MATRIX DELTA(N,N)
C    DELTA(N,N) = FLEXIBILITY MATRIX OF ONE CHORD
C
      SUBROUTINE STIFF(N,NN,XI,E,XPL,KK2,M,SB,FLEX,IPRNTM,DB,BS,LCAR,
     1FLEXI,XKY1,XLB1,BB1,BA1,CY1,XKY2,XLB2,BB2,BA2,CY2,XKY3,XLB3,BB3,
     2BA3,CY3,XKY4,XLB4,BB4,BA4,CY4)
C
      IMPLICIT REAL*8(A-H,O-Z)
      DIMENSION FLEX(M,M),SB(NN,NN),DB(NN,NN),FLEXI(N,N),BS(M,M)
      DIMENSION DELTA( 9, 9)
```

```
C
C     INITIALIZATION OF DELTA AND FLEX MATRICES
C
          DO 100 J=1,N
          DO 100 K=1,N
      100 DELTA(J,K)=0.
          DO 110 J=1,M
          DO 110 K=1,M
      110 FLEX(J,K)=0.
          DO 120 J=1,NN
          DO 120 K=1,NN
      120 SB(J,K)=0.
C
          XL=(N+1)*XPL
          CONST=1./(6.*E*XI*XL)
C
C     FLEXIBILITY MATRIX FOR ONE CHORD
C
          D 1149.       DO 150 K=1,N
          A=J*XPL
          X=K*XPL
          B=XL-A
          IF(K.GT.J) GO TO 140
          DELTA(J,K)=X*(XL*XL-B*B-X*X)*B*CONST
          GO TO 150
      140 DELTA(J,K)=A*(XL-X)*(XL*XL-A*A-(XL-X)*(XL-X))*CONST
      150 CONTINUE
          IF(IPRNTM.NE.1) GO TO 180
          WRITE(KK2,160)
      160 FORMAT( /,'*** FLEXIBILITY MATRIX OF ONE CHORD ***'/)
          DO 170 I=1,N
      170 WRITE(KK2,250)(DELTA(I,J),J=1,N)
      180 CONTINUE
C
C     FLEXIBILITY MATRIX FOR BOTH CHORDS
C
          DO 200 J=1,N
          DO 200 K=1,N
      200 FLEX(J,K)=DELTA(J,K)
          DO 220 J=1,N
          DO 220 K=1,N
      220 FLEXI(J,K)=FLEX(J,K)
          DO 230 J=1,N
          JJ=J+N
          DO 230 K=1,N
          KK=K+N
      230 FLEX(JJ,KK)=FLEX(J,K)
C
          IF(IPRNTM.NE.1) GO TO 280
C
C     WRITE OUT FLEXIBILITY MATRIX FOR CHORDS
C
          WRITE(KK2,240)
      240 FORMAT( /,'*** FLEXIBILITY MATRIX FOR BOTH CHORDS ***'/)
          DO 260 I=1,M
          WRITE(KK2,250)(FLEX(I,J),J=1,M)
      250 FORMAT(1X,11(E10.4,1X)/11(E10.4,1X))
      260 CONTINUE
      280 CONTINUE
C
C     SUBROUTINE "INVERT" INVERTS FLEXIBILITY MATRIX INTO STIFFNESS MATRX
C
          CALL INVERT(DELTA,N,KK2,IPRNTM)
C
          DO 300 I=1,N
          DO 300 J=1,N
      300 SB(I,J)=DELTA(I,J)
          DO 320 I=1,N
          DO 320 J=1,N
      320 BS(I,J)=SB(I,J)
          DO 340 J=1,N
```

```
      JJ=J+N
      DO 340 K=1,N
      KK=K+N
  340 BS(JJ,KK)=BS(J,K)
      DO 360 J=1,N
      JJ=J+N
      DO 360 K=1,N
      KK=K+N
  360 SB(JJ,KK)=SB(J,K)
C
C     ADDITION TO STIFFNESS MATRIX OF CONST CONTRIBUTION OF VEHICLE BODY
C
C     VEHICLE NO. 1
C
      SB(M+1,M+1)=8.*XKY1
      SB(M+2,M+2)=8.*XKY1*(XLB1*XLB1+BB1*BB1)
      SB(M+3,M+3)=8.*XKY1*BA1*BA1
      IF(LCAR.EQ.1) GO TO 380
C
C     VEHICLE NO. 2
C
      SB(M+4,M+4)=8.*XKY2
      SB(M+5,M+5)=8.*XKY2*(XLB2*XLB2+BB2*BB2)
      SB(M+6,M+6)=8.*XKY2*BA2*BA2
      IF(LCAR.EQ.2) GO TO 380
C
C     VEHICLE NO. 3
C
      SB(M+7,M+7)=8.*XKY3
      SB(M+8,M+8)=8.*XKY3*(XLB3*XLB3+BB3*BB3)
      SB(M+9,M+9)=8.*XKY3*BA3*BA3
      IF(LCAR.EQ.3) GO TO 380
C
C     VEHICLE NO. 4
C
      SB(M+10,M+10)=8.*XKY4
      SB(M+11,M+11)=8.*XKY4*(XLB4*XLB4+BB4*BB4)
      SB(M+12,M+12)=8.*XKY4*BA4*BA4
  380 CONTINUE
C
      IF(IPRNTM.NE.1) GO TO 460
      WRITE(KK2,400)
  400 FORMAT(1H1 /,' **** OVERALL STIFF MATRIX OF CHORDS AND VEHICLE BOD
     1Y **** '/)
      DO 420 I=1,NN
  420 WRITE(KK2,440)I,(SB(I,J),J=1,NN)
  440 FORMAT(1X,I2,1X,10(E11.4,1X)/10(E11.4,1X))
  460 CONTINUE
C
C     COMPUTATION OF DAMPING MATRIX OF VEHICLE
C
C     CY = CONSTANT FOR VERTICAL DAMPER OF VEHICLE
C     THE VALUE OF CY IS AT PRESENT TAKEN AS ZERO
C
C     INITIALIZATION OF "DB" MATRIX
C
      DO 480 J=1,NN
      DO 480 K=1,NN
  480 DB(J,K)=0.
C
C     VEHICLE NO. 1
C
      DB(M+1,M+1)=8.*CY1
      DB(M+2,M+2)=8.*CY1*(XLB1*XLB1+BB1*BB1)
      DB(M+3,M+3)=8.*CY1*BA1*BA1
      IF(LCAR.EQ.1) GO TO 500
C
C     VEHICLE NO. 2
C
      DB(M+4,M+4)=8.*CY2
      DB(M+5,M+5)=8.*CY2*(XLB2*XLB2+BB2*BB2)
```

```
      DB(M+6,M+6)=8.*CY2*BA2*BA2
      IF(LCAR.EQ.2) GO TO 500
C
C    VEHICLE NO. 3
C
      DB(M+7,M+7)=8.*CY3
      DB(M+8,M+8)=8.*CY3*(XLB3*XLB3+BB3*BB3)
      DB(M+9,M+9)=8.*CY3*BA3*BA3
      IF(LCAR.EQ.3) GO TO 500
C
C    VEHICLE NO. 4
C
      DB(M+10,M+10)=8.*CY4
      DB(M+11,M+11)=8.*CY4*(XLB4*XLB4+BB4*BB4)
      DB(M+12,M+12)=8.*CY4*BA4*BA4
  500 CONTINUE
      RETURN
      END
C
C  ------------------------------------------------------------------------
C    REF: COMPUTER METHODS IN ADVANCED STRUCTURAL ANALYSIS ,C.K. WANG,
C    INTEXT INTERNATIONAL PUBLISHERS - 1973 PGS 353-354.
C
C    THIS SUBROUTINE INVERTS MATRIX OF N * N SIZE BY GAUSS - JORDON
C    ELIMINATION METHOD
C  ------------------------------------------------------------------------
C
C    A(N,N) = THE ORIGINAL MATRIX
C    N = ACTIVE NO. OF NODAL POINTS
C    B( N, N) = THIS MATRIX IS USED TO STORE THE ORIGINAL MATRIX A(N,N)
C    C( N, N) = THIS MATRIX IS FOR THE UNIT MATRIX A*AINV
C    INDEX( N, N) = THIS DOUBLED-COLUMNED MATRIX IS FOR KEEPING RECORDS
C
      SUBROUTINE INVERT(A,N,KK2,IPRNTM)
C
      IMPLICIT REAL*8(A-H,O-Z)
      DIMENSION INDEX(10,10),A( N, N),B(10,10),C(10,10)
C
      DO 107 I=1,N
      DO 107 J=1,N
  107 B(I,J)=A(I,J)
      DO 108 I=1,N
  108 INDEX(I,1)=0
      II=0
  109 AMAX=-1.
      DO 110 I=1,N
      IF(INDEX(I,1)) 110,111,110
  111 DO 112 J=1,N
      IF(INDEX(J,1)) 112,113,112
  113 TEMP=DABS(A(I,J))
      IF(TEMP-AMAX) 112,112,114
  114 IROW=I
      ICOL=J
      AMAX=TEMP
  112 CONTINUE
  110 CONTINUE
C
      IF(AMAX) 225,115,116
  116 INDEX(ICOL,1)=IROW
      IF(IROW-ICOL) 119,118,119
  119 DO 120 J=1,N
      TEMP=A(IROW,J)
  123 TEMP=A(I,ICOL)
      A(I,ICOL)=0.
      DO 124 J=1,N
  124 A(I,J)=A(I,J)-A(ICOL,J)*TEMP
  122 CONTINUE
C
      GO TO 109
  125 ICOL=INDEX(II,2)
```

```
      IROW=INDEX(ICOL,1)
      DO 126 I=1,N
      TEMP=A(I,IROW)
      A(I,IROW)=A(I,ICOL)
  126 A(I,ICOL)=TEMP
      II=II-1
  225 IF(II) 125,127,125
  127 CONTINUE
      IF(IPRNTM.NE.1) GO TO 8
      WRITE(KK2,128)
  128 FORMAT(/10X,' THE INVERSE OF MATRIX ')
      DO 129 I=1,N
  129 WRITE(KK2,106)I,(A(I,J),J=1,N)
  106 FORMAT( /,I3,5X,10(E11.4,1X))
    8 CONTINUE
C
      DO 130 I=1,N
      DO 130 J=1,N
      C(I,J)=0.
      DO 130 K=1,N
  130 C(I,J)=C(I,J)+B(I,K)*A(K,J)
      IF(IPRNTM.NE.1) GO TO 9
      WRITE(KK2,131)
  131 FORMAT(10X,' THE UNIT MATRIX '/)
      DO 132 I=1,N
  132 WRITE(KK2,106)I,(C(I,J),J=1,N)
    9 CONTINUE
      GO TO 134
  115 WRITE(KK2,133)
  133 FORMAT(1X,' ZERO PIVOT ')
  134 RETURN
      END
C
C  ------------------------------------------------------------------------

C  THIS SUBROUTINE COMPUTES THE EIGEN VALUES
C  ------------------------------------------------------------------------

C
      SUBROUTINE EIGEN(U,W,N,NN,DELTA,EIGV,KK2,IPRNTM)
C
      IMPLICIT REAL*8(A-H,O-Z)
      DIMENSION W(N,N),U(N,N)
      DIMENSION A(10,10),UI(10),UK(10),TEMP(10),EIGV(10)
C
      IF(IPRNTM.NE.1) GO TO 55
      WRITE(6,205)
  205 FORMAT(  /10X,'VECTOR','TRIAL',5X,'EIGEN VALUES',5X,'EIGEN VECTOR
     1S'/)
   55 CONTINUE
      CALL MATMUL(U,W,A,N,N,N)
      DO 10 M=1,NN
      DO 1 I=1,N
    1 UK(I)=1.
      ITRY=0
      M1=M-1
      IF(M-1) 5,5,2
    2 DO 4 I=1,M1
      DO 3 J=1,N
    3 UI(J)=U(J,I)
      CALL VCMAT(UI,W,TEMP,N,N)
      CALL VCVC(TEMP,UI,C,N)
      CALL VCVC(TEMP,UK,CM,N)
      C=CM/C
      CALL SCVC(C,UI,TEMP,N)
      DO 9 J=1,N
    9 UI(J)=UK(J)-TEMP(J)
      S=1./UI(1)
    4 CALL SCVC(S,UI,UK,N)
    5 CALL MATVC(A,UK,TEMP,N,N)
      E=TEMP(1)
```

```
      S=1./E
      CALL SCVC(S,TEMP,UI,N)
      DO 6 I=1,N
      IF(DABS(UI(I)-UK(I))-DELTA) 6,6,8
    8 IF(ITRY-100) 13,13,6
    6 CONTINUE
      CALL MATVC(A, UI,TEMP,N,N)

      CALL SCVC(E,UI,UK,N)
      DO 15 I=1,N
   15 TEMP(I)=TEMP(I)-UK(I)
      IF(IPRNTM.NE.1) GO TO 56
      WRITE(KK2,204)M,ITRY,E,UI(1),TEMP(1)
  204 FORMAT(/,5X,2I10, 3(E15.5))
      WRITE(KK2,206) (UI(I),TEMP(I),I=2,N)
  206 FORMAT(40X,2(E15.5))
   56 CONTINUE
      EIGV(M)=1./E
      DO 7 I=1,N
    7 U(I,M)=UI(I)
      GO TO 10
   13 CALL VCEQ(UI,UK,N)
      ITRY=ITRY+1
      IF(M-1) 5,5,2
   10 CONTINUE
      RETURN
      END
C
C   -----------------------------------------------------------------

C    REAL MATRIX MULTIPLICATION ( CALCULATES C=A*B)
C    A(M,N) = INPUT ARRAY 'A'
C    B(N,P) = INPUT ARRAY 'B'
C    C(M,P) = OUTPUT ARRAY 'C'
C   -----------------------------------------------------------------

C
      SUBROUTINE MATMUL(A,B,C,M,N,P)
C
      IMPLICIT REAL*8(A-H,O-Z)
      INTEGER P
      DIMENSION A( M, N),B( N, P),C( M, P),X(10),Y(10),Z(10)
      DO 1 I=1,M
      DO 1 J=1,P
    1 C(I,J)=0.
      DO 2 I=1,M
      DO 2 J=1,P
      DO 2 K=1,N
    2 C(I,J)=A(I,K)*B(K,J)+C(I,J)
      RETURN
C
C   -----------------------------------------------------------------

C    REAL MULTIPLICATION OF MATRIX WITH VECTOR (CALCULATES Z=A*X)
C    A(M,N) = INPUT ARRAY 'A'
C    X(N) = INPUT VECTOR 'X'
C    Z(M) = OUTPUT VECTOR 'Z'
C   -----------------------------------------------------------------

C
      ENTRY MATVC(A,X,Z,M,N)
      DO 5 I=1,M
    5 Z(I)=0.
      DO 6 I=1,M
      DO 6 J=1,N
    6 Z(I)=A(I,J)*X(J)+Z(I)
      RETURN
C
C   -----------------------------------------------------------------

C    MULTIPLICATION OF SCALAR WITH VECTOR (CALCULATES Y=S*X)
```

```
C     X(N) = INPUT VECTOR 'X'
C     S = INPUT SCALAR 'S'
C     Y(N) = OUTPUT VECTOR 'Y'
C   ------------------------------------------------------------------

C
       ENTRY SCVC(S,X,Y,N)
       DO 7 I=1,N
     7 Y(I)=S*X(I)
       RETURN
C
C   ------------------------------------------------------------------

C     MULTIPLICATION OF SCALAR WITH MATRIX ( CALCULATES B=S*A)
C     S = INPUT SCALAR 'S'
C     A(M,N) = INPUT ARRAY 'A'
C     B(M,N) = OUTPUT ARRAY 'B'
C   ------------------------------------------------------------------

C
       ENTRY SCMAT(S,A,B,M,N)
       DO 8 I=1,M
       DO 8 J=1,N
     8 B(I,J)=S*A(I,J)
       RETURN
C
C   ------------------------------------------------------------------

C     MULTIPLICATION OF VECTOR WITH VECTOR ( CALCULATES S=X*Y )
C     S = OUTPUT SCALAR
C     X(N) = INPUT VECTOR
C     Y(N) = INPUT VECTOR
C   ------------------------------------------------------------------

C
       ENTRY VCVC(X,Y,S,N)
       S=0.
       DO 9 I=1,N
     9 S=S+X(I)*Y(I)
       RETURN
C
C   ------------------------------------------------------------------

C     MULTIPLICATION OF VECTOR WITH MATRIX ( CALCULATES X=Z*A )
C     Z(N) = INPUT VECTOR
C     A(N,N) = INPUT ARRAY 'A'
C     X(N) = OUTPUT ARRAY 'X'
C   ------------------------------------------------------------------

C
       ENTRY VCMAT(Z,A,X,M,N)
       DO 10 J=1,N
       X(J)=0.
       DO 10 K=1,M
    10 X(J)=X(J)+Z(K)*A(K,J)
       RETURN
C
C   ------------------------------------------------------------------

C     VECTOR SUBSTITUTION ( EQUATES Y=X )
C     X(N) = INPUT VECTOR
C     Y(N) = OUTPUT VECTOR
C   ------------------------------------------------------------------

C
       ENTRY VCEQ(X,Y,N)
       DO 13 I=1,N
    13 Y(I)=X(I)
       RETURN
       END
C
```

```
C
C   ------------------------------------------------------------------
C      REF:INTRODUCTION TO STRUCTURAL DYNAMICS, J.M. BIGGS, MCGRAW-HILL
C      BOOK COMPANY - 1965.
C      THIS SUBROUTINE CARRIES OUT DIRECT STEP BY STEP INTEGRATION BY
C      LINEAR ACCELERATION USING NEWMARK'S BETA METHOD
C   ------------------------------------------------------------------
C
C      INCR = COUNT OF TIME INCREMENTS
C      DELT = TIME INCREMENT
C      XM(NN,NN) = MASS MATRIX
C      XK(NN,NN) = STIFFNESS MATRIX
C      F(NN) = FORCE VECTOR
C      UO(NN) = INITIAL DISPLACEMENT VECTOR
C      VO(NN) = INITIAL VELOCITY VECTOR
C      AAO(NN) = INITIAL ACCELERATION VECTOR
C      UU(NN) = DISPLACEMENT VECTOR
C      V(NN) = VELOCITY VECTOR
C      A(NN) = ACCELERATION VECTOR
C      XC(NN,NN) = DAMPING MATRIX
C      EPS = SMALL NO. TO TEST WHETHER ANY DIAGONAL ELEMENT IS ZERO OR NOT
C      UN1(NN) = SUBSTITUTION FOR UO(NN)
C      U(NN) =
C      REF(NN) =
C      EF(NN) = EFFECTIVE LOAD VECTOR
C      XKE(NN,NN) =
C
       SUBROUTINE INTGR1(INCR,DELT,XM,XK,F,XC,NN,UO,VO,AAO,UU,V,A,
      1EPS)
C
       IMPLICIT REAL*8(A-H,O-Z)
       DIMENSION XM(NN,NN),XK(NN,NN),F(NN),UO(NN),VO(NN),UU(NN),V(NN),
      1XC(NN,NN),A(NN),AAO(NN),UN1(30),U(30),REF(30),EF(30),XKE(30,30)
C
       IF(INCR.GE.2) GO TO 100
C
C     COMPUTATION OF CONSTANTS FOR INTEGRATION
C     VALUE OF BETA IS TAKEN AS 0.25
C
       ALPHA=.5
       BETA=.25
       AO=1./(BETA*DELT*DELT)
       A1=ALPHA/(BETA*DELT)
       A2=1./(BETA*DELT)
       A3=(.5/BETA)-1.
       A4=(ALPHA/BETA)-1.
       A5=.5*DELT*((ALPHA/BETA)-2.)
       A6=DELT*(1.-ALPHA)
       A7=ALPHA*DELT
C
C     FORMULATION OF EFFECTIVE STIFFNESS MATRIX
C
   100 DO 200 J=1,NN
       DO 200 K=1,NN
   200 XKE(J,K)=XK(J,K)+AO*XM(J,K)+A1*XC(J,K)
C
C     COMPUTATION OF EFFECTIVE LOAD VECTOR
C
       DO 400 J=1,NN
       REF(J)=0.
       DO 300 K=1,NN
   300 REF(J)=REF(J)+XM(J,K)*(AO*UO(K)+A2*VO(K)+A3*AAO(K))+XC(J,K)*
      1(A1*UO(K)+A4*VO(K)+A5*AAO(K))
   400 EF(J)=F(J)+REF(J)
C
C     SOLUTION FOR DISPLACEMENT VECTOR AT (T+DELTA T)
C
       CALL SOLVE(NN,XKE,EF,U,EPS)
```

```
C
C     SOLUTION FOR VELOCITY AND ACCELERATION VECTOR AT (T+DELTA T)
C
      DO 500 J=1,NN
      A(J)=AO*(U(J)-UO(J))-A2*VO(J)-A3*AAO(J)
  500 V(J)=VO(J)+A6*AAO(J)+A7*A(J)
C
C     RESETTING DISPLACEMENT VECTORS FOR SECOND TIME STEP
C
      DO 600 J=1,NN
      UN1(J)=UO(J)
      UO(J)=U(J)
      VO(J)=V(J)
      AAO(J)=A(J)
  600 UU(J)=U(J)
  800 CONTINUE
      RETURN
      END
C
C  -------------------------------------------------------------------
C     REF: THE COMPONENT ELEMENT METHOD IN DYNAMICS - LEVY AND WILKINSON
C     - MCGRAW-HILL BOOK COMPANY - 1976 PGS 17-19
C     THIS SUBROUTINE CARRIES OUT STEP BY STEP INTEGRATION USING THE
C     FINITE DIFFERENCE EXPANSION BY HOUBOLT METHOD.
C  -------------------------------------------------------------------

C
C     INCR = COUNT OF TIME INCREMENTS
C     DELT = TIME INCREMENT
C     XM(NN,NN) = MASS MATRIX
C     XK(NN,NN) = STIFFNESS MATRIX
C     F(NN) = FORCE VECTOR
C     UO(NN) = INITIAL DISPLACEMENT VECTOR
C     VO(NN) = INITIAL VELOCITY VECTOR
C     AAO(NN) = INITIAL ACCELERATION VECTOR
C     UU(NN) = DISPLACEMENT VECTOR
C     V(NN) = VELOCITY VECTOR
C     A(NN) = ACCELERATION VECTOR
C     XC(NN,NN) = DAMPING MATRIX
C     EPS = SMALL NO. TO TEST WHETHER ANY DIAGONAL ELEMENT IS ZERO OR NOT

C     UN1(NN) = SUBSTITUTION FOR UO(NN)
C     U(NN) =
C     REF(NN) =
C     EF(NN) = EFFECTIVE LOAD VECTOR
C     XKE(NN,NN) = EFFECTIVE STIFFNESS MATRIX
C     N = ACTIVE NO OF NODAL POINTS
C     M = 2 *N
C     NN = M+9
C
      SUBROUTINE INTGR2(INCR,DELT,XM,XK,F,XC,NN,UO,VO,AAO,UU,V,A,
     1EPS)
C
      IMPLICIT REAL*8(A-H,O-Z)
      DIMENSION XM(NN,NN),XK(NN,NN),F(NN),UO(NN),VO(NN),UU(NN),V(NN),
     1XC(NN,NN),A(NN),AAO(NN),UN1(30),U(30),REF(30),EF(30),XKE(30,30)
C
      IF(INCR.GE.2) GO TO 100
C
      AO=2./(DELT*DELT)
      A1=11./(6.*DELT)
      A2=5./(DELT*DELT)
      A3=3./DELT
      A4=-2.*AO
      A5=-A3/2.
      A6=AO/2.
      A7=A3/9.
      DO 50 J=1,NN
      UN1(J)=UO(J)-DELT*VO(J)+AAO(J)/AO
   50 U(J)=UN1(J)+2.*DELT*VO(J)
C
```

```
C     COMPUTATION OF EFFECTIVE STIFFNESS MATRIX
C
  100  DO 200 J=1,NN
       DO 200 K=1,NN
  200 XKE(J,K)=XK(J,K)+AO*XM(J,K)+A1*XC(J,K)
C
C     COMPUTATION OF EFFECTIVE FORCE VECTOR
C
       DO 400 J=1,NN
       REF(J)=0.
       DO 300 K=1,NN
  300 REF(J)=REF(J)+XM(J,K)*(A2*U(K)+A4*UO(K)+A6*UN1(K))+XC(J,K)*
     1(A3*U(K)+A5*UO(K)+A7*UN1(K))
  400 EF(J)=F(J)+REF(J)
C
C     SOLUTION DISPLACEMENT VECTOR AT (T+DELTA T)
C
       CALL SOLVE(NN,XKE,EF,UU,EPS)
C
C     EVALUATION OF ACCELERATIONS AND VELOCITIES AT TIME (T+DELTA T)
C
       DO 500 J=1,NN
       A(J)=AO*UU(J)-A2*U(J)-A4*UO(J)-A6*UN1(J)
  500 V(J)=A1*UU(J)-A3*U(J)-A5*UO(J)-A7*UN1(J)
C
C     RESETTING VALUES FOR NEXT TIME STEP
C
       DO 600 J=1,NN
       UN1(J)=UO(J)
       UO(J)=U(J)
  600 U(J)=UU(J)
  800 CONTINUE
       RETURN
       END
C
C
C
C   --------------------------------------------------------------------

C     REF:MECHANICAL VIBRATIONS BY S. S. RAO   PP486-488 ADDISON-WESLEY
C     PUBLISHING COMPANY.
C
C     THIS SUBROUTINE CARRIES OUT DIRECT STEP BY STEP INTEGRATION USING
C     WILSON THETA METHOD - WHICH ASSUMES THAT THE ACCELERATION VARIES
C     LINEARLY BETWEEN TWO INSTANTS OF TIME.
C   --------------------------------------------------------------------

C
C     INCR = COUNT OF TIME INCREMENTS
C     DELT = TIME INCREMENT
C     XM(NN,NN) = MASS MATRIX
C     XK(NN,NN) = STIFFNESS MATRIX
C     F(NN) = FORCE VECTOR
C     UO(NN) = INITIAL DISPLACEMENT VECTOR
C     VO(NN) = INITIAL VELOCITY VECTOR
C     AAO(NN) = INITIAL ACCELERATION VECTOR
C     UU(NN) = DISPLACEMENT VECTOR
C     V(NN) = VELOCITY VECTOR
C     A(NN) = ACCELERATION VECTOR
C     XC(NN,NN) = DAMPING MATRIX
C     EPS = SMALL NO. TO TEST WHETHER ANY DIAGONAL ELEMENT IS ZERO OR NOT

C     UN1(NN) = SUBSTITUTION FOR UO(NN)
C     U(NN) = DISPLACEMENT AT (I+THETA) INTERVAL
C     REF(NN) =
C     EF(NN) = EFFECTIVE LOAD VECTOR
C     XKE(NN,NN) = EFFECTIVE STIFFNESS MATRIX
C
       SUBROUTINE INTGR3(INCR,DELT,XM,XK,F,XC,NN,UO,VO,AAO,UU,V,A,EPS)
C
       IMPLICIT REAL*8(A-H,O-Z)
```

```
      DIMENSION XM(NN,NN),XK(NN,NN),F(NN),UO(NN),VO(NN),UU(NN),V(NN),
     1XC(NN,NN),A(NN),AAO(NN),          U(30),REF(30),EF(30),XKE(30,30)
     2,REFO(30),FO(30),F1(30),REX(30)

      A3=6./((THET**3)*(DELT*DELT))
      A4=6./((THET*THET)*DELT)
      A5=(DELT*DELT)/6.
C
C   INITIATION
C
   25 CONTINUE
      DO 50 J=1,NN
      F1(1)=F(1)
      IF(INCR.EQ.1) FO(J)=F(J)
      IF(INCR.NE.1) FO(J)=F1(J)
      REF(J)=0.
   50 CONTINUE
C
C   FORMULATIE STIFFNESS MATRIX
C
  100 DO 200 J=1,NN
      DO 200 K=1,NN
  200 XKE(J,K)=XK(J,K)+AO*XM(J,K)+A1*XC(J,K)
C
C   COMPUTATION OF EFFECTIVE LO788. C
      DO 400 J=1,NN
      REFO(J)=0.
      DO 300 K=1,NN
  300 REX(J)=XM(J,K)*(AO*UO(J)+2.*A1*VO(J)+2.*AAO(J))+XC(J,K)*(A1*
     1UO(J)+2.*VO(J)+A2*AAO(J))
      REFO(J)=REFO(J)+REF(J)+REX(J)
  400 EF(J)=F(J)+REFO(J)
C
C   SOLUTION FOR DISPLACEMENT VECTOR AT (T+DELTA T)
C
      CALL SOLVE(NN,XKE,EF,U,EPS)
C
C   SOLUTION FOR DISPLACEMENT VELOCITY AND ACCELERATION VECTORS
C   AT (T+DELTA T)
C
      DO 500 J=1,NN
      A(J)=A3*(U(J)-UO(J))-A4*VO(J)+(1.-3./THET)*AAO(J)
      V(J)=VO(J)+0.5*DELT*(A(J)+AAO(J))
  500 UU(J)=UO(J)+DELT*VO(J)+A5*(A(J)+2.*AAO(J))
C
C   RESETTING DISPLACEMENT VECTORS FOR SECOND TIME STEP
C
      DO 600 J=1,NN
      UO(J)=UU(J)
      VO(J)=V(J)
      AAO(J)=A(J)
      F1(J)=FO(J)+(REFO(J)-FO(J)-REX(J))/THET
      REF(J)=FO(J)+THET*(F1(J)-FO(J))
  600 CONTINUE
  800 CONTINUE
      RETURN
      END
C
C ---------------------------------------------------------------------

C THIS SUBROUTINE SOLVES SERIES OF SIMULTANEOUS EQUATIONS
C REF: NUMERICAL AND MATRIX METHODS IN STRUCTURAL MECHANICS WITH
C APPLICATIONS TO COMPUTERS, P.C. WANG - JOHN WILEY & SONS - 1966 -
C PGS 290-294.
C ---------------------------------------------------
C
      SUBROUTINE SOLVE(NN,A,U,V,EPS)
C
C  A(NM,NM) = COEFFICIENTS OF THE UNKNOWNS IN THE EQUATIONS
C  U(NM) = CONSTANTS AT THE RIGHT HAND SIDE OF THE EQUATIONS
C  V(NM) = RESULT OF THE UNKNOWNS IN SEQUENCE
```

```
C    NM = NUMBER OF EQUATIONS
C    EPS = SMALL NUMBER TO TEST WHETHER ANY DIAGONAL ELEMENT IS ZERO OR
C          NOT.
C
       IMPLICIT REAL*8(A-H,O-Z)
       DIMENSION A(30,30),U(NN),V(NN)
C
       DO 2000 I=1,NN
       K=I
       IF(I-NN) 1000,1400,1000
C
C    TEST TO SEE WHETHER THE DIAGONAL ELEMENT IS ZERO OR NOT.
C
 1000 IF(DABS(A(I,I))-EPS) 1100,1100,1400
C
C    ADD SUBSEQUENT EQUATIONS TO THE CURRENT ONES.
C
 1100 K=K+1
       IF(K.GT.NN) K=NN
       U(I)=U(I)+U(K)
       DO 1200 J=1,NN
 1200 A(I,J)=A(I,J)+A(K,J)
 1300 GO TO 1000
 1400 DIV=A(I,I)
       U(I)=U(I)/DIV
C
C    DIVIDE ALL ELEMENTS OF I-TH EQUATION BY A(I,I)
C
       DO 1500 J=1,NN
 1500 A(I,J)=A(I,J)/DIV
C
C    REDUCE THE I-TH ELEMENT OF THE OTHER EQUATIONS TO ZERO
C
       DO 2000 MM=1,NN
       DELT=A(MM,I)
       IF(DABS(DELT)-EPS) 2000,2000,1600
 1600 IF(MM-I) 1700,2000,1700
 1700 U(MM)=U(MM)-U(I)*DELT
       DO 1800 J=1,NN
 1800 A(MM,J)=A(MM,J)-A(I,J)*DELT
 2000 CONTINUE
       DO 2500 J=1,NN
 2500 V(J)=U(J)
       RETURN
       END
C
C  ---------------------------------------------------------------------

C    THIS SUBROUTINE COMPUTES STATIC DISPLACEMENTS - FLEXIBILITY METHOD
C  ---------------------------------------------------------------------

C
       SUBROUTINE STATIC(A,M,B,NN,US,KK2)
C
C    A(M,M) = FLEXIBILITY MATRIX
C    B(NN) = NODAL LOAD VECTOR
C    US(M) = DISPLACEMENT VECTOR
C
       IMPLICIT REAL *8(A-H,O-Z)
       DIMENSION A(M,M),B(NN),US(M)
       DIMENSION A(M,M),B(NN),US(M)
C
C    DISPLACEMENT=FLEXIBILITY MATRIX * NODAL LOAD VECTOR
C
       DO 1 J=1,M
       US(J)=0.
       DO 1 K=1,M
       US(J)=A(J,K)*B(K)+US(J)
     1 CONTINUE
       RETURN
       END
```

```
C
C  ------------------------------------------------------------------
C     THIS SUBROUTINE COMPUTES THE LOAD OR FORCE AT THE WHEEL - RAIL
C     INTERFACE FOR ANY WHEEL(S) WHICH MAY FALL UNDER THE INFLUENCE
C     OF A DISTANCE OF 'DLTX' FROM A NODAL POINT.
C  ------------------------------------------------------------------
C
      SUBROUTINE CONFOR(N,M,NN,G,UU,AC,XKY1,UM1,SM1,XLB1,BA1,XKY2,UM2,
     1SM2,XLB2,BA2,XKY3,UM3,SM3,XLB3,BA3,XKY4,UM4,SM4,XLB4,BA4,FAC1,FAC2
     2,FAC3,LCAR,NW,Y,XPL,FF,DT,VEL,NP,NU)
C
      IMPLICIT REAL *8(A-H,O-Z)
      INTEGER FAC1(NW),FAC2(NW),FAC3(NW)
      DIMENSION UU(NN),AC(NN),Y(NW)
      DIMENSION BB(18),CC(18),DD(18),FF( M)
      COMMON/BLOCK 1/XLAMD1,XLAMD2,ZETA1,ZETA2
      IF(LCAR.EQ.1) NWLT=8
      IF(LCAR.EQ.2) NWLT=16
      IF(LCAR.EQ.3) NWLT=24
      IF(LCAR.EQ.4) NWLT=32
C
C     INITIALIZATION OF ARRAYS
C
      AA=0.
      DO 300 K=1,M
      CC(K)=0.
      DD(K)=0.
      BB(K)=0.
      FF(K)=0.
  300 CONTINUE
C
C     VERIFICATION OF WHEEL PRESENCE BETWEEN TWO NODAL POINTS
C
      DO 1200 I=1,NP
      X1=I*XPL
      X2=(I-1)*XPL
      L=N+I
      KK=1
      DO 1100 JJM=1,NW
      KK=-KK
      IF(KK) 350,400,400
  350 FAT1=XLAMD1
      FAT2=XLAMD2
      GO TO 430
  400 FAT1=ZETA1
      FAT2=ZETA2
  430 CONTINUE
      IF(Y(JJM).GT.X1.OR.Y(JJM).LT.X2) GO TO 1100
      X=Y(JJM)-X2
      ALPHA=X/XPL
      BETA=1.-ALPHA
      C10=FAT2*BETA
      C11=FAT2*ALPHA
      C12=FAT1*BETA
      C13=FAT1*ALPHA
      IF(JJM.GT.24) GO TO 900
      IF(JJM.GT.16) GO TO 700
      IF(JJM.GT.8) GO TO 500
C
C     VEHICLE NO. 1
C
      AA=(SM1+UM1)*G
      IF(I.GT.N.OR.L.GT.M) GO TO 470
      BB(I)=XKY1*(UU(M+1)+FAC1(JJM)*XLB1*UU(M+2)+FAC3(JJM)*BA1*
     1UU(M+3))
      CC(I)=-XKY1*(C11*UU(I+1)+C10*UU(I)+C13*UU(L+1)+C12*UU(L))
      DD(I)=-UM1*(C11*AC(I+1)+C10*AC(I)+C13*AC(L+1)+C12*AC(L))
  450 CONTINUE
```

```
  460 CC(L)=-XKY1*(C11*UU(L+1)+C10*UU(L)+C13*UU(I+1)+C12*UU(I))
      DD(L)=-UM1*(C11*AC(L+1)+C10*AC(L)+C13*AC(I+1)+C12*AC(I))
  470 GO TO 1000
C
C     VEHICLE NO. 2
C
  500 AA=(SM2+UM2)*G
      IF(I.GT.N.OR.L.GT.M) GO TO 570
      BB(I)=XKY2*(UU(M+4)+FAC1(JJM)*XLB2*UU(M+5)+FAC3(JJM)*BA2*
     1UU(M+6))
      CC(I)=-XKY2*(C11*UU(I+1)+C10*UU(I)+C13*UU(L+1)+C12*UU(L))
      DD(I)=-UM2*(C11*AC(I+1)+C10*AC(I)+C13*AC(L+1)+C12*AC(L))
  550 CONTINUE
  560 CC(L)=-XKY2*(C11*UU(L+1)+C10*UU(L)+C13*UU(I+1)+C12*UU(I))
      DD(L)=-UM2*(C11*AC(L+1)+C10*AC(L)+C13*AC(I+1)+C12*AC(I))
  570 GO TO 1000
C
C     VEHICLE NO. 3
C
  700 AA=(SM3+UM3)*G
      IF(I.GT.N.OR.L.GT.M) GO TO 770
      BB(I)=XKY3*(UU(M+7)+FAC1(JJM)*XLB3*UU(M+8)+FAC3(JJM)*BA3*
     1UU(M+9))
      CC(I)=-XKY3*(C11*UU(I+1)+C10*UU(I)+C13*UU(L+1)+C12*UU(L))
      DD(I)=-UM3*(C11*AC(I+1)+C10*AC(I)+C13*AC(L+1)+C12*AC(L))
  750 CONTINUE
  760 CC(L)=-XKY3*(C11*UU(L+1)+C10*UU(L)+C13*UU(I+1)+C12*UU(I))
      DD(L)=-UM3*(C11*AC(L+1)+C10*AC(L)+C13*AC(I+1)+C12*AC(I))
  770 GO TO 1000
C
C     VEHICLE NO. 4
C
  900 AA=(SM4+UM4)*G
      IF(I.GT.N.OR.L.GT.M) GO TO 970
      BB(I)=XKY4*(UU(M+10)+FAC1(JJM)*XLB4*UU(M+11)+FAC3(JJM)*BA4*
     1UU(M+12))
      CC(I)=-XKY4*(C11*UU(I+1)+C10*UU(I)+C13*UU(L+1)+C12*UU(L))
      DD(I)=-UM4*(C11*AC(I+1)+C10*AC(I)+C13*AC(L+1)+C12*AC(L))
  950 CONTINUE
  960 CC(L)=-XKY4*(C11*UU(L+1)+C10*UU(L)+C13*UU(I+1)+C12*UU(I))
      DD(L)=-UM4*(C11*AC(L+1)+C10*AC(L)+C13*AC(I+1)+C12*AC(I))
  970 GO TO 1000
 1000 IF(I.GT.N.OR.L.GT.M) GO TO 1075
 1025 FF(I)=AA+BB(I)+CC(I)+DD(I)
 1050 FF(L)=AA+BB(L)+CC(L)+DD(L)
 1075 IF(JJM.GE.NWLT) GO TO 1200
 1100 CONTINUE
 1200 CONTINUE
      RETURN
      END
C
$ENTRY
      1.65D  6    386.40D000   347.22D-04
    654.14D000    11.05D000    70.72D000    1.98D+07     1.17D+06
    484.42D000     4.53D000    56.02D000    1.66D+07     1.28D+06
    529.50D000     4.53D000    61.66D000    1.66D+07     1.28D+06
    157.40D000     4.53D000    15.10D000    0.27D+07     0.24D+06
   3324.00D000   204.00D000    54.00D000    29.50D000    0.00D000    000.00D000

  11020.00D000   190.25D000    34.00D000    29.50D000    0.00D000    138.25D000

  11020.00D000   190.25D000    34.00D000    29.50D000    0.00D000     82.50D000

   1600.00D000   164.88D000    34.00D000    29.50D000    0.00D000    118.50D000

      9     0     1     4
    512.00D000    13.80D000  7569.79D000    0
    10   322000    0.01D-01  1760.00D-00     6.20D-02
     60.97D000    10.32D-01   600.32D-01
+1+1+1+1-1-1-1-1+1+1+1+1-1-1-1-1+1+1+1+1-1-1-1-1+1+1+1+1-1-1-1-1
+1+1-1-1+1+1-1-1+1+1-1-1+1+1-1-1+1+1-1-1+1+1-1-1+1+1-1-1+1+1-1-1
```

2037. +1-1+1-1+1-1+1-1+1-1+1-1+1-1+1-1+1-1+1-1+1-1+1-1+1-1+1-1+1-1+1-1+1-1
2038. /*

FIGURES

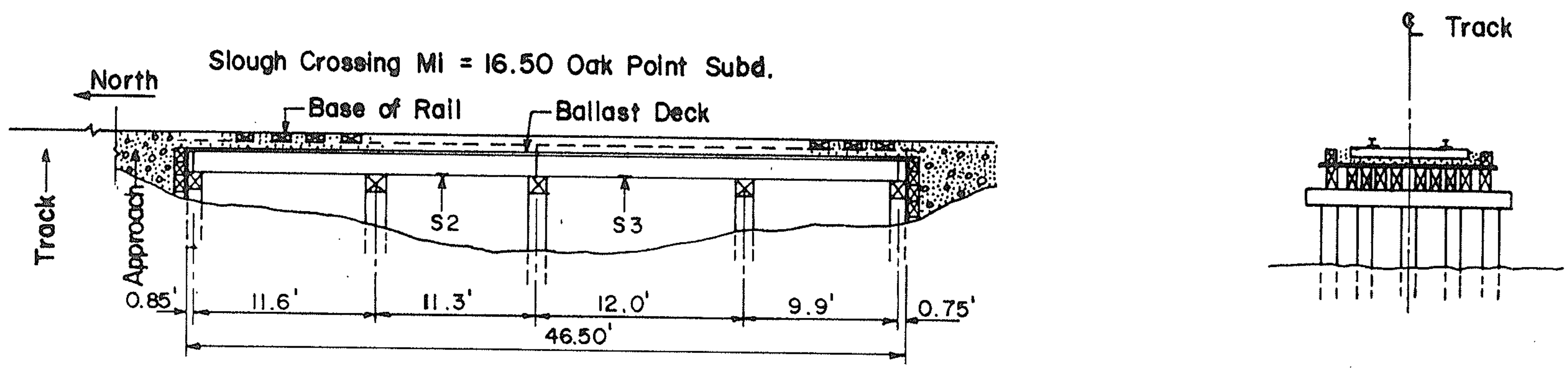

Figure 3.1 Elevation and typical cross-section of the ballast-deck bridge

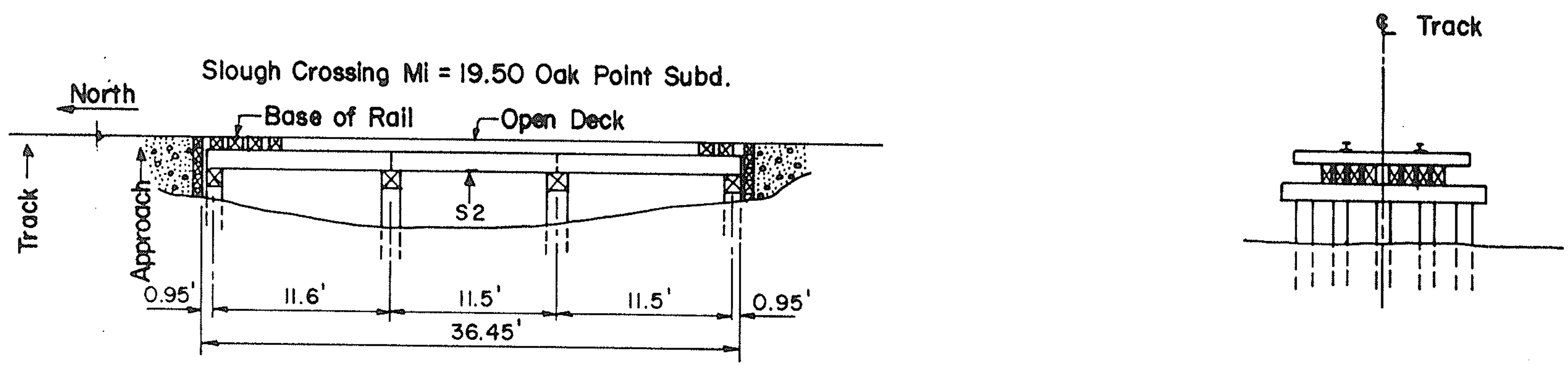

Figure 3.2 Elevation and typical cross section of the open-deck bridge

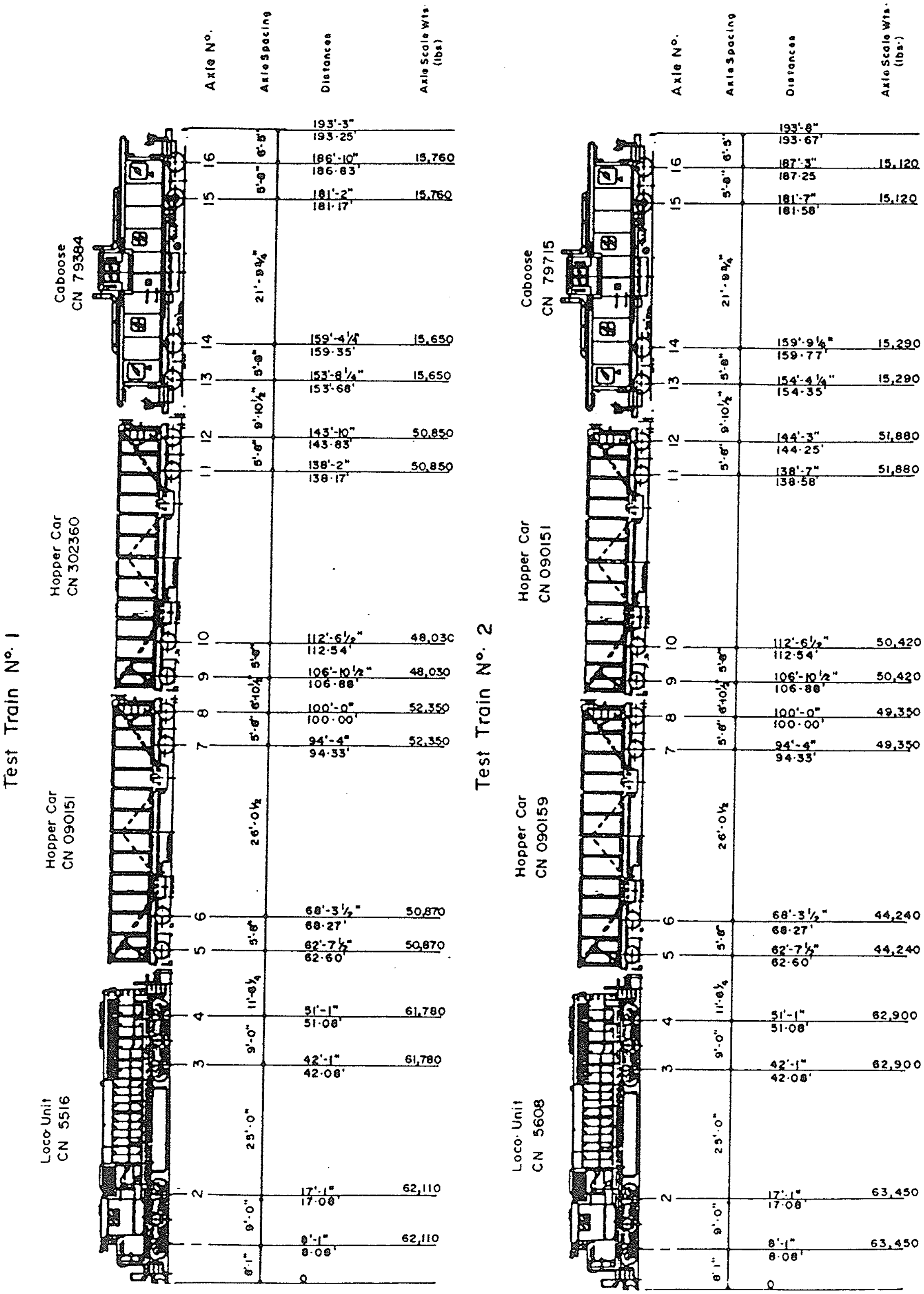

Figure 3.3 Arrangement of locomotives and cars in test trains No. 1 and 2

Figure 3.4 Photograph showing a typical test train

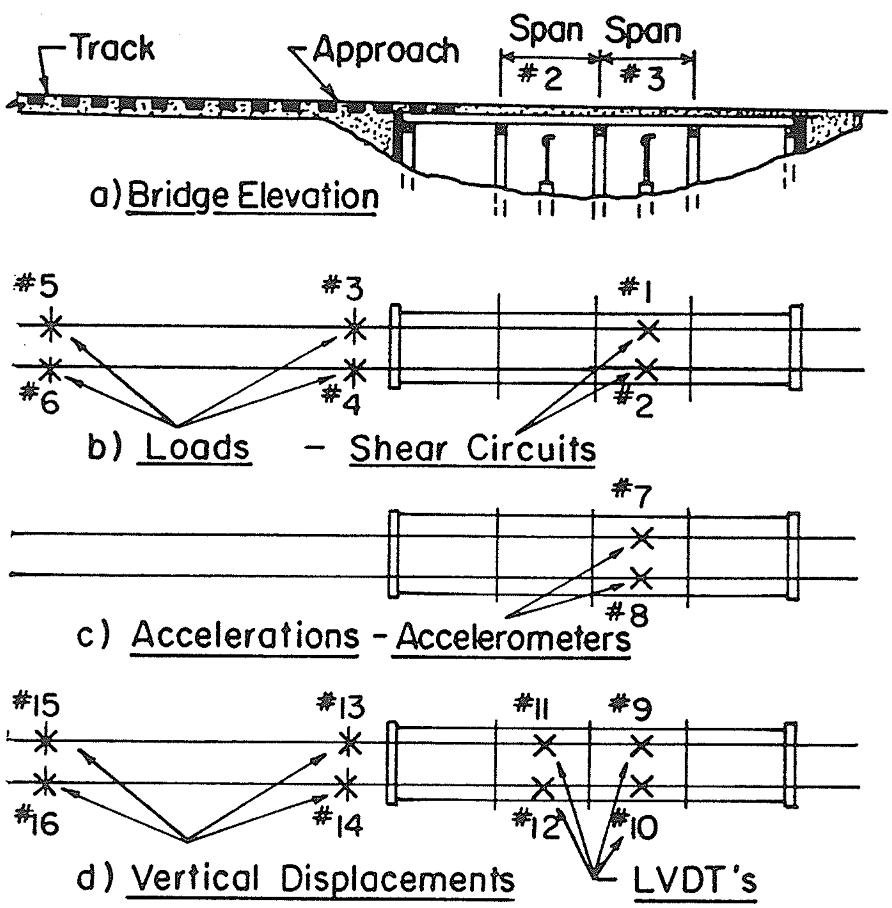

Figure 3.5 Location of shear circuits, LVDT's and accelerometers - ballast deck bridge site

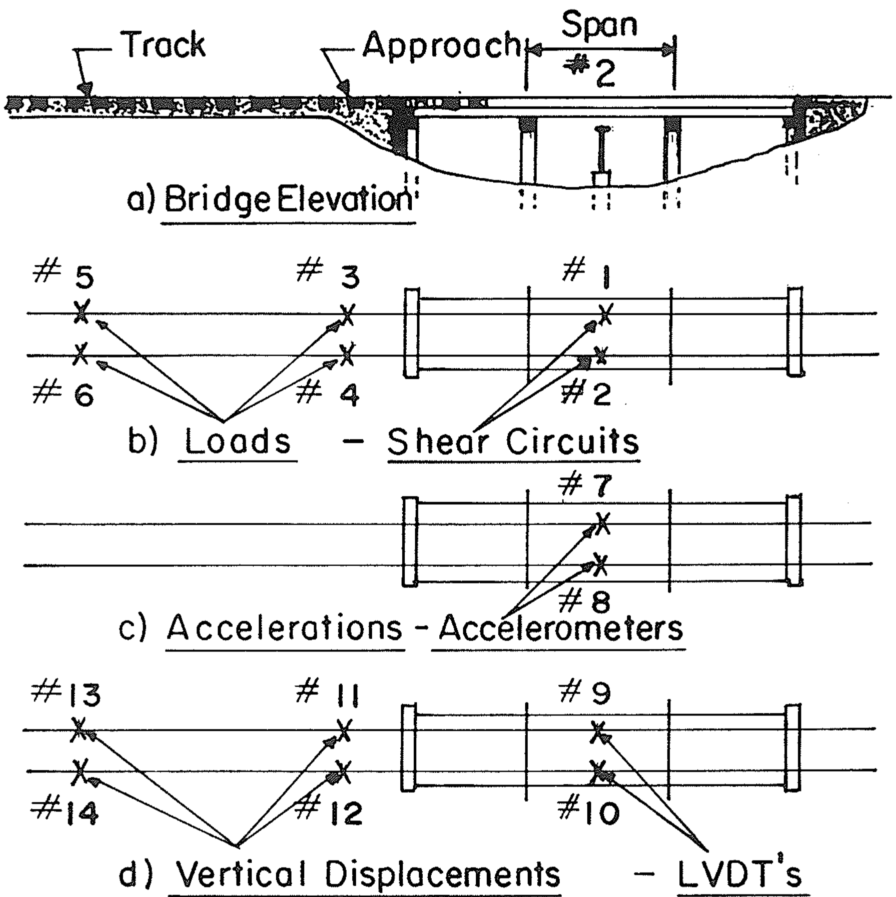

Figure 3.6 Location of shear circuits, LVDT's and accelerometers - open deck bridge site

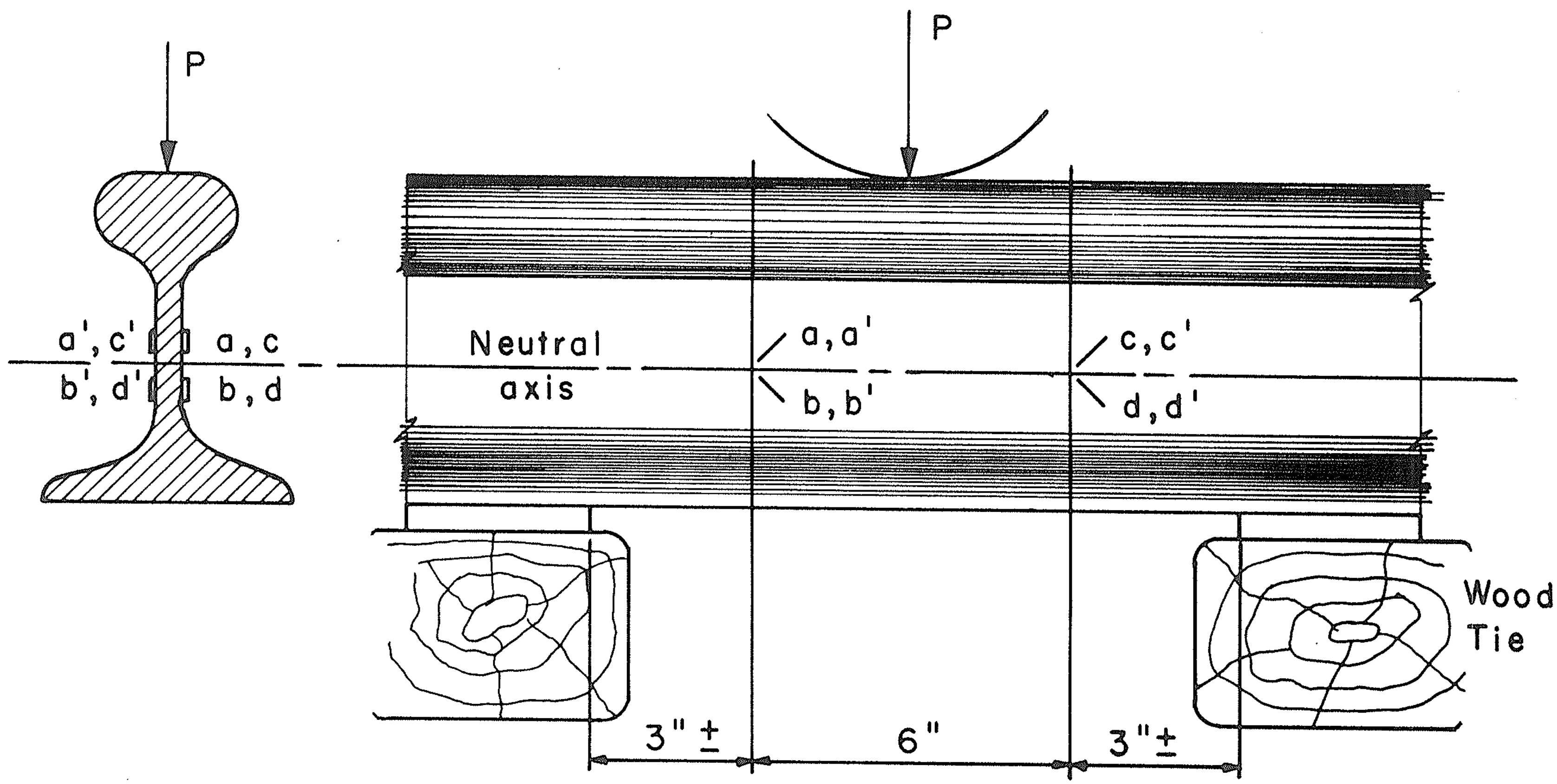

Figure 3.7 Detail of strain gauges in shear-load circuit

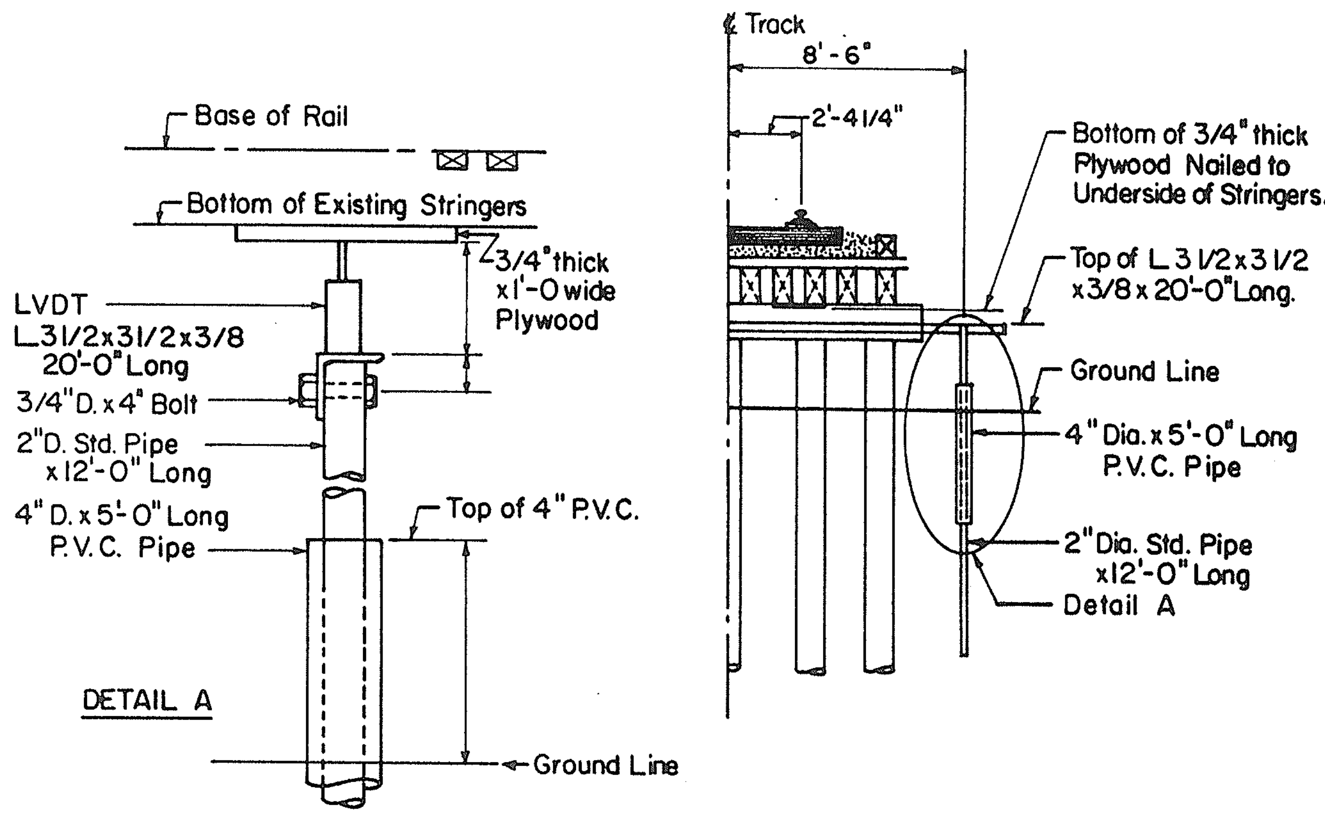

Figure 3.8 Typical support system for LVDT's

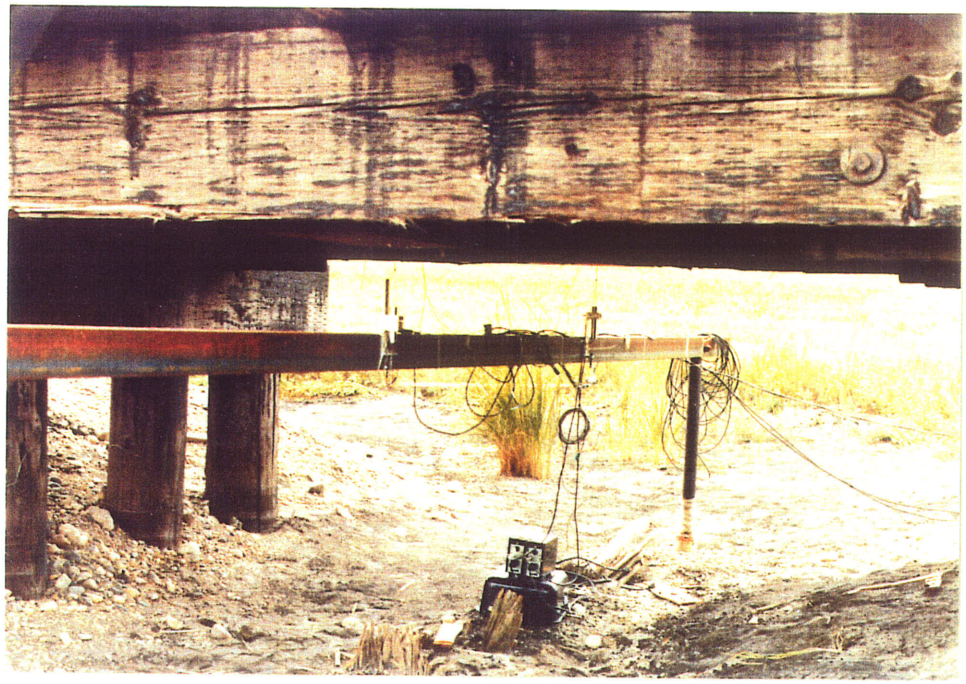

Figure 3.9 Photograph showing typical support system for LVDT's

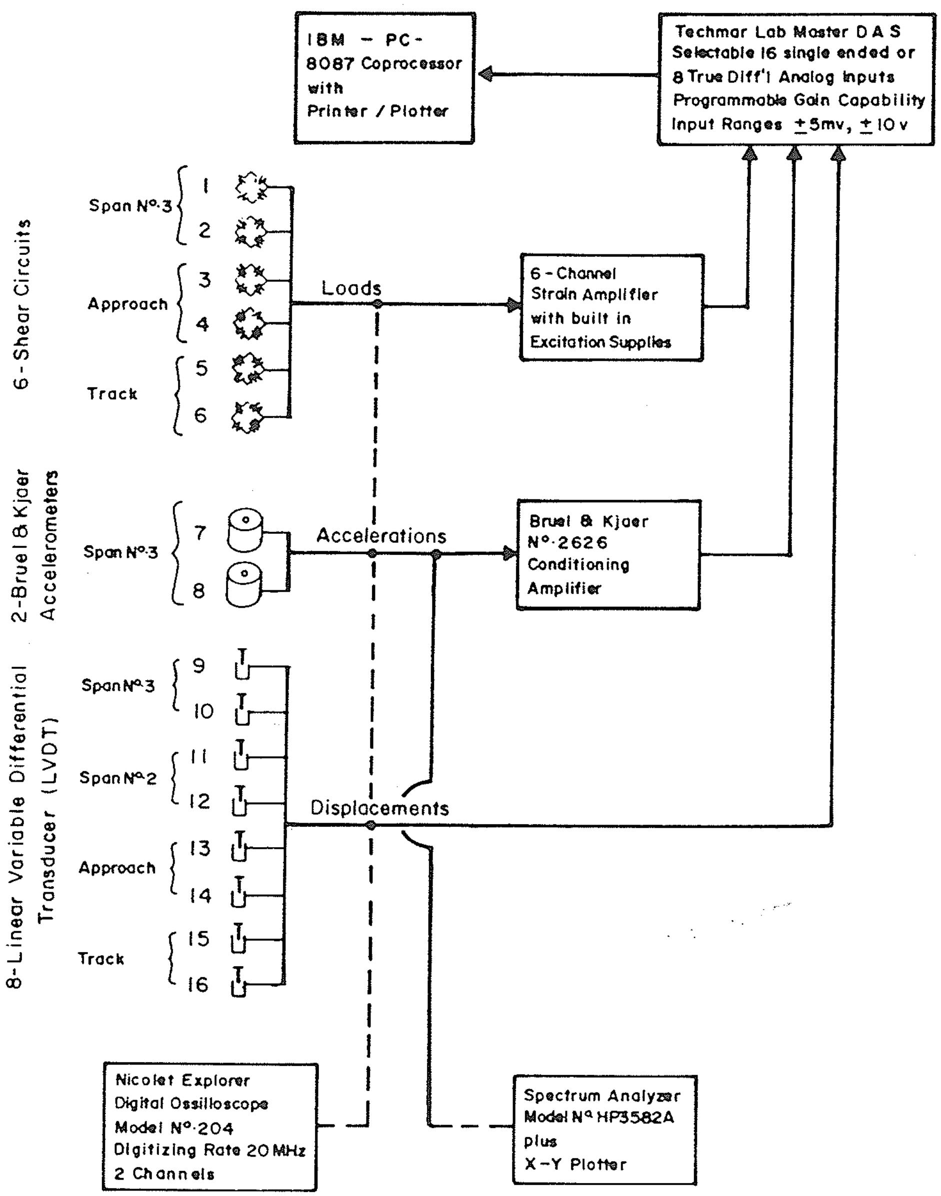

Figure 3.10 Typical outline of circuitry for dynamic tests

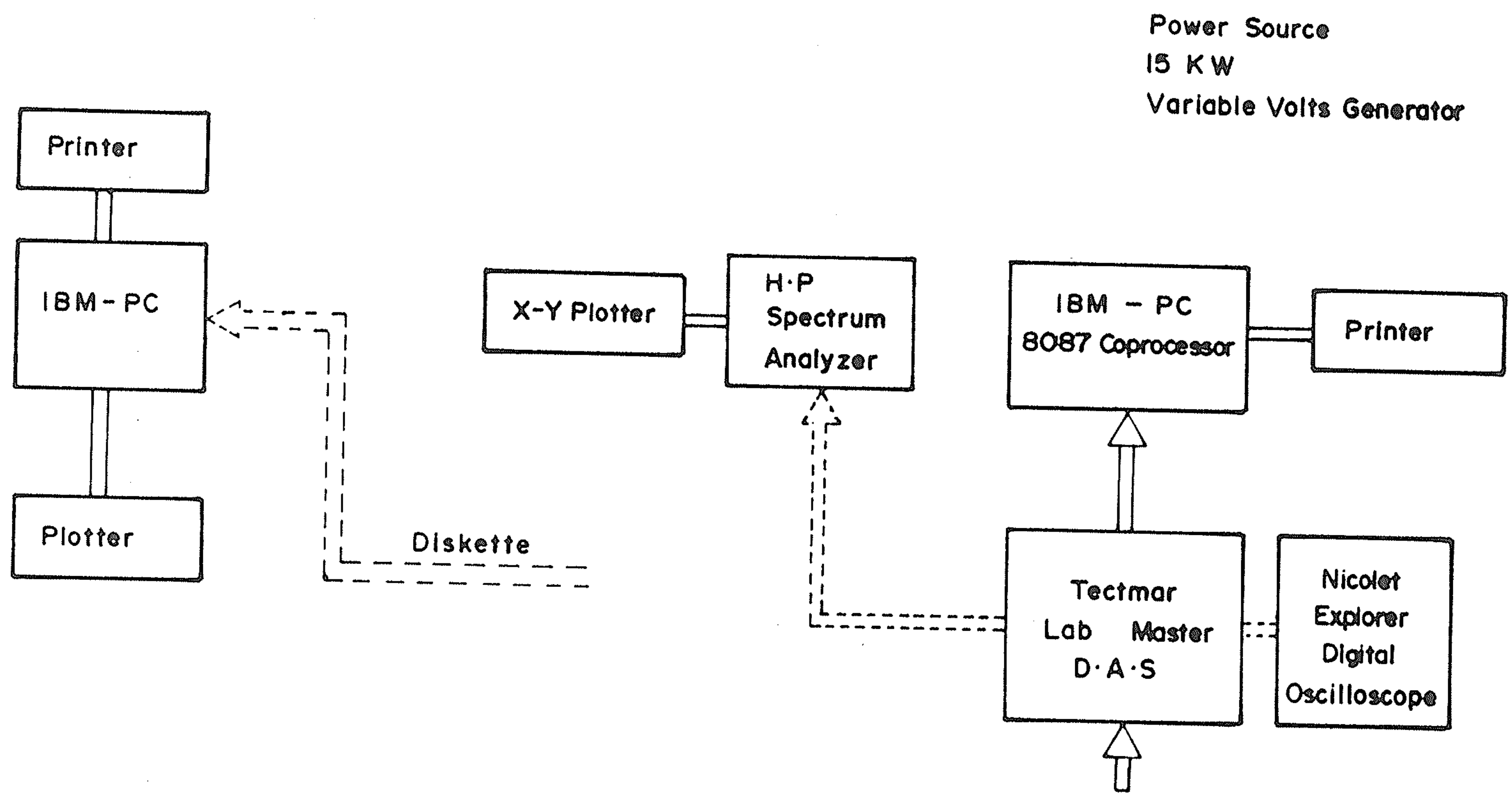

Figure 3.11 Test equipment in truck trailer

Figure 3.12 Photograph showing test equipment in truck trailer

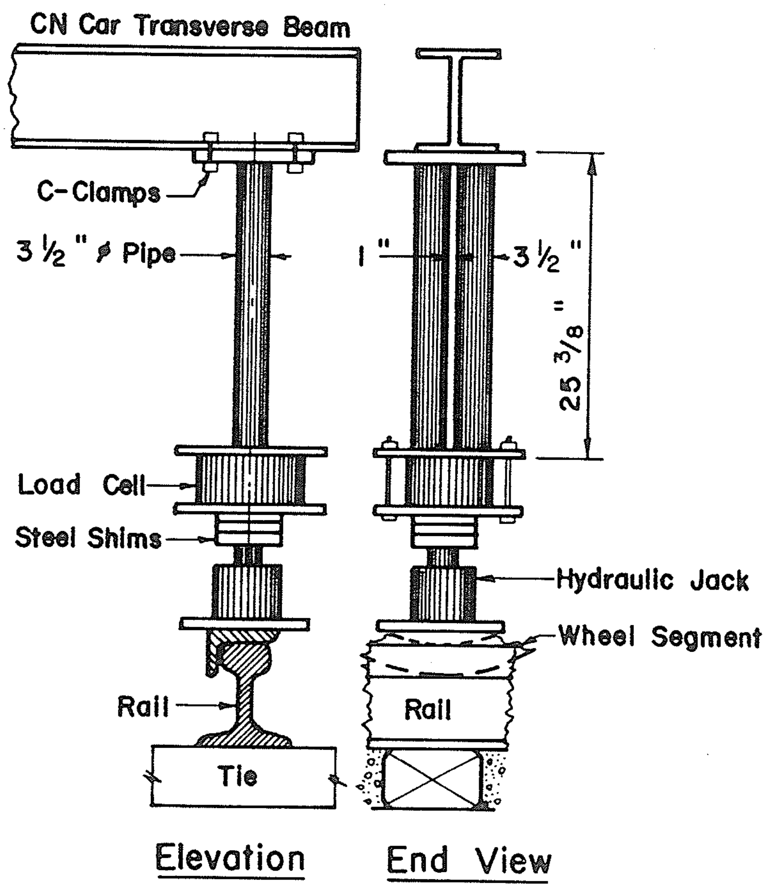

Figure 3.13 Set-up for calibration tests

Figure 3.14 Photograph showing calibration test in progress

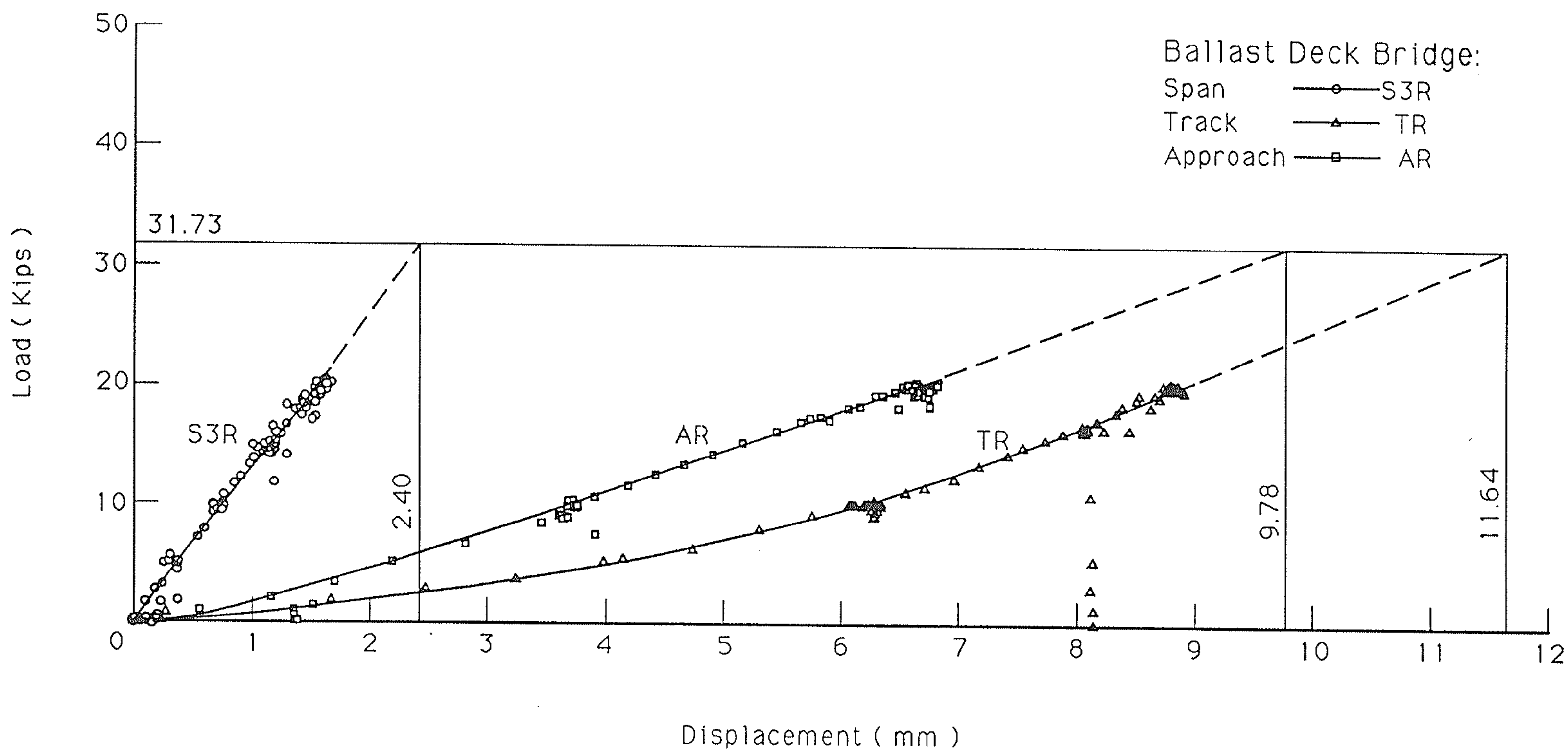

Figure 3.15 Load-displacement characteristics
BDB Site - Locations S3, A and T (given in Fig. 3.5)
- Test Train No. 1

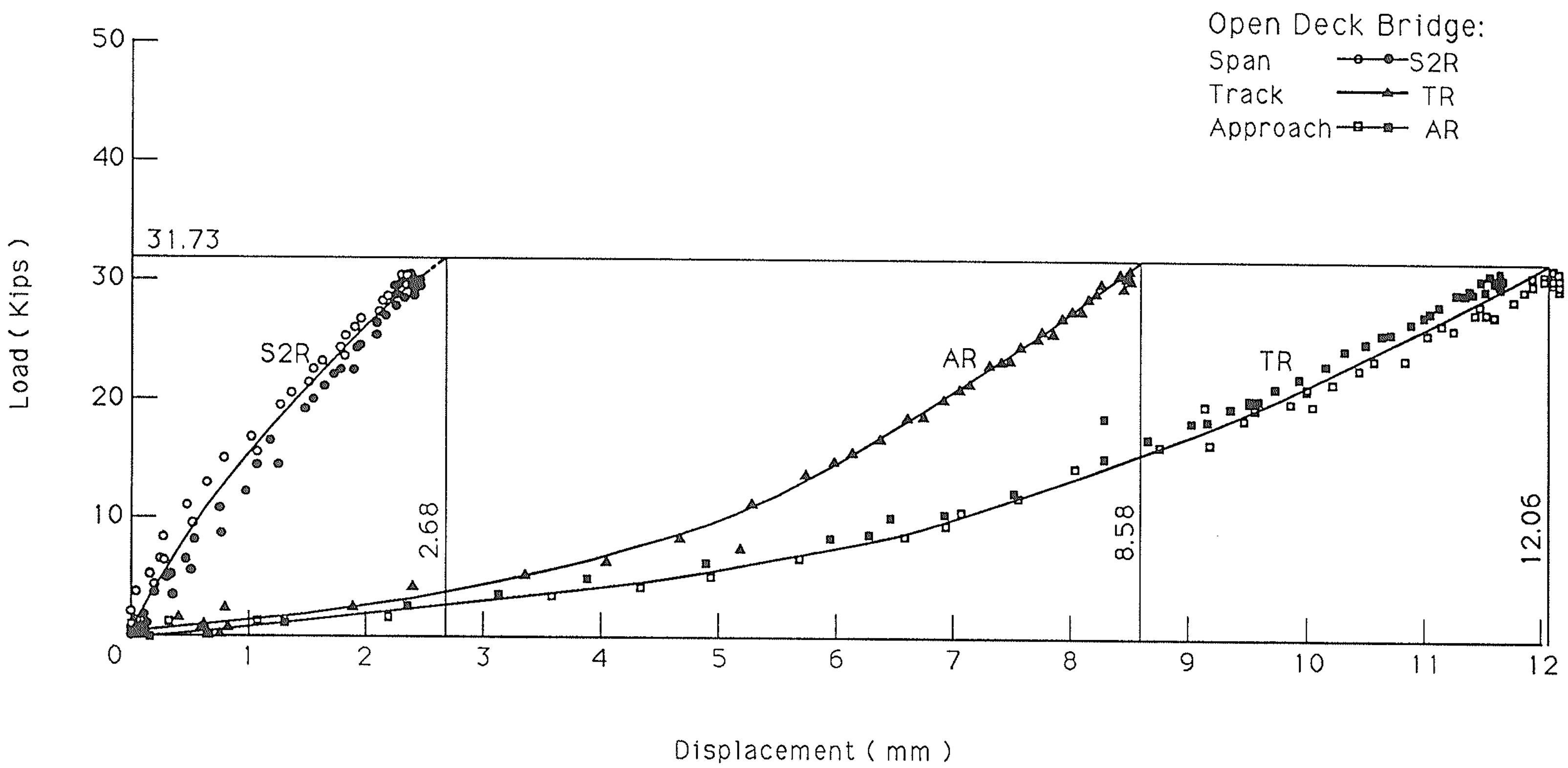

Figure 3.16 Load-displacement characteristics
ODB Site - Locations S2, A and T (given in Fig. 3.6)
- Test Train No. 2

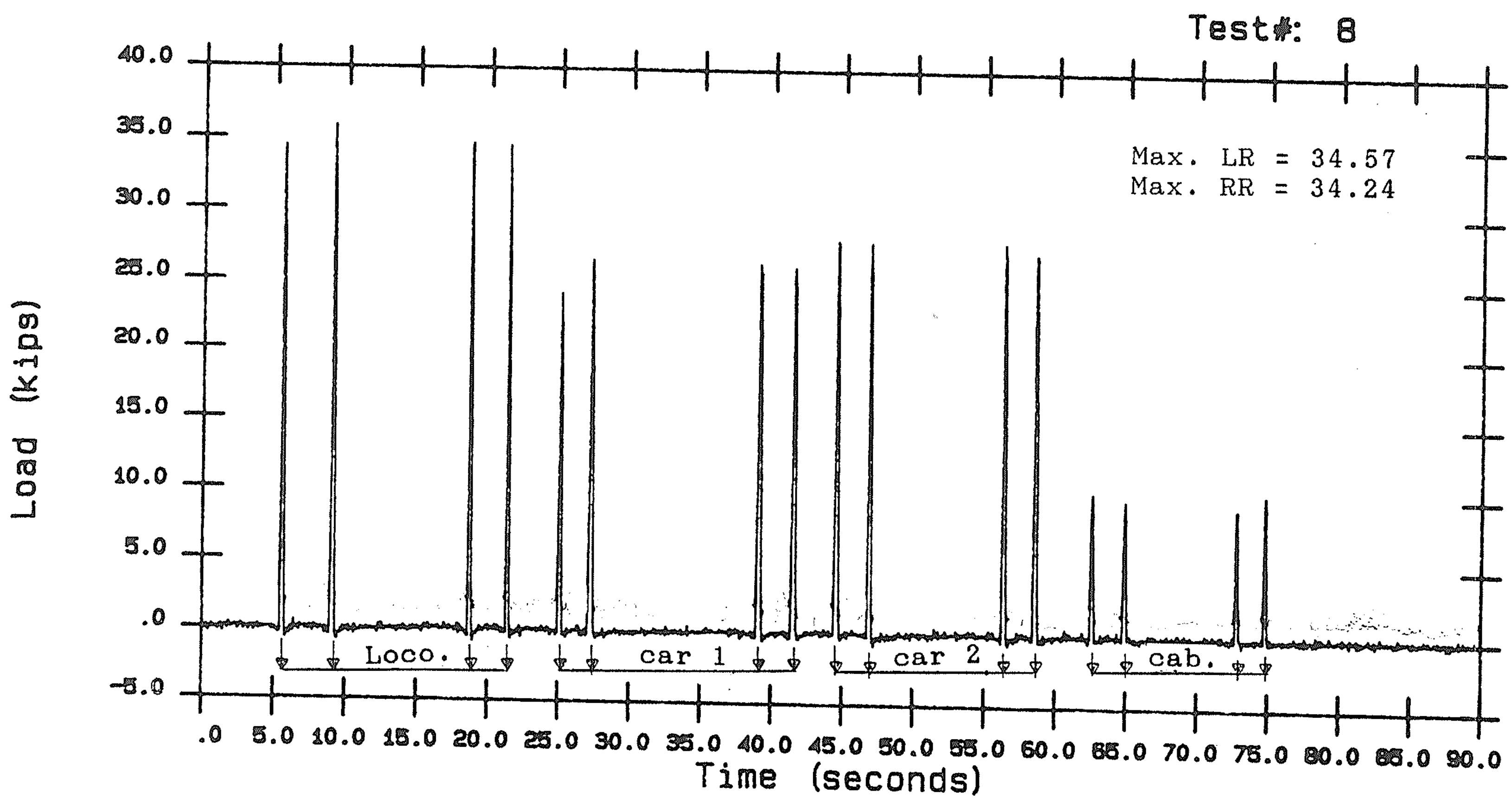

Figure 3.17 Loads at wheel-rail interfaces versus time
BDB Site - Midpoint of Span S3 - Test Train No. 2
Speed 1 mph

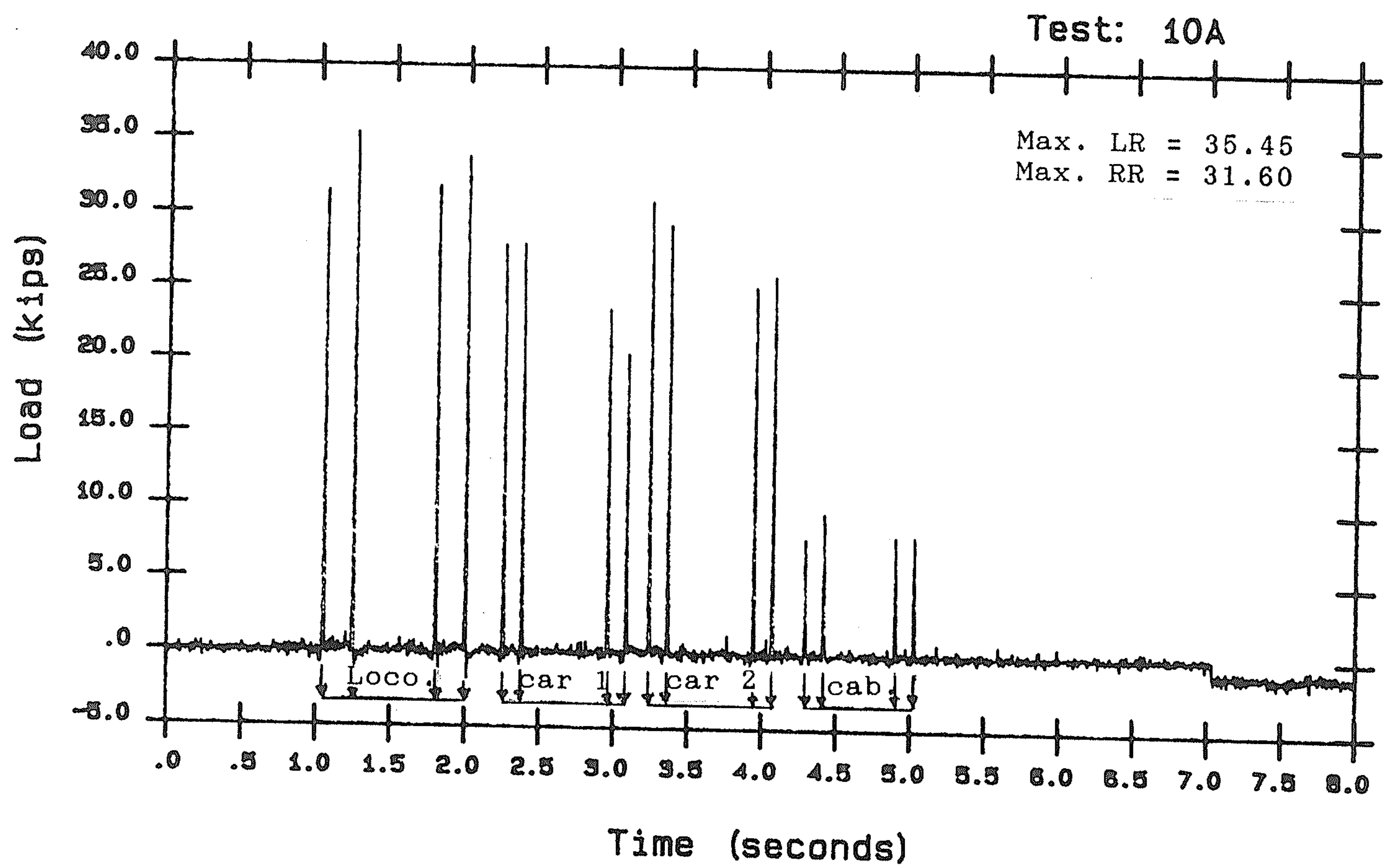

Figure 3.18 Loads at wheel-rail interfaces versus time
BDB Site - Midpoint of Span S3 - Test Train No. 2
Speed 30 mph

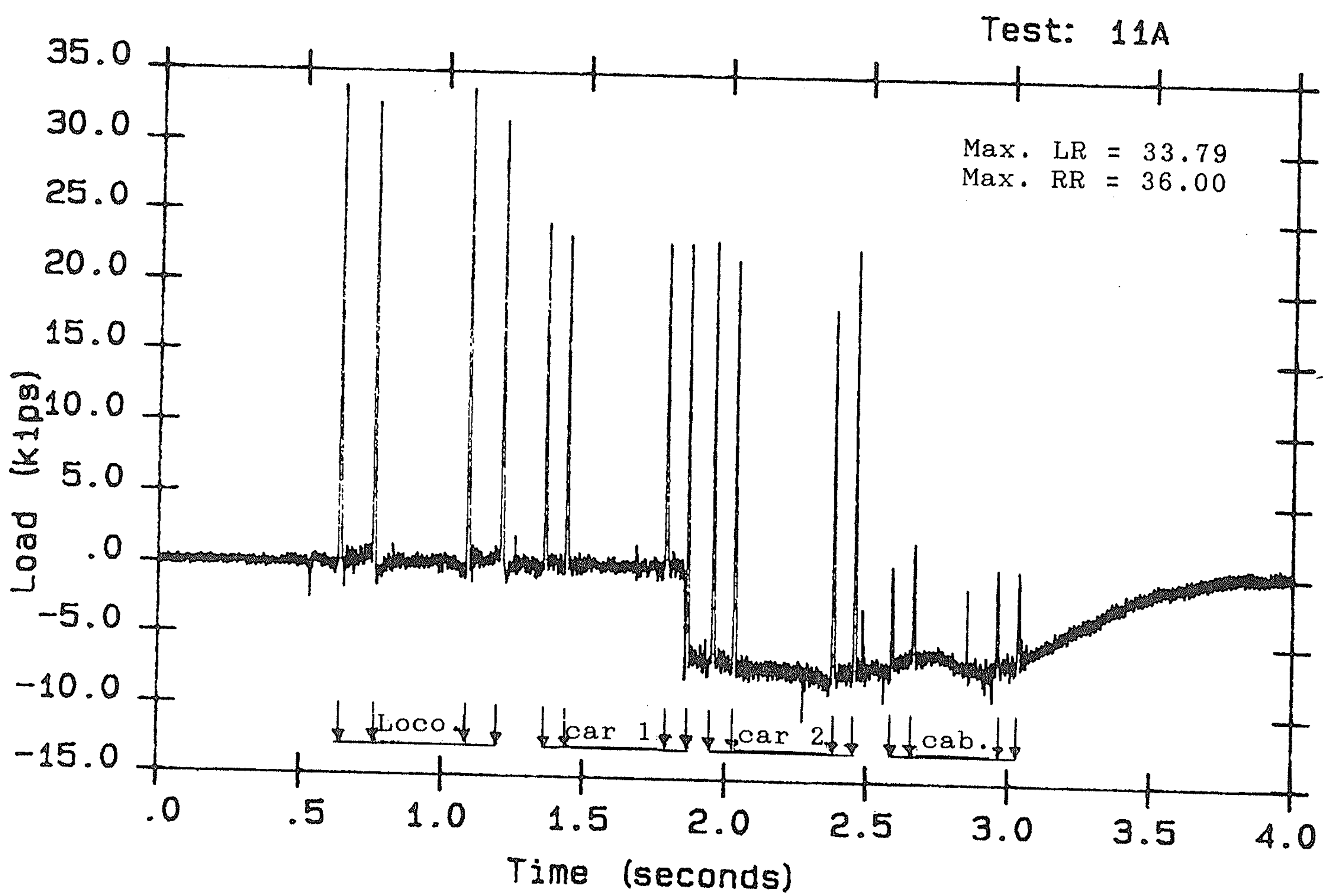

Figure 3.19 Loads at wheel-rail interfaces versus time
BDB Site - Midpoint of Span S3 - Test Train No. 2
Speed 50 mph

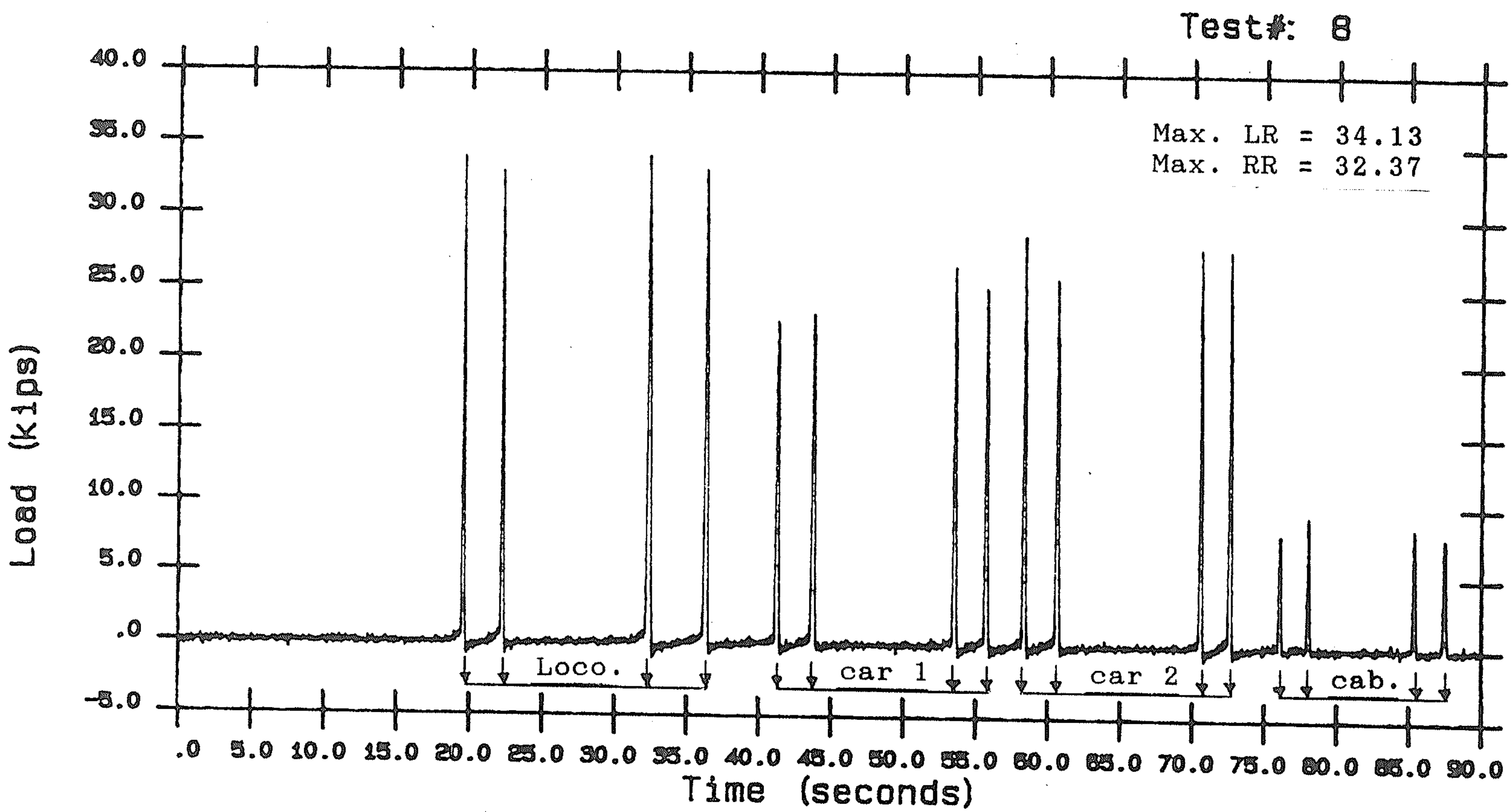

Figure 3.20 Loads at wheel-rail interfaces versus time
BDB Site - Bridge approach - Test Train No. 2
Speed 1 mph

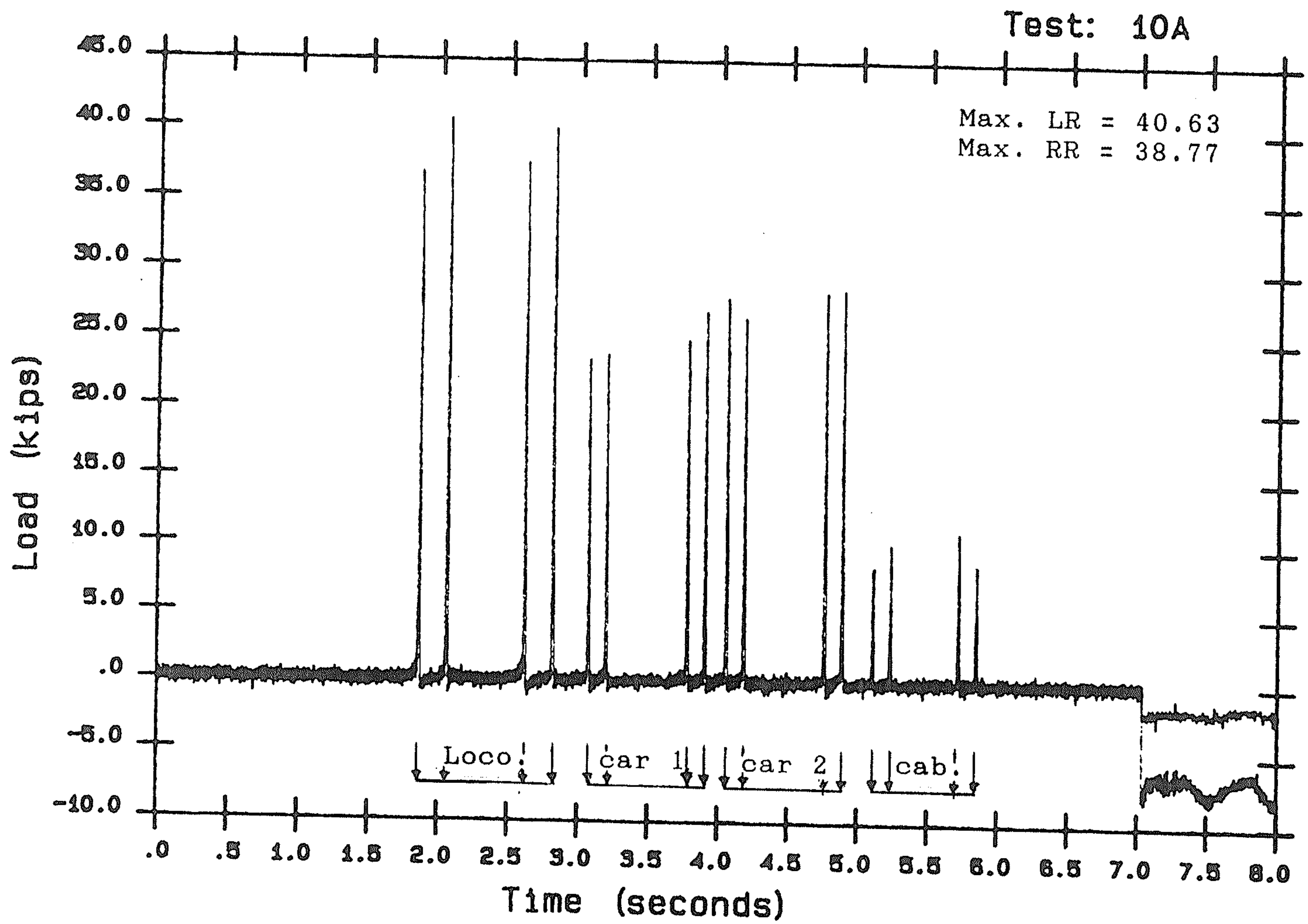

Figure 3.21 Loads at wheel-rail interfaces versus time
BDB Site - Bridge approach - Test Train No. 2
Speed 30 mph

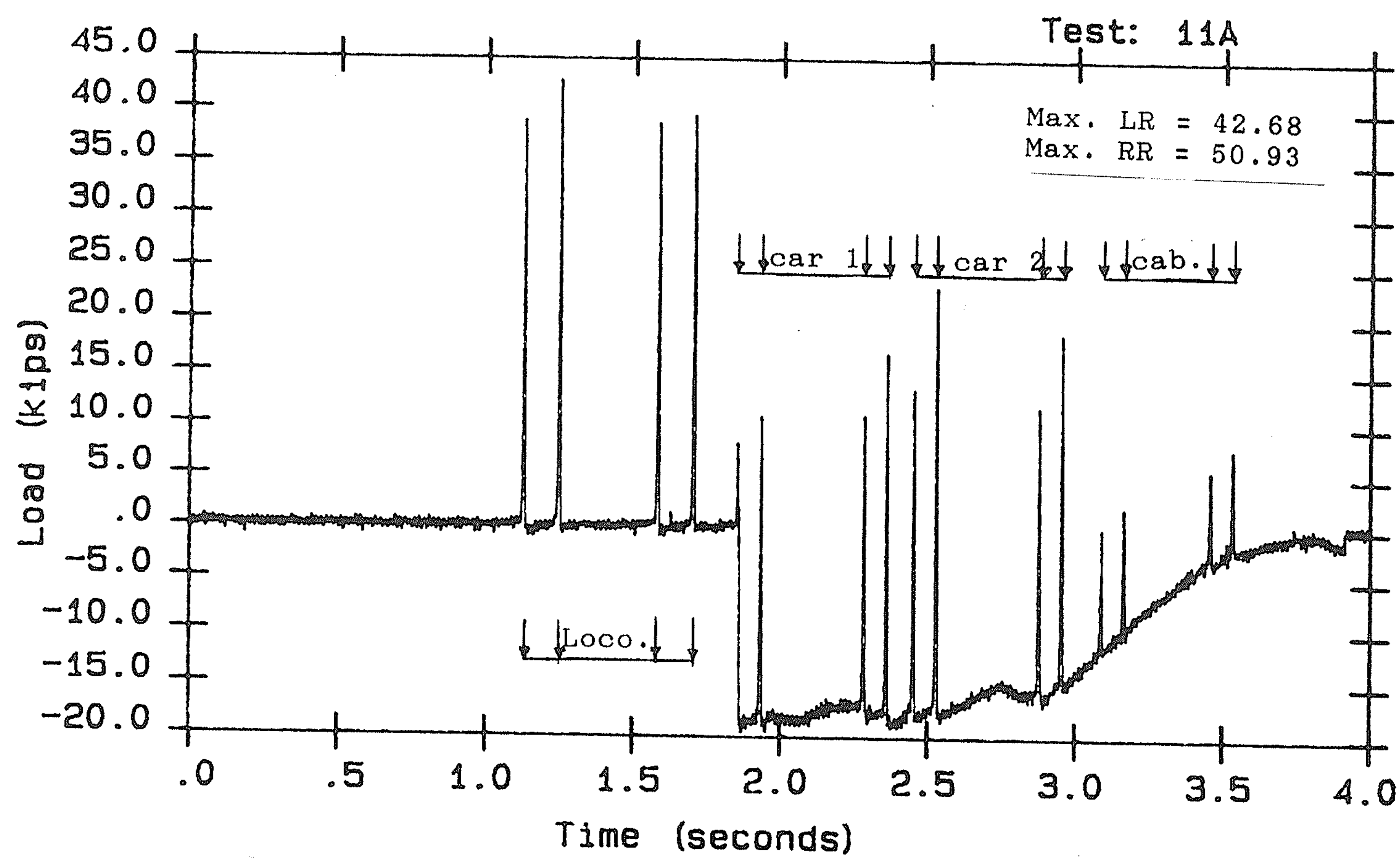

Figure 3.22 Loads at wheel-rail interfaces versus time
BDB Site - Bridge approach - Test Train No. 2
Speed 50 mph

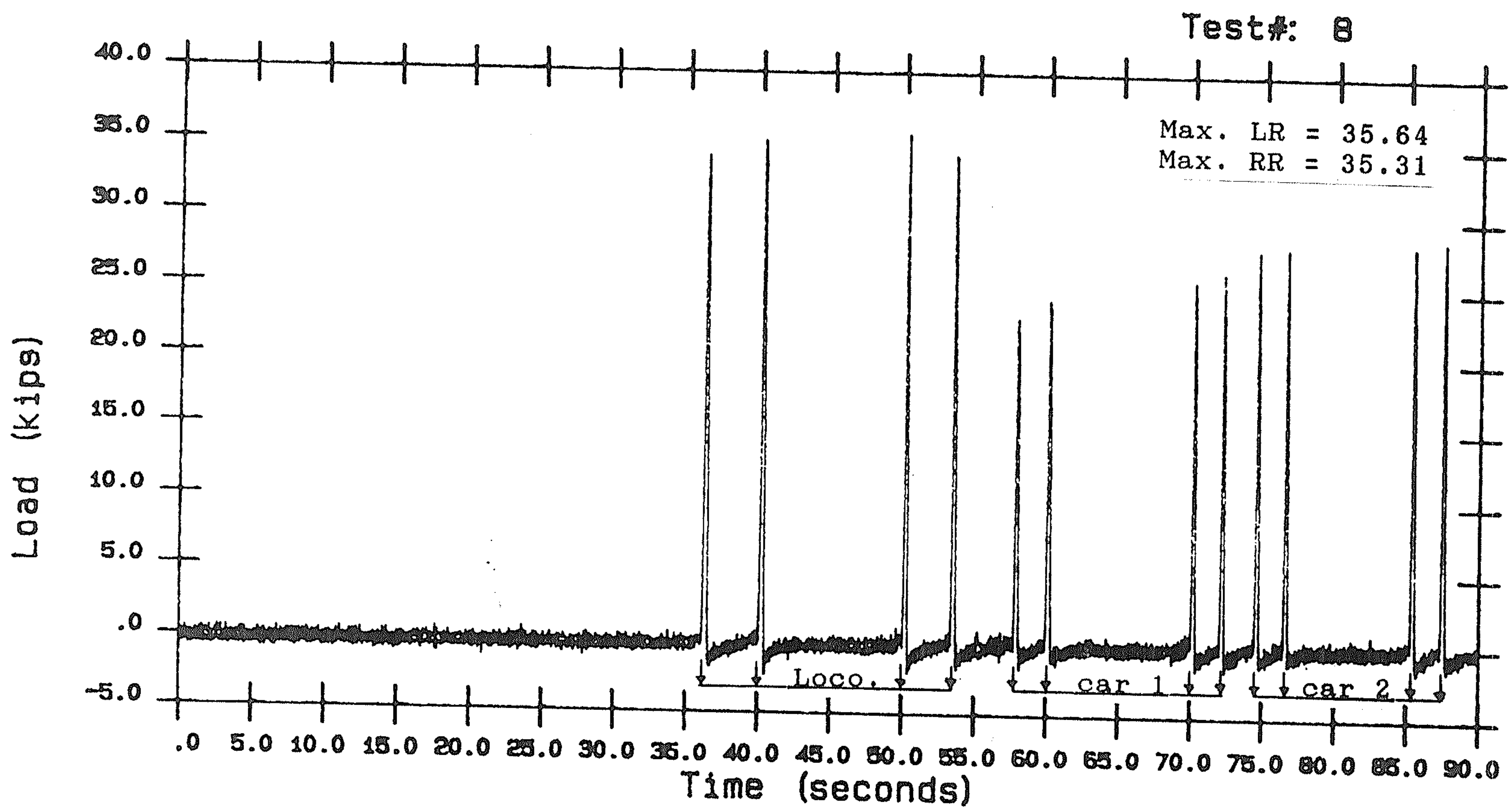

Figure 3.23 Loads at wheel-rail interfaces versus time
BDB Site - Normal track section - Test Train No. 2
Speed 1 mph

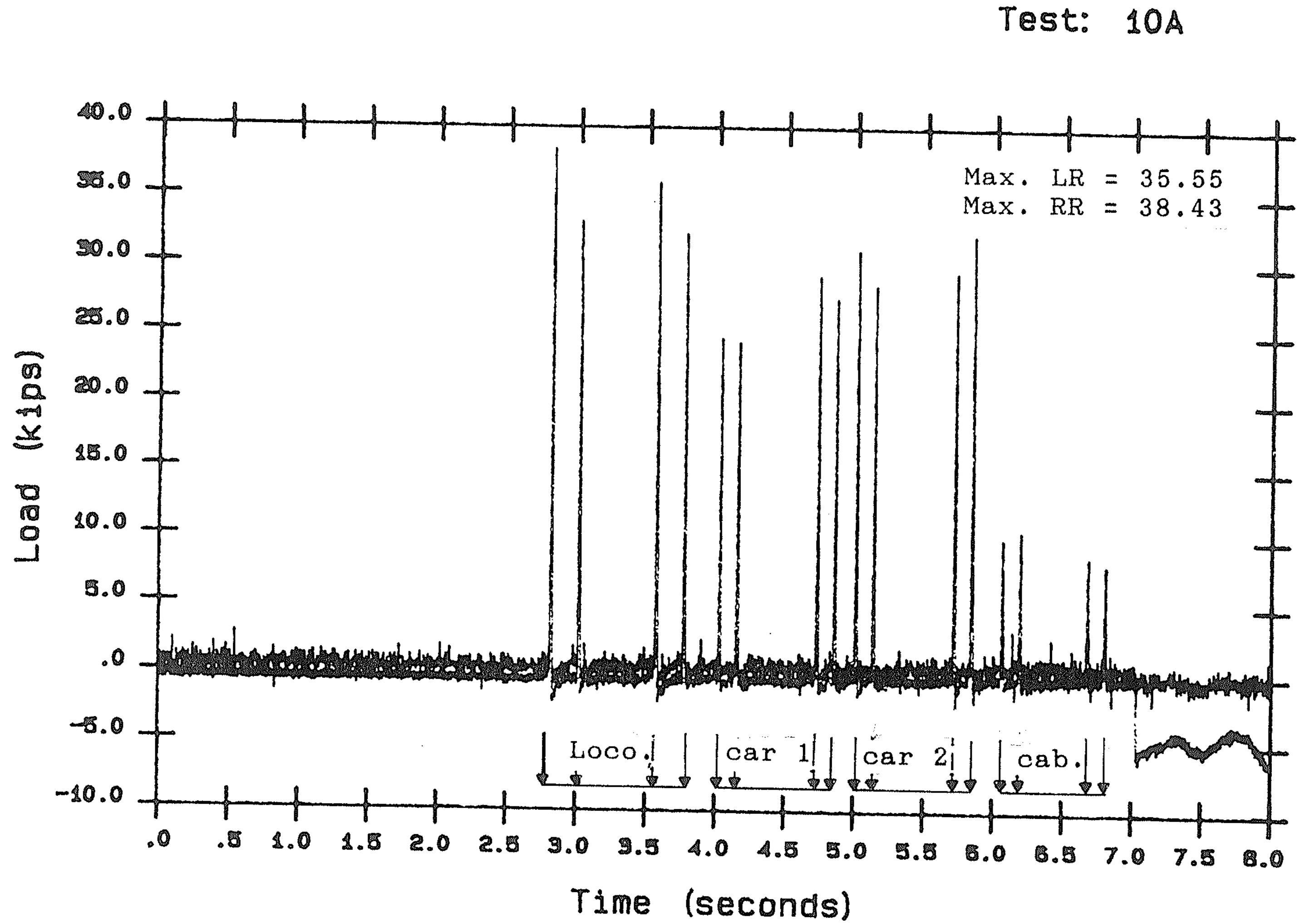

Figure 3.24 Loads at wheel-rail interfaces versus time
BDB Site - Normal track section - Test Train No. 2
Speed 30 mph

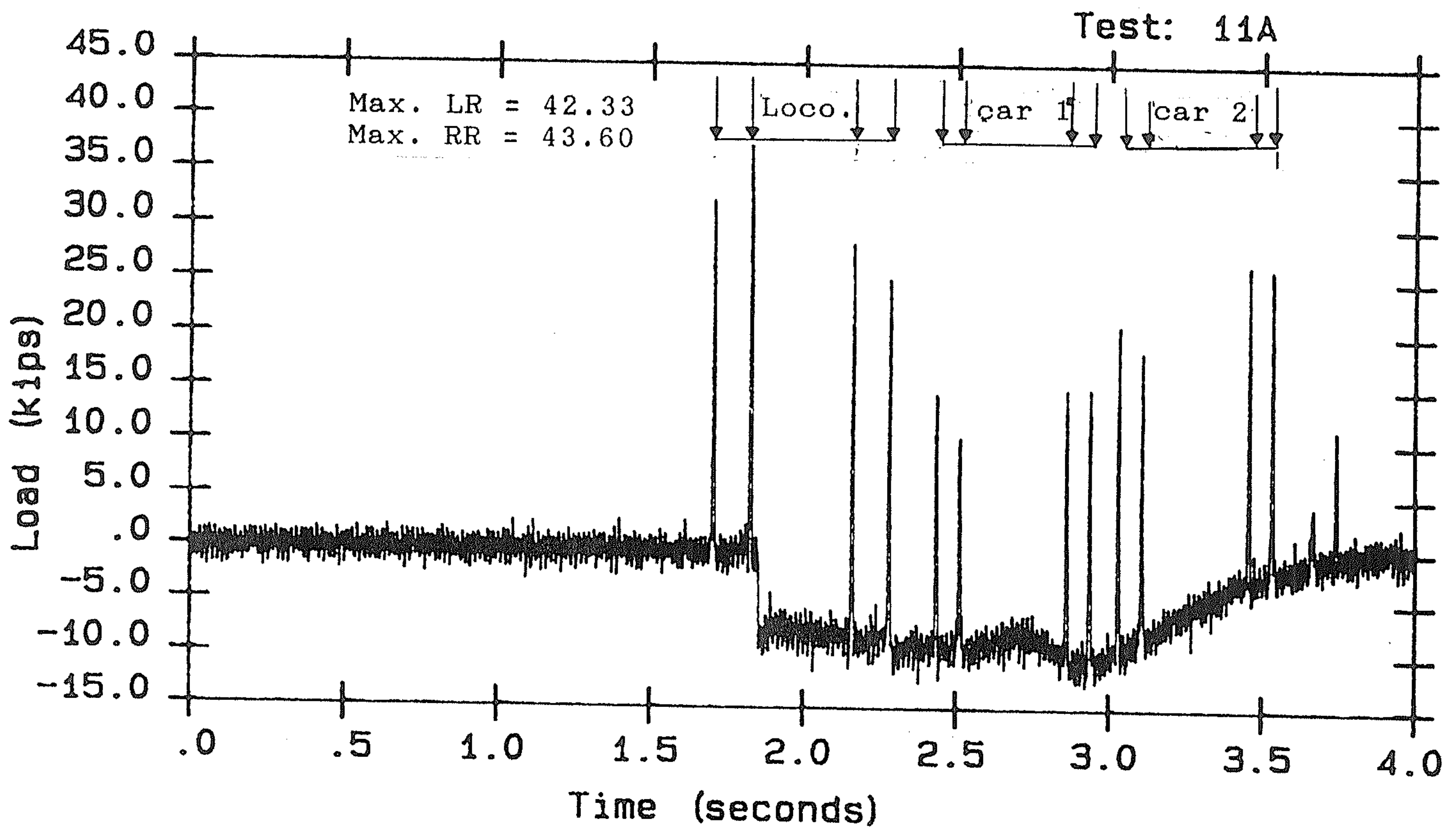

Figure 3.25 Loads at wheel-rail interfaces versus time
BDB Site - Normal track section - Test Train No. 2
Speed 50 mph

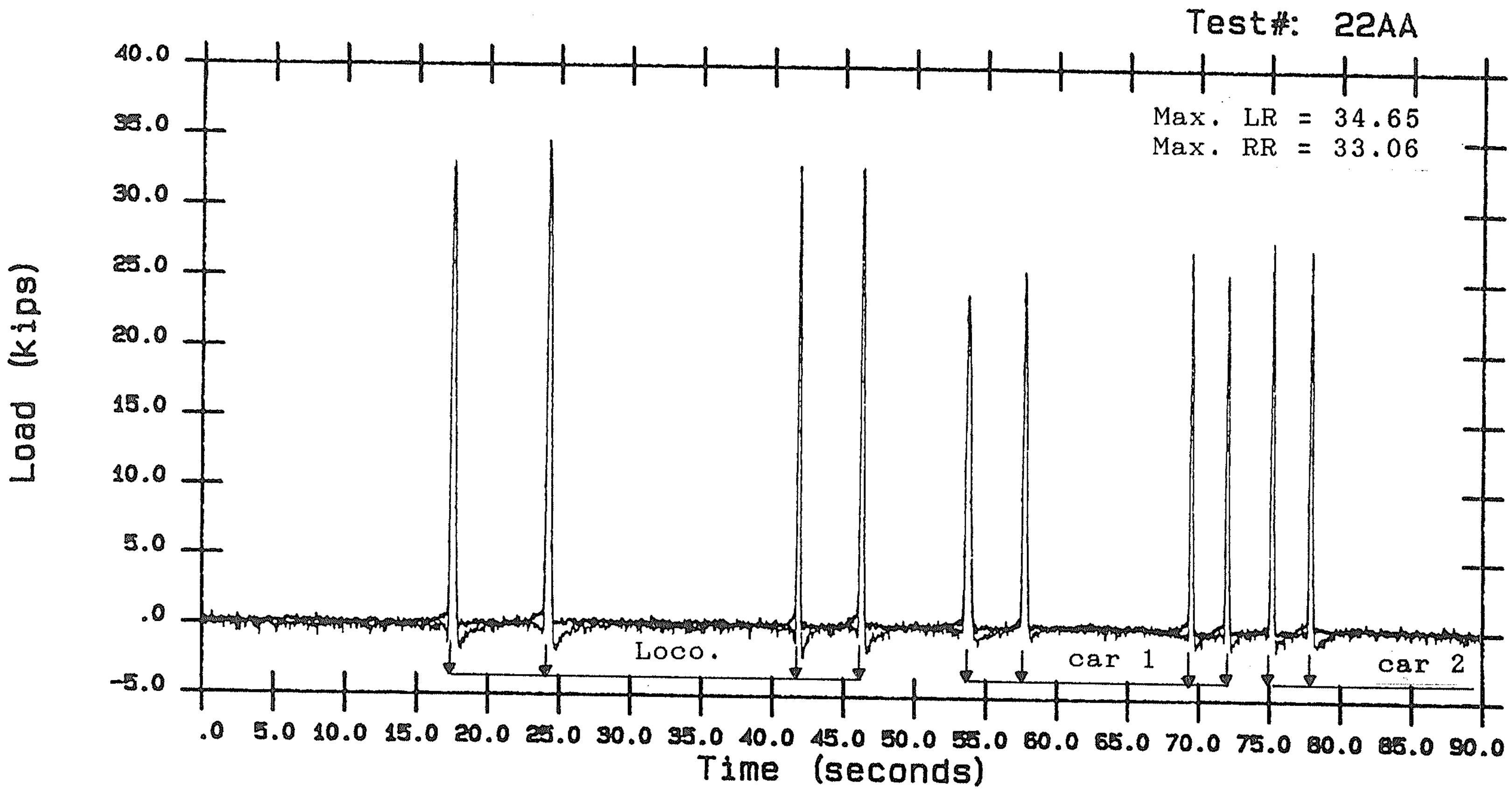

Figure 3.26 Loads at wheel-rail interfaces versus time
ODB Site - Midpoint of span S2 - Test Train No. 2
Speed 1 mph

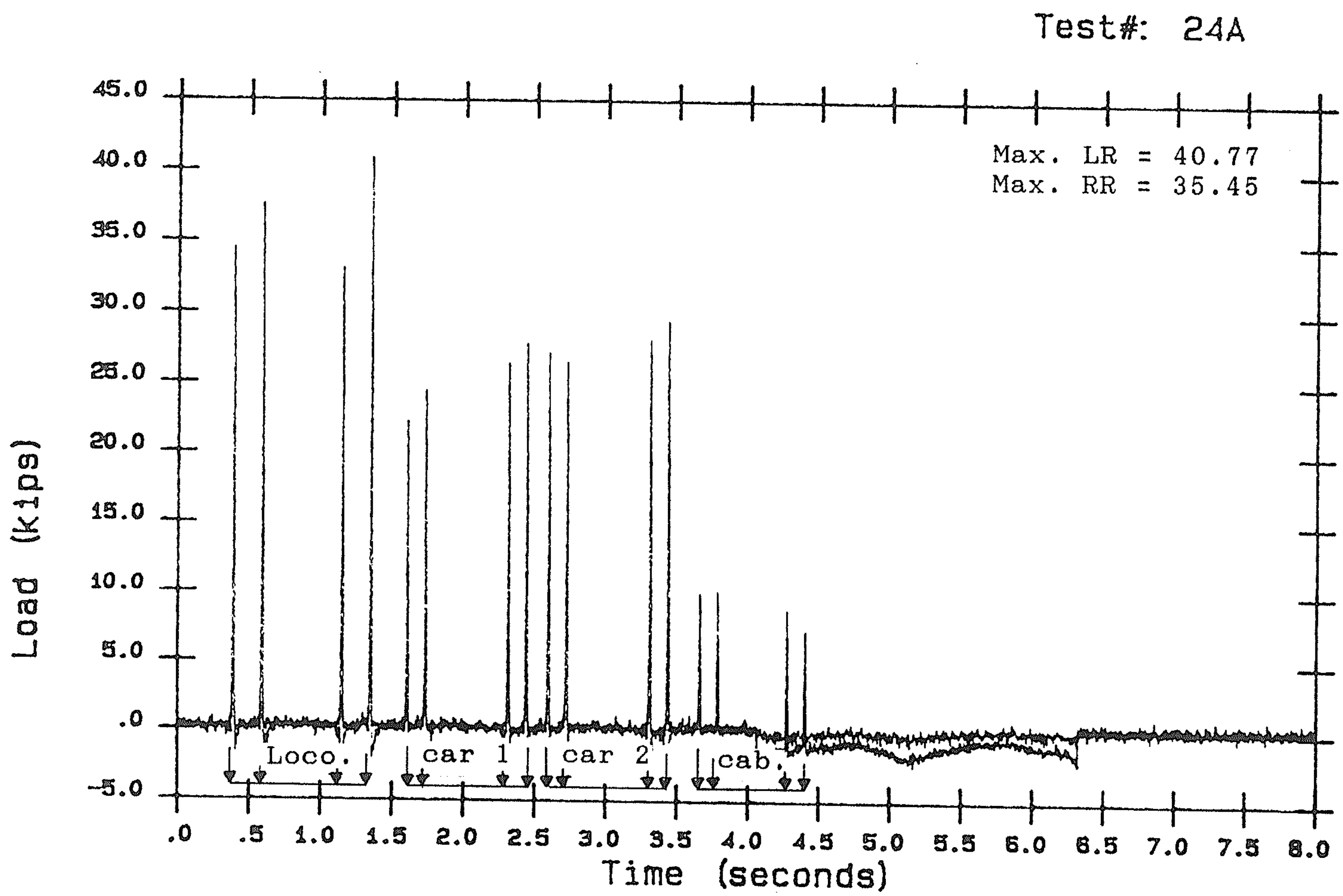

Figure 3.27 Loads at wheel-rail interfaces versus time
ODB Site - Midpoint of Span S2 - Test Train No. 2
Speed 30 mph

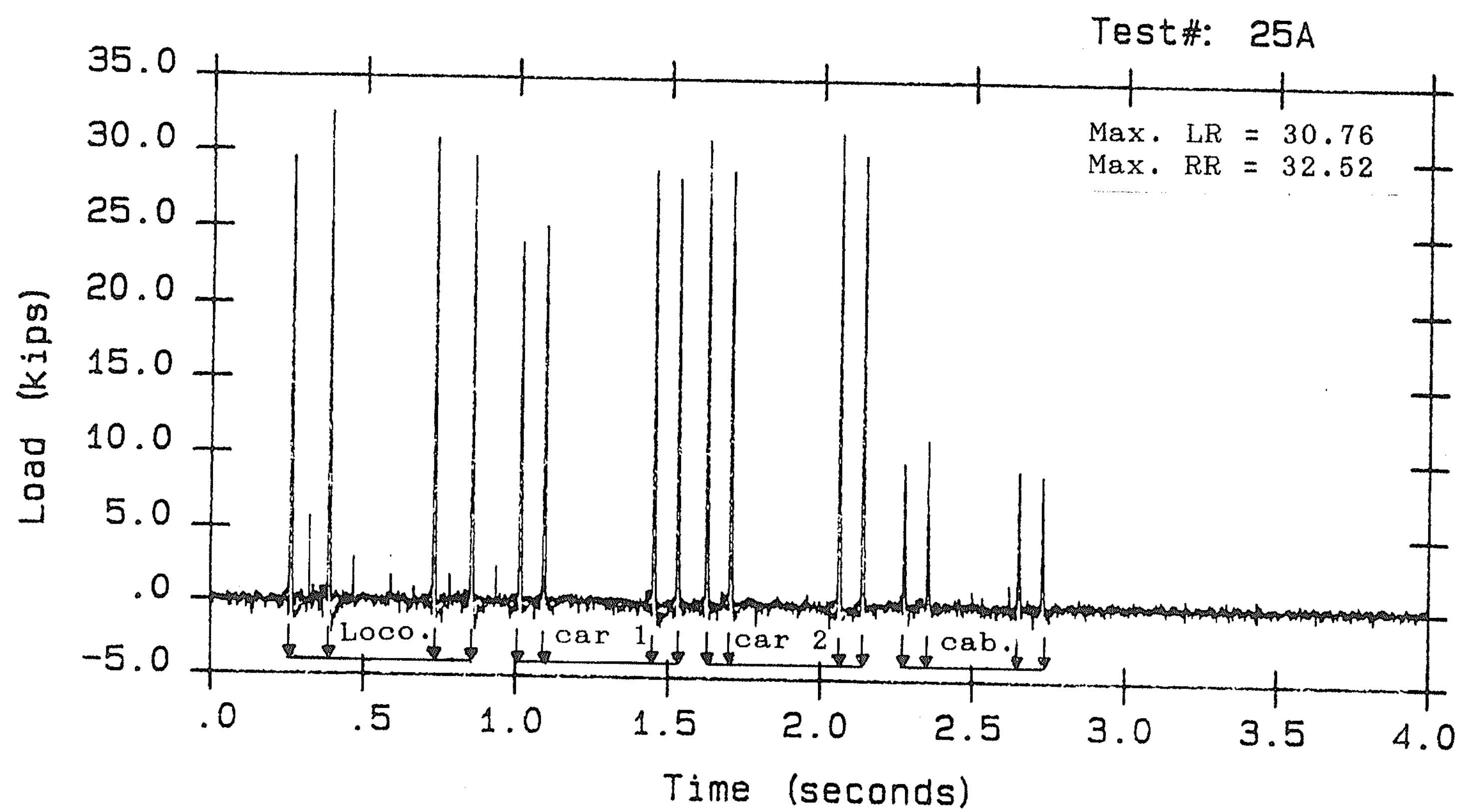

Figure 3.28 Loads at wheel-rail interfaces versus time
ODB Site - Midpoint of Span S2 - Test Train No. 2
Speed 50 mph

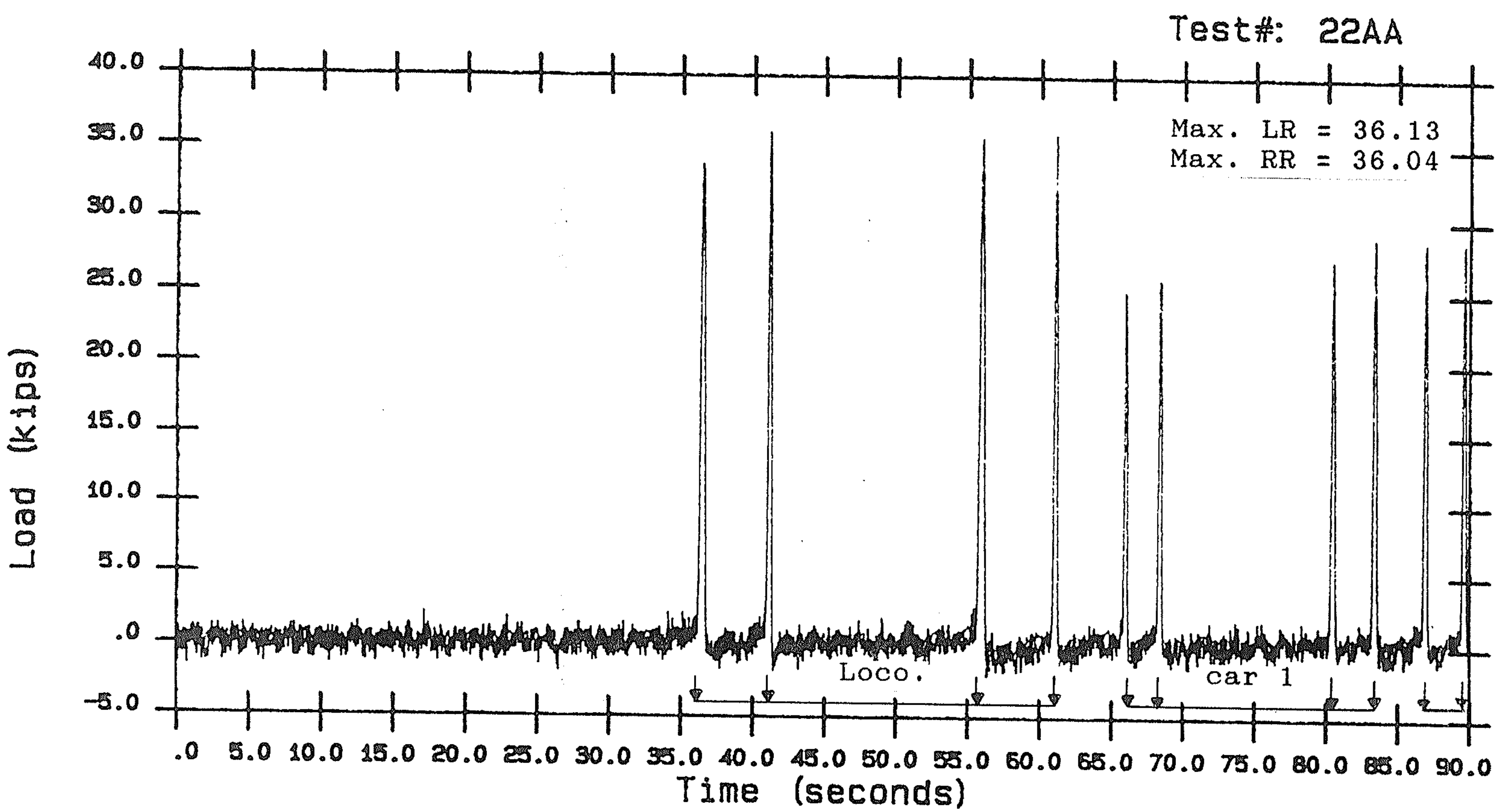

Figure 3.29 Loads at wheel-rail interfaces versus time
ODB Site - Bridge approach - Test Train No. 2
Speed 1 mph

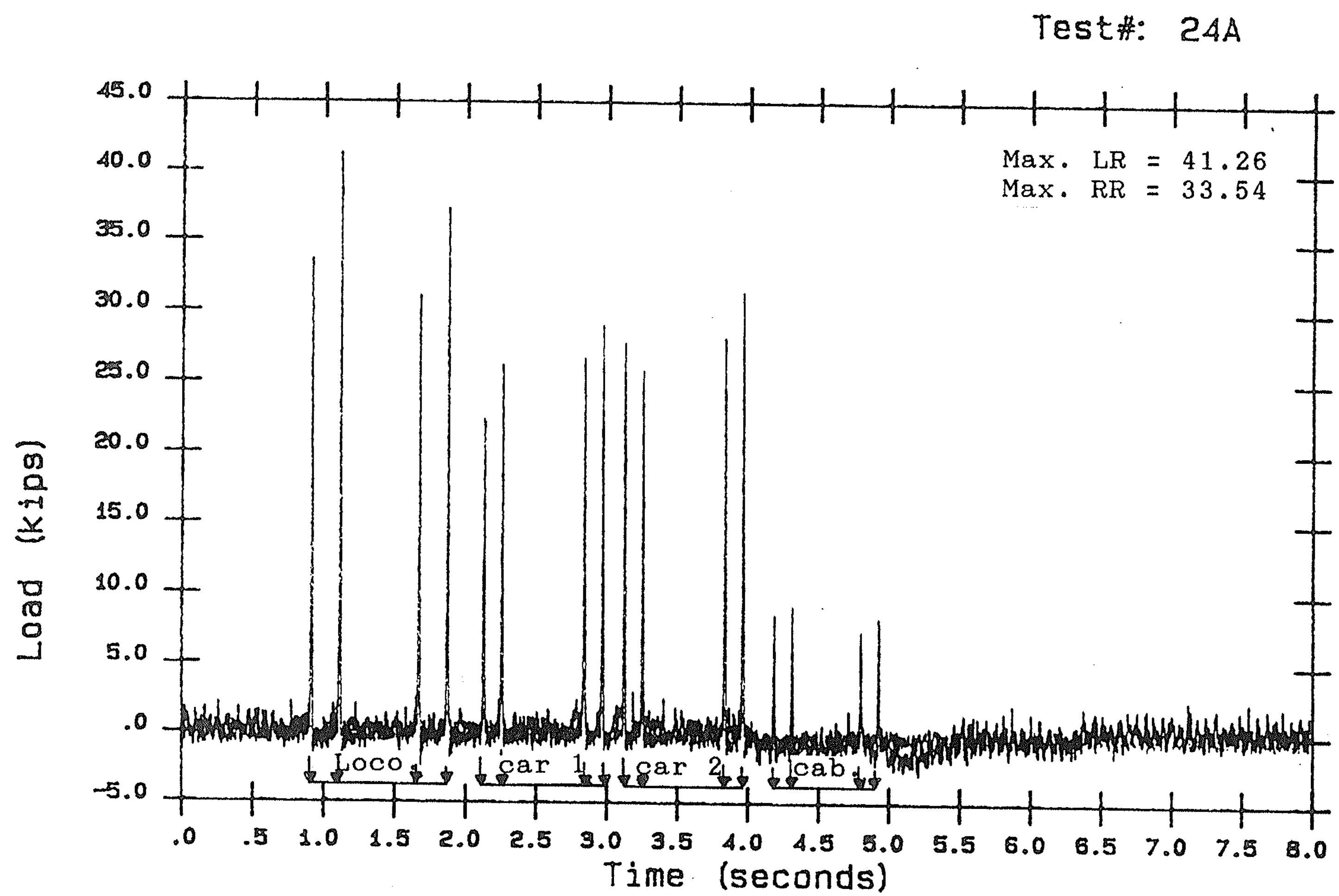

Figure 3.30 Loads at wheel-rail interfaces versus time
ODB Site - Bridge approach - Test Train No. 2
Speed 30 mph

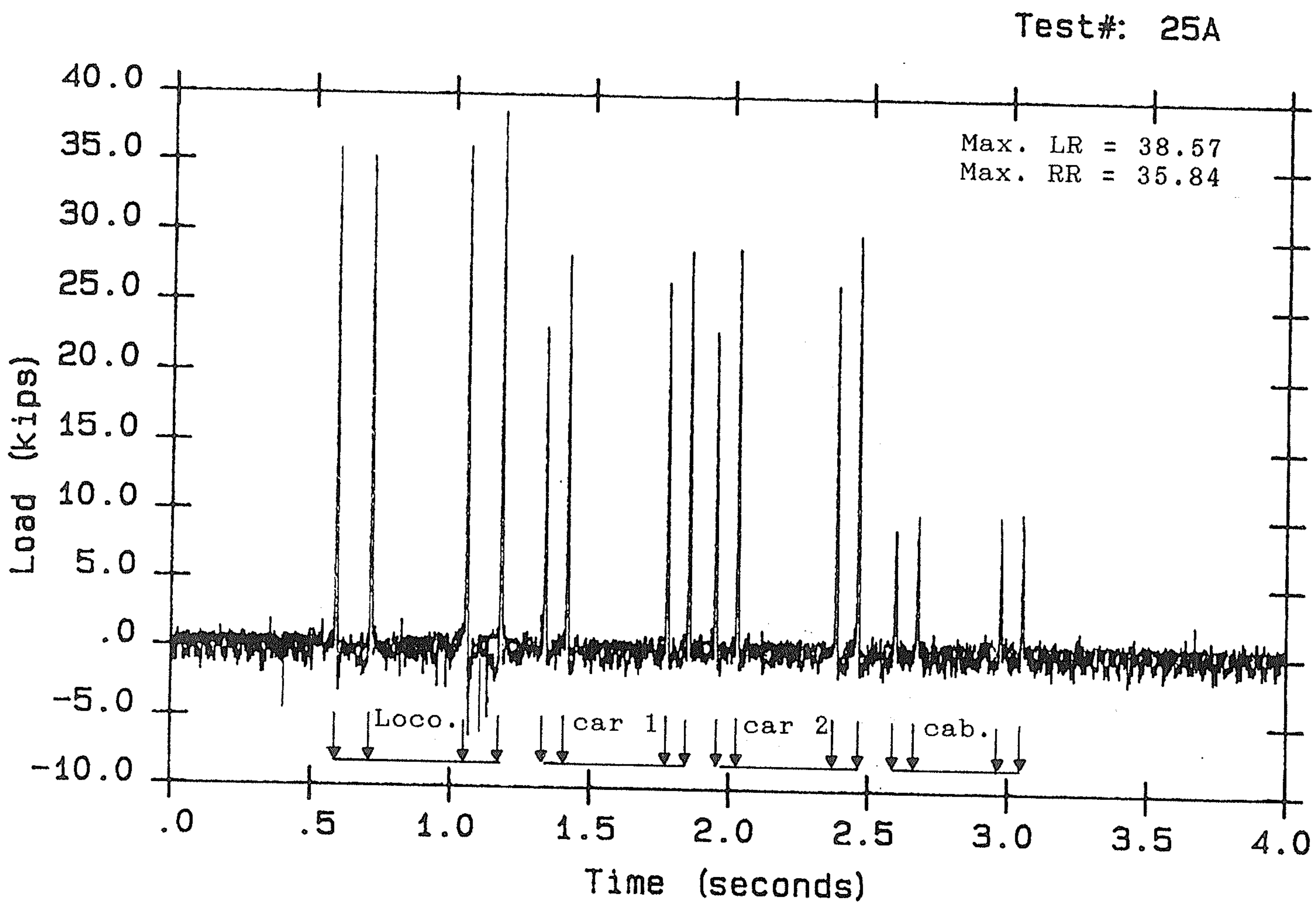

Figure 3.31 Loads at wheel-rail interfaces versus time
BDB Site - Bridge approach - Test Train No. 2
Speed 50 mph

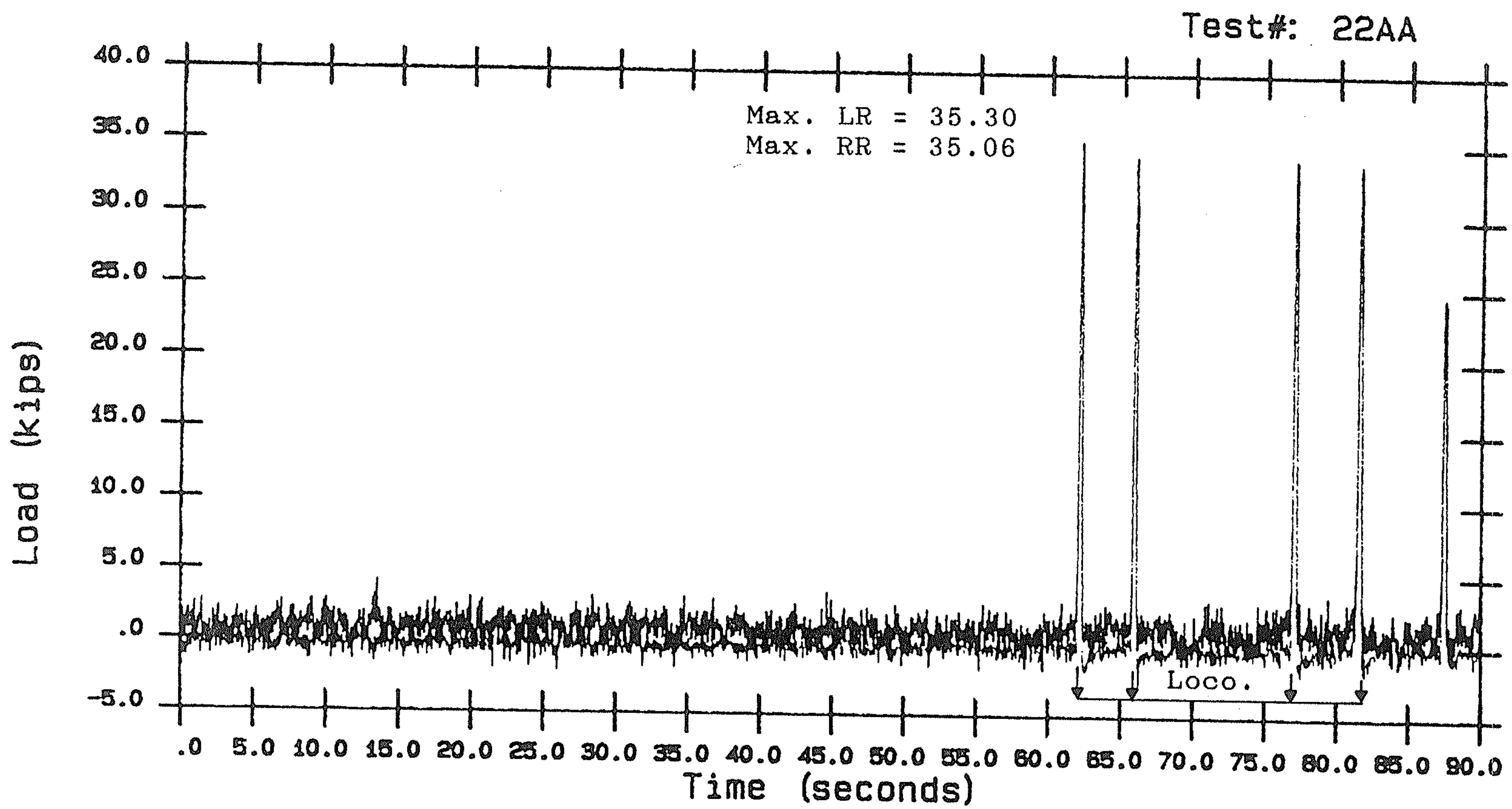

Figure 3.32 Loads at wheel-rail interfaces versus time
Test Site 3 - Normal track section - Test Train No. 2
Speed 1 mph

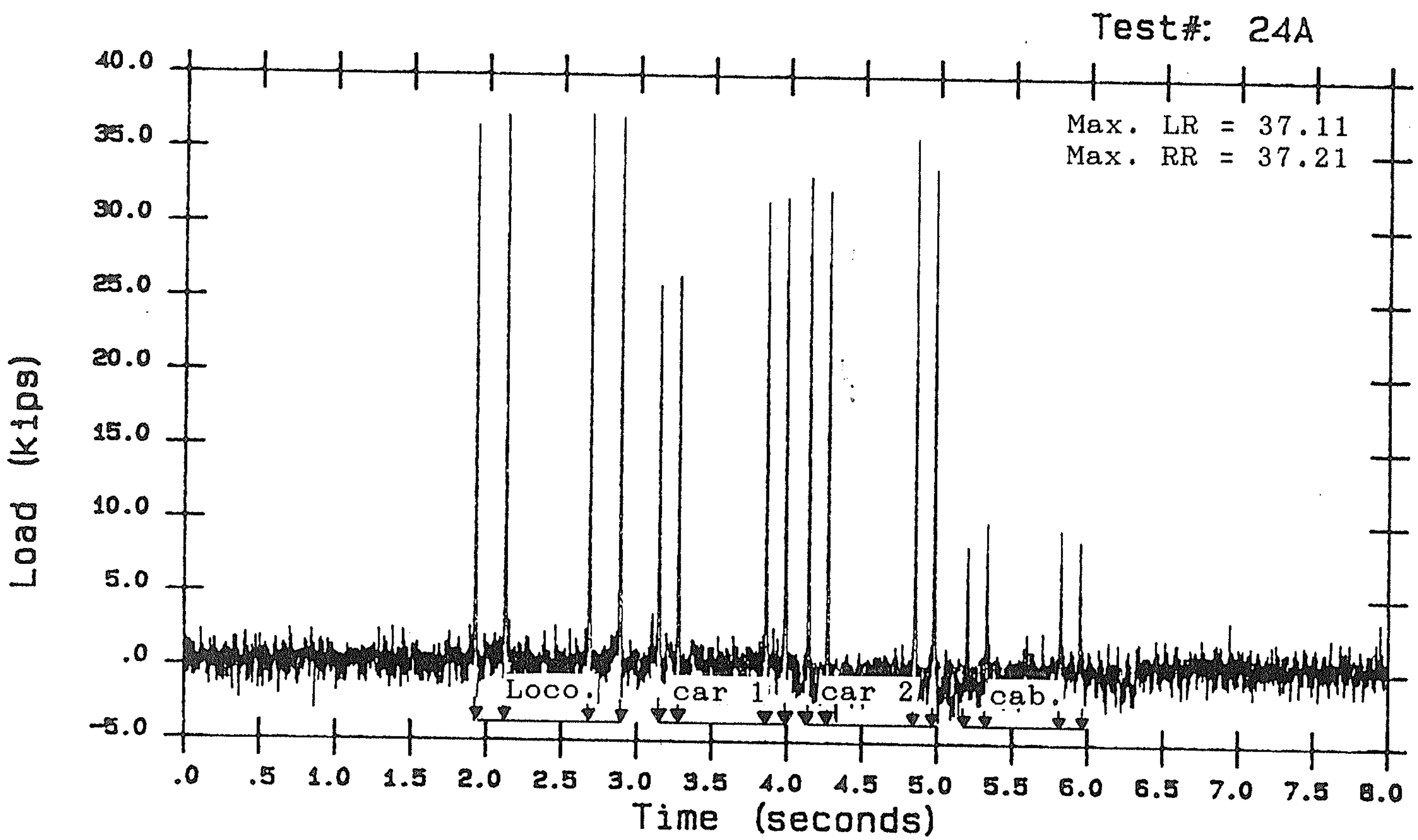

Figure 3.33 Loads at wheel-rail interfaces versus time
ODB Site - Normal track section - Test Train No. 2
Speed 30 mph

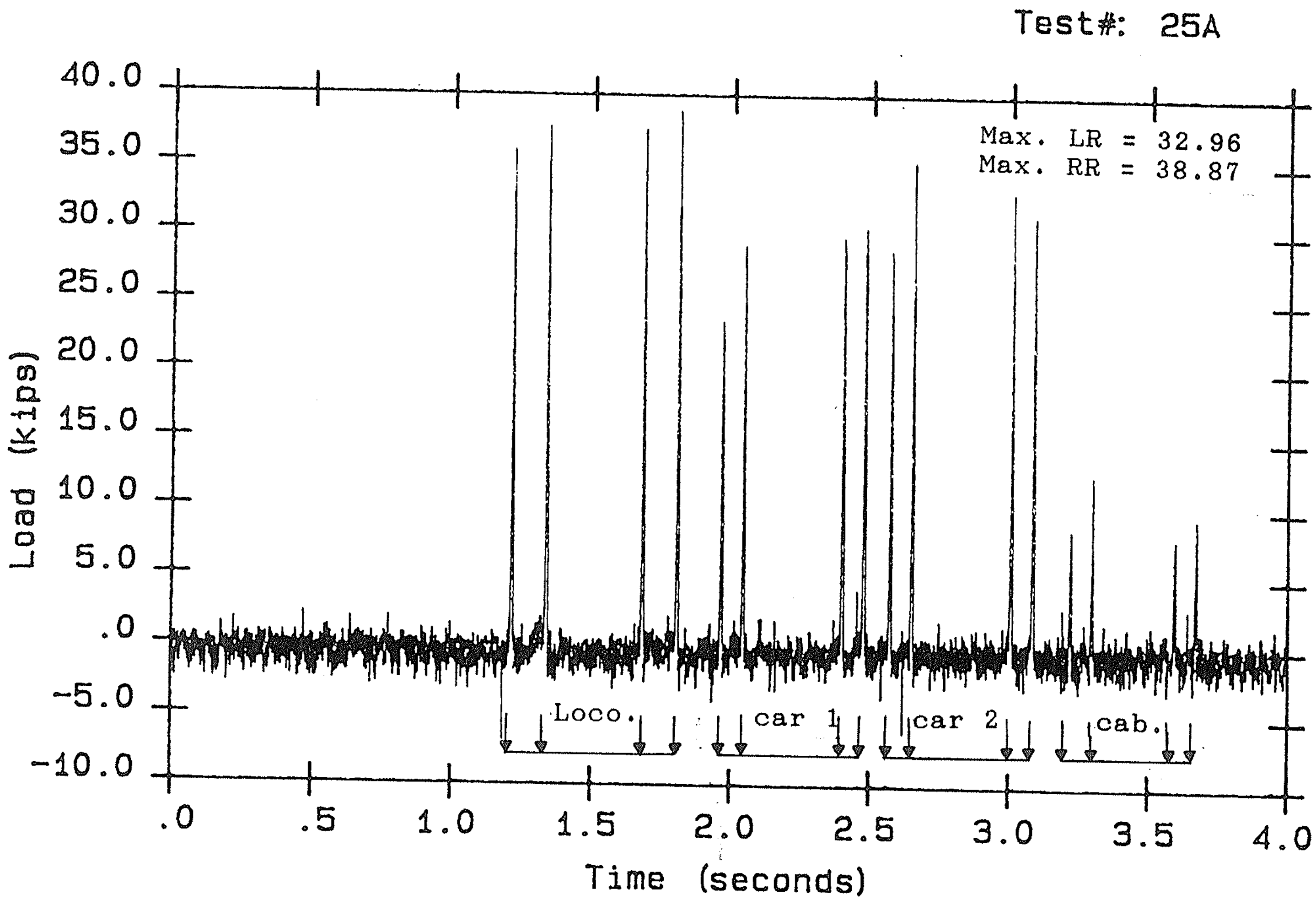

Figure 3.34 Loads at wheel-rail interfaces versus time
ODB Site - Normal track section - Test Train No. 2
Speed 50 mph

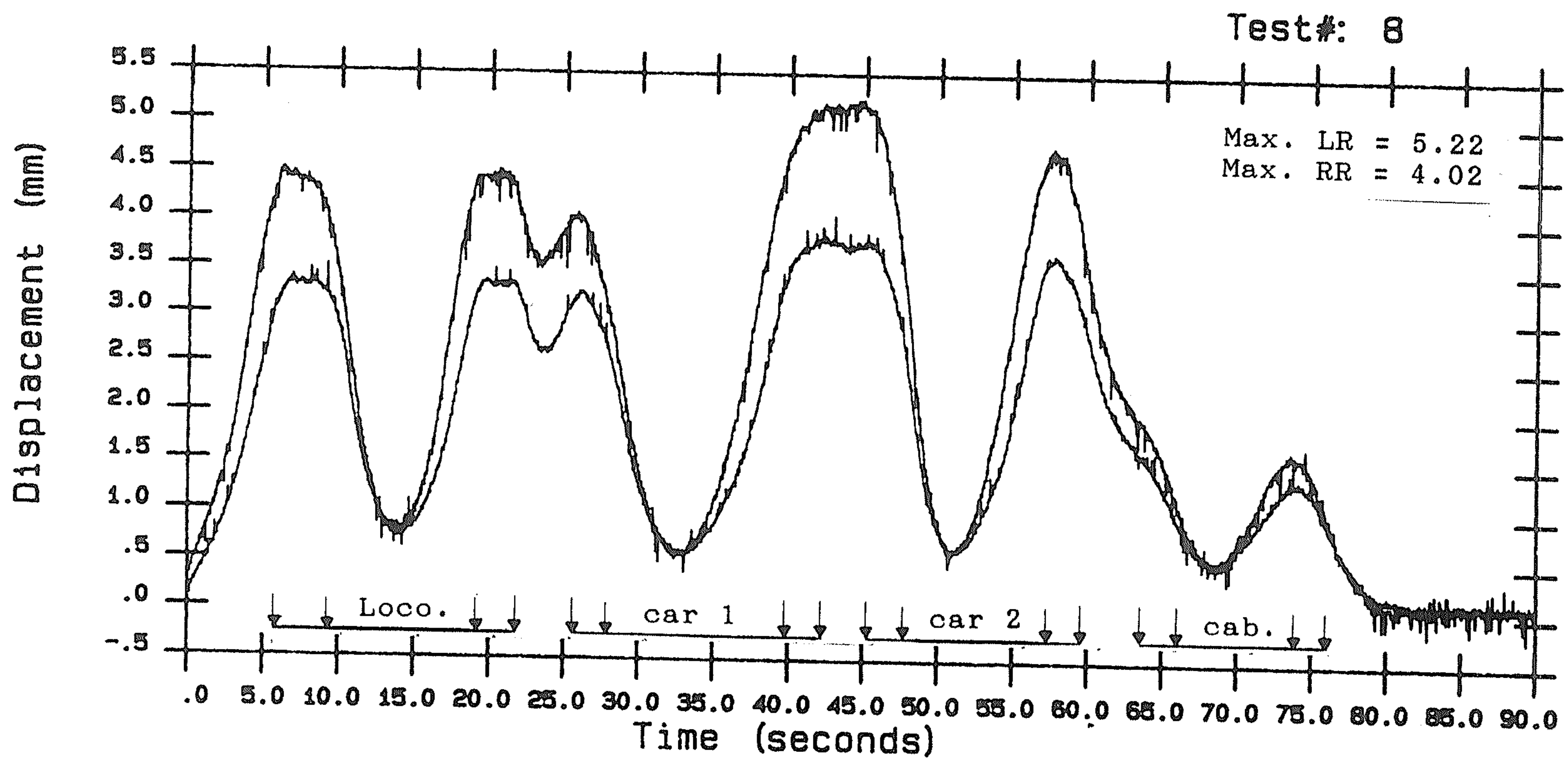

Figure 3.35 Vertical displacement versus time
BDB Site - Midpoint of Span S3 - Test Train No. 2
Speed 1 mph

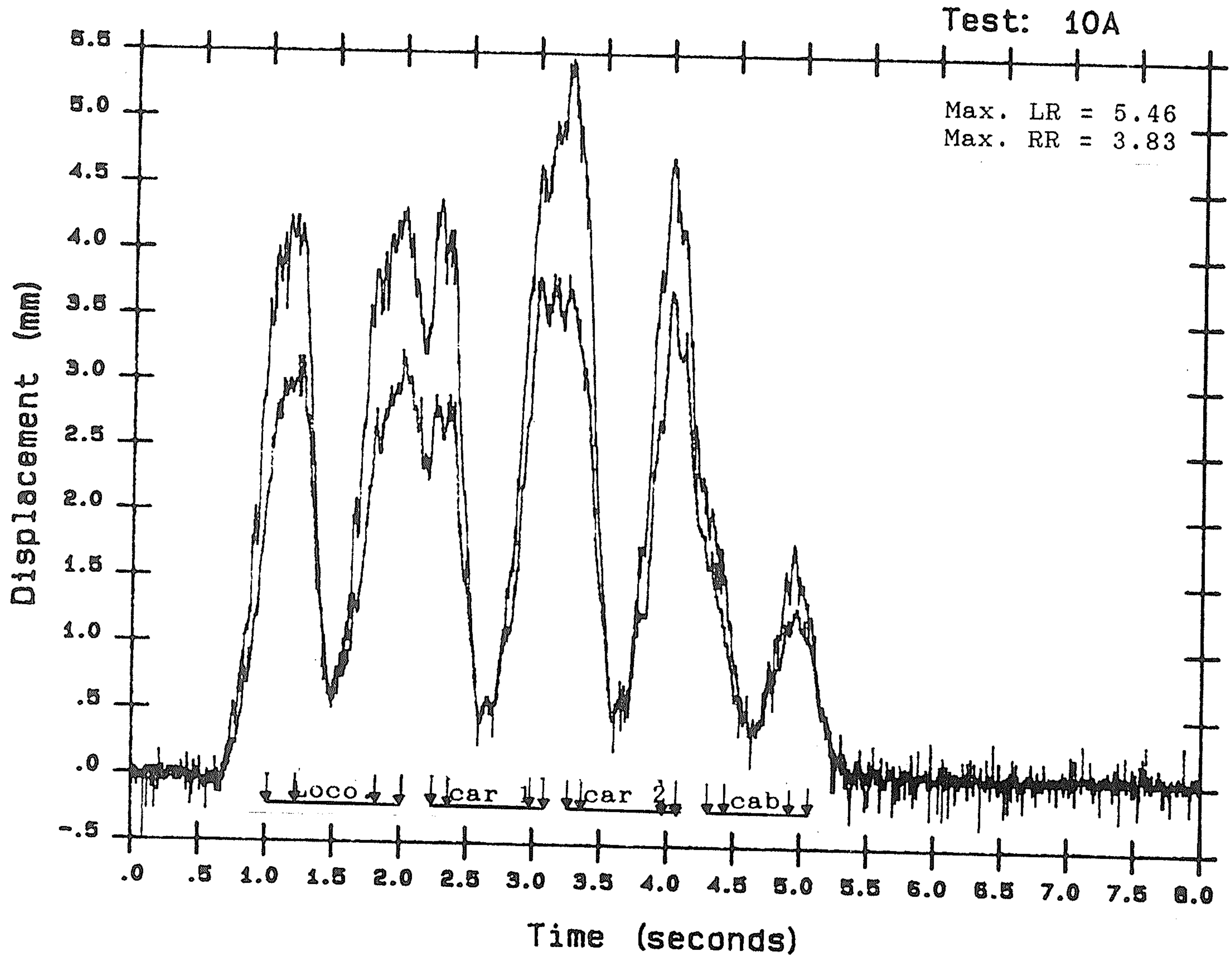

Figure 3.36 Vertical displacement versus time
BDB Site - Midpoint of Span S3 - Test Train No. 2
Speed 30 mph

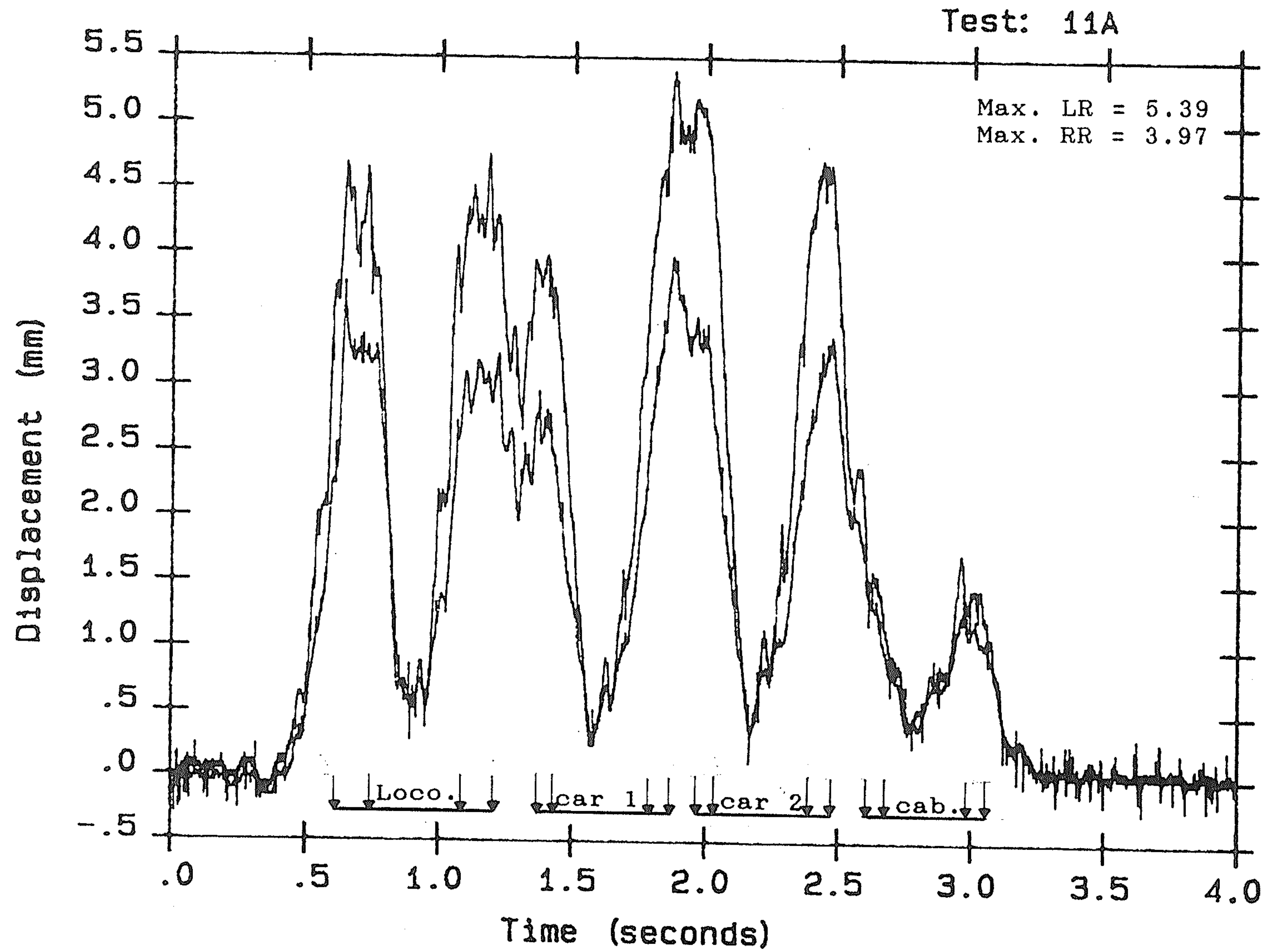

Figure 3.37 Vertical displacement versus time
BDB Site - Midpoint of Span S3 - Test Train No. 2
Speed 50 mph

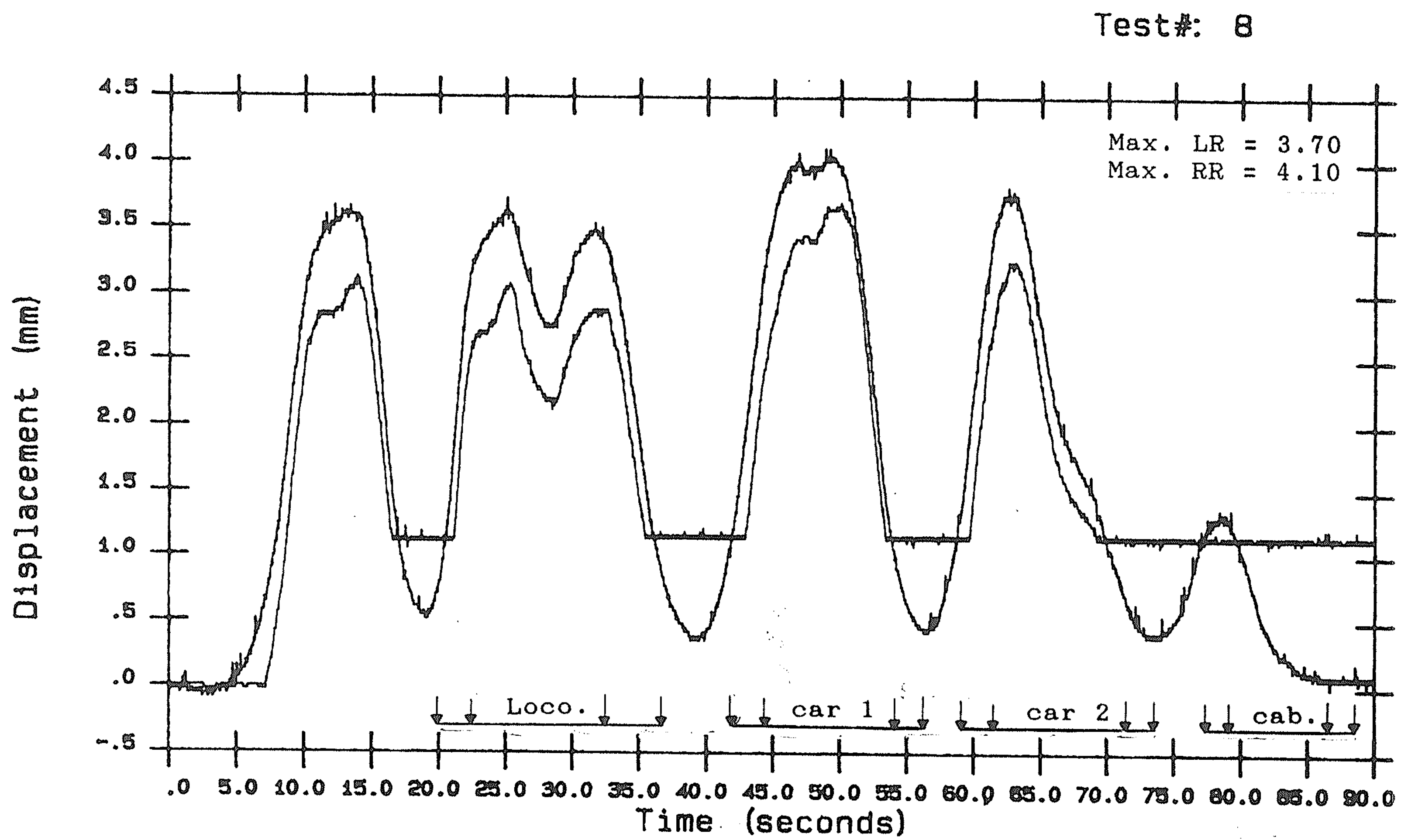

Figure 3.38 Vertical displacement versus time
BDB Site - Midpoint of Span S2 - Test Train No. 2
Speed 1 mph

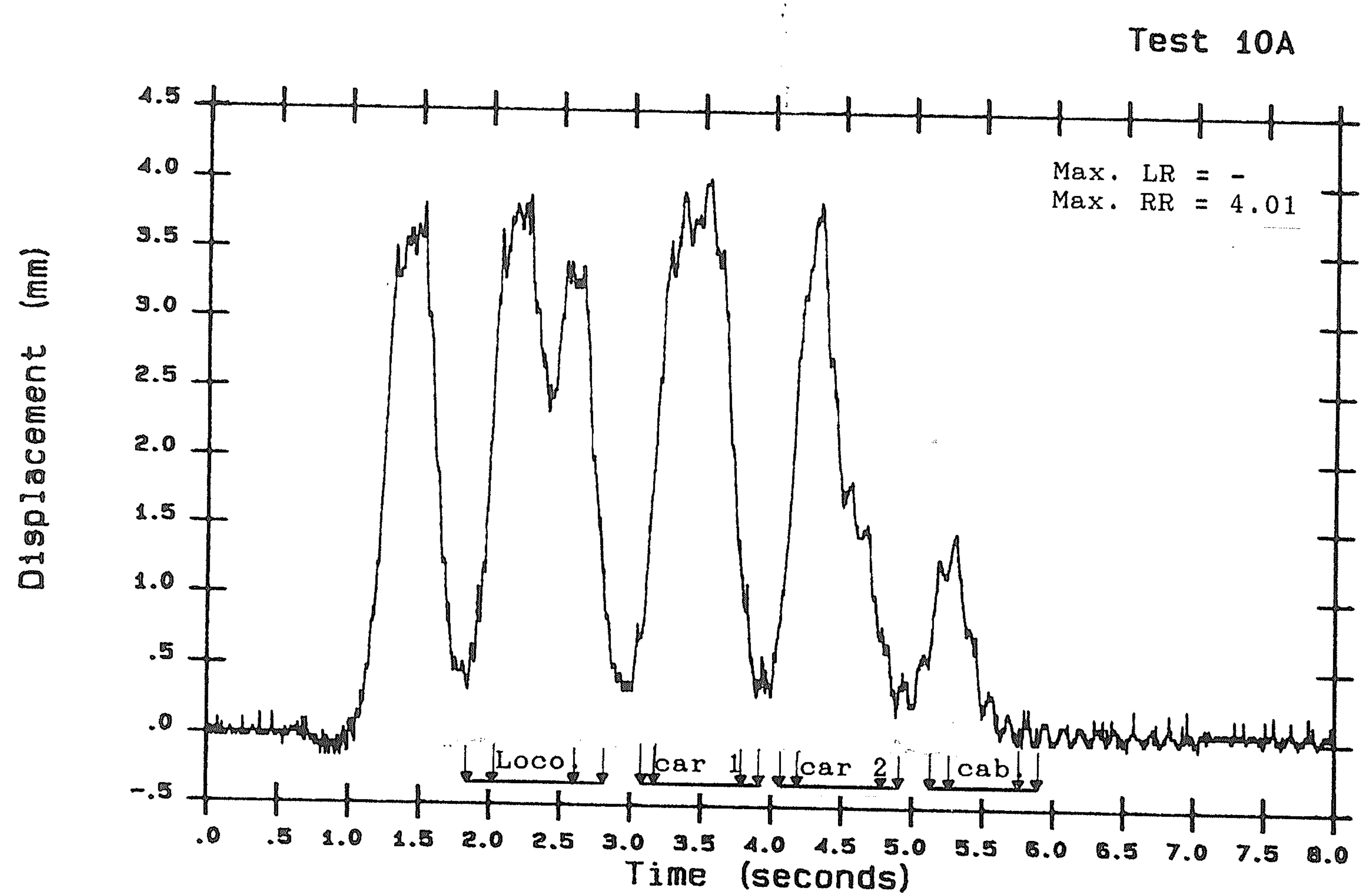

Figure 3.39 Vertical displacement versus time
BDB Site - Midpoint of Span S2 - Test Train No. 2
Speed 30 mph

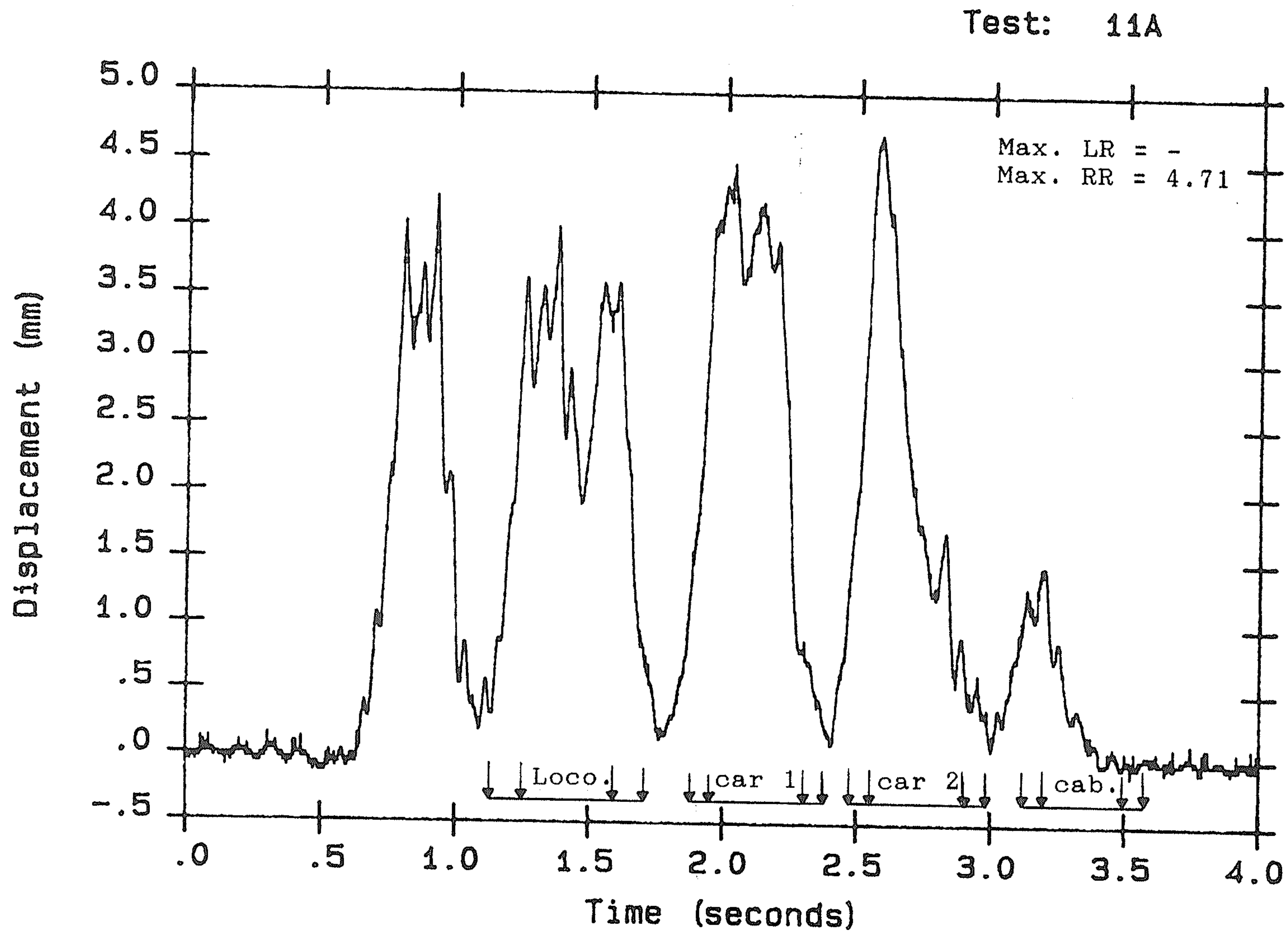

Figure 3.40 Vertical displacement versus time
BDB Site - Midpoint of Span S2 - Test Train No. 2
Speed 50 mph

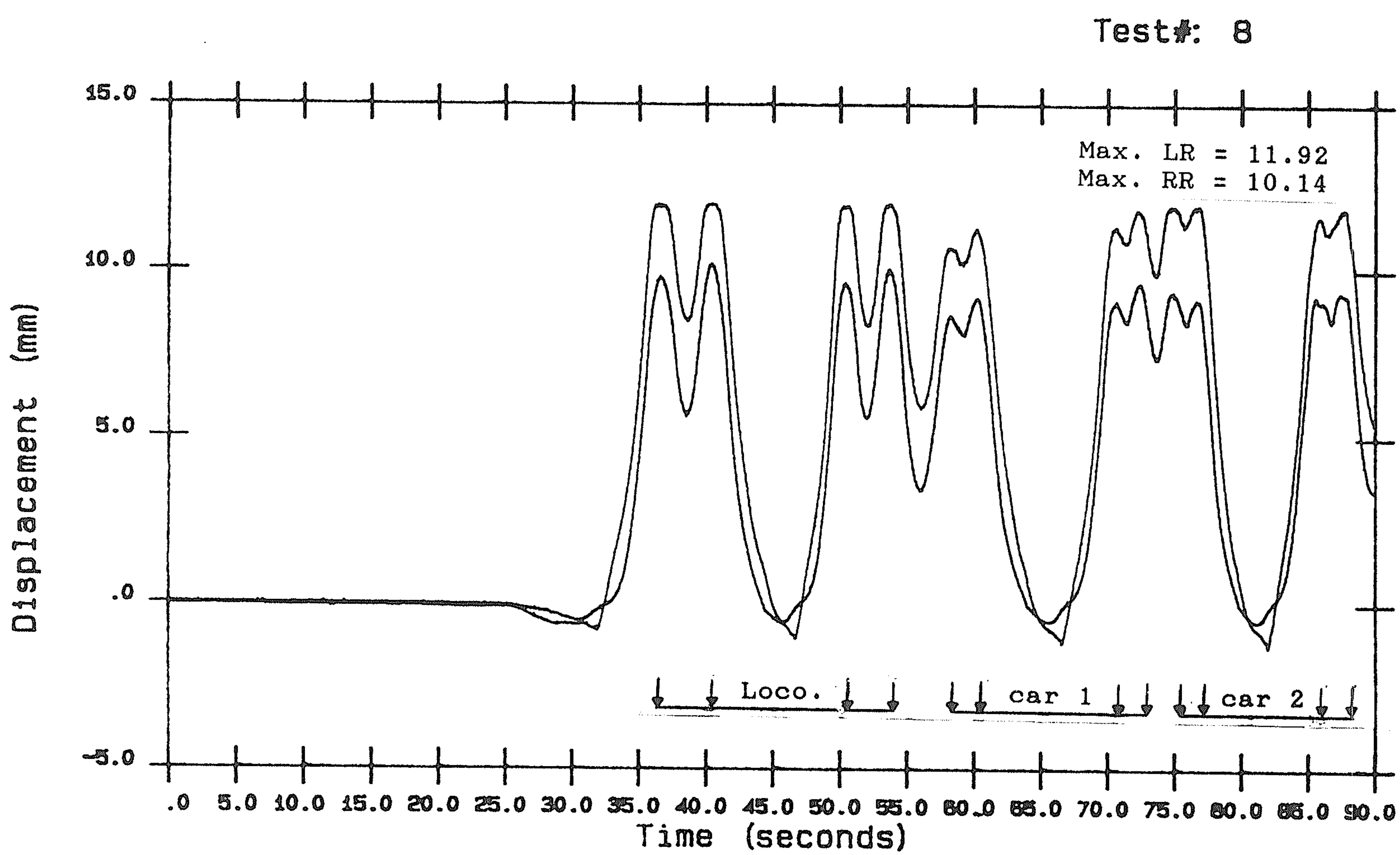

Figure 3.41 Vertical displacement versus time
BDB Site - Normal track section - Test Train No. 2
Speed 1 mph

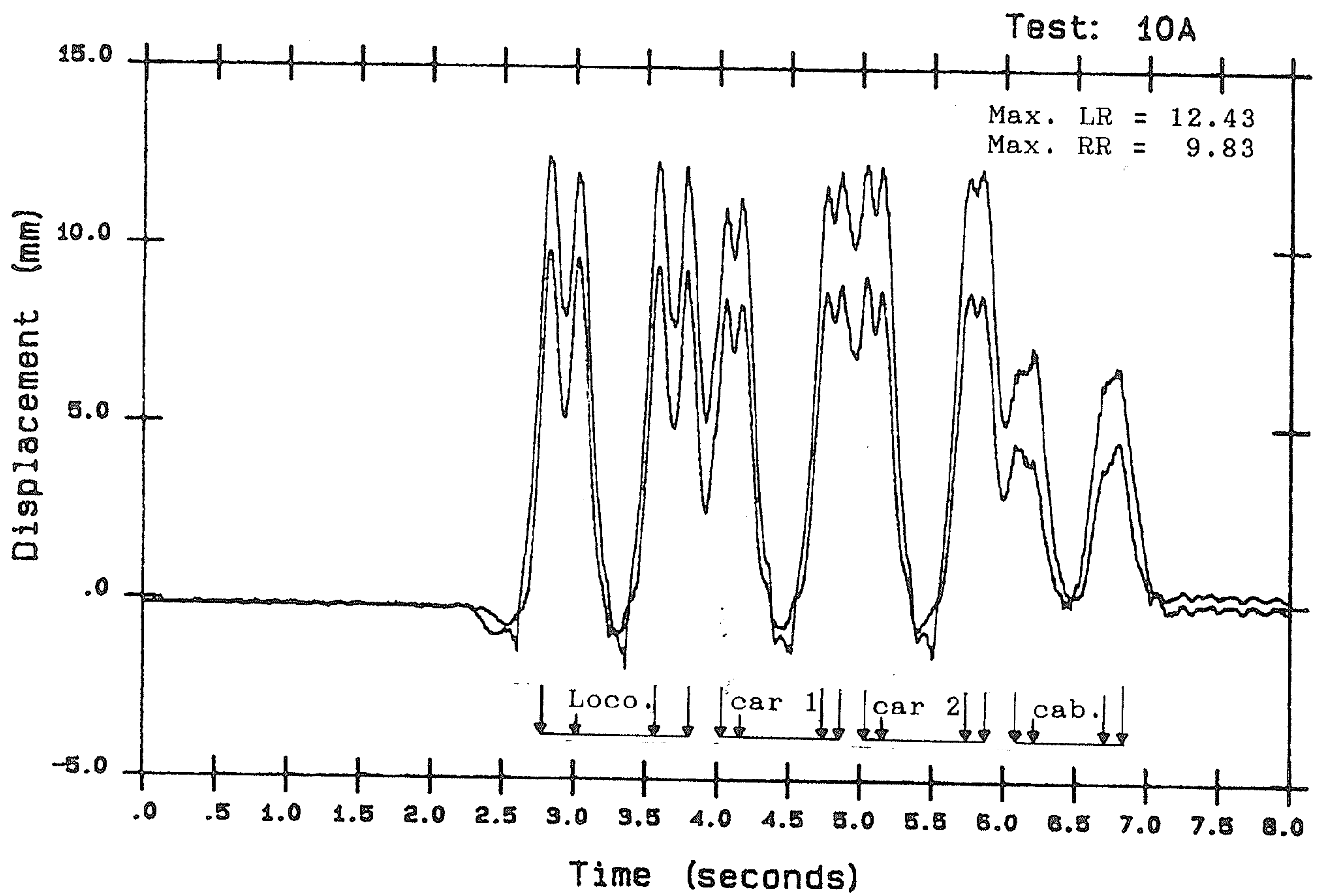

Figure 3.42 Vertical displacement versus time
BDB Site - Normal track section - Test Train No. 2
Speed 30 mph

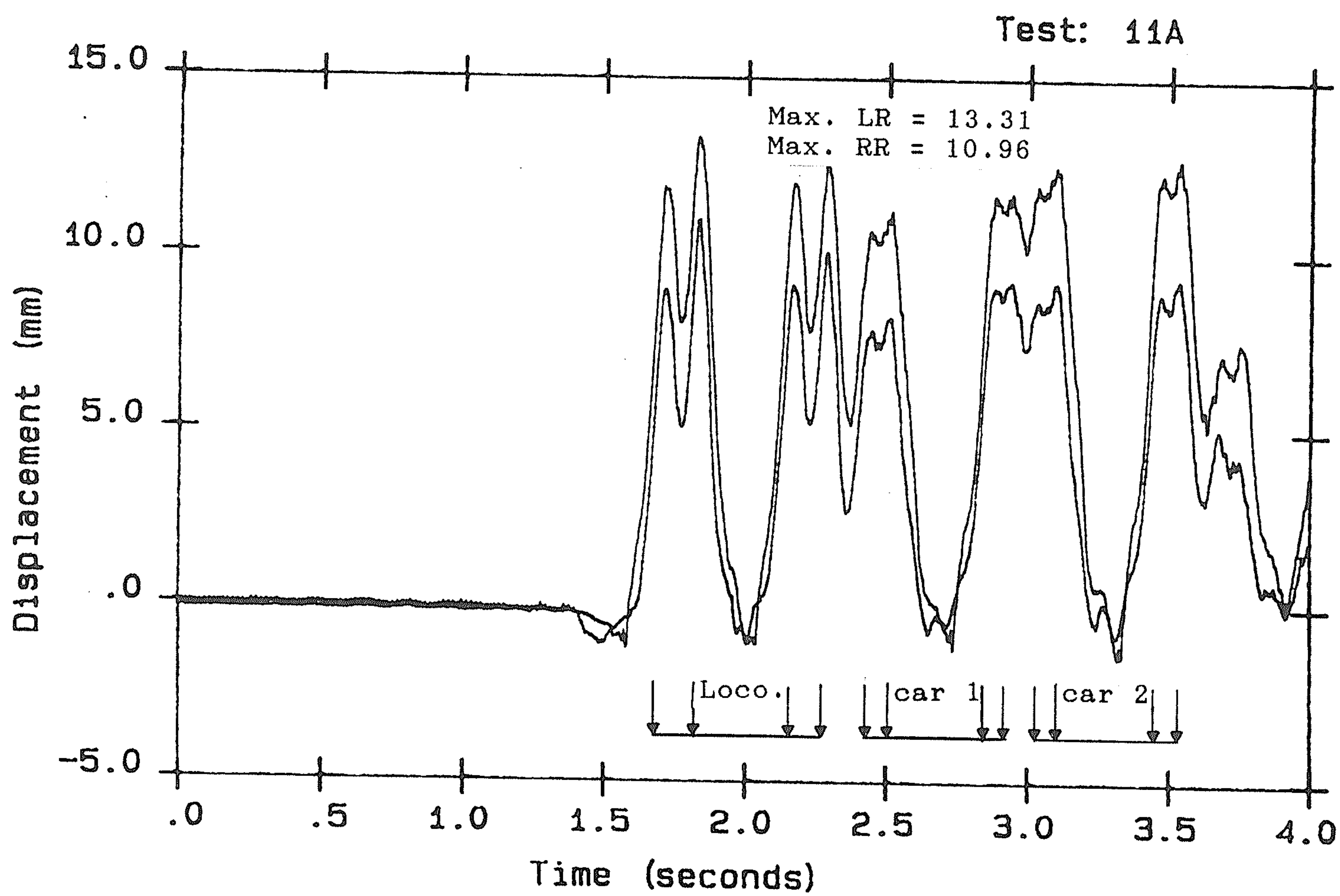

Figure 3.43 Vertical displacement versus time
BDB Site - Normal track section - Test Train No. 2
Speed 50 mph

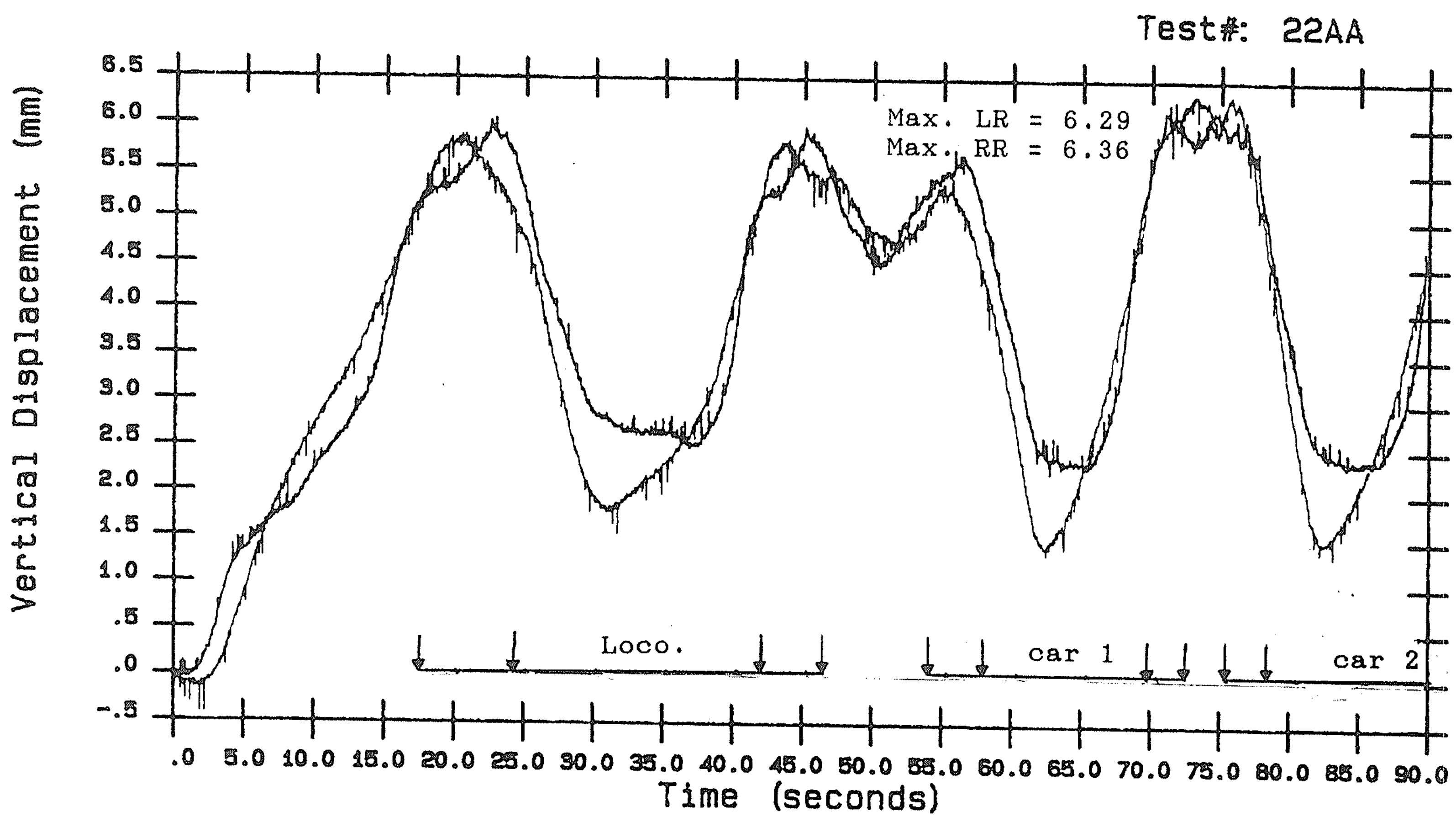

Figure 3.44 Vertical displacement versus time
ODB Site - Midpoint of span S2 - Test Train No. 2
Speed 1 mph

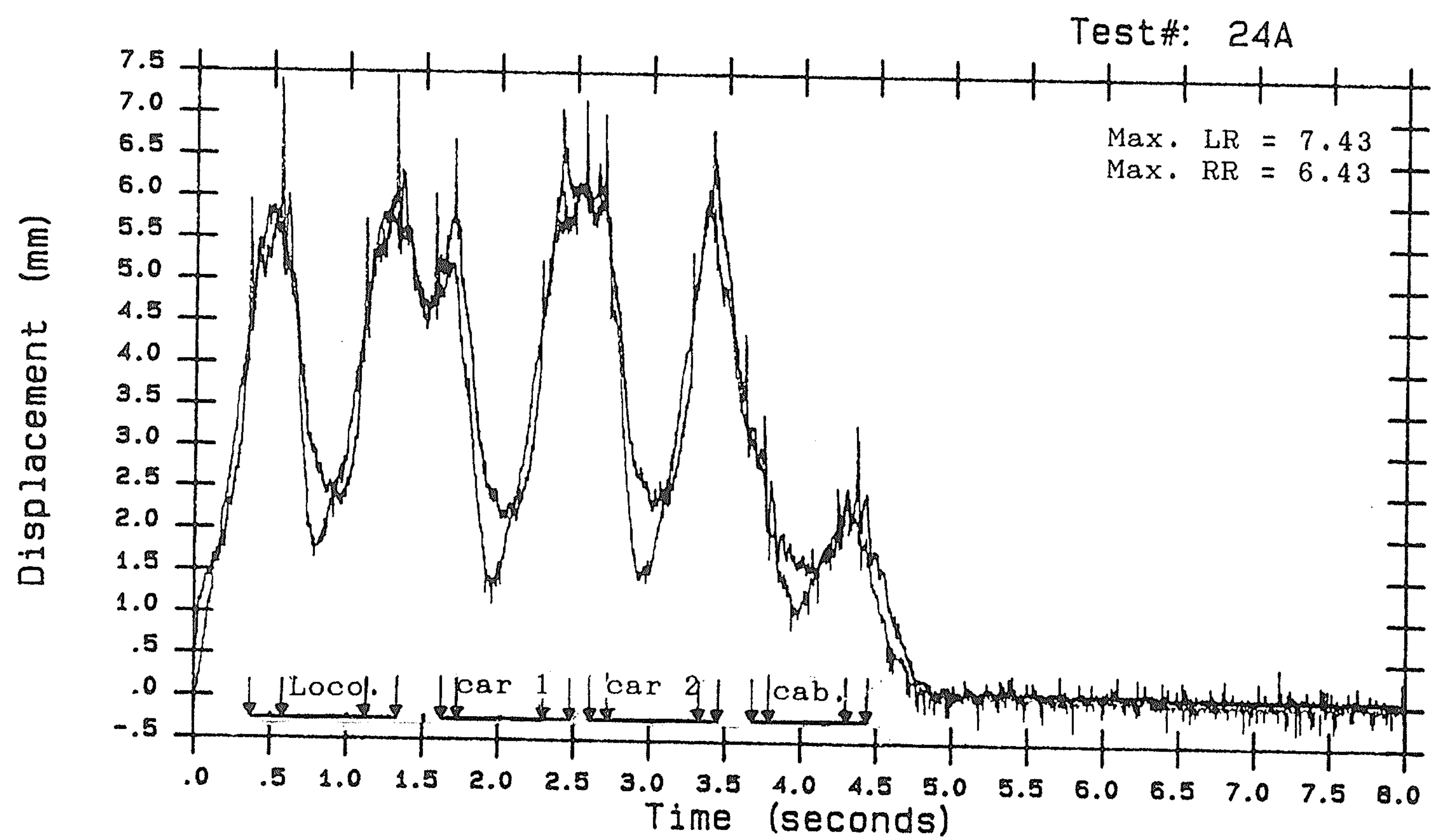

Figure 3.45 Vertical displacement versus time
ODB Site - Midpoint of Span S2 - Test Train No. 2
Speed 30 mph

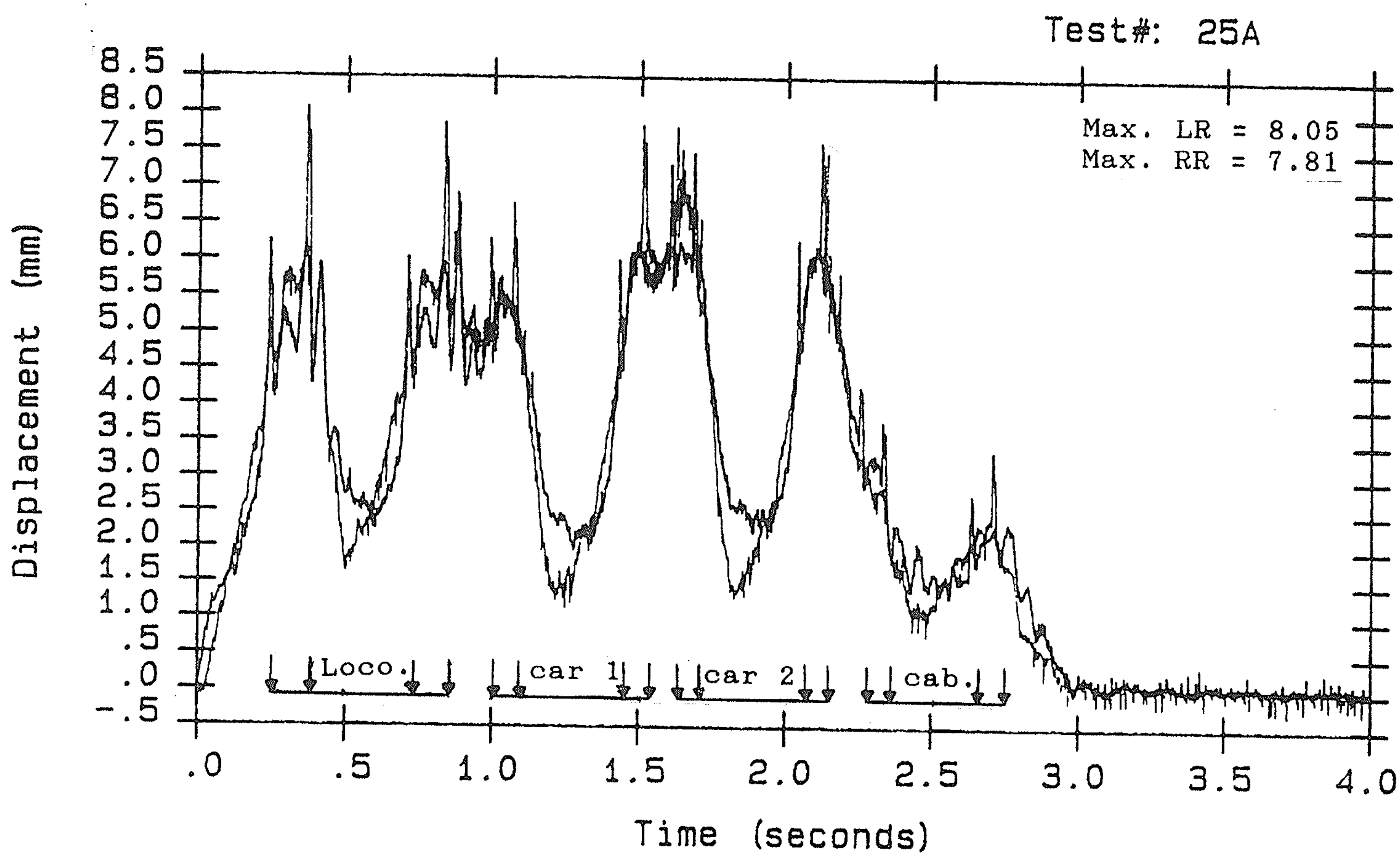

Figure 3.46 Vertical displacement versus time
ODB Site - Midpoint of Span S2 - Test Train No. 2
Speed 50 mph

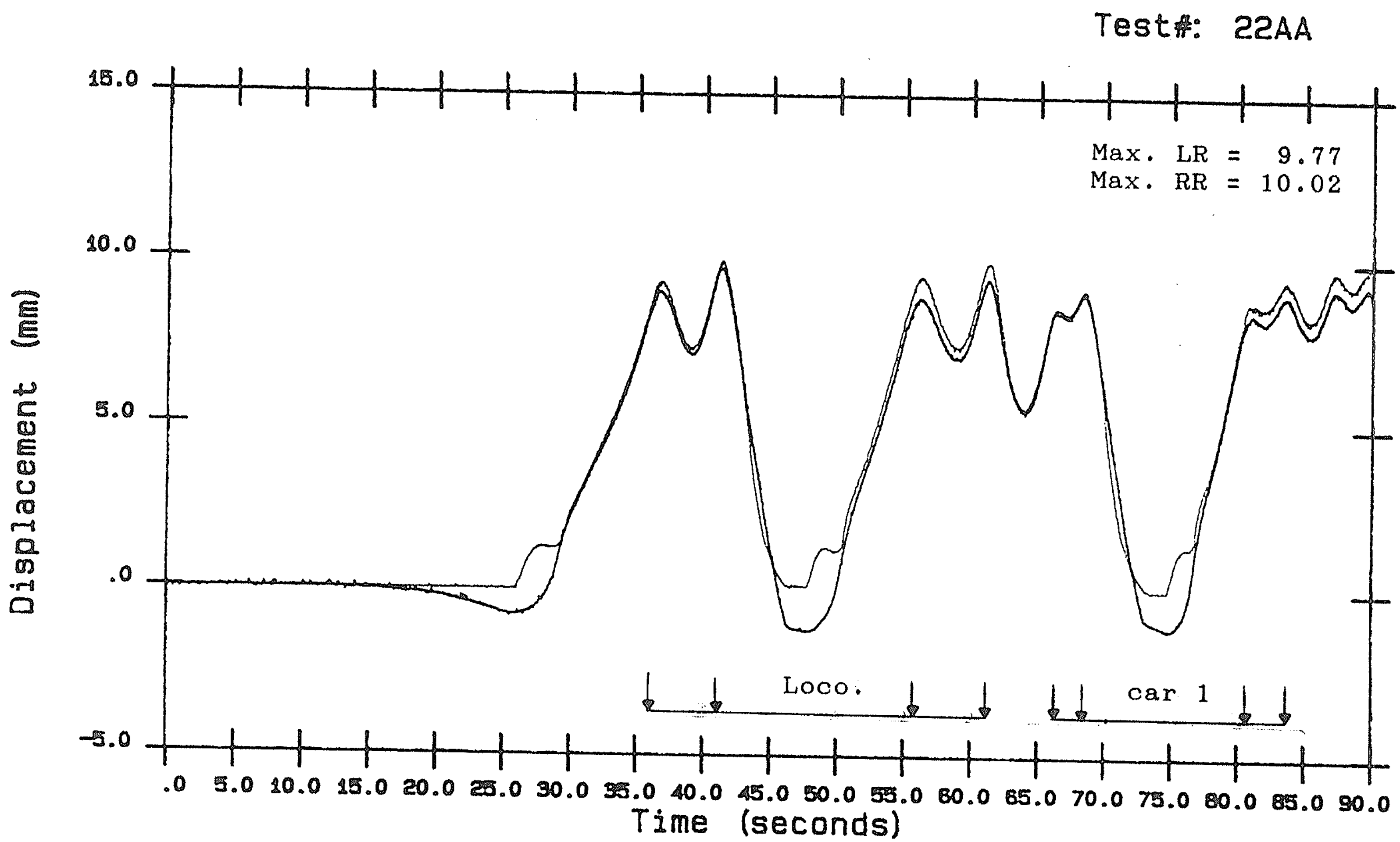

Figure 3.47 Vertical displacement versus time
ODB Site - Bridge approach - Test Train No. 2
Speed 1 mph

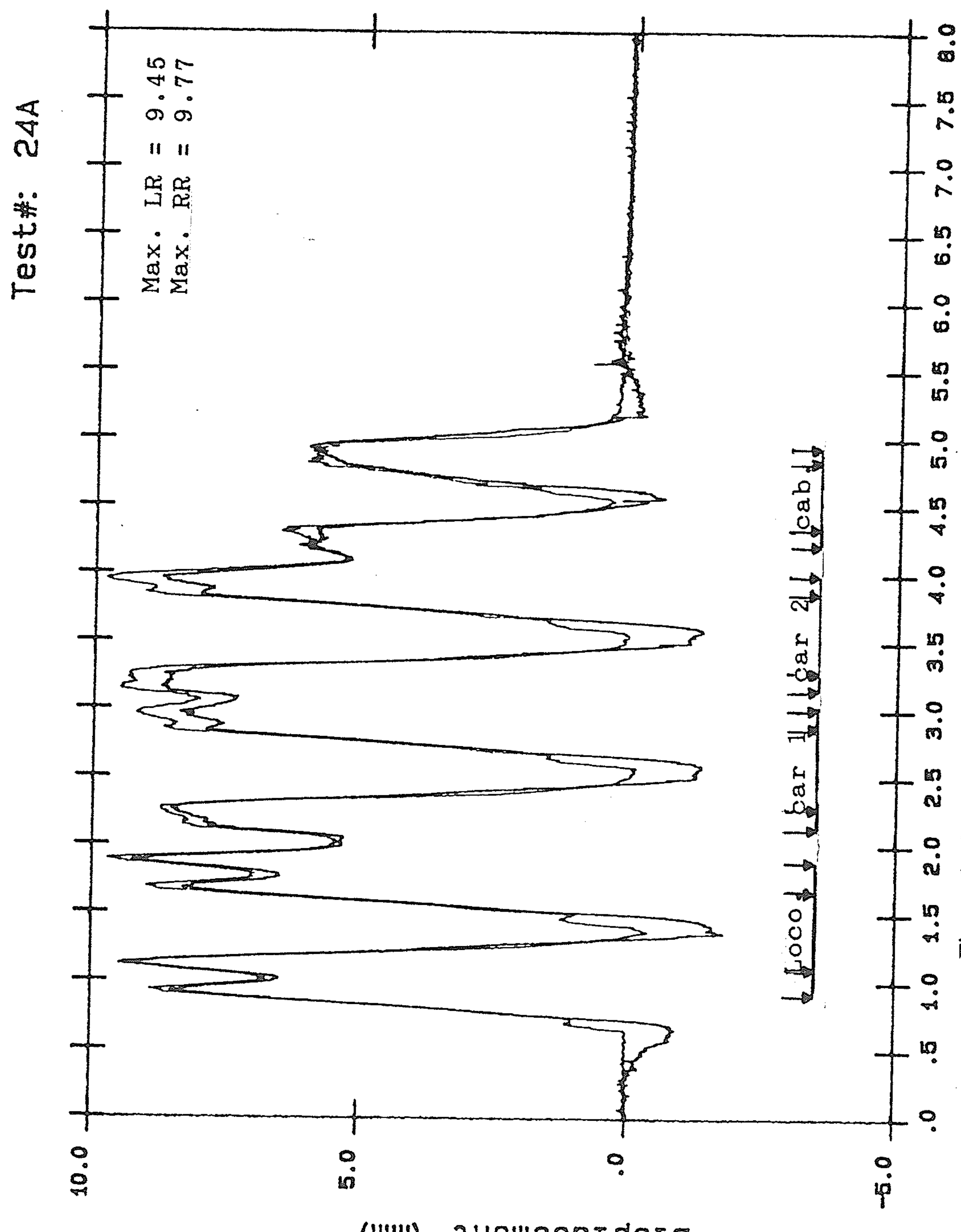

Figure 3.48

Vertical displacement versus time
ODB Site - Bridge approach - Test Train No. 2
Speed 30 mph

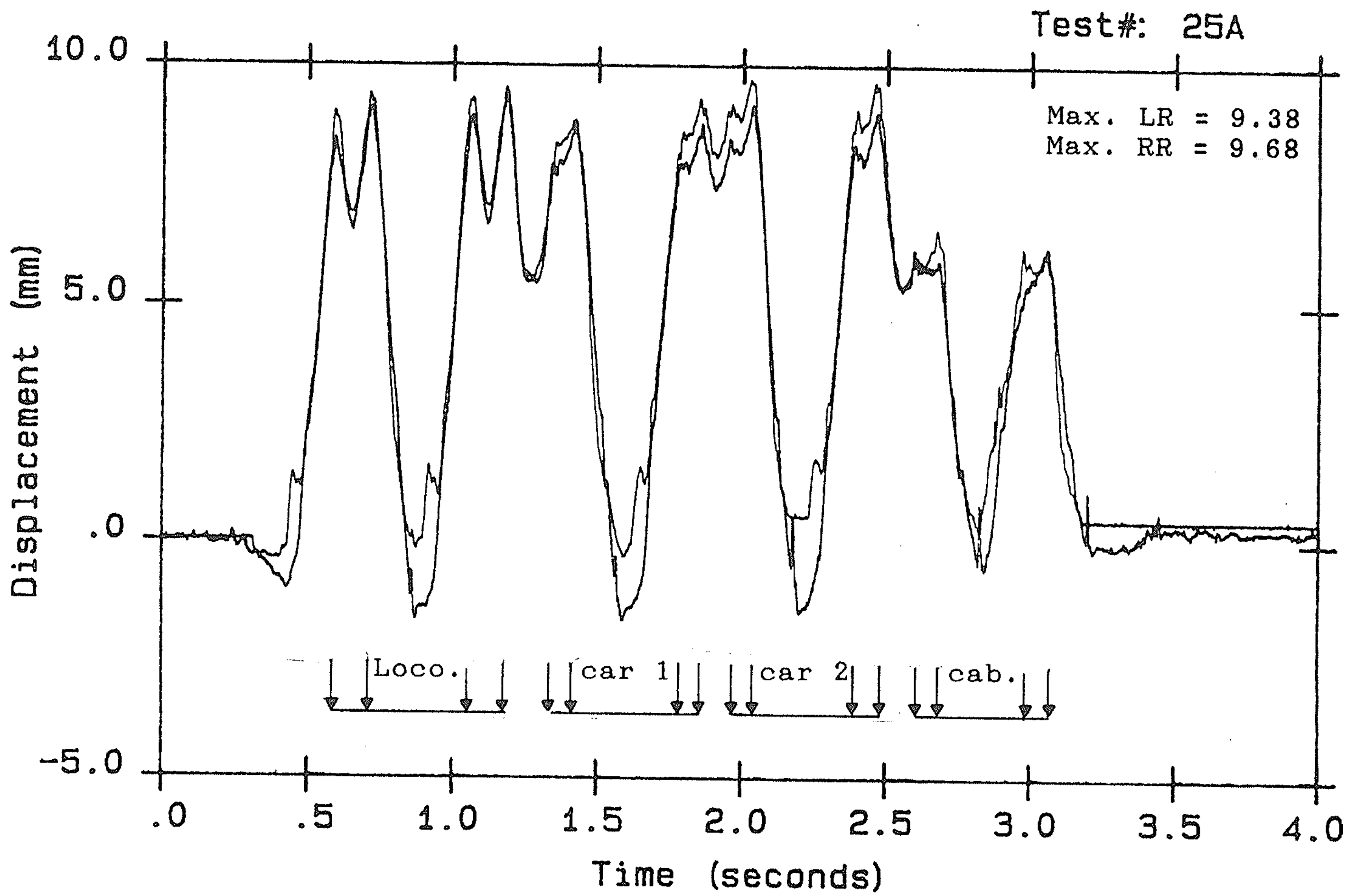

Figure 3.49 Vertical displacement versus time
ODB Site - Bridge approach - Test Train No. 2
Speed 50 mph

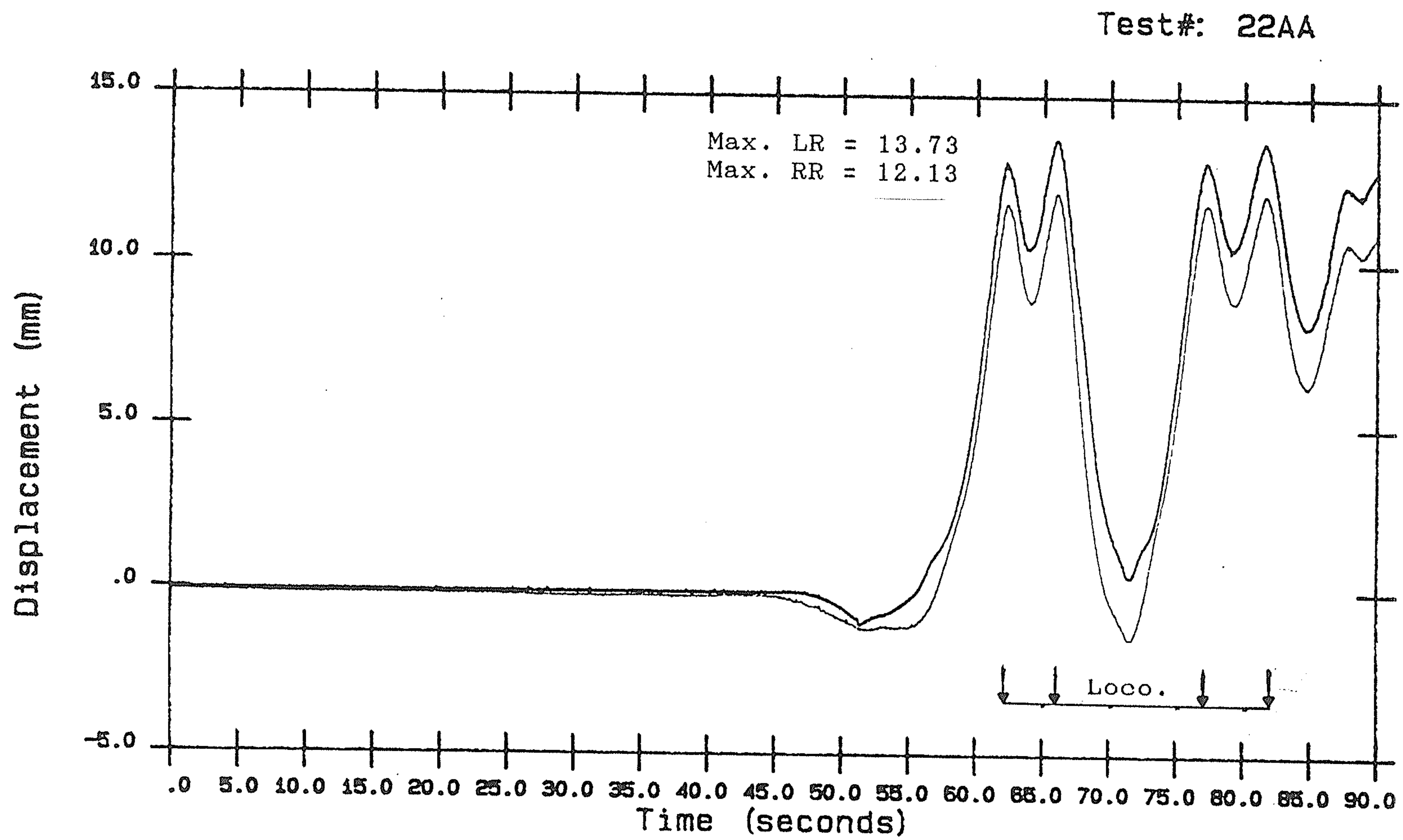

Figure 3.50 Vertical displacement versus time
ODB Site - Normal track section - Test Train No. 2
Speed 1 mph

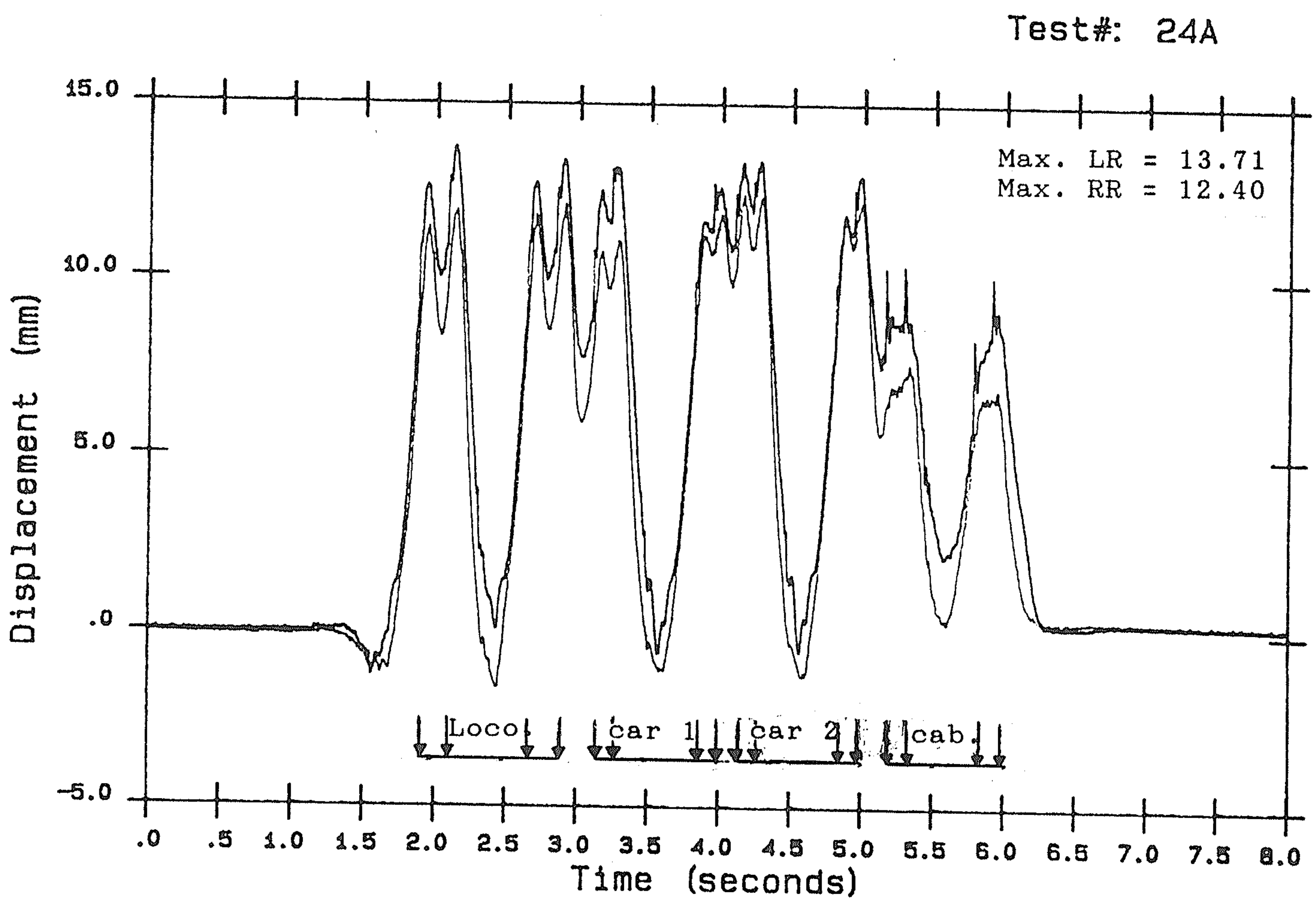

Figure 3.51 Vertical displacement versus time
ODB Site - Normal track section - Test Train No. 2
Speed 30 mph

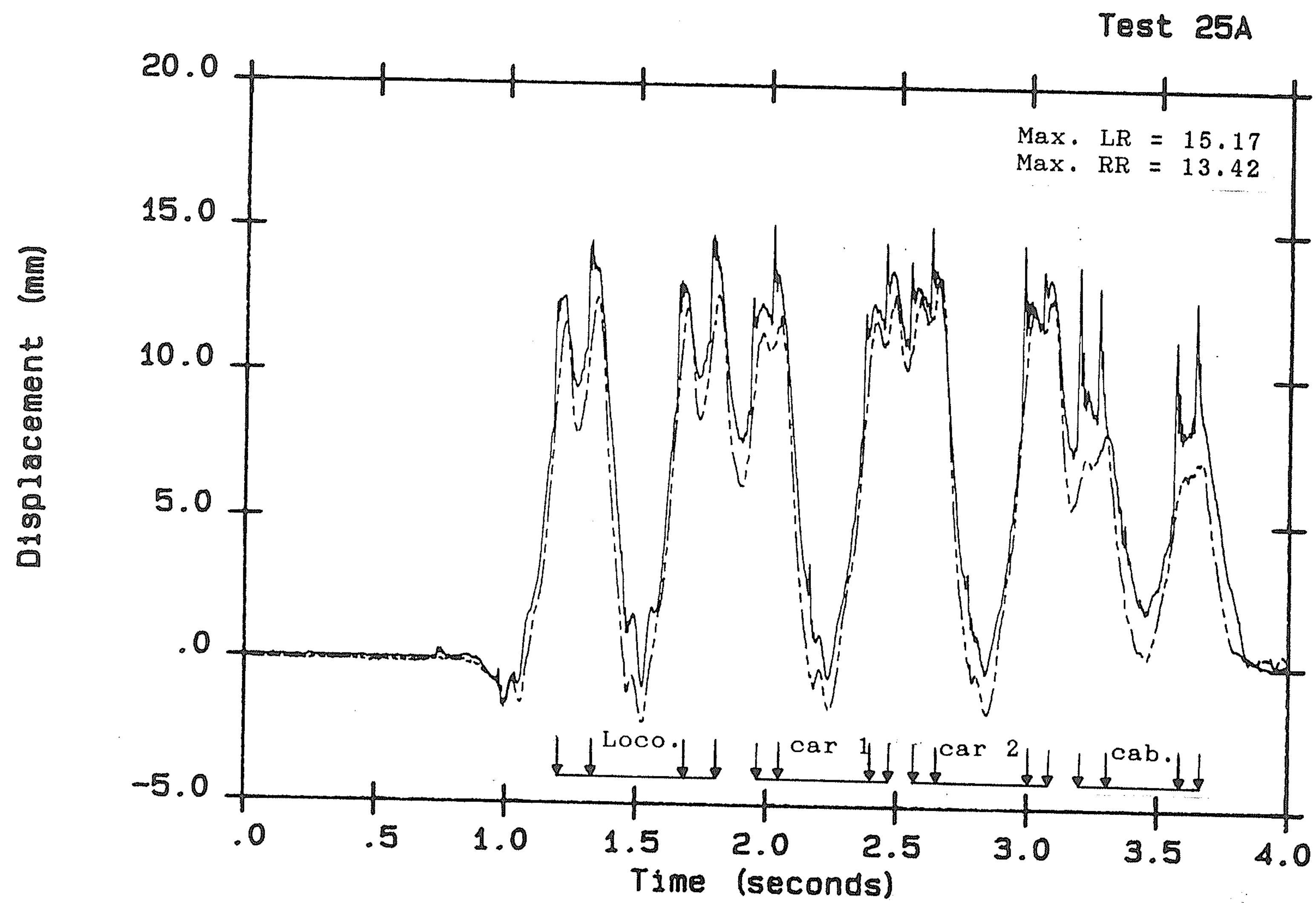

Figure 3.52 Vertical displacement versus time
ODB Site - Normal track section - Test Train No. 2
Speed 50 mph

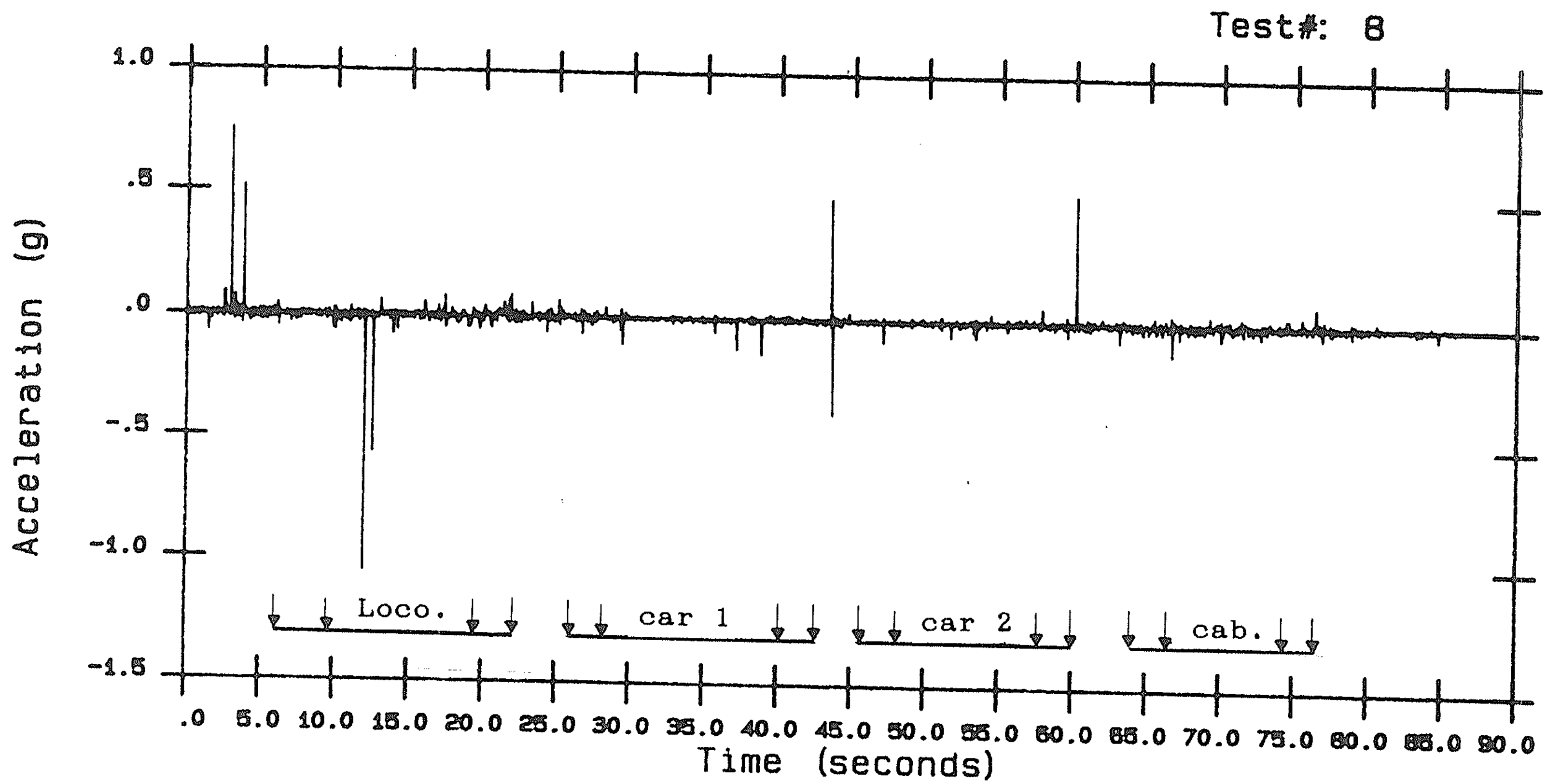

Figure 3.53 Acceleration versus time
BDB Site - Midpoint of Span S3 - Test Train No. 2
Speed 1 mph

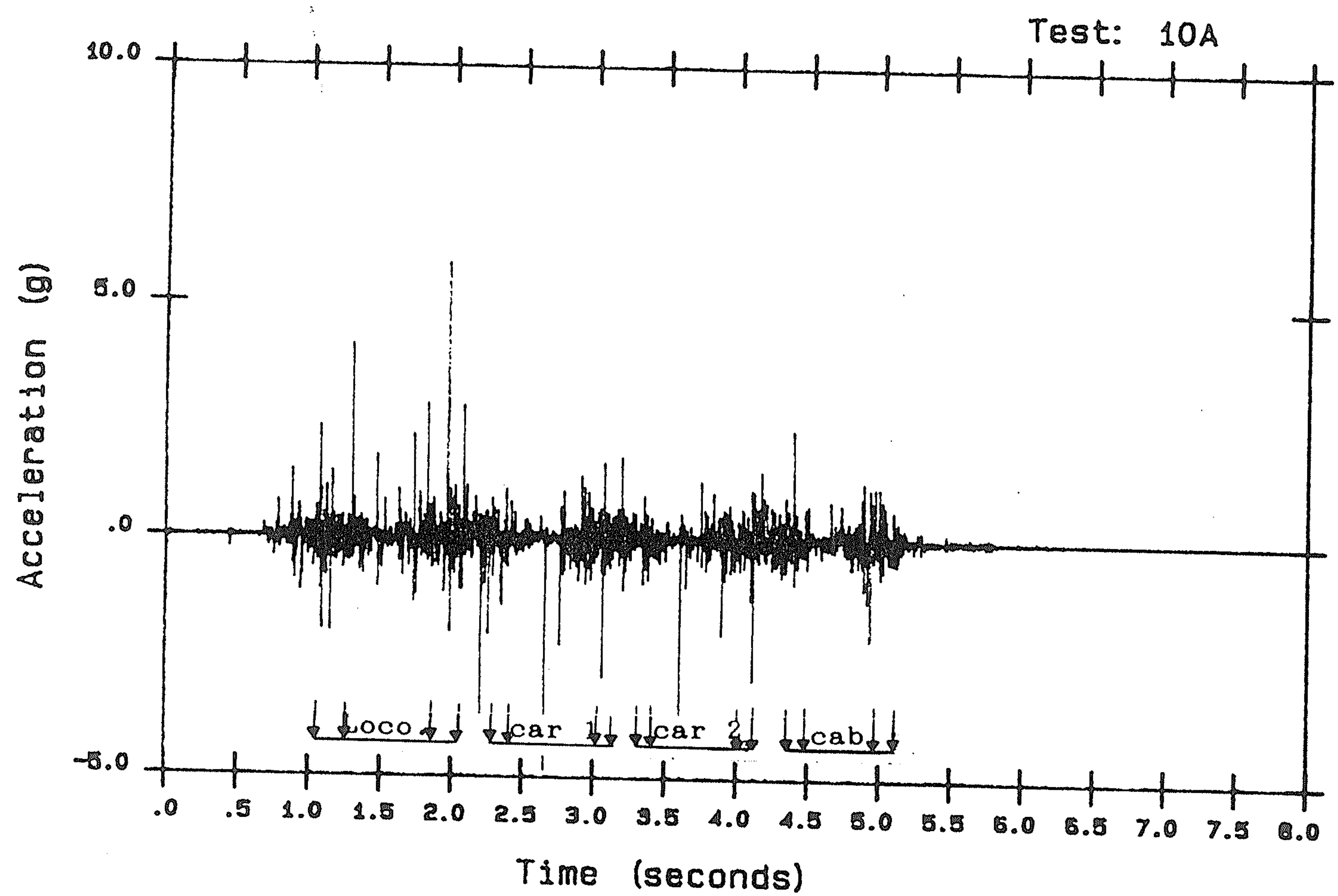

Figure 3.54 Accelèration versus time
BDB Site - Midpoint of Span S3 - Test Train No. 2
Speed 30 mph (Channel #1 not working)

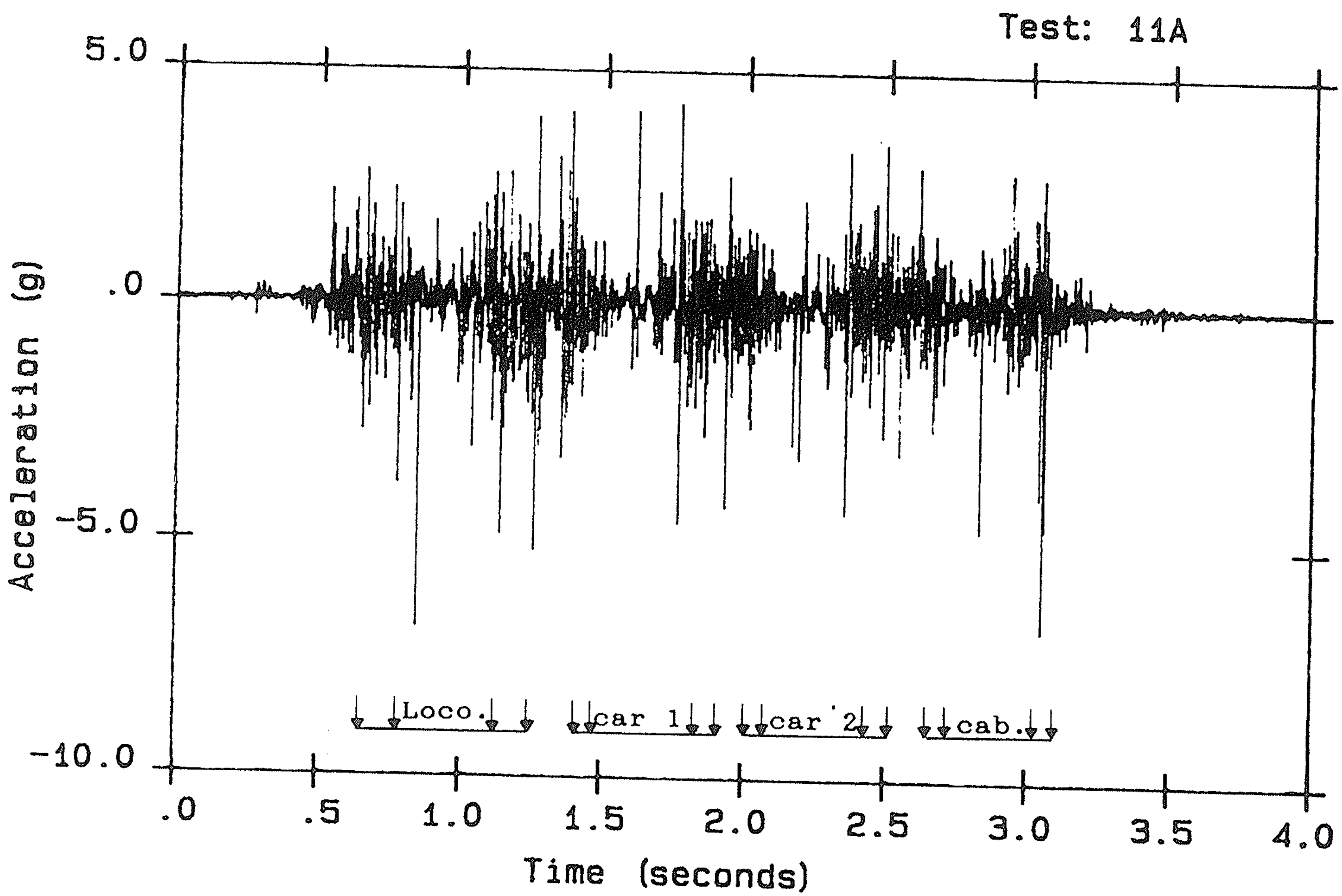

Figure 3.55 Acceleration versus time
BDB Site - Midpoint of Span S3 - Test Train No. 2
Speed 50 mph

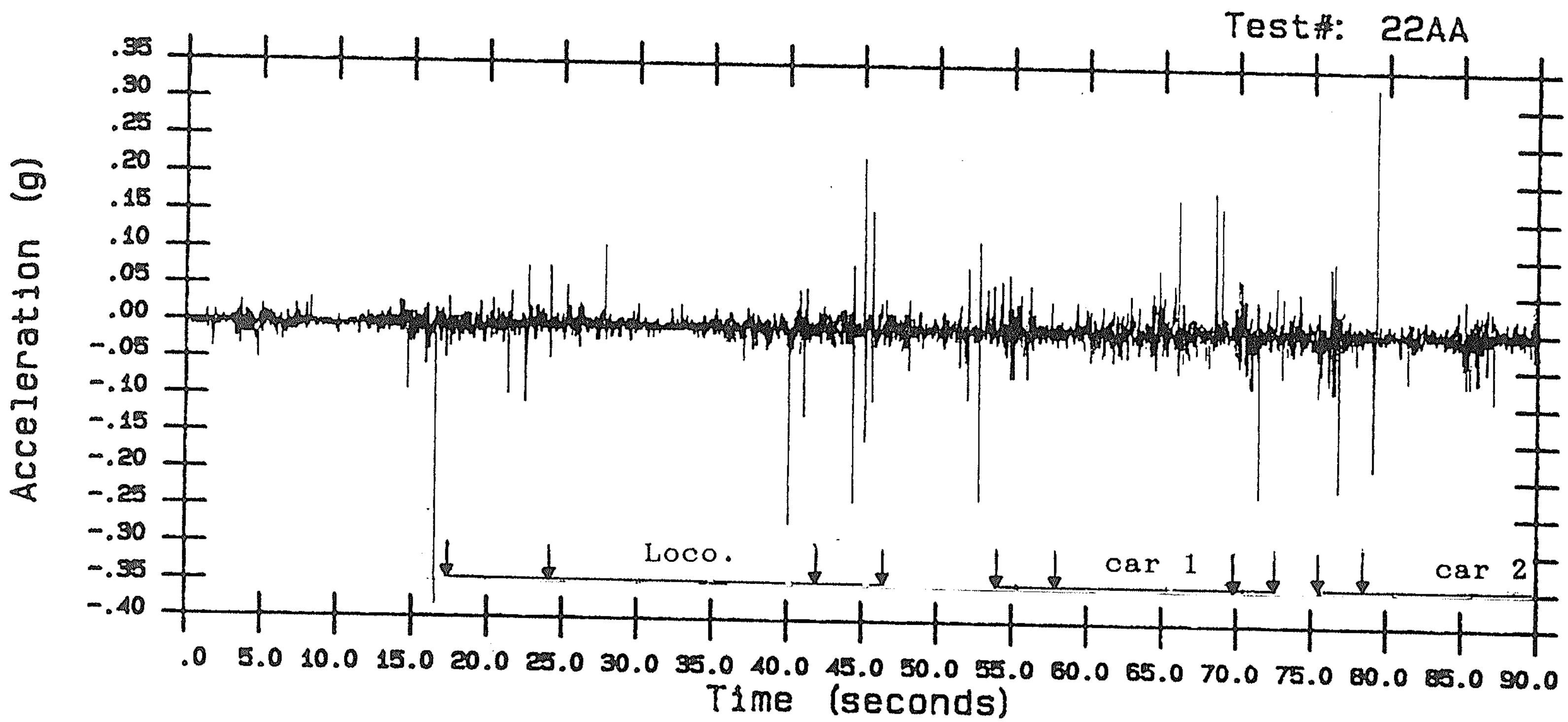

Figure 3.56 Acceleration versus time
ODB Site - Midpoint of Span S2 - Test Train No. 2
Speed 1 mph

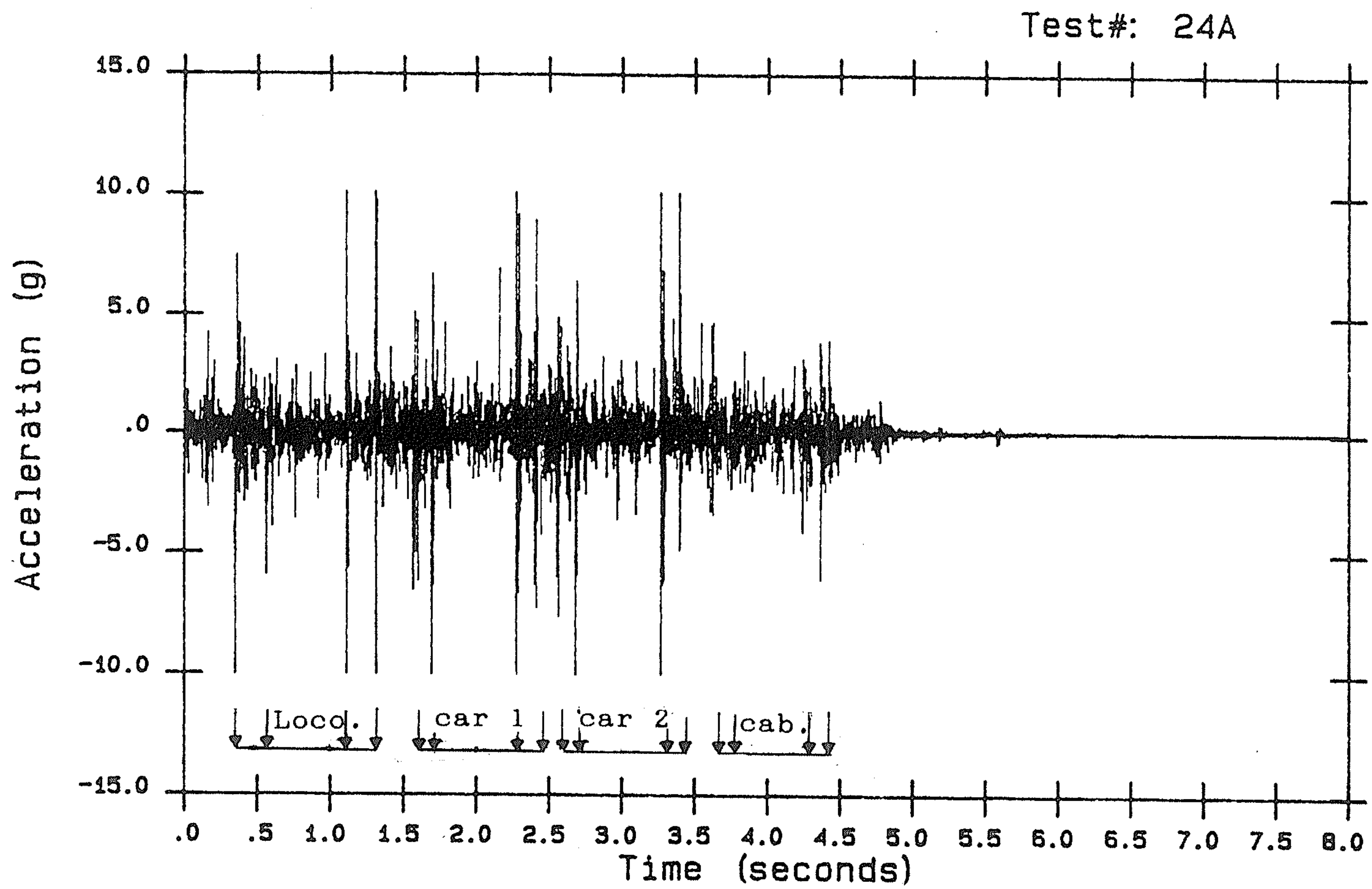

Figure 3.57 Acceleration versus time
ODB Site - Midpoint of Span S2 - Test Train No. 2
Speed 30 mph

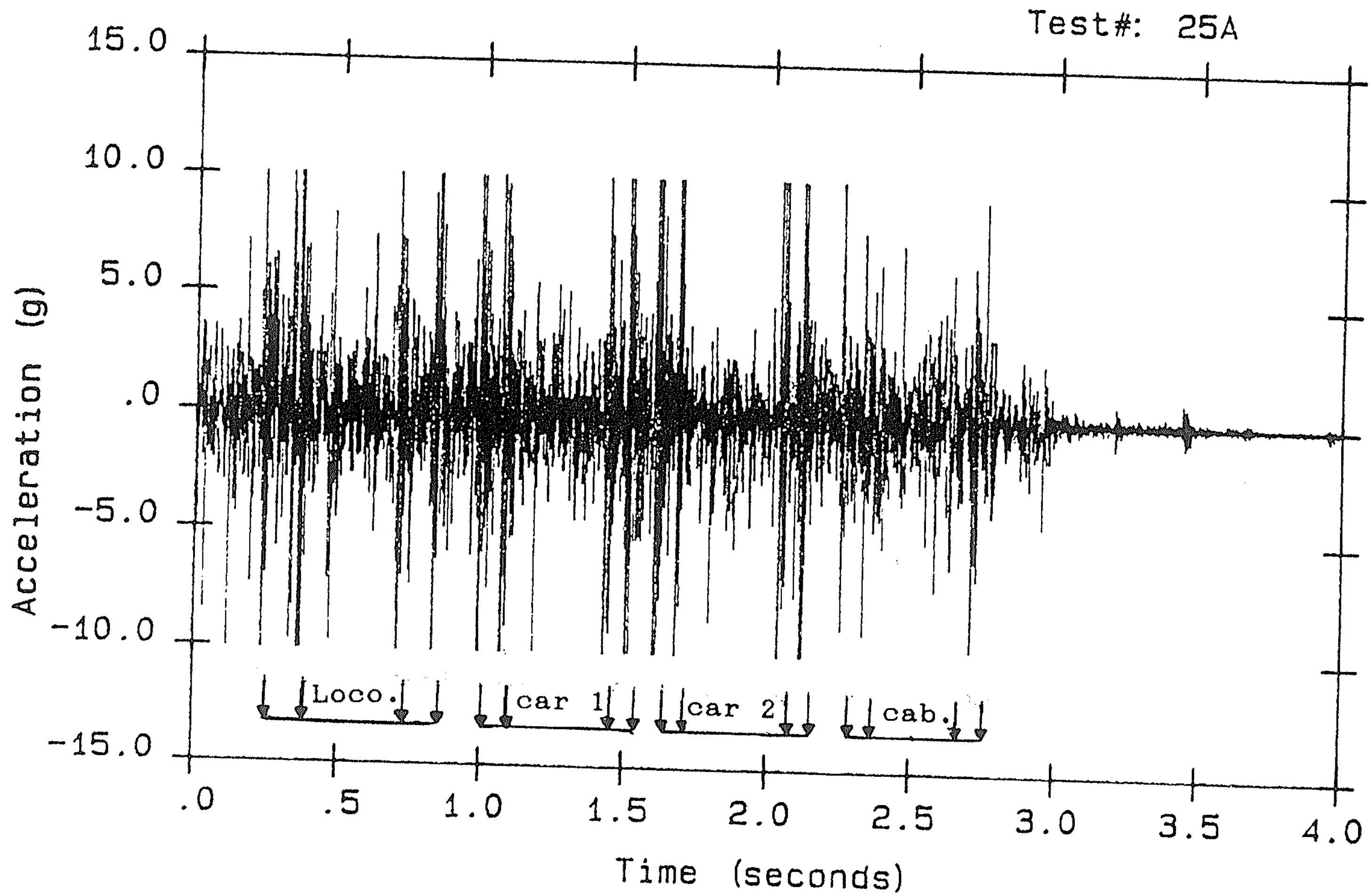

Figure 3.58 Acceleration versus time
ODB Site - Midpoint of Span S2 - Test Train No. 2
Speed 50 mph

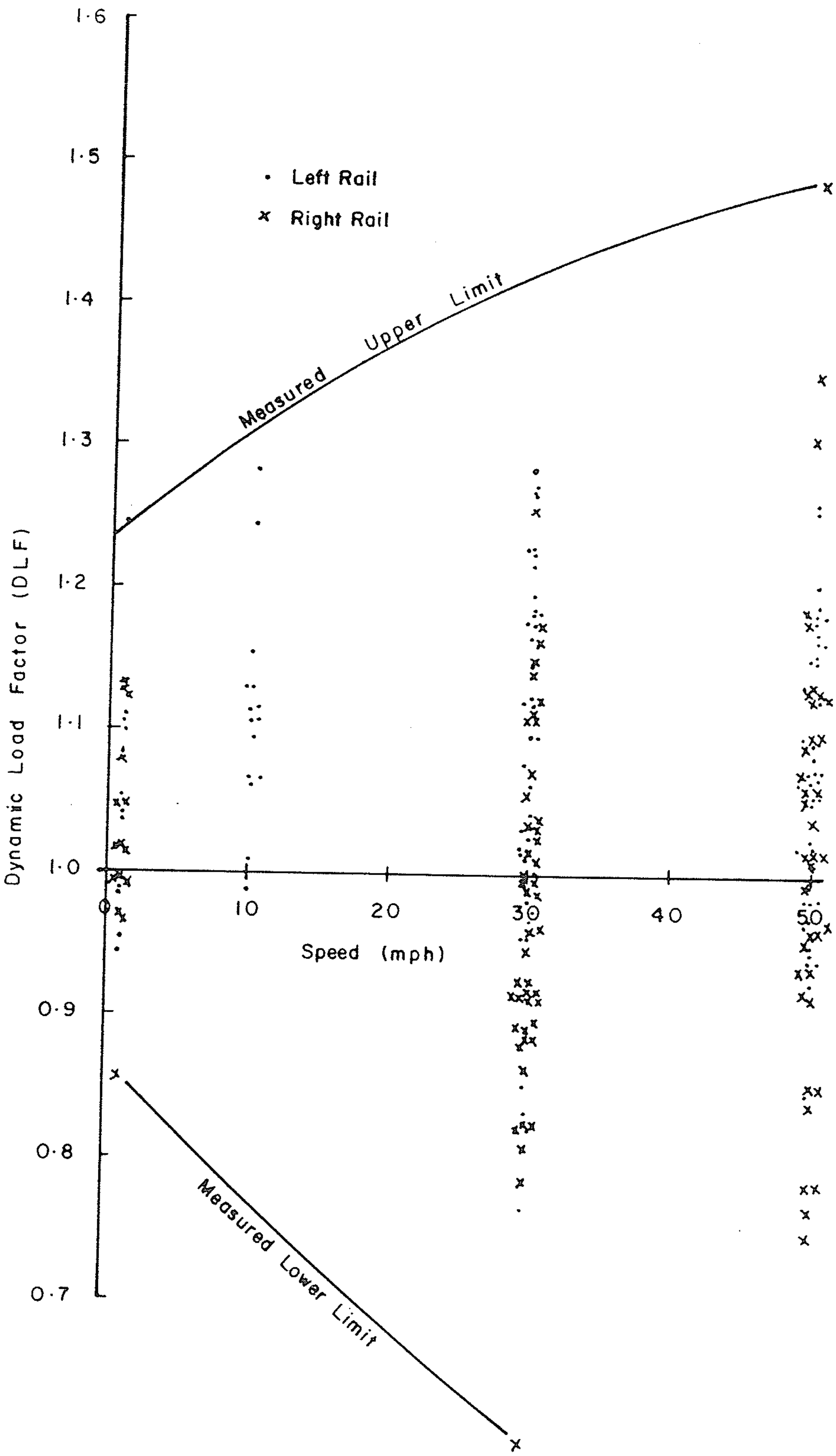

Figure 3.59 Dynamic load factors versus speed
BDB Site - Midpoint of Span S3 - Test Train No. 2

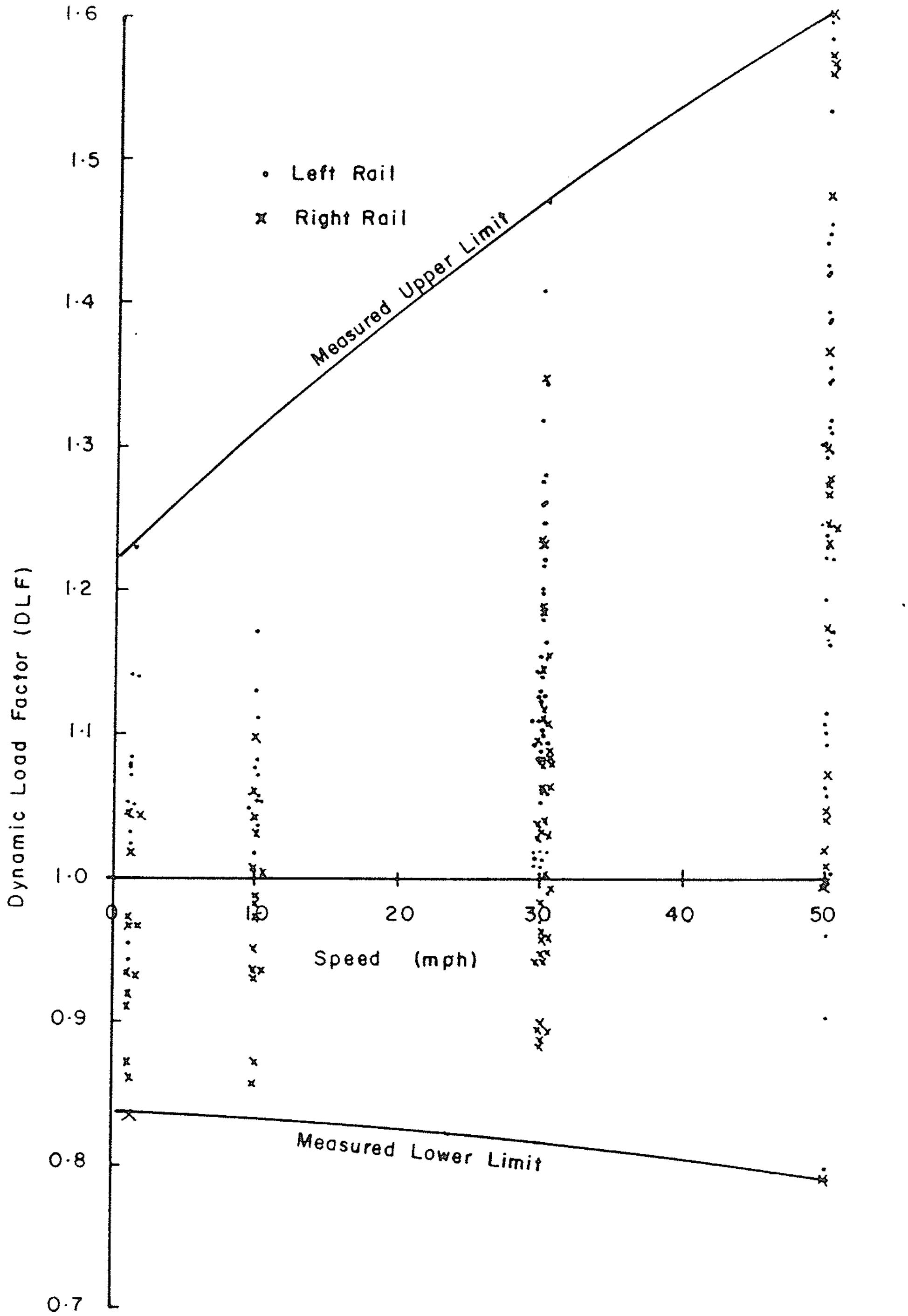

Figure 3.60 Dynamic load factors versus speed
BDB Site - Bridge Approach - Test Train No. 2

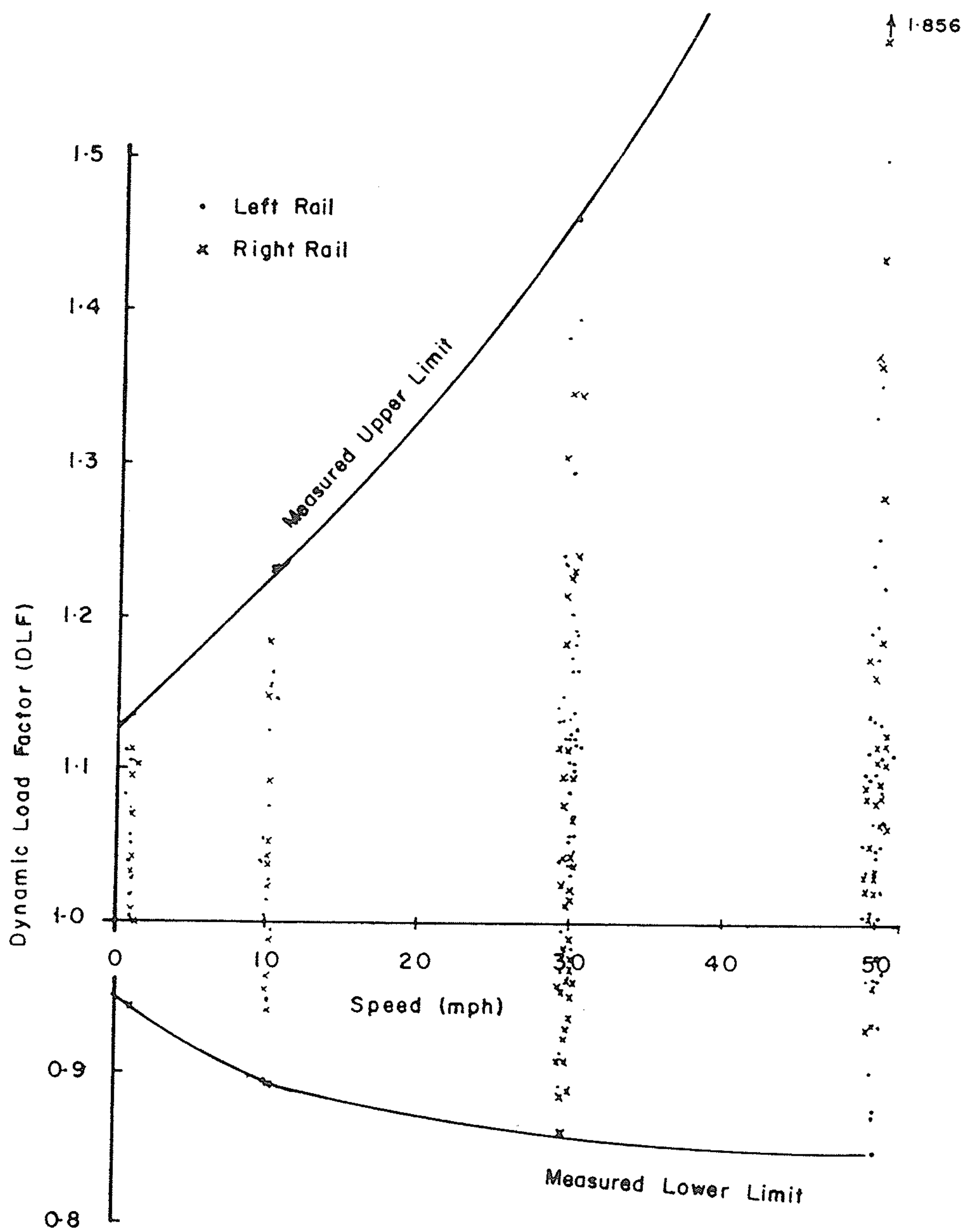

Figure 3.61 Dynamic load factors versus speed
BDB Site - Normal track section - Test Train No. 2

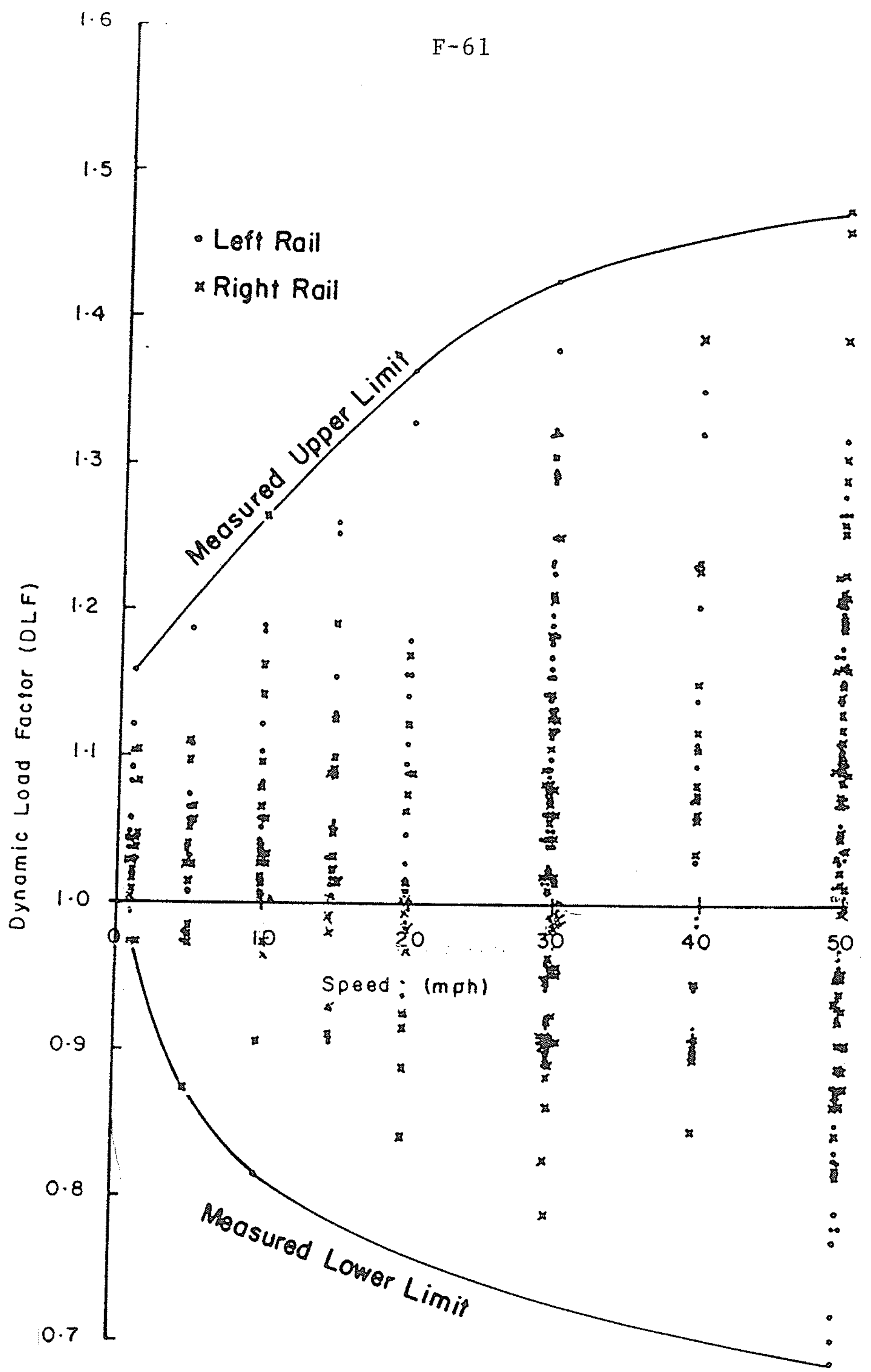

Figure 3.62 Dynamic load factors versus speed
ODB Site - Midpoint of Span S3 - Test Train No. 2

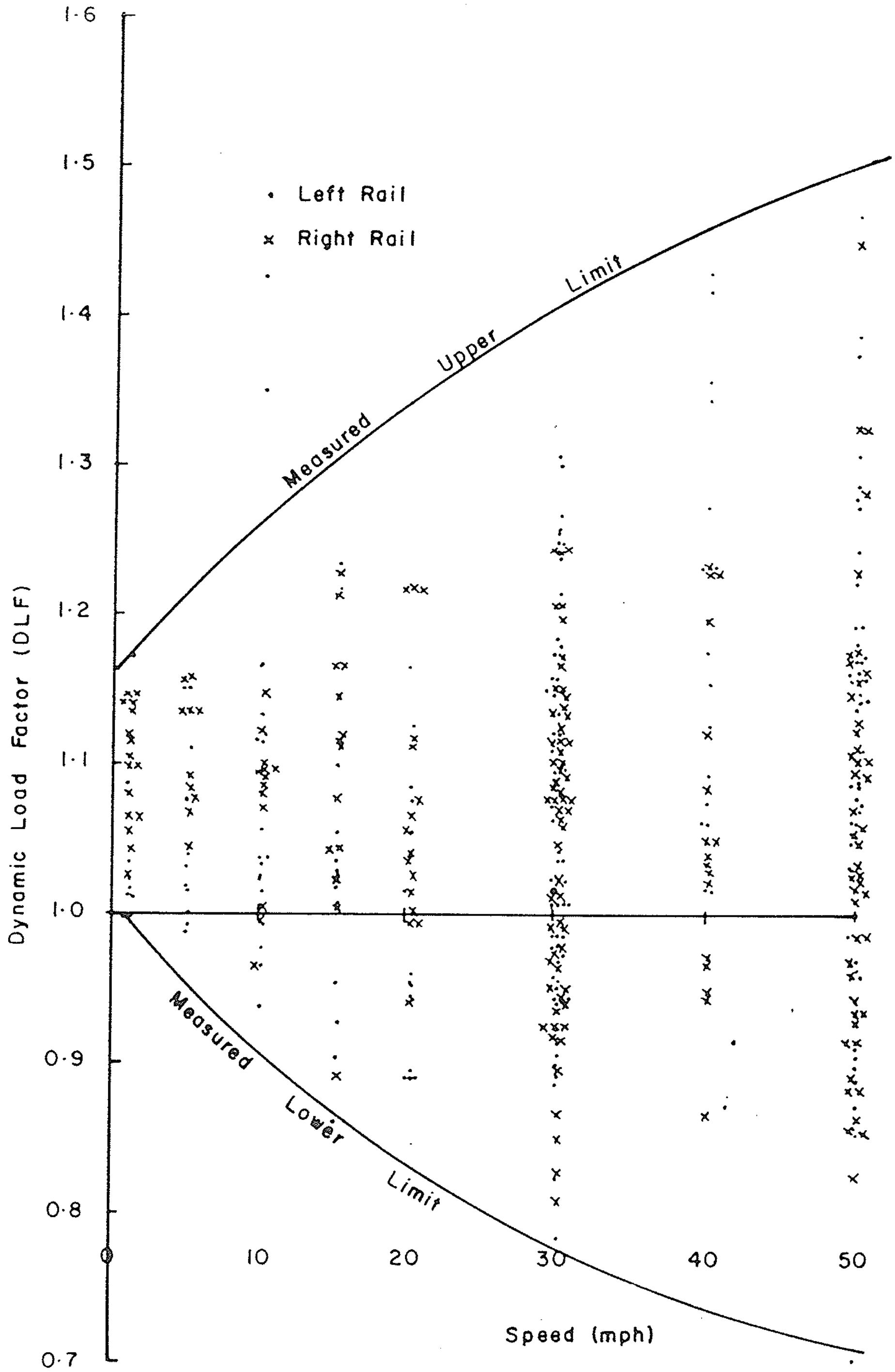

Figure 3.63 Dynamic load factors versus speed
ODB Site - Bridge Approach - Test Train No. 2

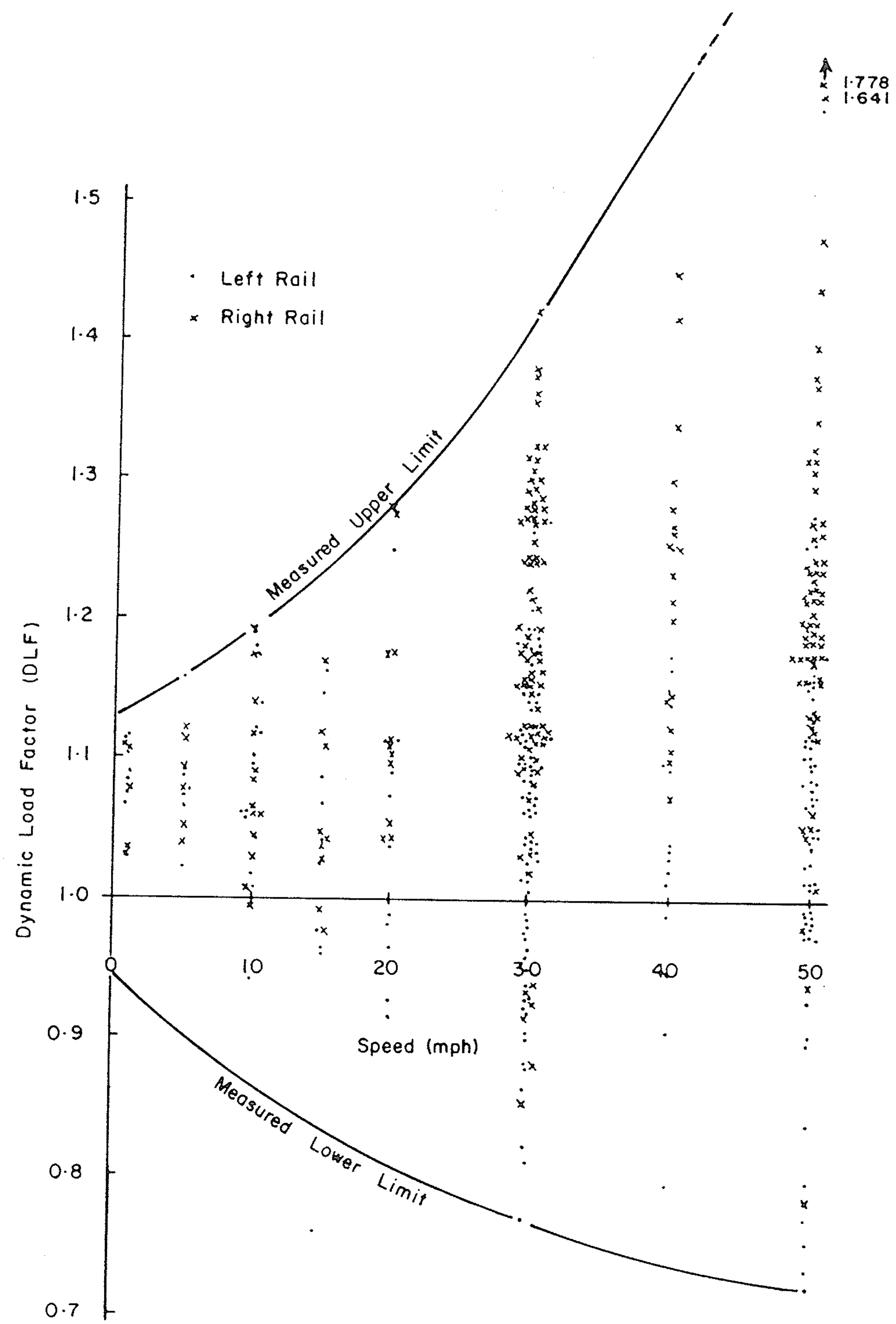

Figure 3.64 Dynamic load factors versus speed
ODB Site - Normal track section - Test Train No. 2

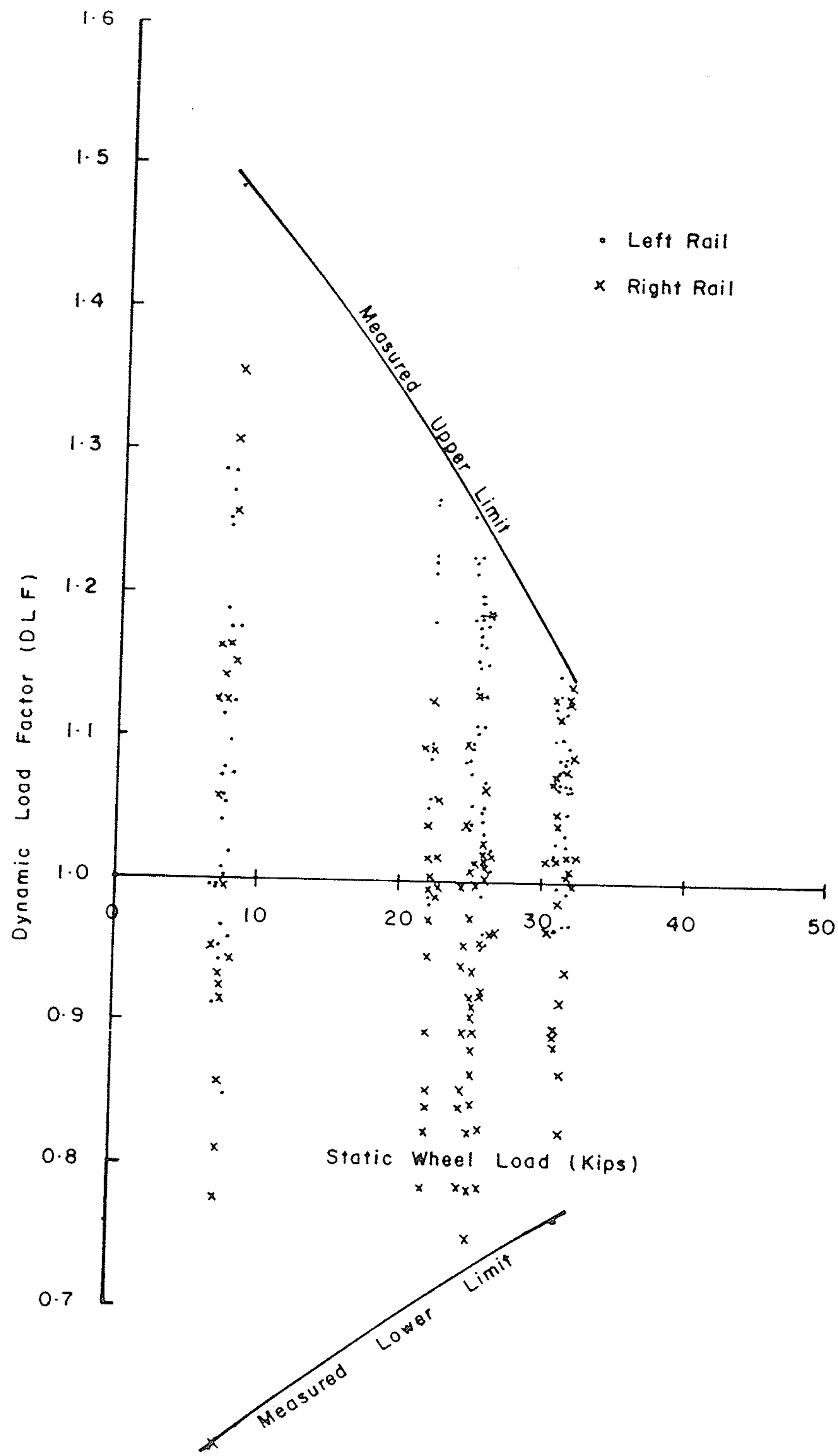

Figure 3.65 Dynamic load factors versus static wheel load
BDB Site - Midpoint of span S3 - Test Train No. 2

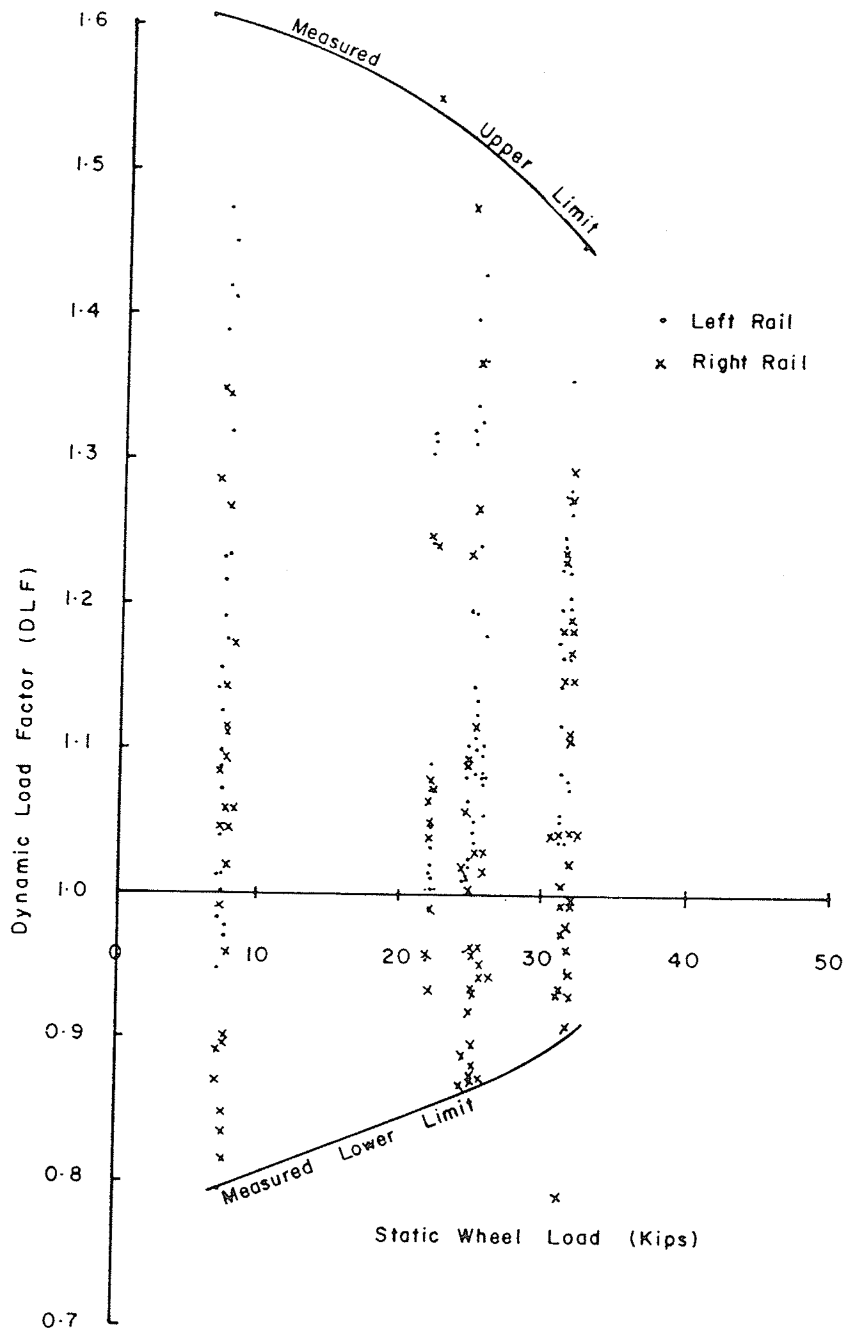

Figure 3.66 Dynamic load factors versus static wheel load
BDB Site - Bridge approach - Test Train No. 2

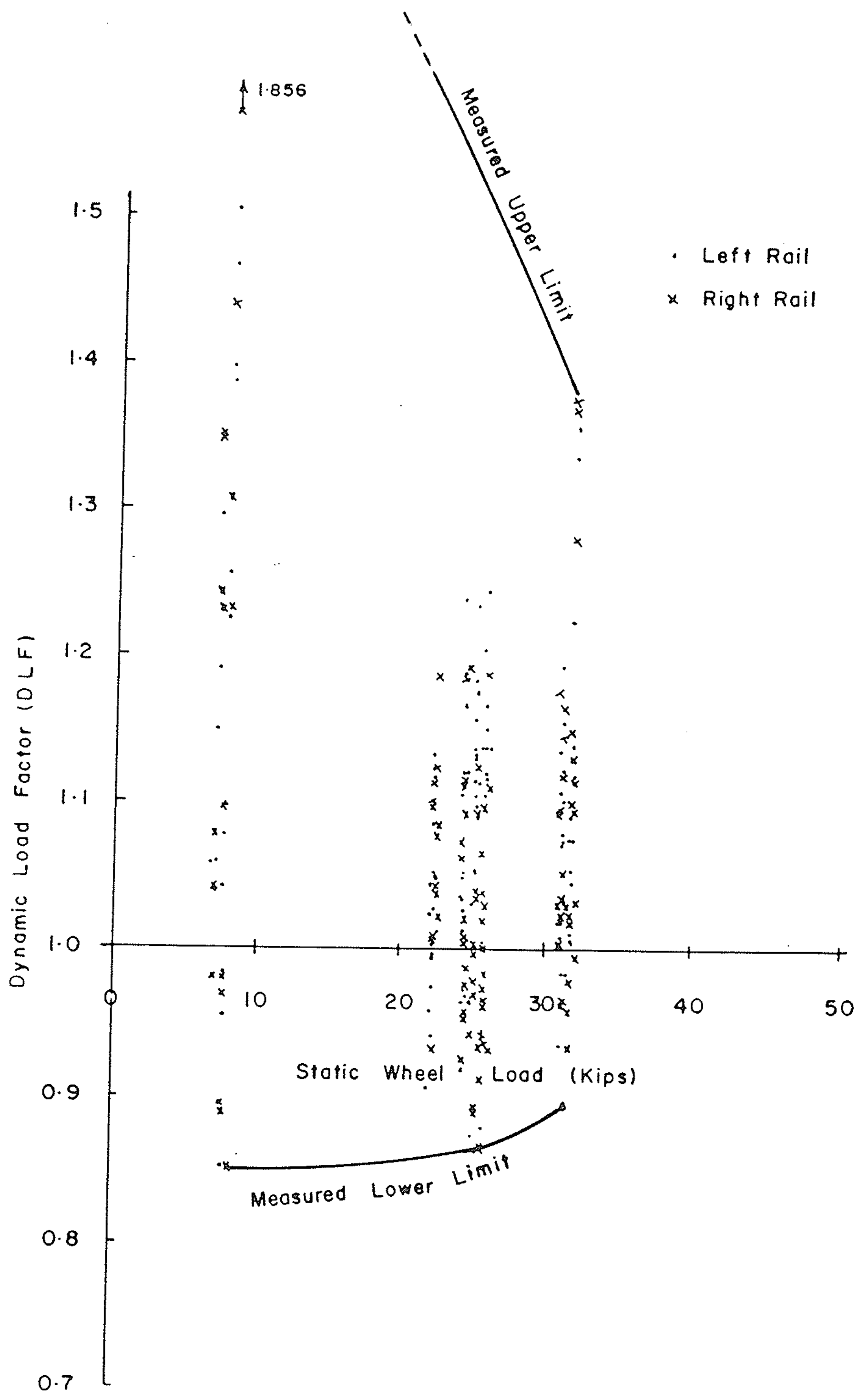

Figure 3.67 Dynamic load factors versus static wheel load
BDB Site - Normal track section - Test Train No. 2

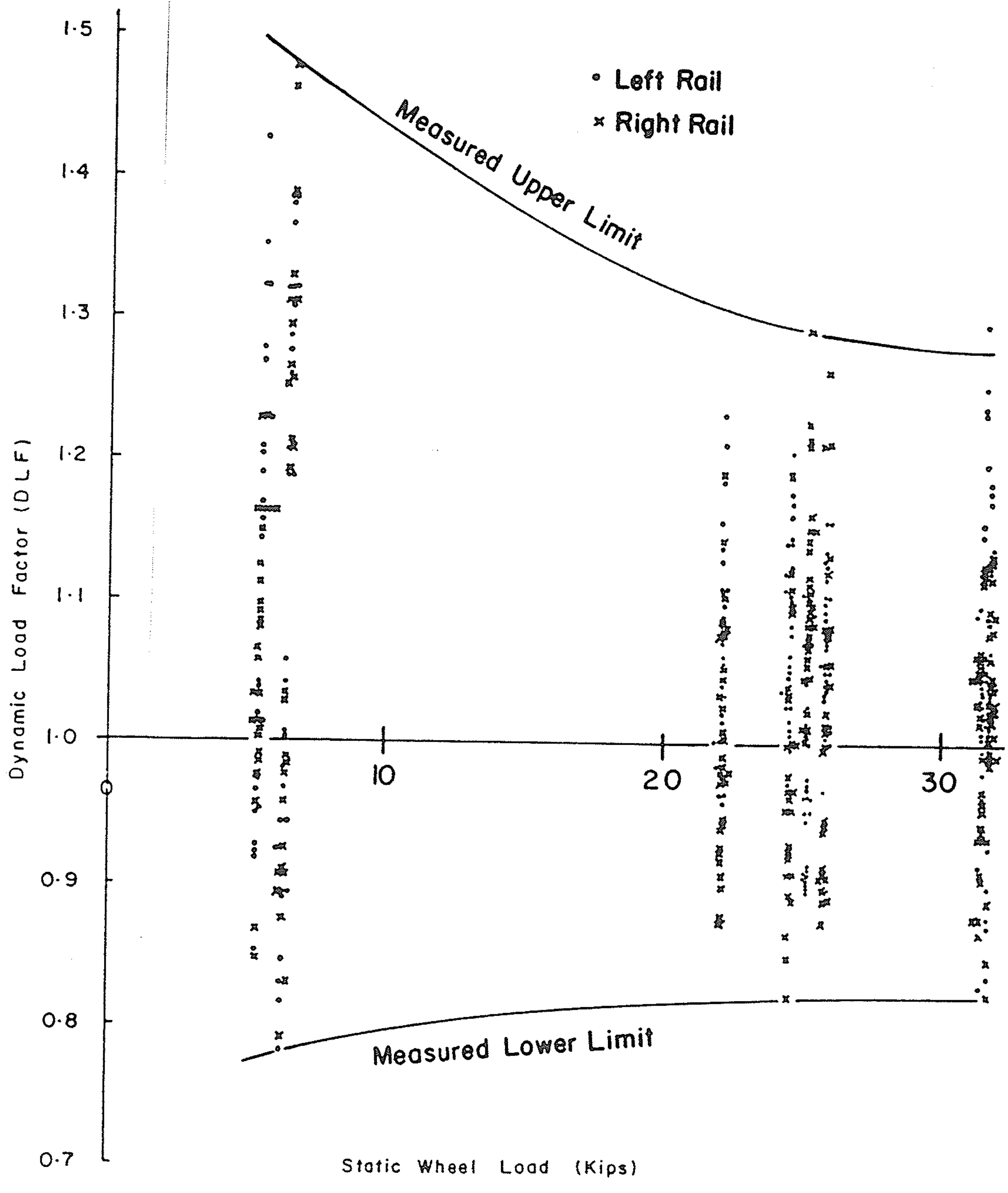

Figure 3.68 Dynamic load factors versus static wheel load
ODB Site - Midpoint of span S3 - Test Train No. 2

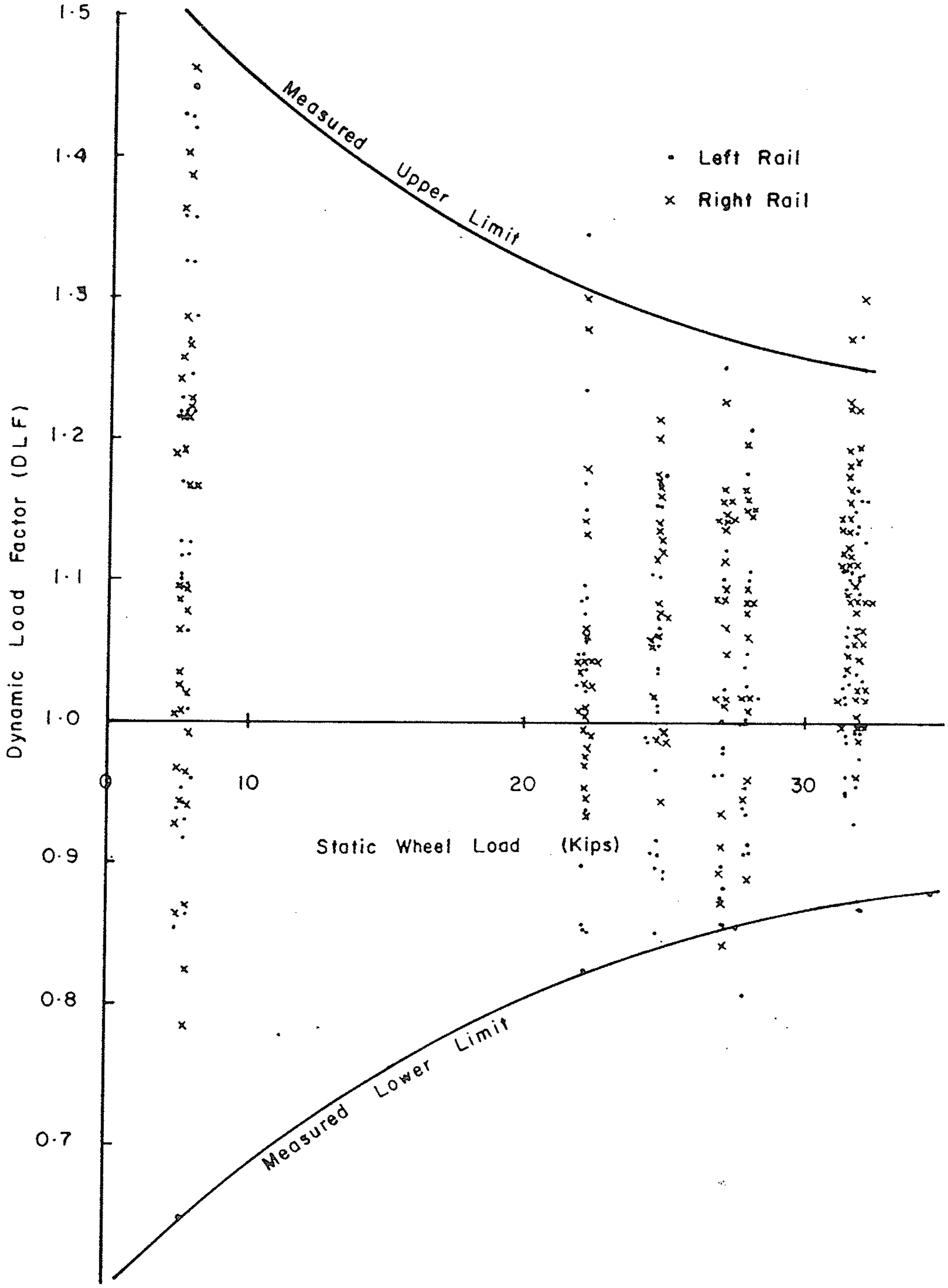

Figure 3.69 Dynamic load factors versus static wheel load
ODB Site - Bridge approach - Test Train No. 2

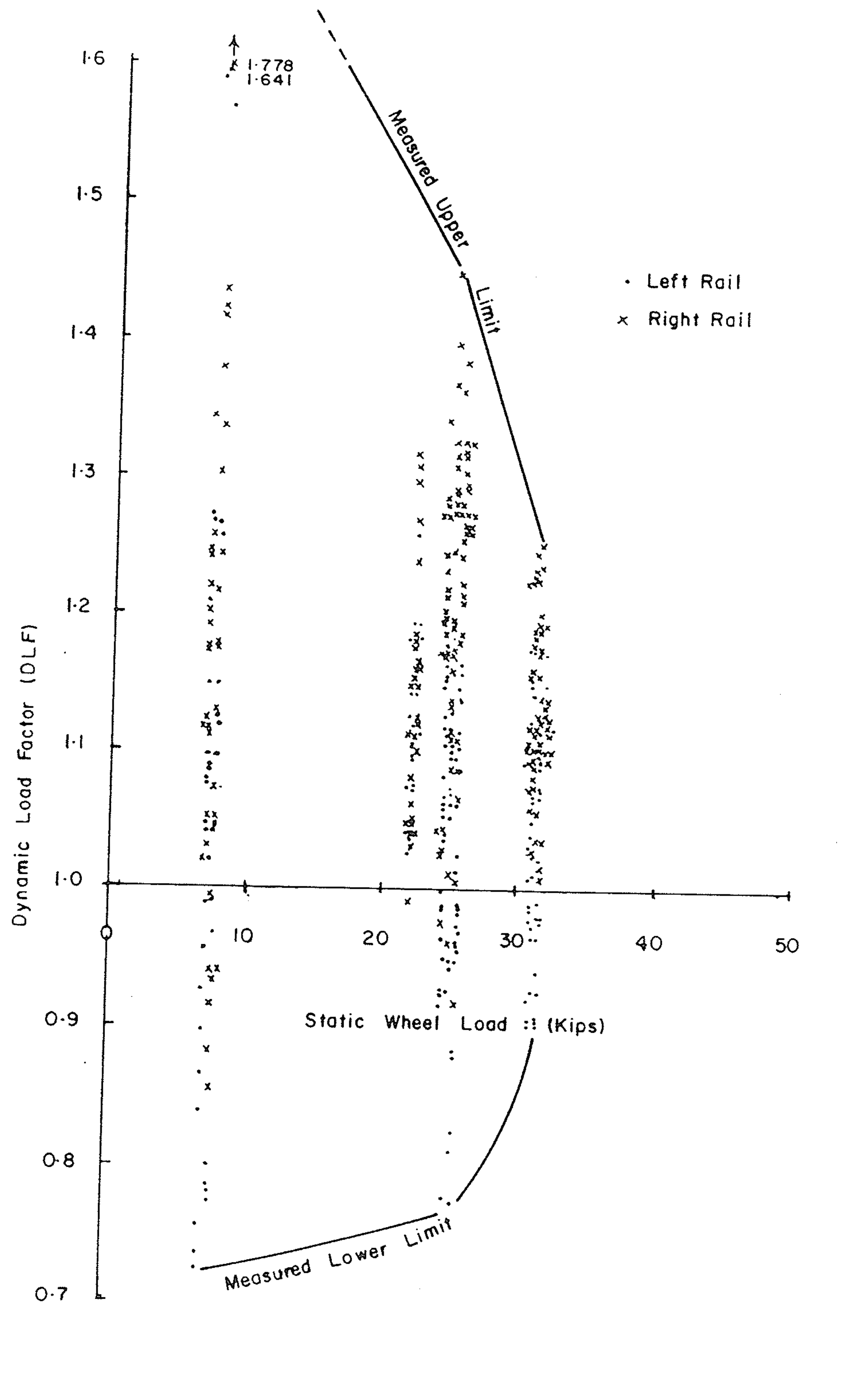

Figure 3.70 Dynamic load factors versus static wheel load
ODB Site - Normal track section - Test Train No. 2

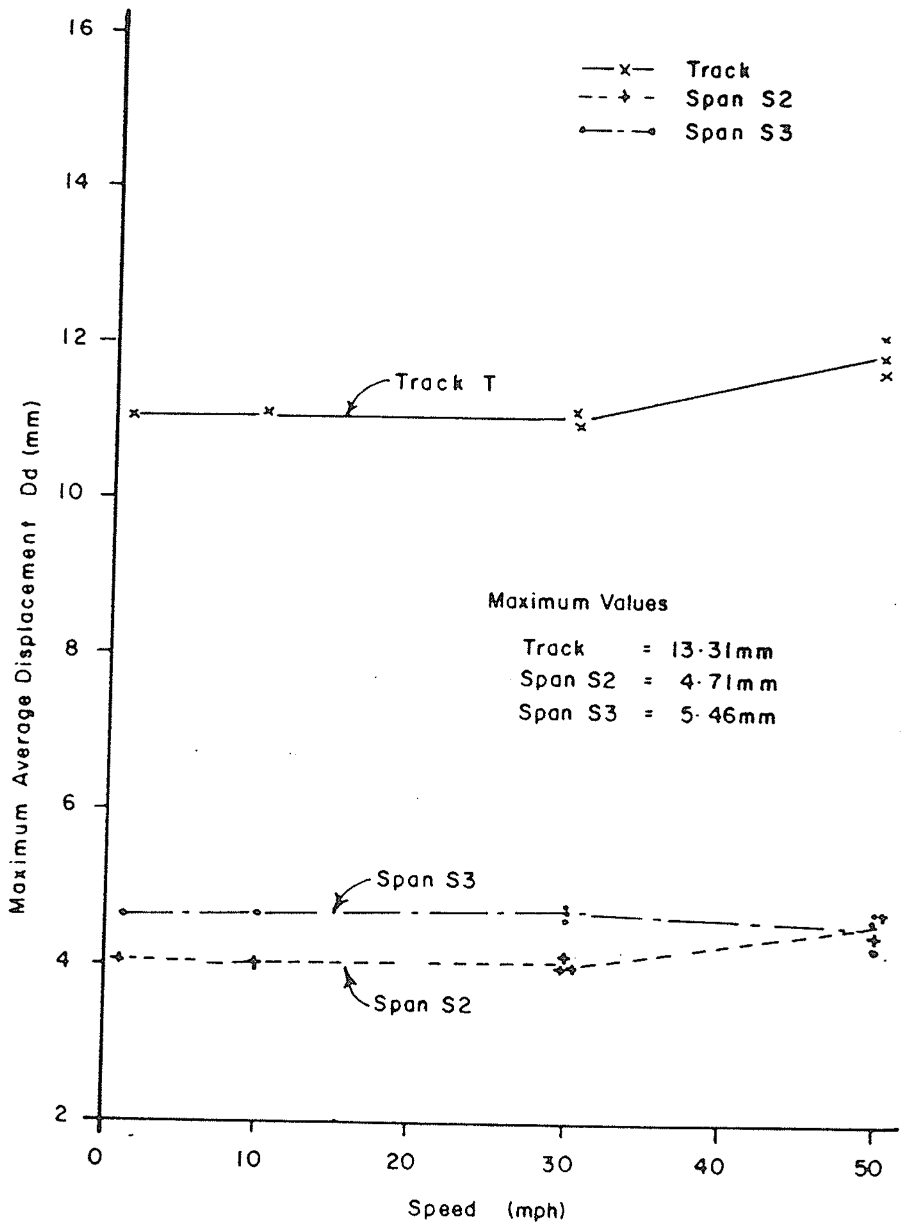

Figure 3.71 Maximum displacement at midpoint of span S3 and span S2 and track section - BDB Site - Test train no. 2

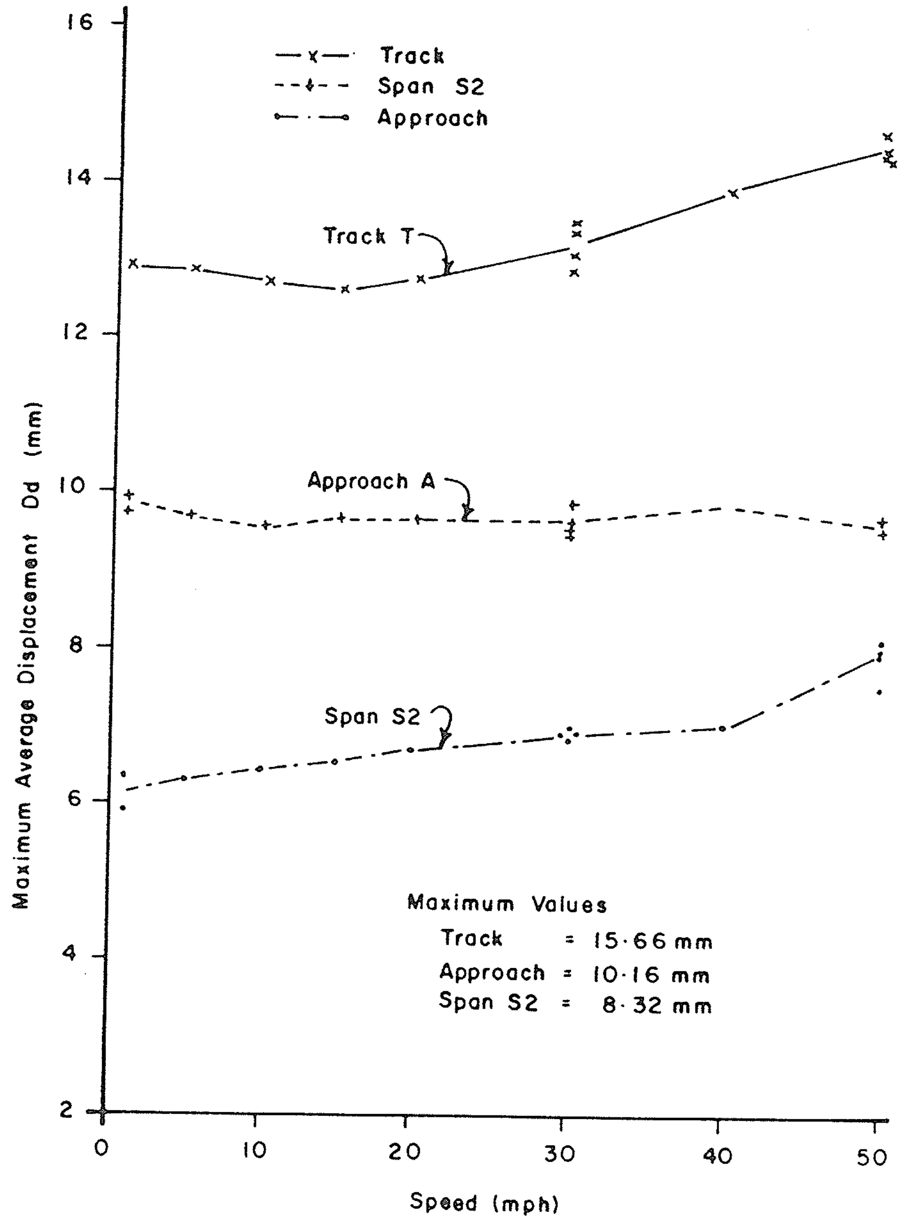

Figure 3.72 Maximum displacements at midpoint of span S2, bridge approach and track section - ODB Site - Test train no. 2

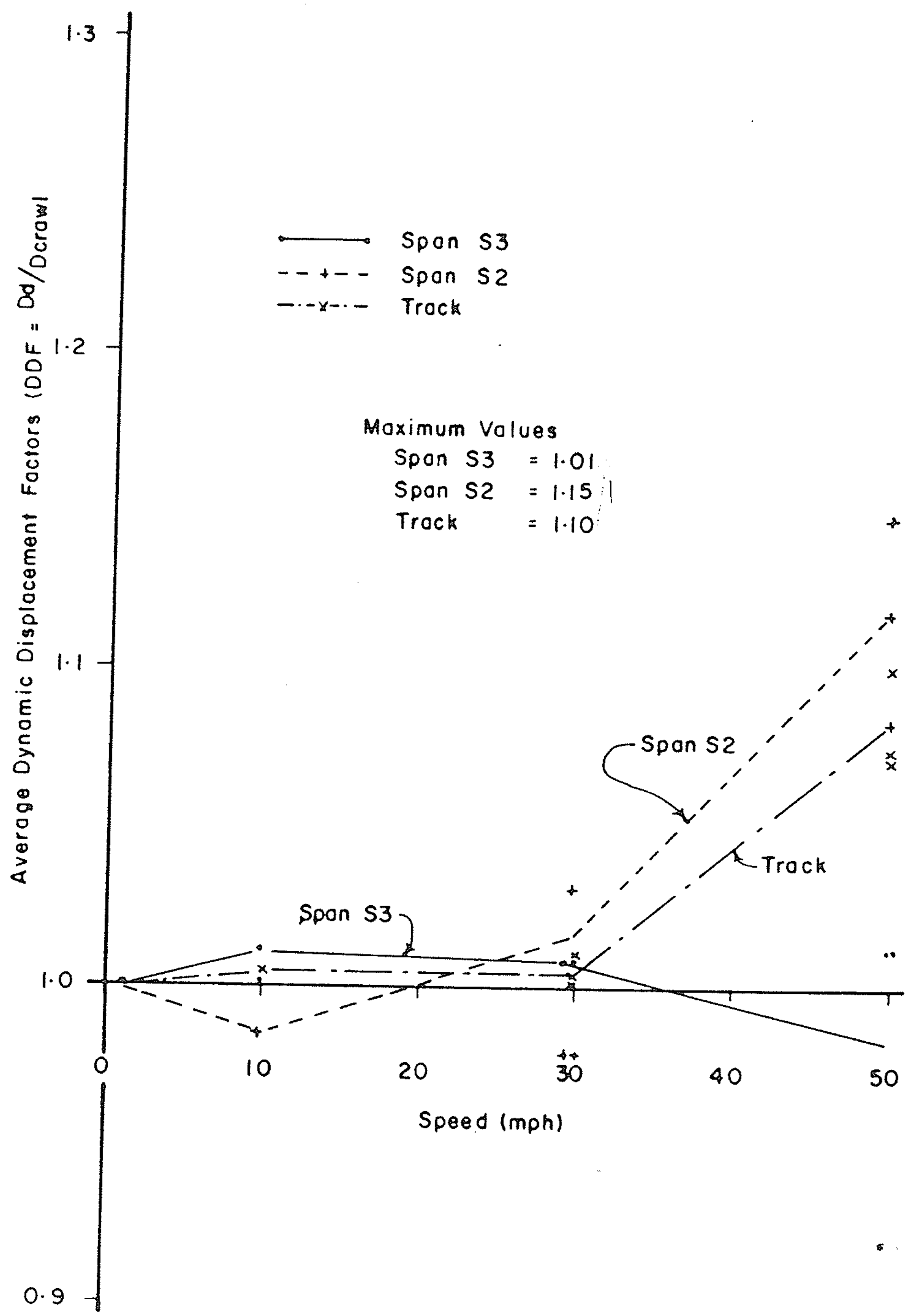

Figure 3.73 Dynamic displacement factors, DDF versus speed
BDB Site - Mid-point of Spans S3, S2, and Track Section

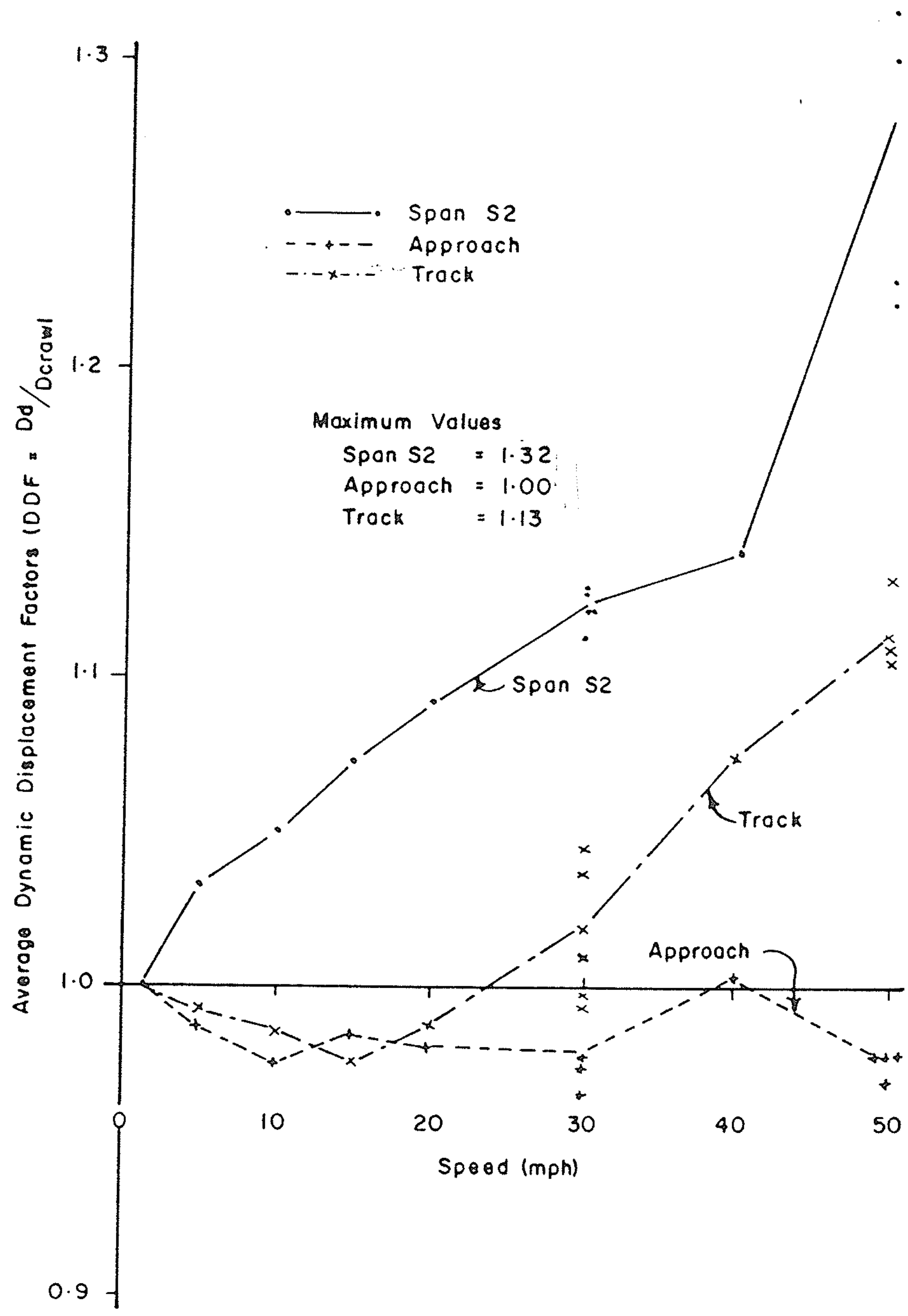

Figure 3.74 Dynamic displacement factors, DDF versus speed
ODB Site - Mid-point of span S2, Bridge approach and track section

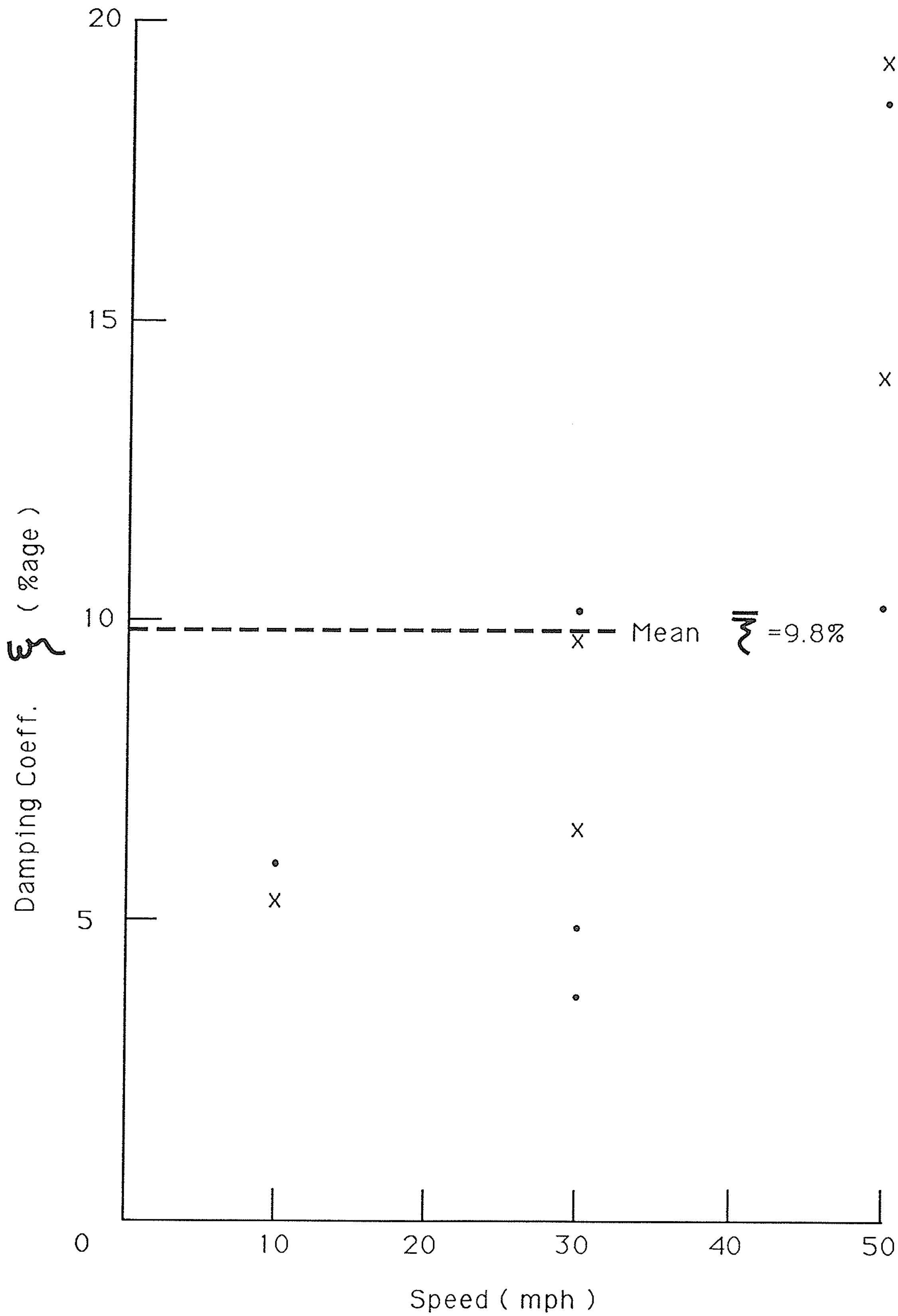

Figure 3.75 Damping coefficient versus train speed - Test train No. 2 - Ballast deck bridge span S3

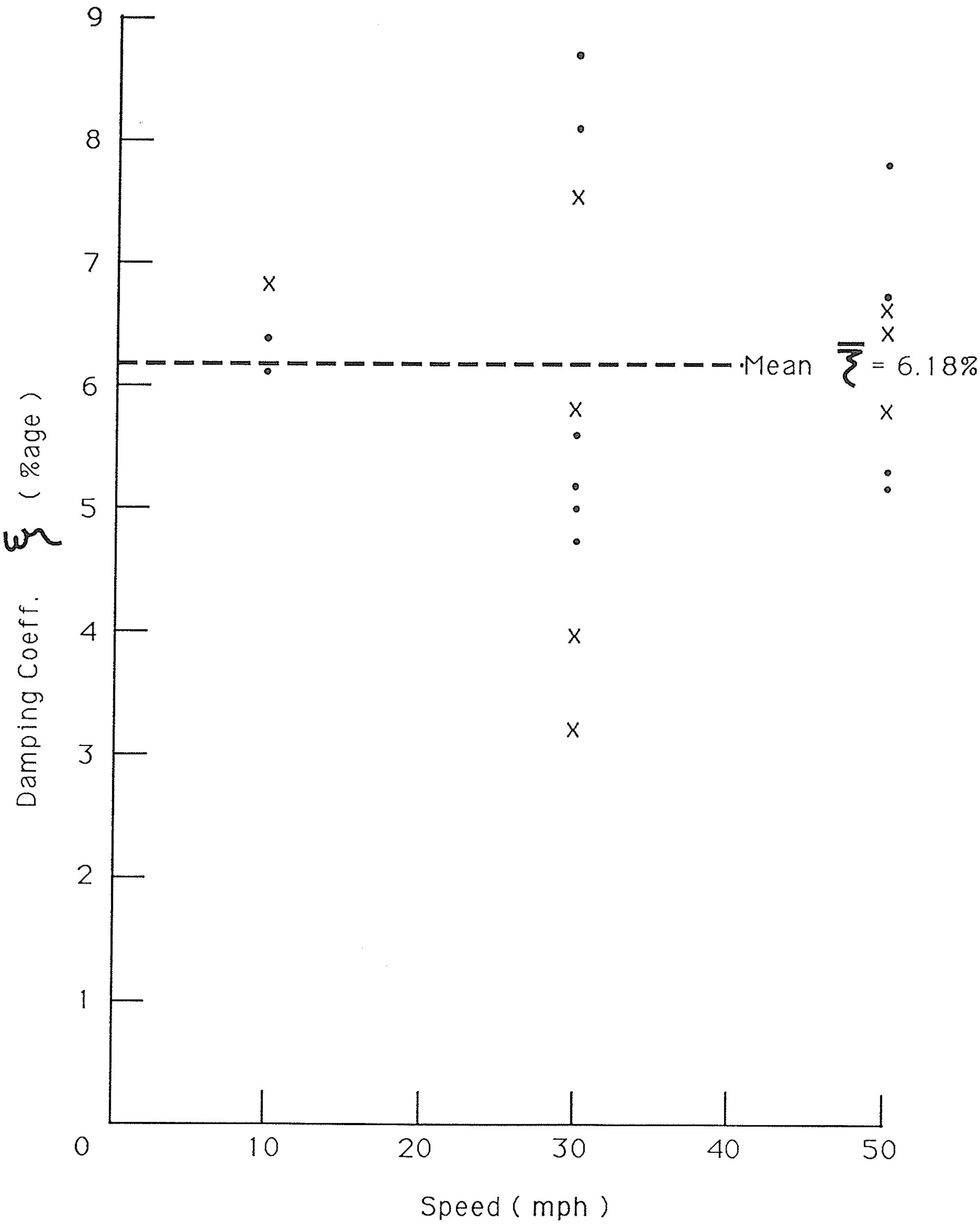

Figure 3.76 Damping coefficient versus train speed - Test train No. 2 - Open deck bridge span S2

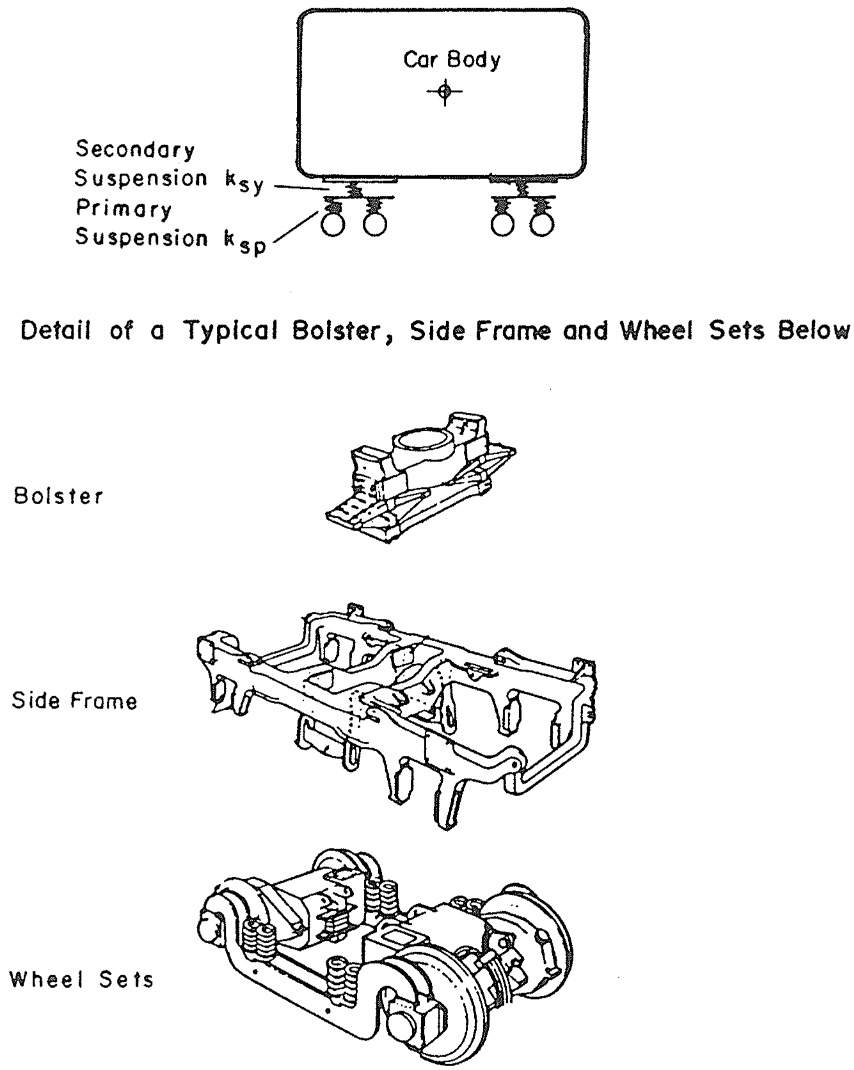

Figure 4.1 Vehicle suspension system

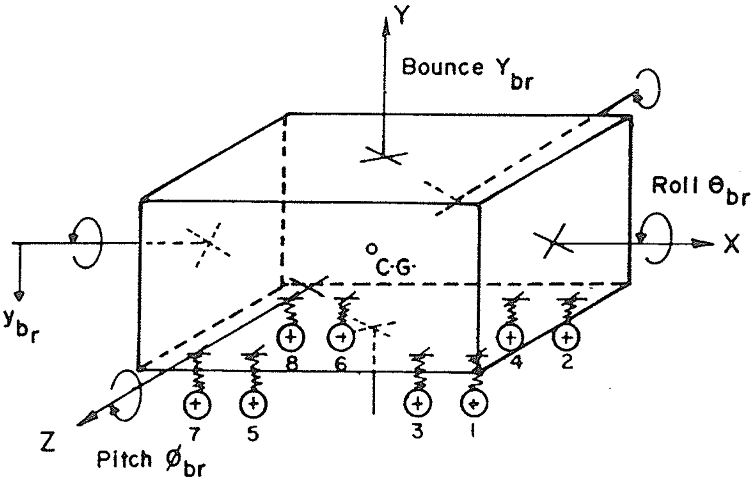

a) Vehicle Body Motions

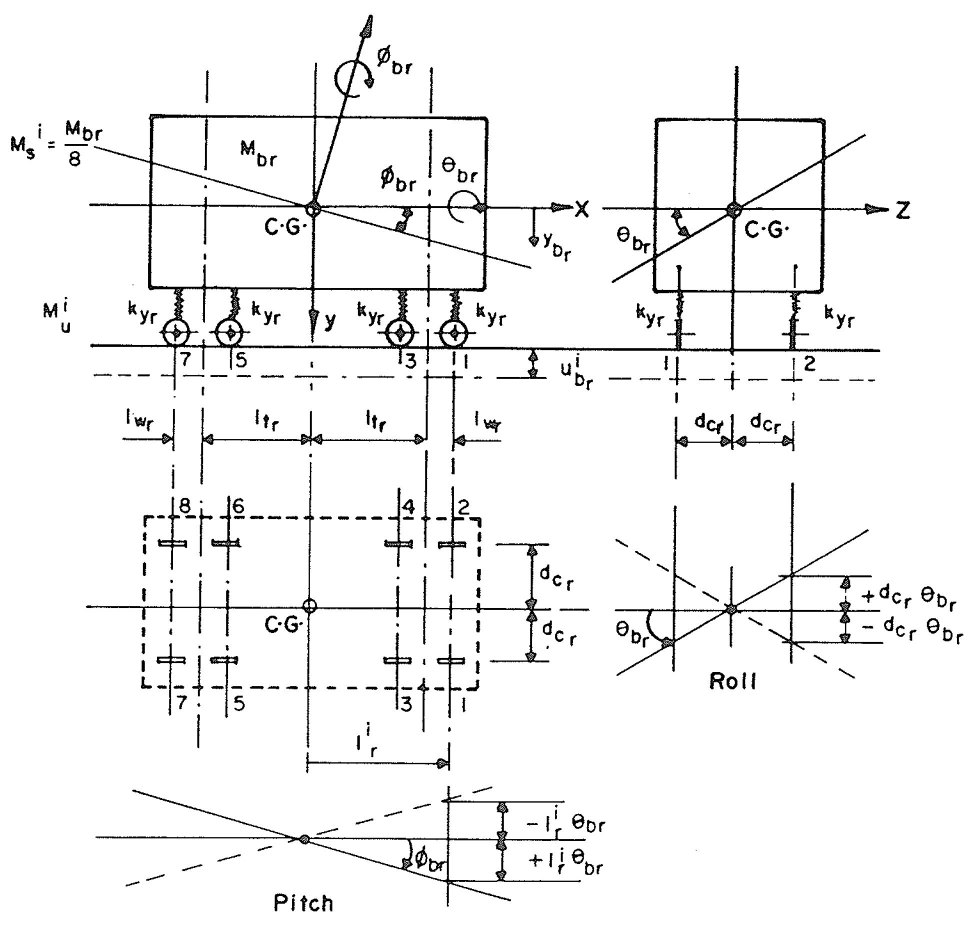

b) Vehicle Model Notation

Figure 4.2 Idealized vehicle model

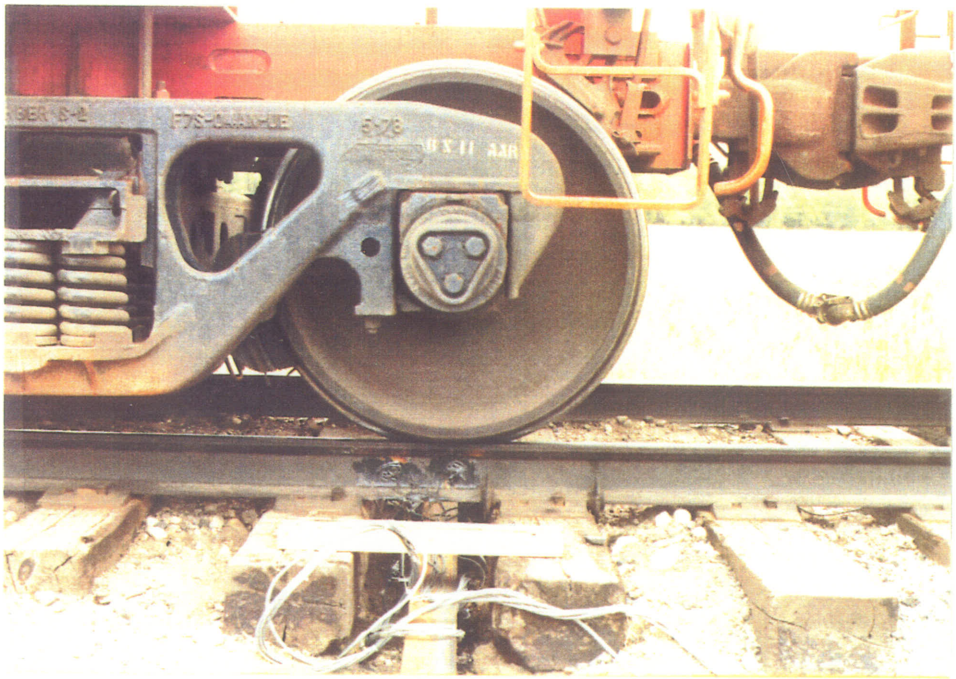

Figure 4.3 Photograph showing wheel-rail contact point

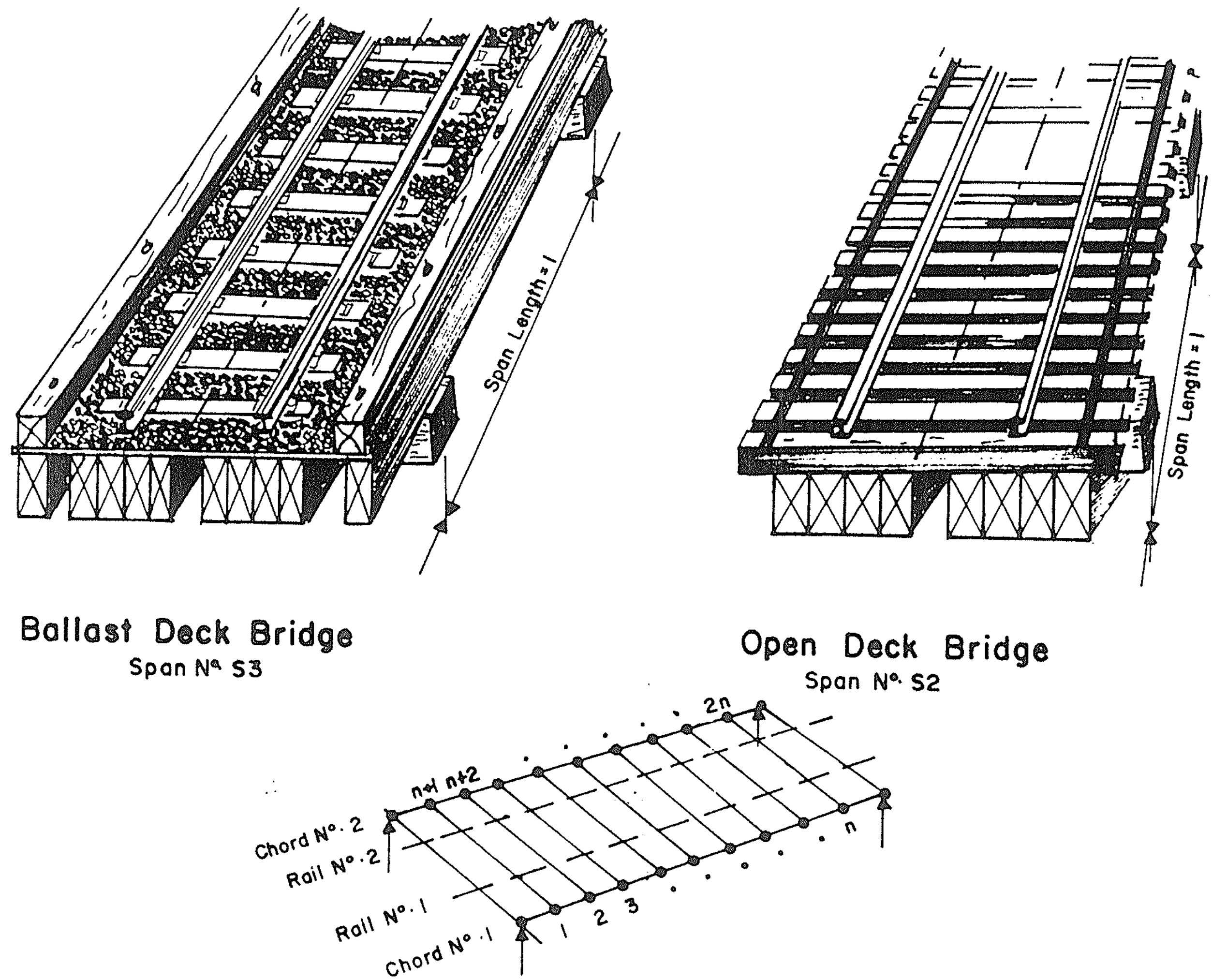

Figure 4.4 Ballast and open deck bridge spans

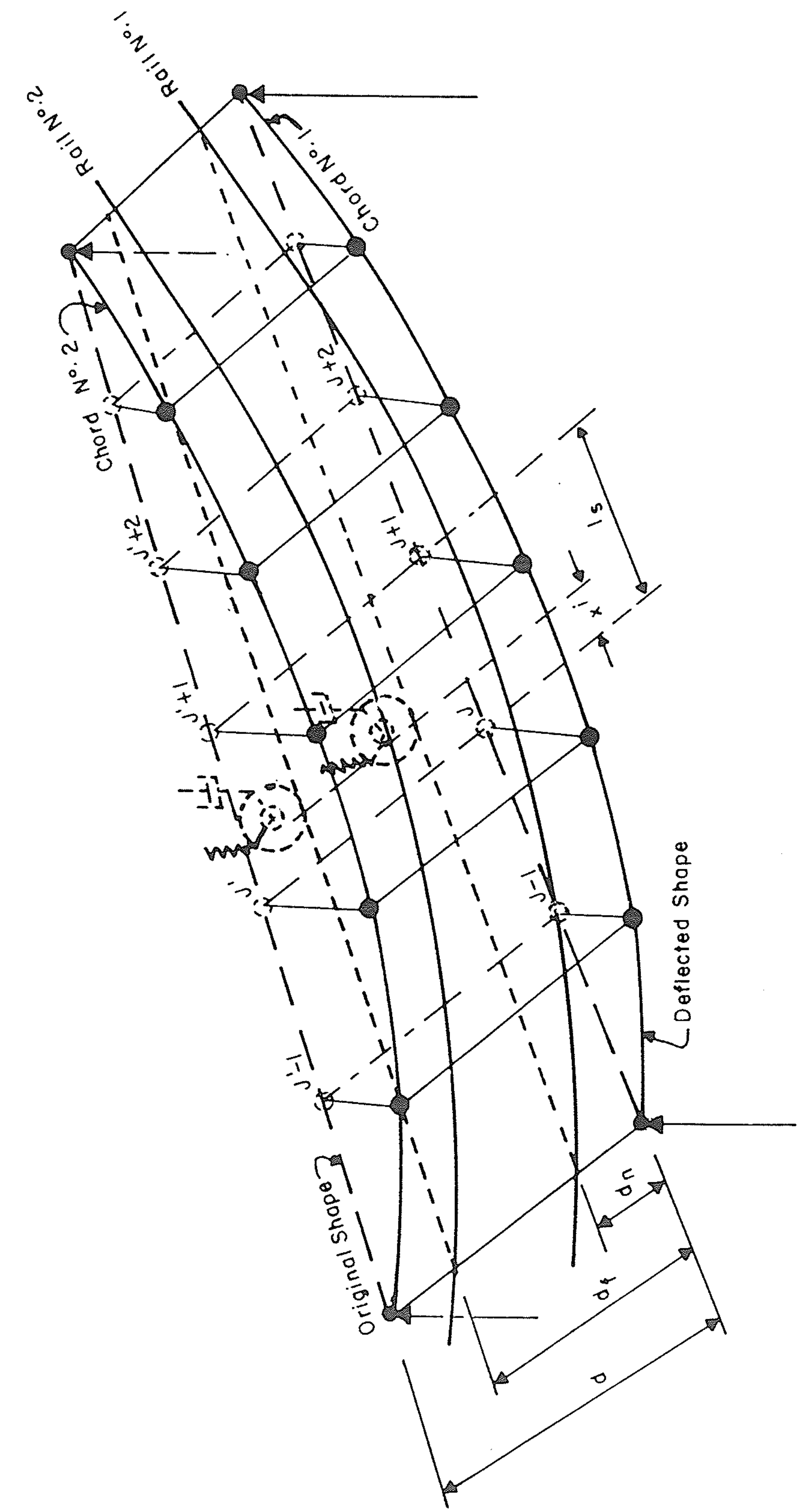

Figure 4.5 Idealized bridge span model

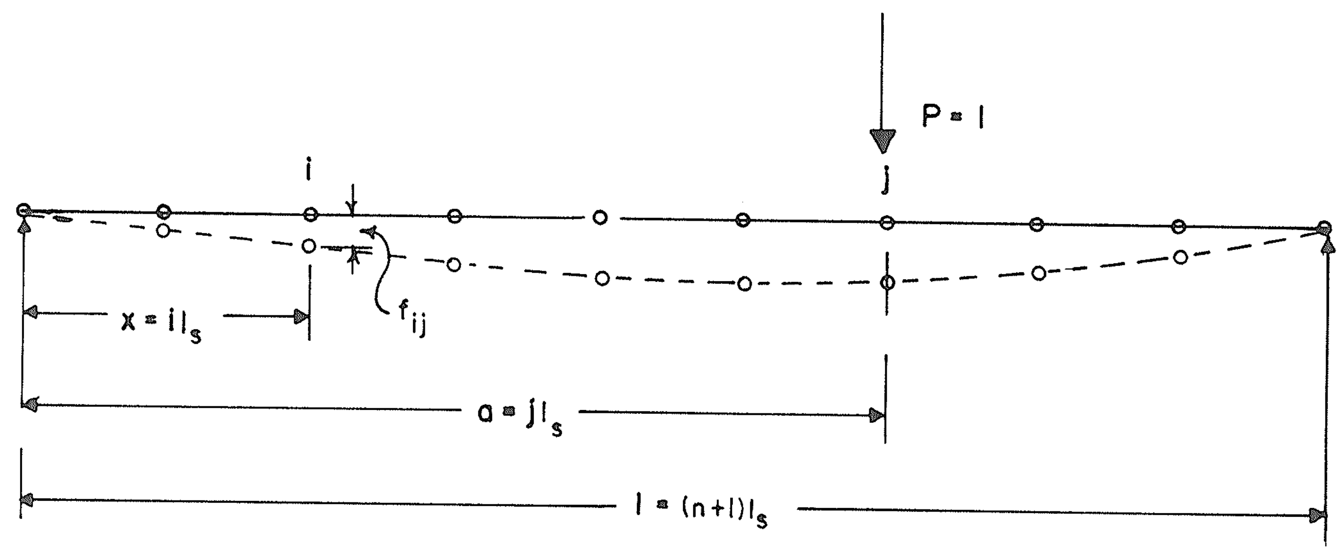

Figure 4.6 Flexibility influence coefficient - simple span

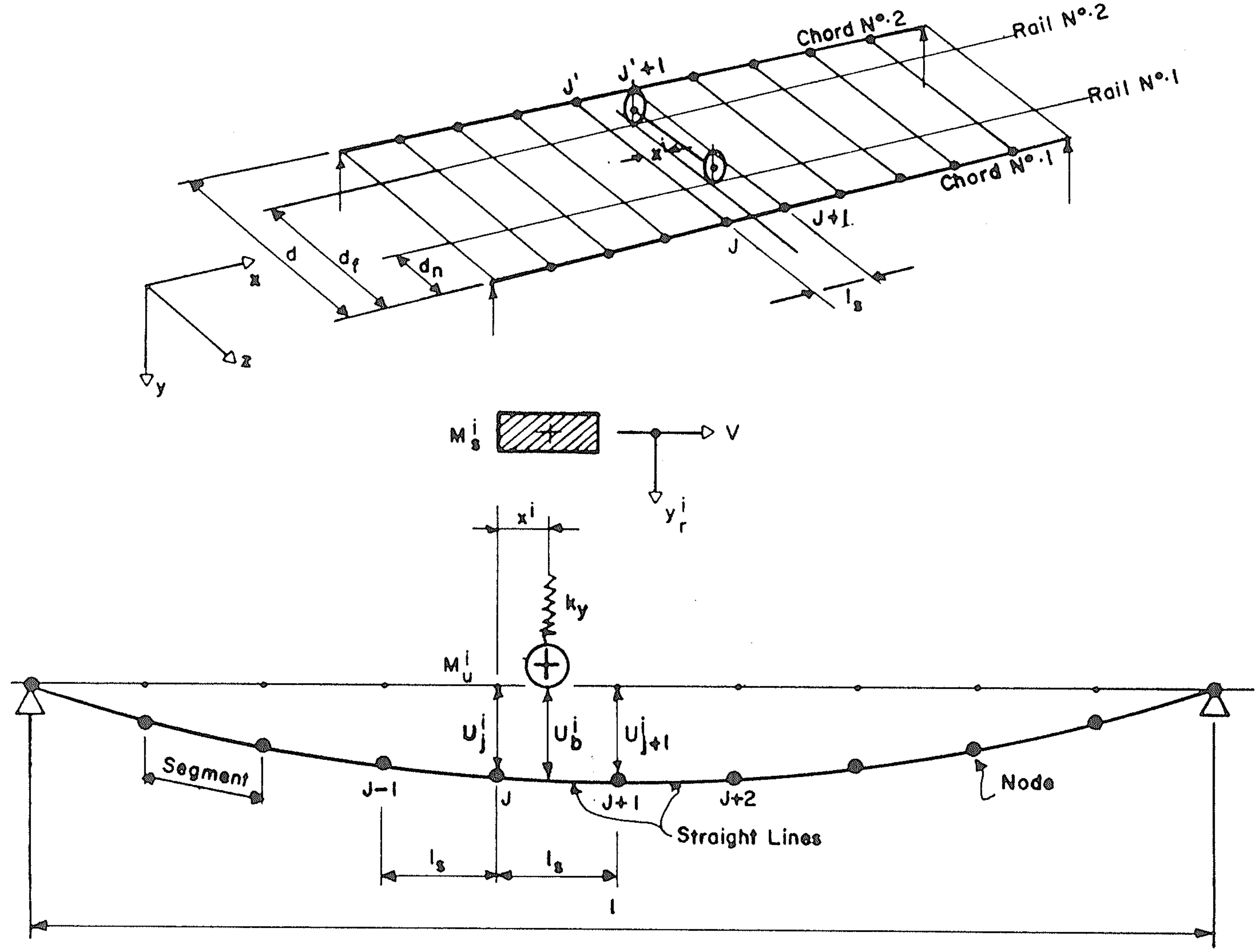

Figure 4.7 Vehicle-Bridge interaction

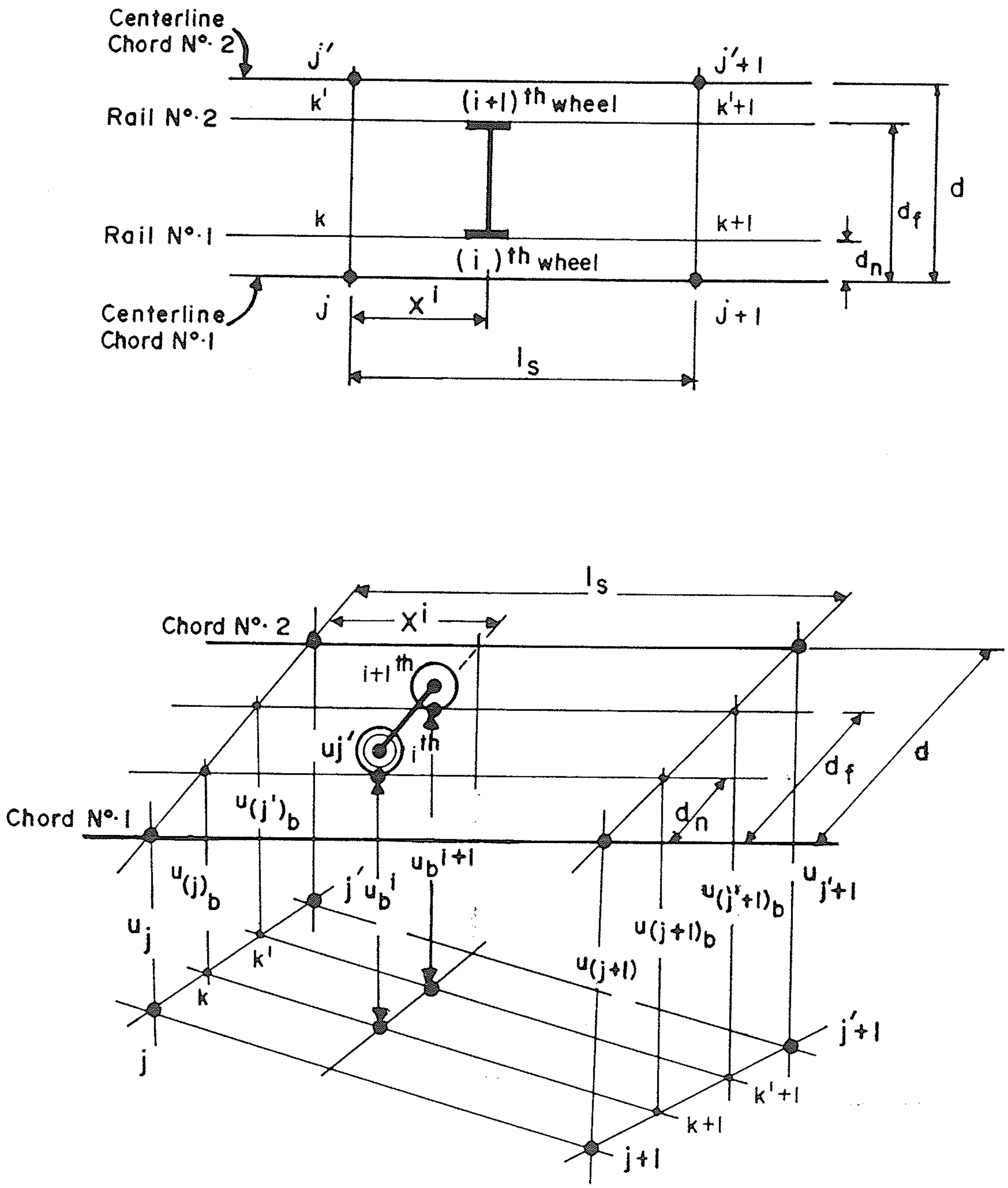

Figure 4.8 Relationship between displacements under i[th] wheel and its neighbouring nodal points j and j+1

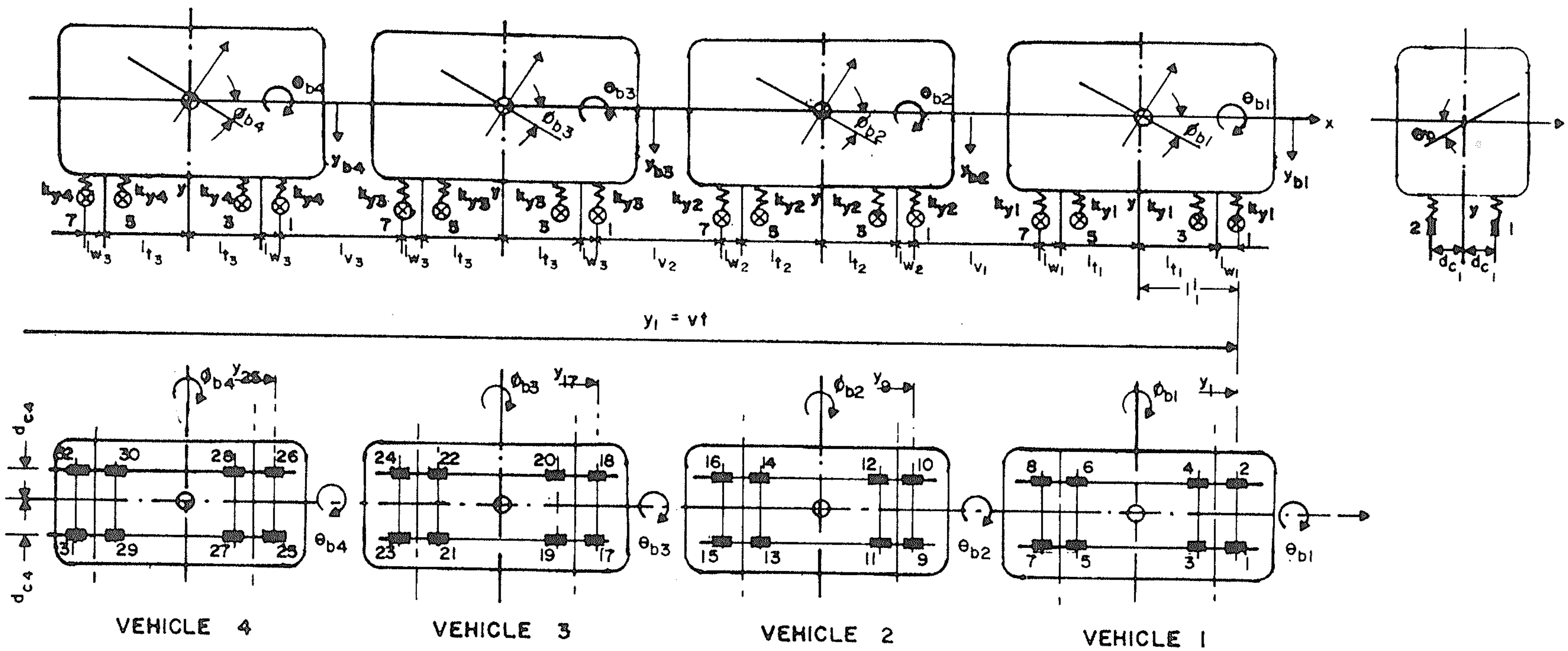

Figure 4.9 Location of wheels on chord segments

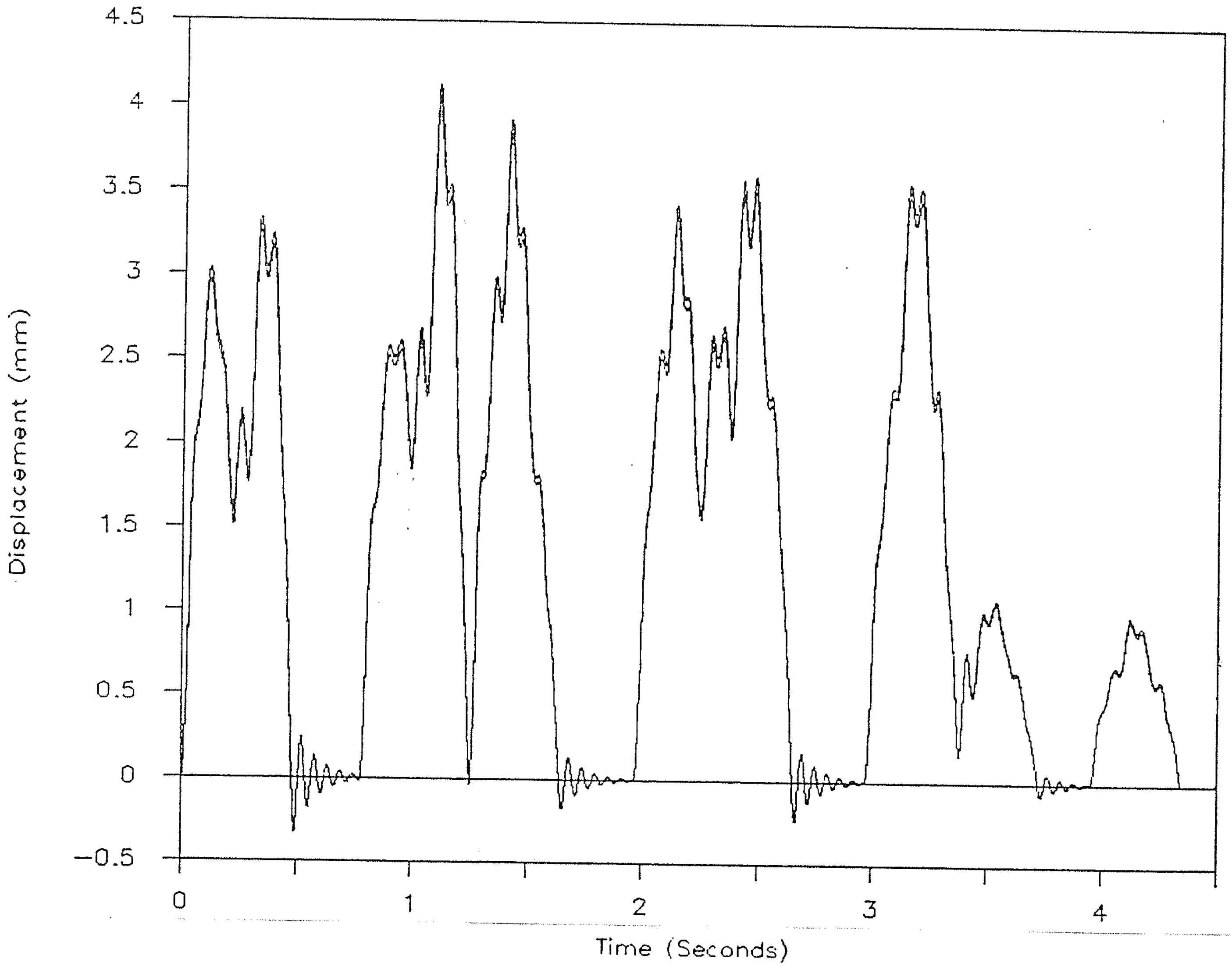

Figure 4.10 Typical predicted vertical displacement versus time
Midpoint of ballast-deck span S3 - Test Train No. 2
Speed 30 mph

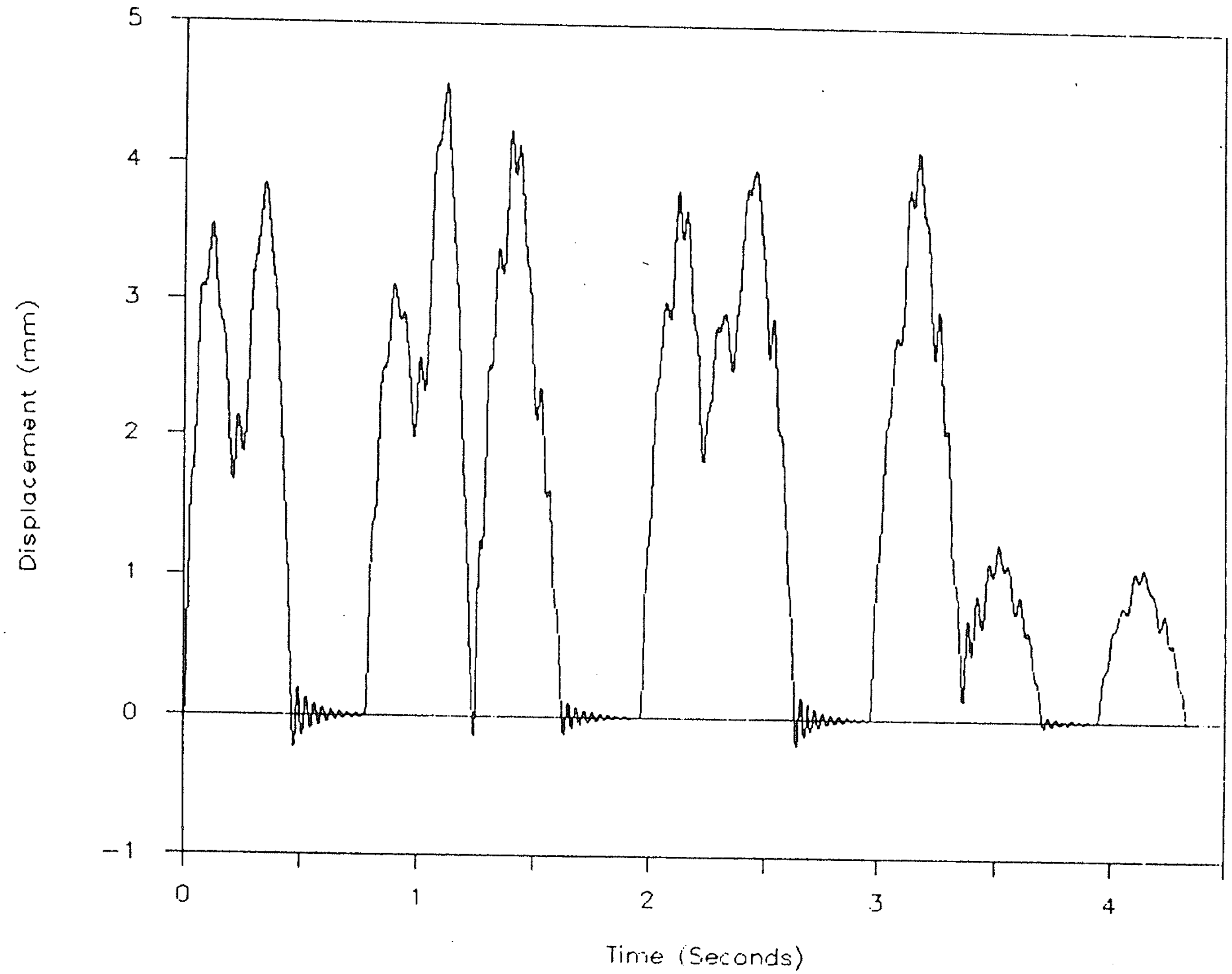

Figure 4.11 Typical predicted vertical displacement versus time
Midpoint of open-deck span S2 - Test Train No. 2
Speed 30 mph

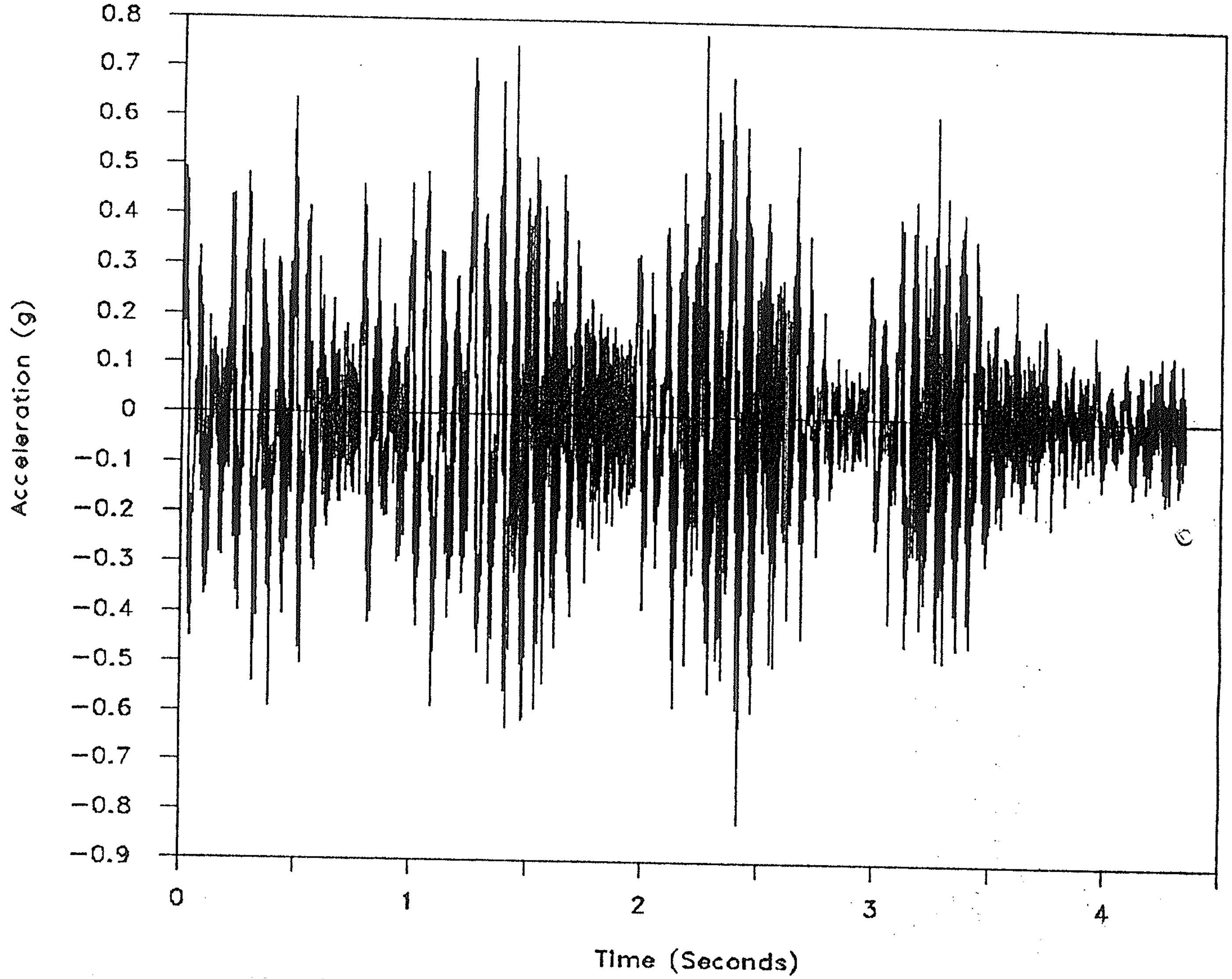

Figure 4.12 Typical predicted acceleration versus time
Midpoint of ballast-deck span S3 - Test Train No. 2
Speed 30 mph

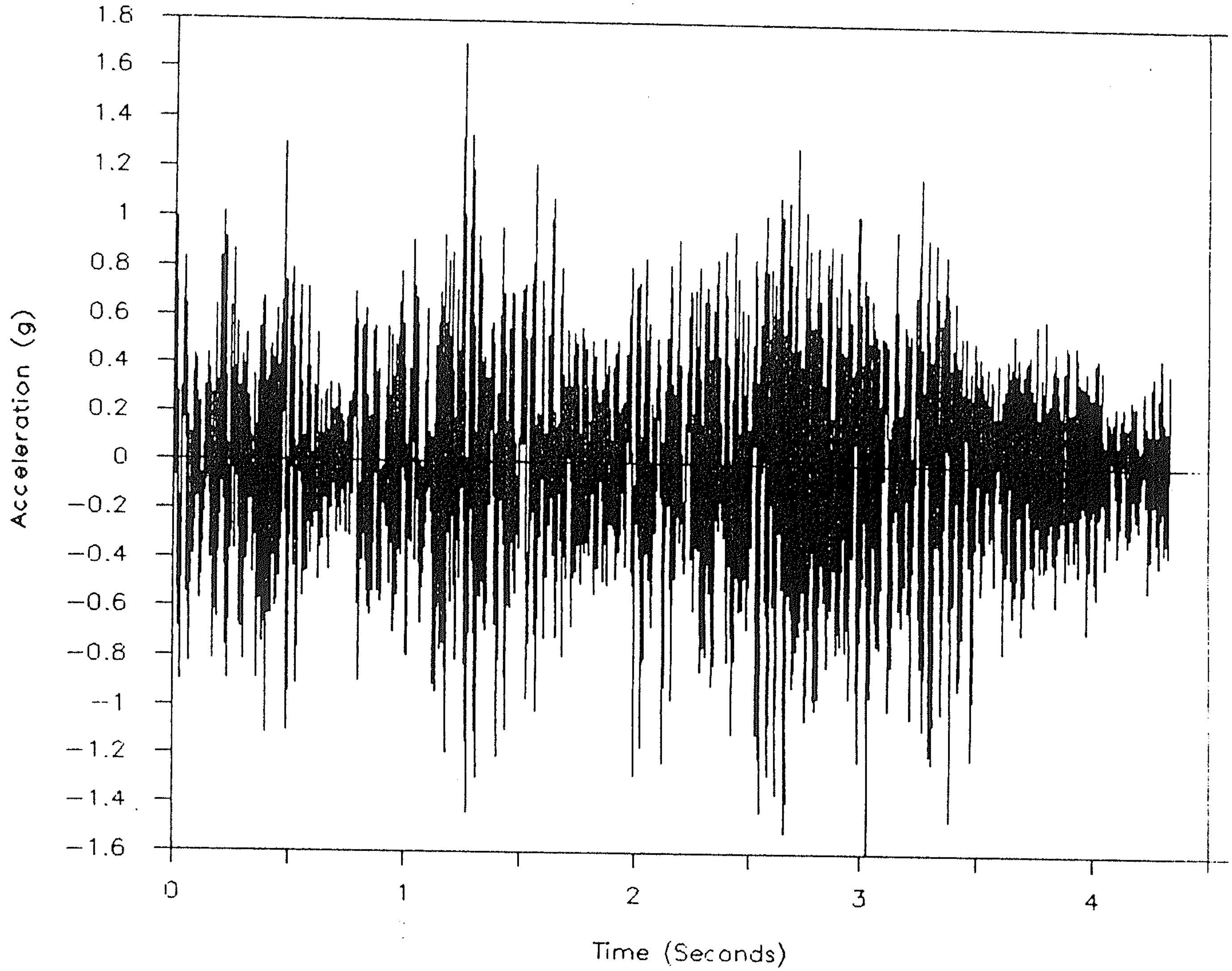

Figure 4.13 Typical predicted acceleration versus time
Midpoint of open-deck span S2 - Test Train No. 2
Speed 30 mph

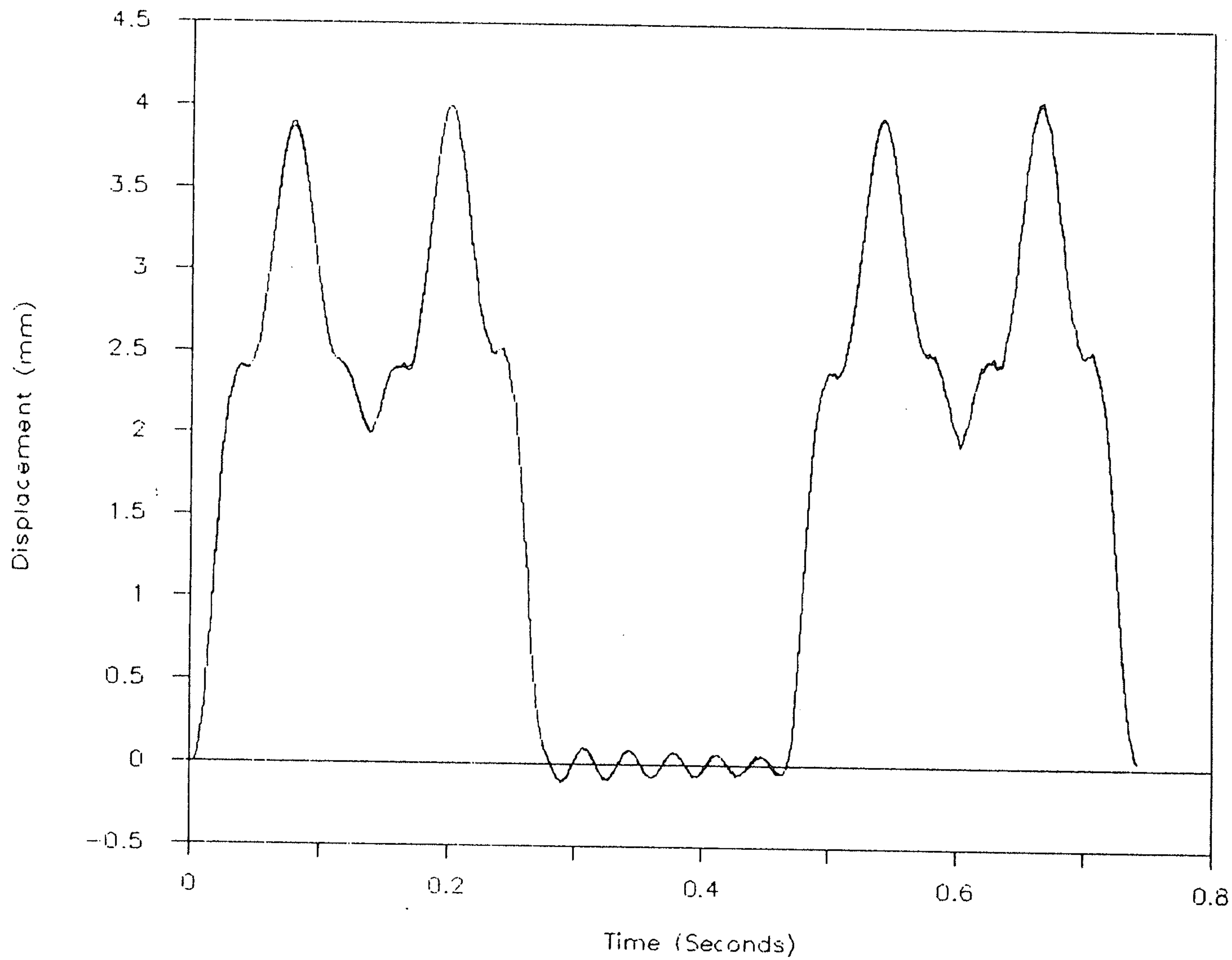

Figure 4.14 Predicted vertical displacement versus time
Midpoint of open-deck span S2 - Locomotive of Test Train No. 2 - Speed 30 mph

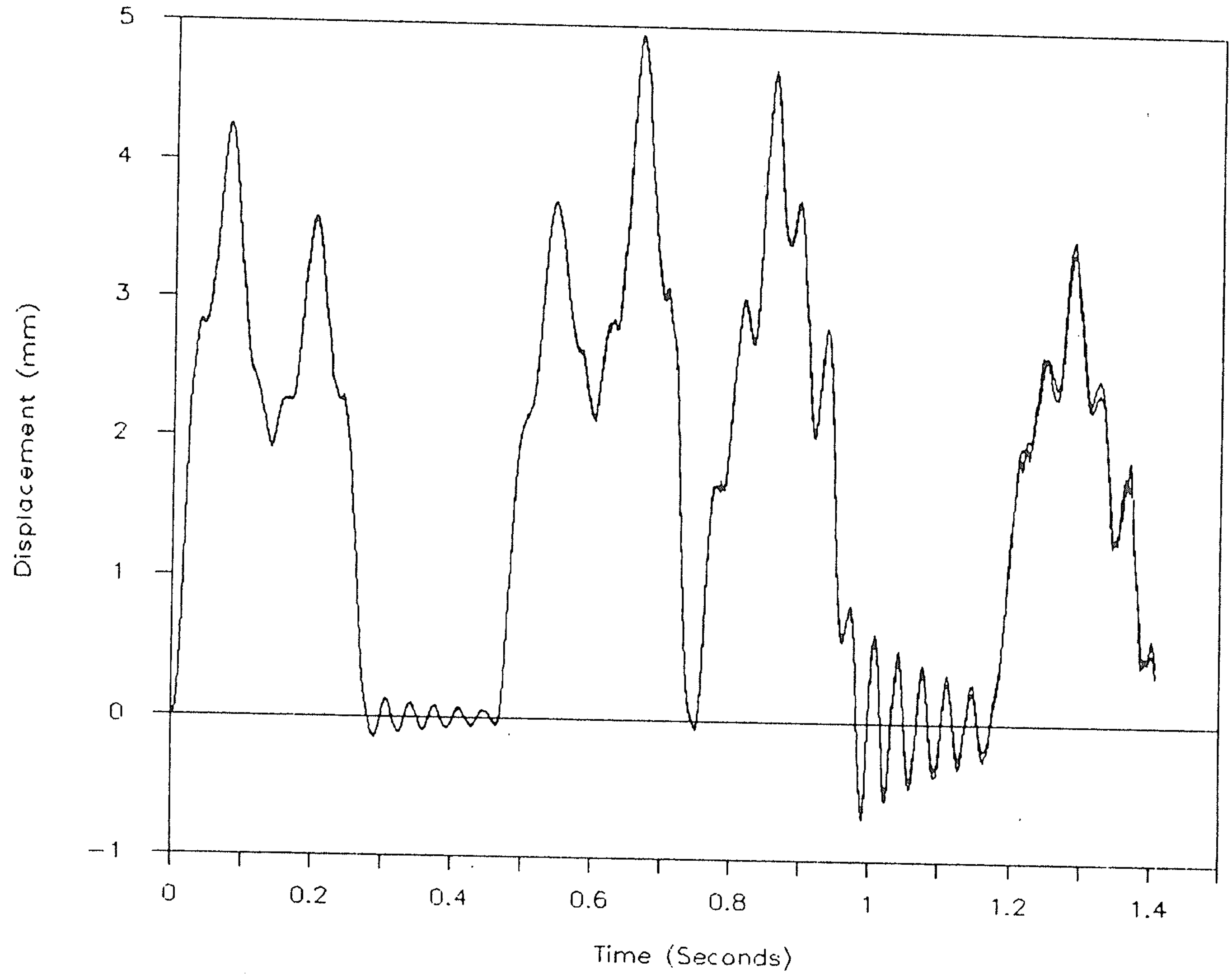

Figure 4.15 Predicted vertical displacement versus time
Midpoint of open-deck span S2 - Locomotive and one car of test train no. 2 - Speed 30 mph

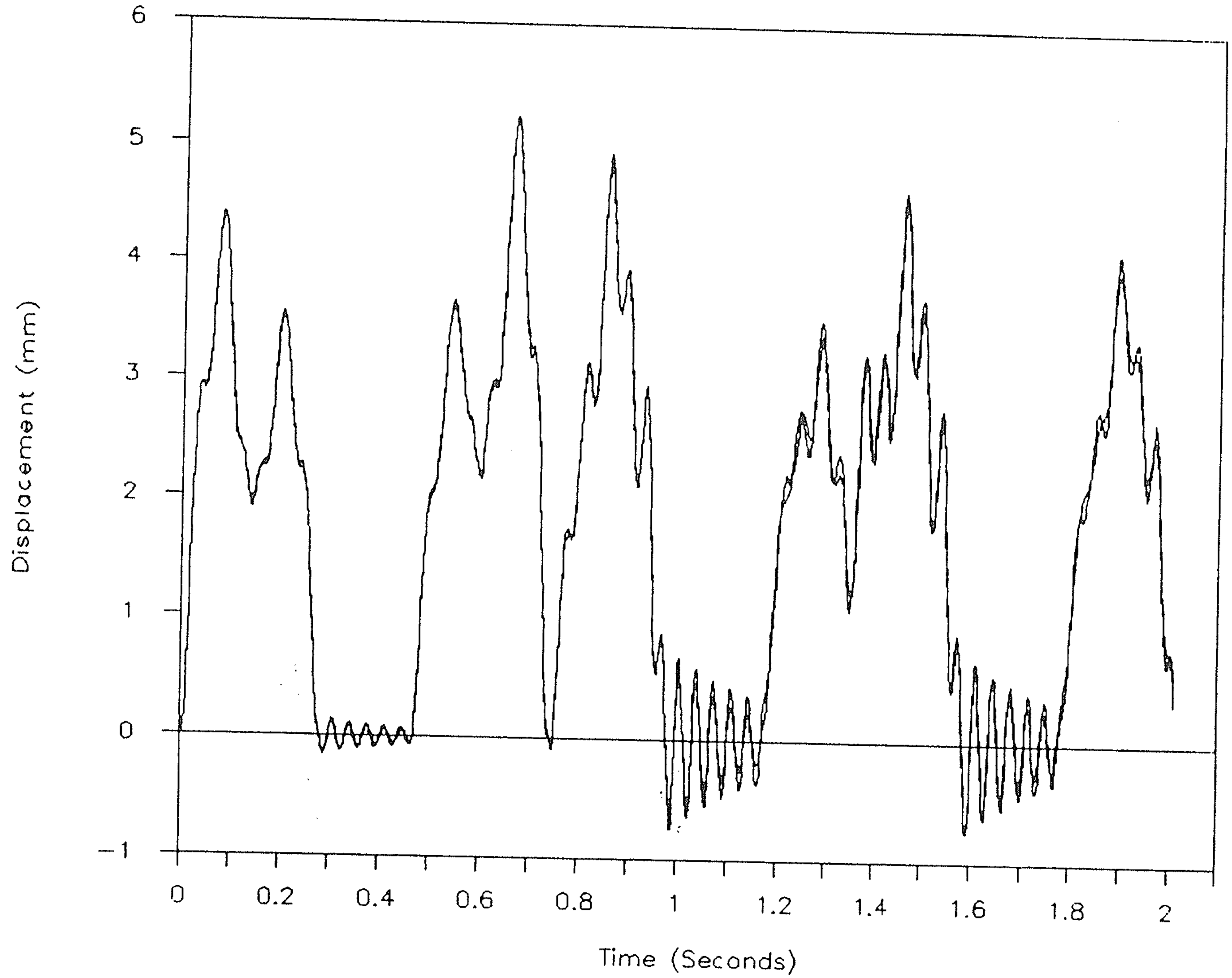

Figure 4.16 Predicted vertical displacement versus time
Midpoint of open-deck span S2 - Locomotive and two cars of test train No. 2 - speed 30 mph

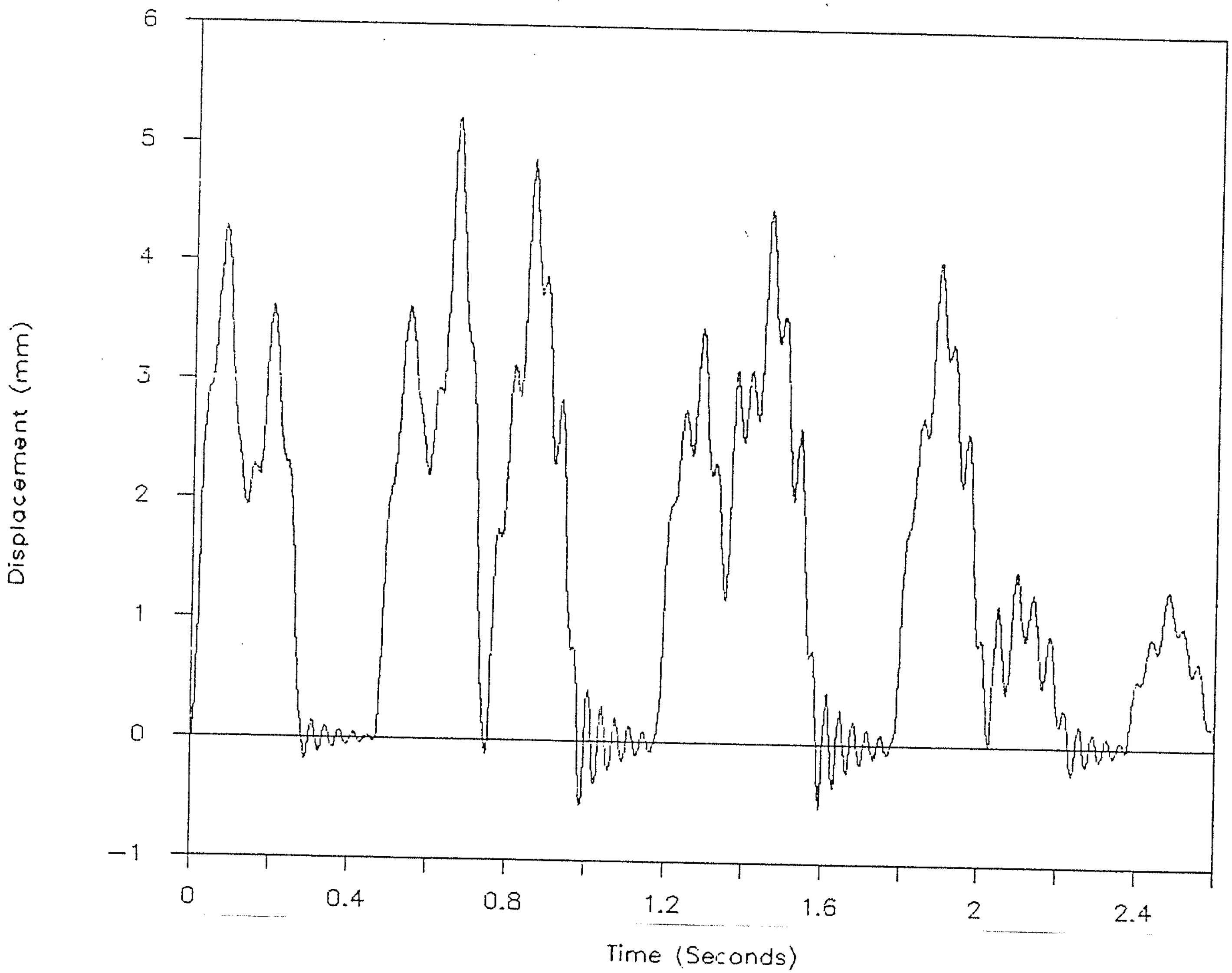

Figure 4.17 Predicted vertical displacement versus time
Midpoint of open-deck span S2 - Test Train No. 2 - Speed 50 mph - no low spot approach

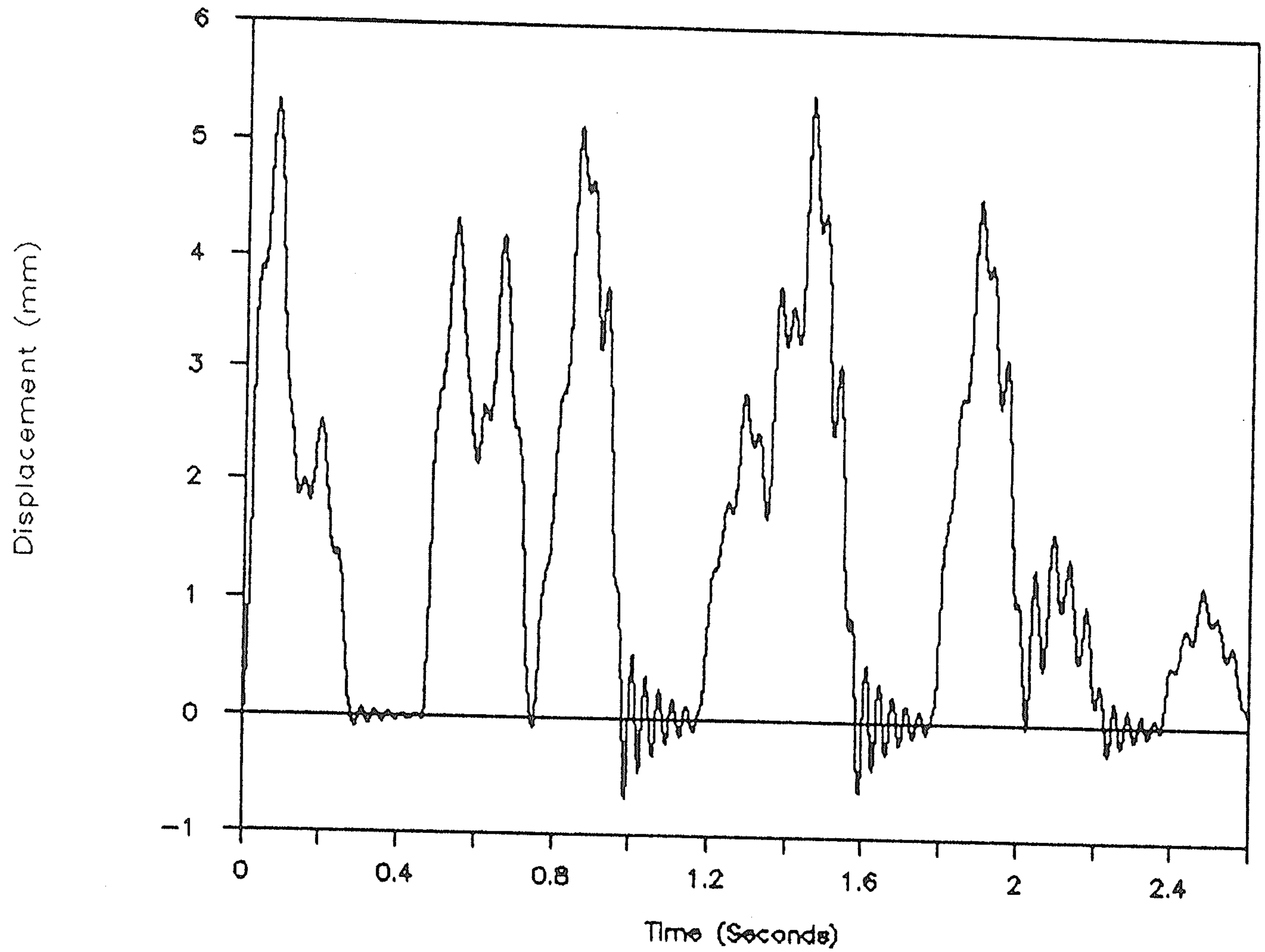

Figure 4.18 Predicted vertical displacement versus time
Midpoint of open-deck span S2 - Test Train No. 2 - Speed 50 mph -
Low spot at approach = 0.5 in

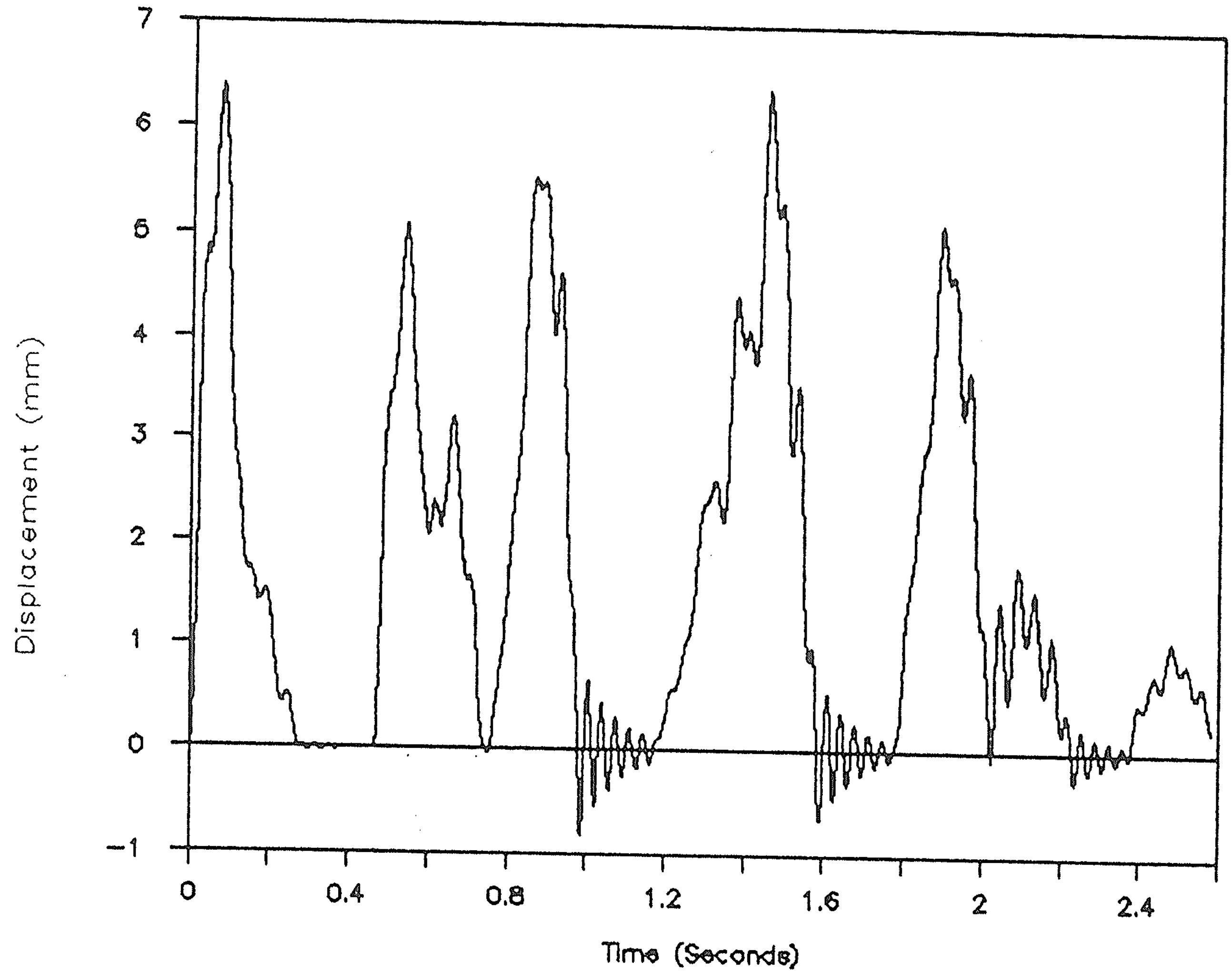

Figure 4.19 Predicted vertical displacement versus time
Midpoint of open-deck span S2 - Test Train No. 2 - Speed 50 mph -
Low spot at approach = 1.0 in

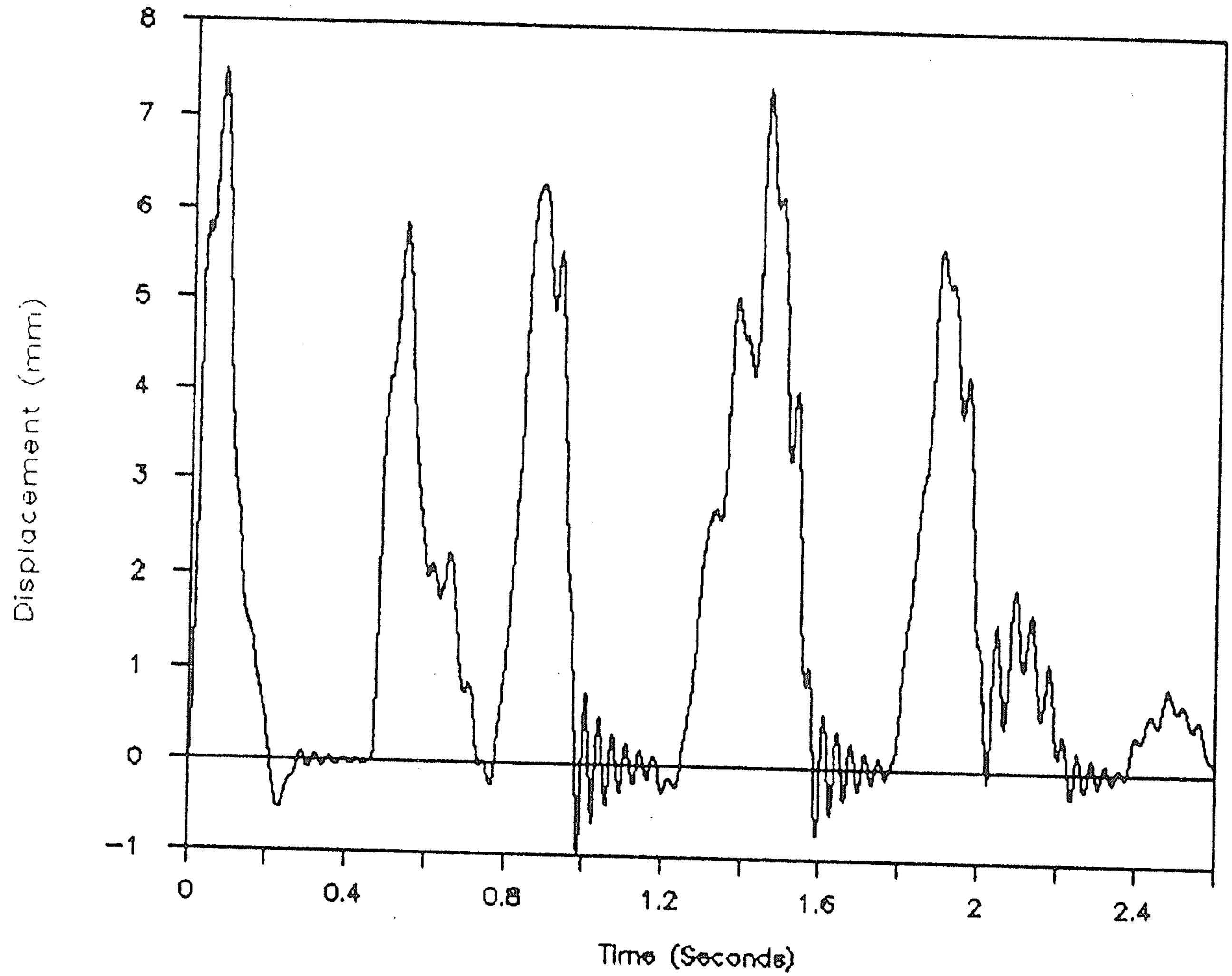

Figure 4.20 Predicted vertical displacement versus time
Midpoint of open-deck span S2 - Test train No. 2 - speed 50 mph - Low spot at approach = 1.5 in

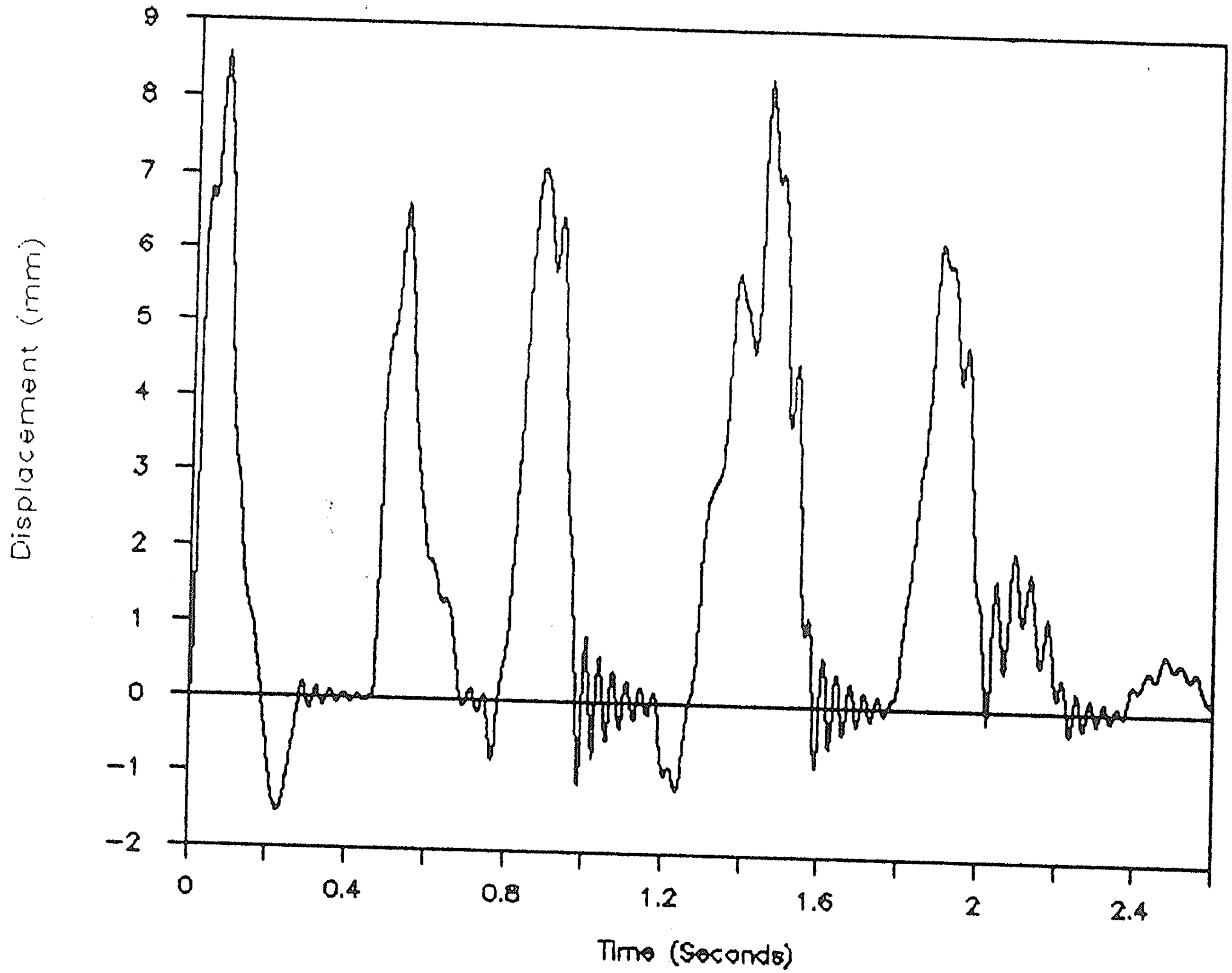

Figure 4.21 Predicted vertical displacement versus time
Midpoint of open deck span S2 - Test Train No. 2 - speed 50 mph - Low spot at approach = 2.0 in

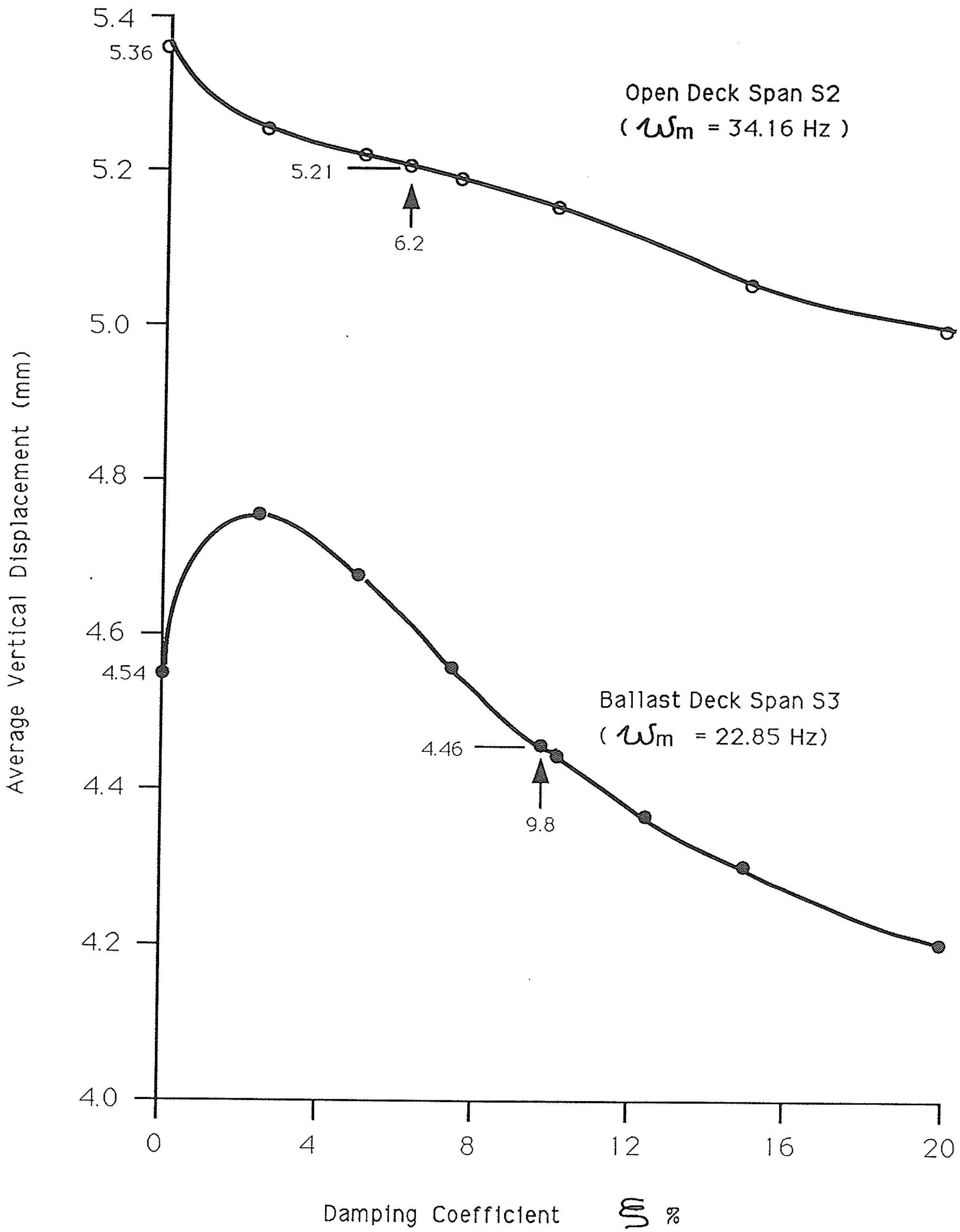

Fig. 4.22 Effect of Damping Coefficient on Predicted Vertical Displacement
Test Train No.2 - Speed 50 mph

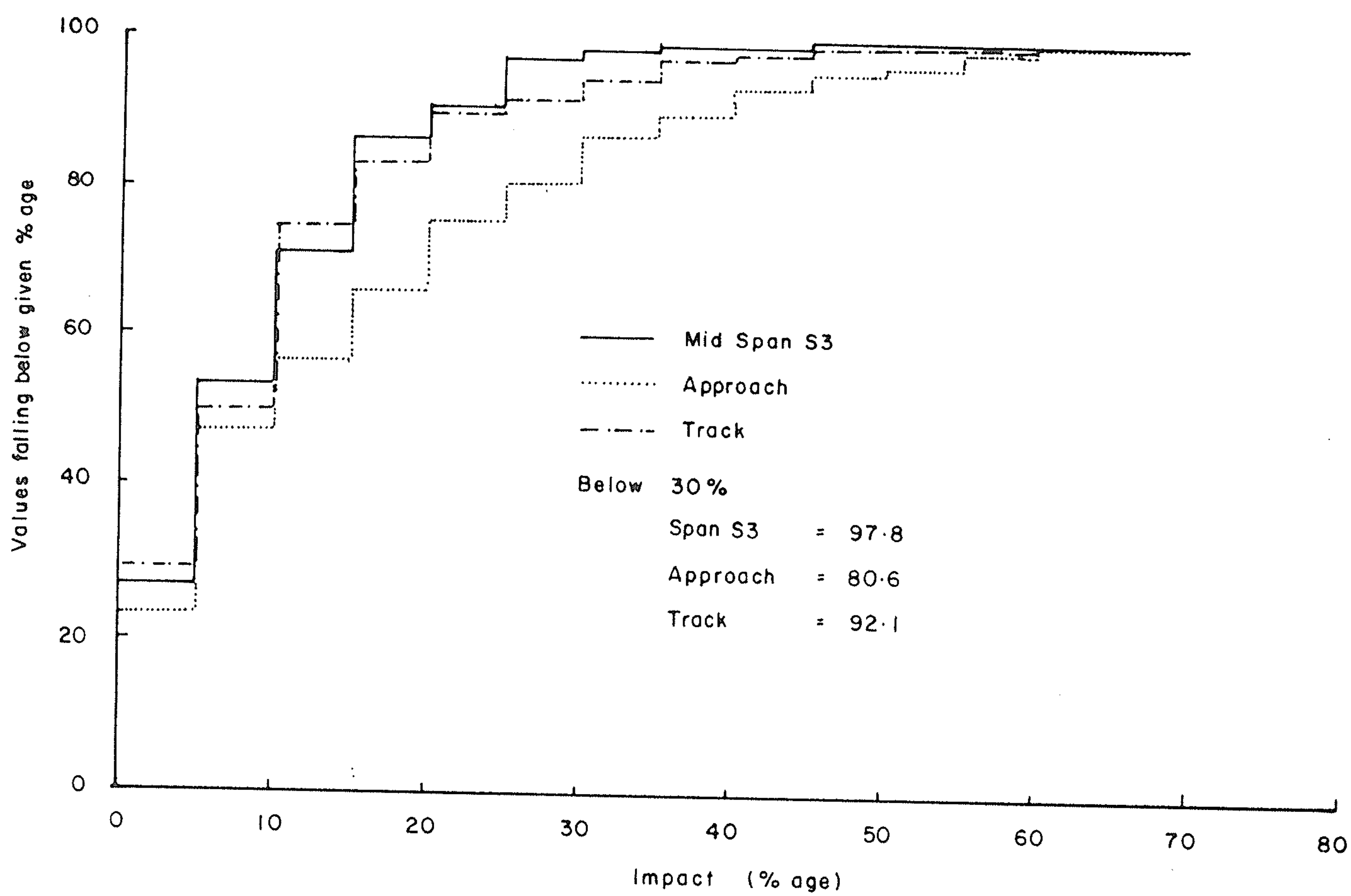

Figure 5.1 Percentage of DLF values falling below given percent of impact - bridge span S3, bridge approach and track section, BDB Site

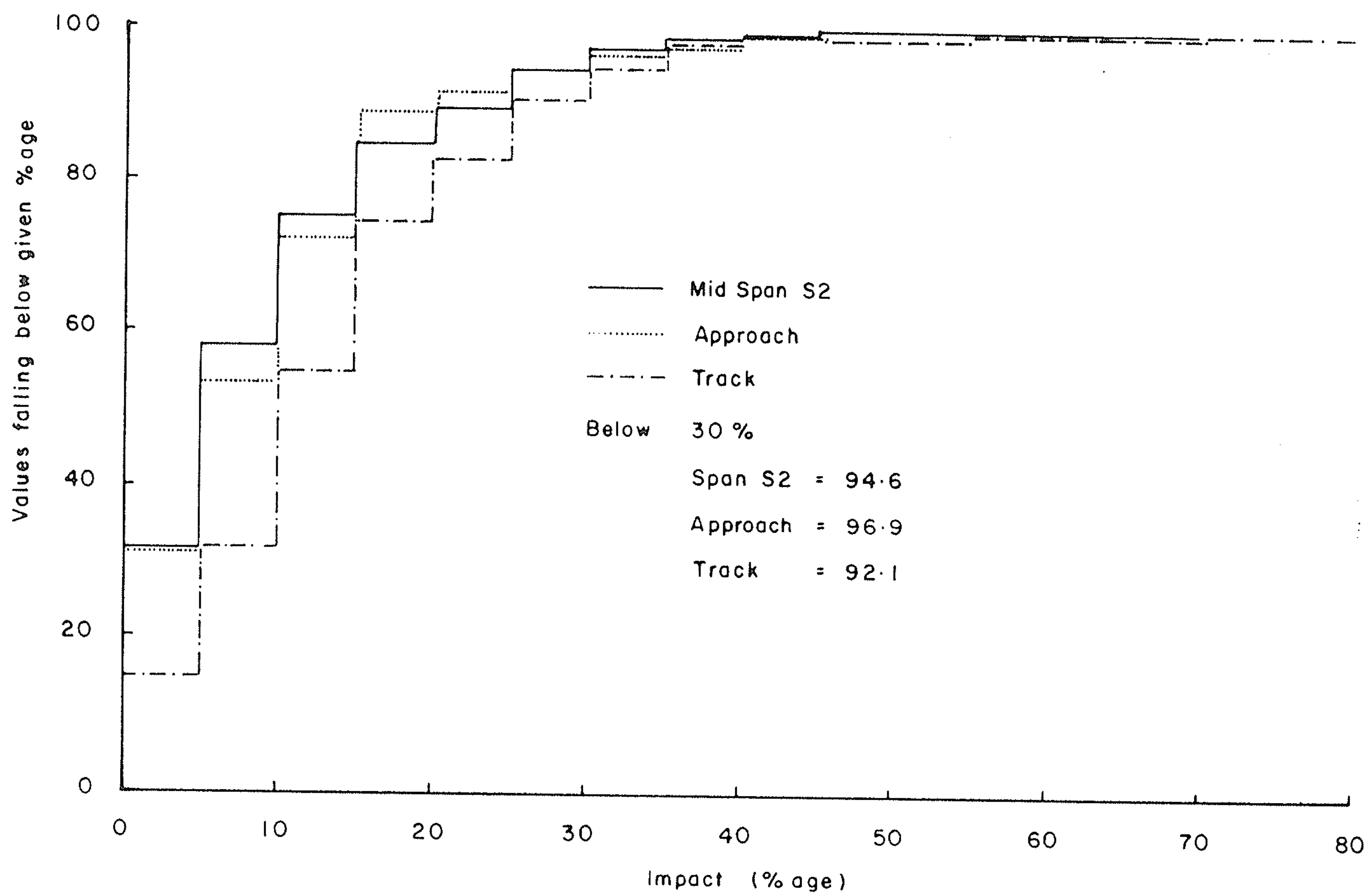

Figure 5.2 Percentage of DLF values falling below given percent of impact - bridge span S2, bridge approach and track section, ODB Site

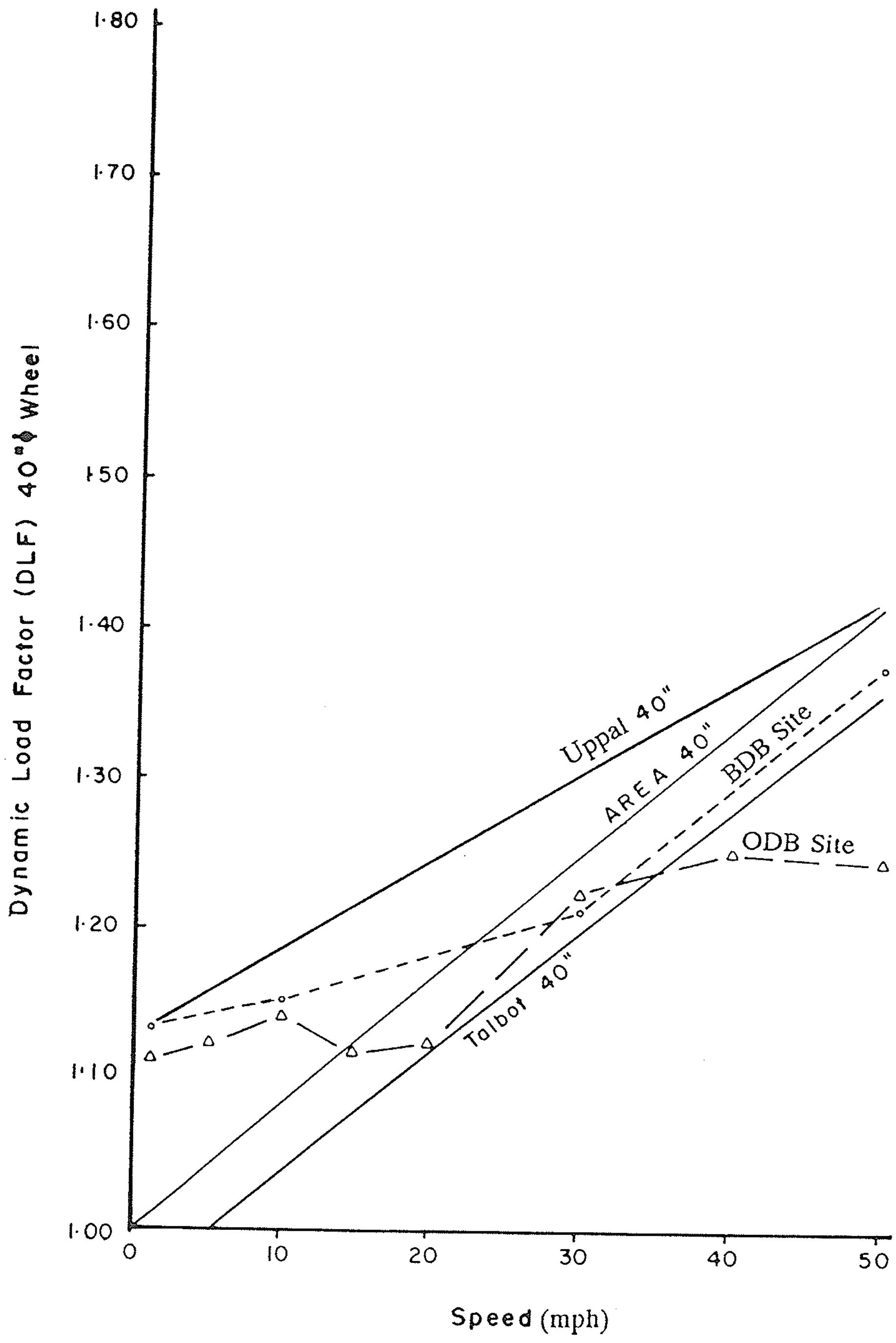

Figure 5.3 Comparison of theoretical with measured dynamic load factors, DLF - 40" dia. wheels

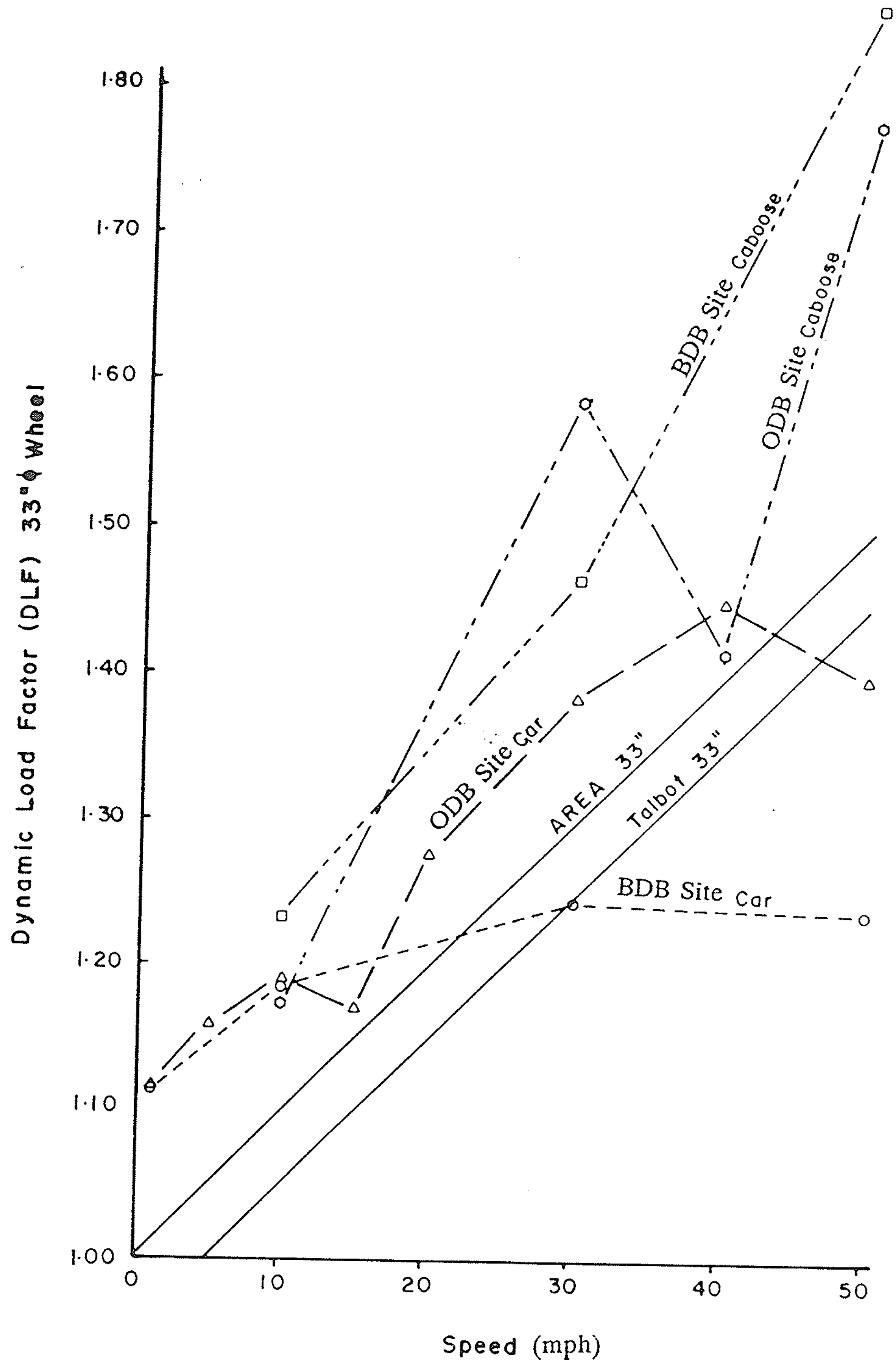

Figure 5.4 Comparison of theoretical with measured dynamic load factors, DLF - 33" dia. wheels

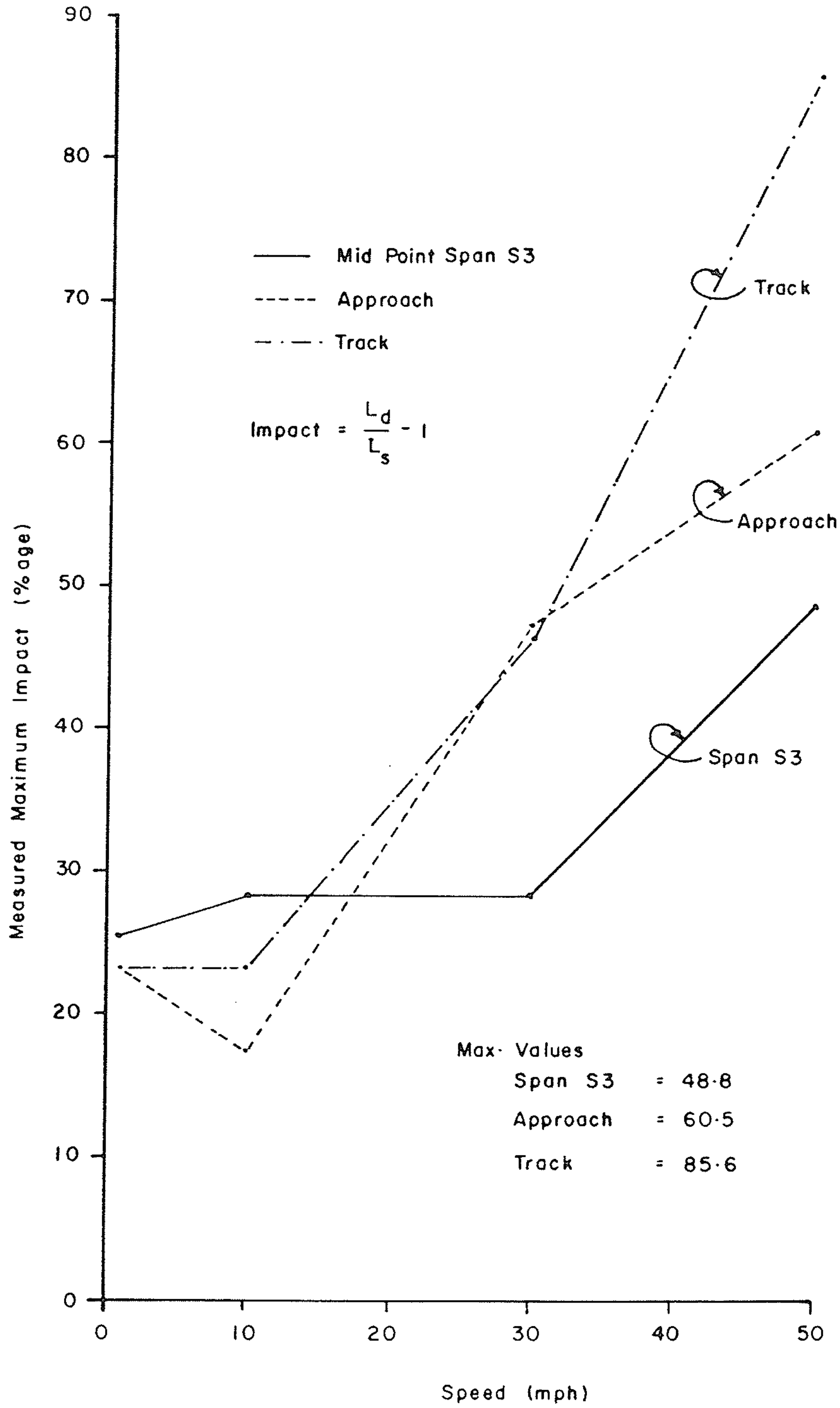

Figure 5.5 Measured maximum impact versus speed
Test train no. 2 - BDB Site

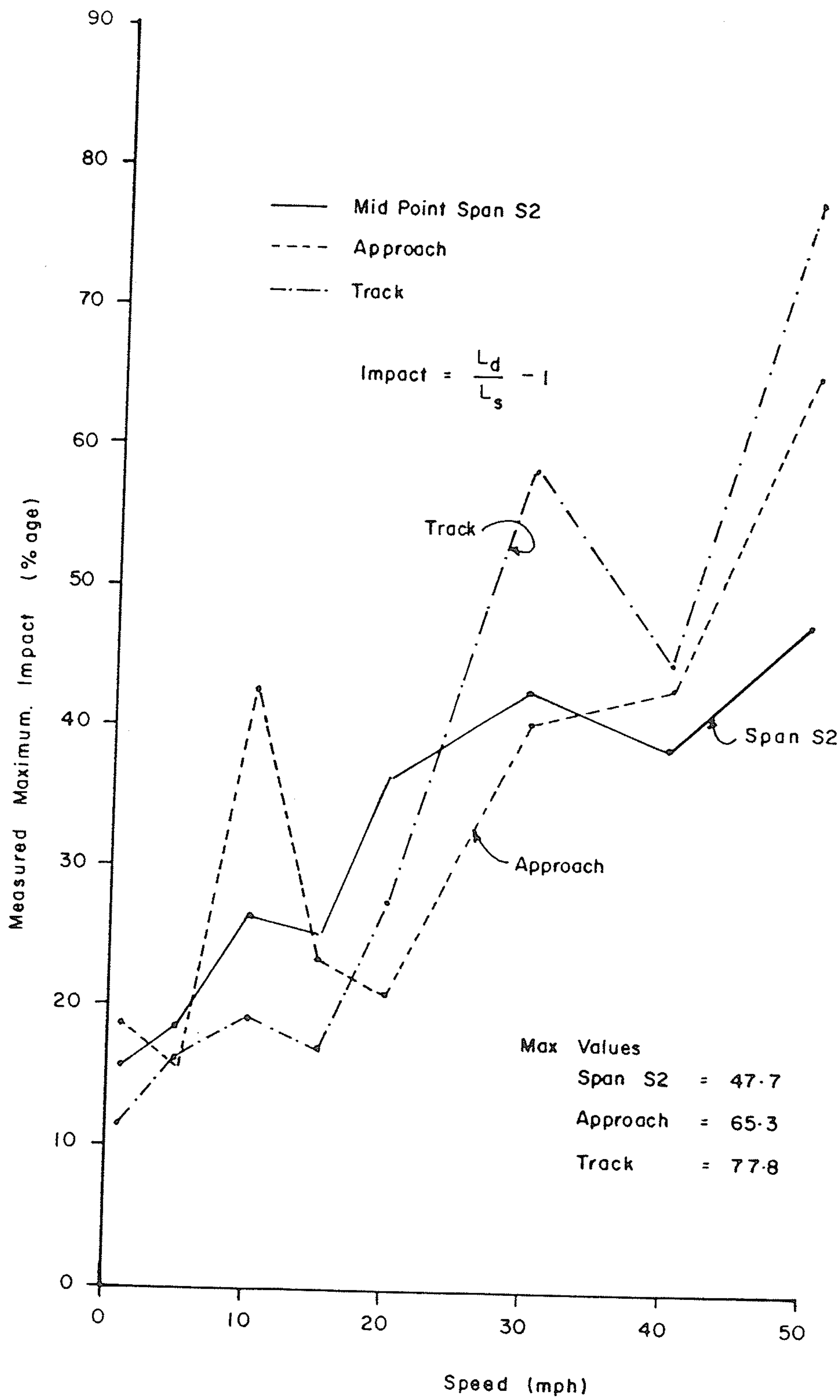

Figure 5.6 Measured maximum impact versus speed
Test train no. 2 - ODB Site

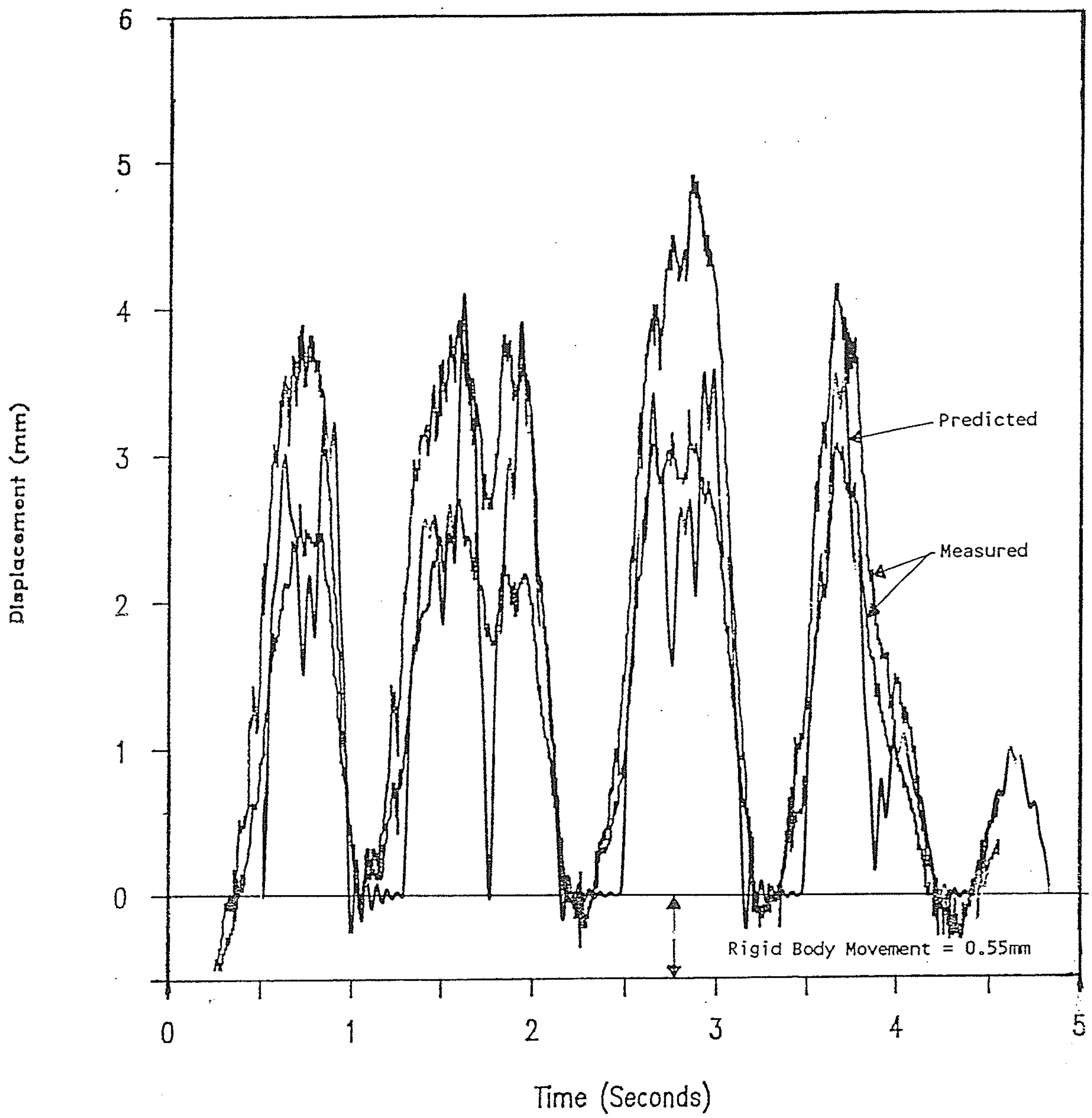

Figure 5.7 Comparison between measured and predicted displacement versus time - BDB Span S3 - Test train No. 2 at 30 mph

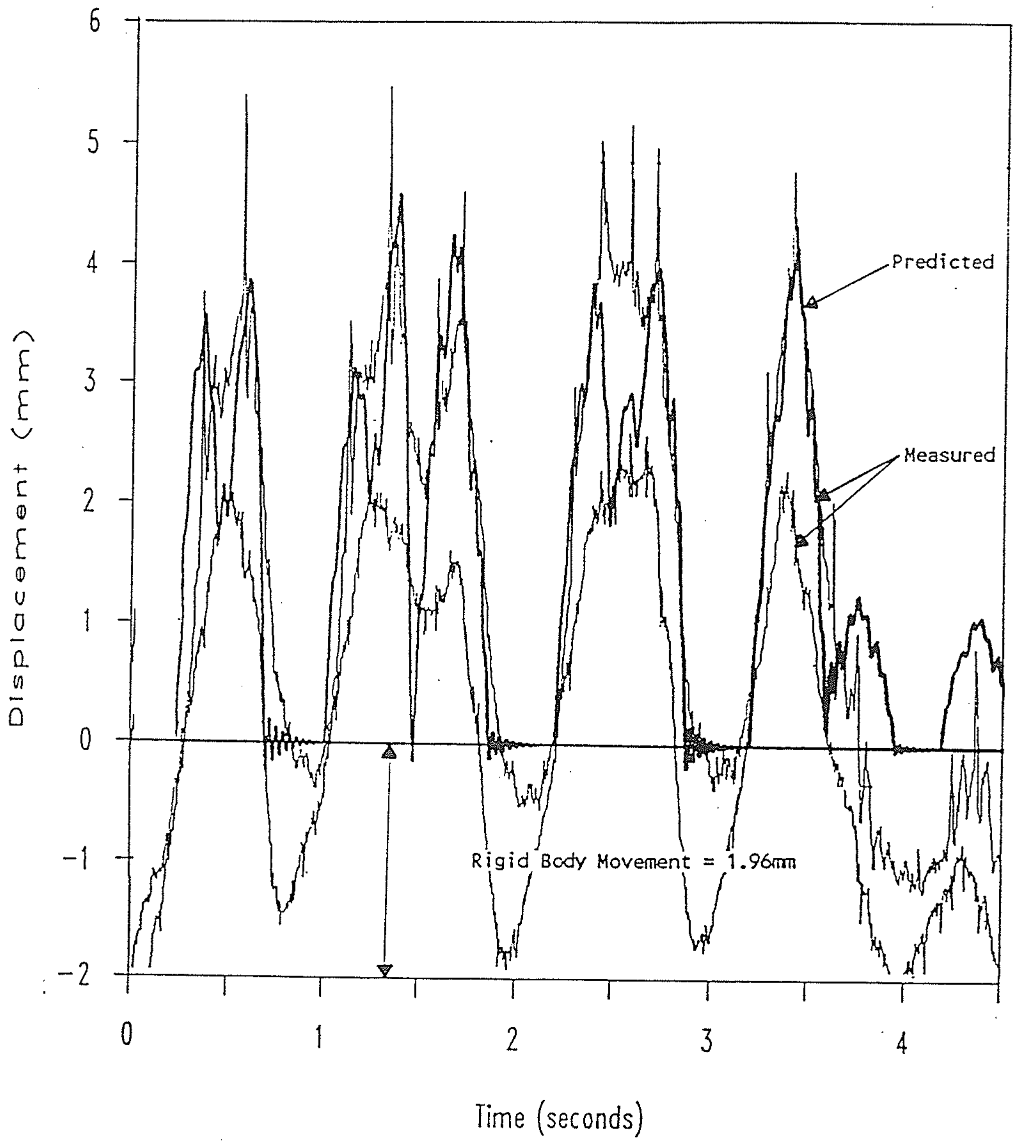

Figure 5.8 Comparison between measured and predicted displacement versus time - ODB Span S2 - Test train No. 2 at 30 mph